FINAL REPORT
FDOT CONTRACT NUMBER: BDV31-977-100

DURABILITY EVALUATION OF TERNARY MIX DESIGNS FOR EXTREMELY AGGRESSIVE EXPOSURES PHASE II

Submitted to
Research.Center@dot.state.fl.us
The Florida Department of Transportation Research Center
605 Suwannee Street, MS 30 Tallahassee, FL 32399

c/o Dr. Harvey DeFord, Ph.D.
Structures Materials Research Specialist
State Materials Office

Submitted by:

Dr. Kyle A. Riding (kyle.riding@essie.ufl.edu) (Principal Investigator)
Dr. Christopher C. Ferraro (Co-Principal Investigator)
Hossein Mosavi
Mohammed Hussain Alyami
Mohammed Almarshoud
Raid Alrashidi

November 2020

Department of Civil Engineering
Engineering School of Sustainable Infrastructure and Environment
College of Engineering
University of Florida
Gainesville, Florida 32611

DISCLAIMER

The opinions, findings, and conclusions expressed in this publication are those of the authors and not necessarily those of the State of Florida Department of Transportation or the U.S. Department of Transportation.

Prepared in cooperation with the State of Florida Department of Transportation and the U.S. Department of Transportation.

APPROXIMATE CONVERSIONS TO SI UNITS (from FHWA)				
Symbol	**When You Know**	**Multiply By**	**To Find**	**Symbol**
Length				
in	inches	25.4	millimeters	mm
ft	feet	0.305	meters	m
yd	yards	0.914	meters	m
mi	miles	1.61	kilometers	km
Area				
in^2	square inches	645.2	square millimeters	mm^2
ft^2	square feet	0.093	square meters	m^2
yd^2	square yard	0.836	square meters	m^2
mi^2	square miles	2.59	square kilometers	km^2
Volume				
fl oz	fluid ounces	29.57	milliliters	mL
gal	gallons	3.785	liters	L
ft^3	cubic feet	0.028	cubic meters	m^3
yd^3	cubic yards	0.765	cubic meters	m^3
NOTE: volumes greater than 1000 L shall be shown in m^3				
Mass				
oz	ounces	28.35	grams	g
lb	pounds	0.454	kilograms	kg
Temperature (exact degrees)				
°F	Fahrenheit	5 (F-32)/9 or (F-32)/1.8	Celsius	°C
Illumination				
fc	foot-candles	10.76	lux	lx
fl	foot-Lamberts	3.426	candela/m^2	cd/m^2
Force and Pressure or Stress				
lbf	pound-force	4.45	newtons	N
lbf/in^2	pound-force per square inch	6.89	kilopascals	kPa

TECHNICAL REPORT DOCUMENTATION PAGE

1. Report No.	2. Government Accession No.	3. Recipient's Catalog No.
4. Title and Subtitle Durability Evaluation of Ternary Mix Designs for Extremely Aggressive Exposures Phase II		5. Report Date August 2020
		6. Performing Organization Code
7. Author(s) Kyle A. Riding, Christopher C. Ferraro, Hossein Mosavi, Mohammed Hussain Alyami, Mohammed Almarshoud, Raid Alrashidi,		8. Performing Organization Report No.
9. Performing Organization Name and Address Department of Civil and Coastal Engineering Engineering School of Sustainable Infrastructure & Environment University of Florida 365 Weil Hall – P.O. Box 116580 Gainesville, FL 32611-6580		10. Work Unit No. 11. Contract or Grant No. BDV31-977-100
12. Sponsoring Agency Name and Address Florida Department of Transportation 605 Suwannee Street, MS 30 Tallahassee, FL 32399		13. Type of Report and Period Covered Final Report 14. Sponsoring Agency Code
15. Supplementary Notes None		

16. Abstract

Concrete made with low transport properties can be very durable even in extremely aggressive environments. This study examined the ability of resistivity testing to determine transport properties for concrete containing ternary blends of portland cement with supplemental cementitious materials. The penetrability of the concrete was tested using rapid chloride migration, rapid chloride permeability, water absorption, water permeability, volume of permeable voids, surface resistivity, bulk resistivity, and bulk diffusion. These tests were performed between 28 and 365 days of age of concrete. Extracted pore solution resistivity was measured to calculate the concrete formation factor. Chloride binding measurements were used to calculate effective diffusion coefficients. Little benefit was seen in increasing the silica fume dosage above 6% in RCMT and bulk resistivity tests. Resistivity samples cured in simulated pore solution showed better correlations to secondary absorption rate and water permeability than fog-room-cured samples. Formation factor performed marginally better for SPS-cured samples against secondary absorption rate than bulk resistivity. Chloride ingress calculations performed using formation factor were shown to conservatively simulate measured profiles. Chloride ingress simulated using formation factor from moist-room-cured samples were shown to be closer to the measured profiles than samples cured in simulated pore solution. Measurements performed on samples collected from piles with 12 years of marine exposure validated the laboratory results.

17. Keywords.	18. Distribution Statement
Concrete Permeability; Electrical Test Methods, Formation Factor	No restrictions.

19. Security Classif. (of this report)	20. Security Classif. (of this page)	21. Pages	22. Price
Unclassified	Unclassified		

ACKNOWLEDGMENTS

The Florida Department of Transportation (FDOT) is acknowledged for funding this project. The assistance of Dr. H. D. DeFord, Jose Armenteros, Ghulam Mujtaba, Ivan Lasa, Patrick Upshaw, Ron Simmons, and Teresa Risher is gratefully acknowledged. The advice of Dr. Michael Thomas is also gratefully acknowledged.

EXECUTIVE SUMMARY

1.1 Background

Chloride-induced reinforcement corrosion is the largest cause of deterioration for reinforced concrete [1–3]. A majority of the deterioration mechanisms in concrete are driven by the water and ion transport properties of concrete. Supplementary cementitious materials (SCMs) have been shown to improve many aspects of concrete performance, especially the chloride transport properties. Rapid test methods are needed in order to quantify the benefits of these SCMs on transport properties for project acceptance. Concrete resistivity has been used in recent years as a rapid measure of the concrete resistance to chloride ingress. There have been some concerns about the ability of resistivity to measure the durability of concrete containing ternary blends of supplementary cementitious materials. Concrete electrical resistivity measurements are known to be influenced by the pore solution composition, which can be significantly affected by the use of SCMs [4]. Formation factor has shown promise in its ability to correct for concrete pore solution effects on concrete resistivity [5].

1.2 Research Objectives

The overall research goal of this project is to be able to reliably use a rapid test that can evaluate the permeability of concrete which is directly related to the concrete long-term durability. The end-use environment determines the level of resistance that is needed to perform adequately. The test method must be rapid, provide a good correlation to penetration provided by the concrete microstructure, and have known thresholds that relate to required penetration resistance for a given level of exposure in chloride or sulfate-bearing environments. The research objective of this project is to determine if resistivity testing used to quantify the formation factor can be used as rapid test methods to determine concrete transport properties for qualification testing of concrete

containing multiple SCMs. In order to determine the suitability of electrical testing and the formation factor as an indication of concrete transport properties, this research seeks to determine the correlation between electrical and transport properties of concrete in mixtures of binary and ternary mix designs at different ages. A critical part of the research is to also link the laboratory testing to field performance of structures. This was achieved by testing concrete electrical properties and chloride concentrations of concrete that has been exposed to marine conditions and comparing their properties to similar mixtures in the lab condition. Additionally, concrete prisms were made for exposure to a 5% sulfate solution to determine the degree of correlation between sulfate durability and transport properties.

1.3 Main Findings

Project findings can be summarized as follows:

- An empirical equation has been developed to estimate the pore solution resistivity from the w/cm and oxide composition.
- Samples cured in SPS showed better correlations to secondary absorption rate and water permeability than samples cured in the fog room.
- Formation factor showed slightly better correlation for SPS-cured samples against secondary absorption rate than bulk resistivity.
- Little benefit was seen in increasing the silica fume dosage above 6% in RCMT and bulk resistivity tests.
- Bulk resistivity was shown to correlate adequately (R^2 = 0.76 to 0.80) with the concrete apparent diffusion coefficient.
- Chloride ingress calculations performed using effective diffusion coefficients calculated from formation factor were shown to conservatively simulate measured profiles. Formation factor from moist-room-cured samples were shown to be closer to the measured profiles than samples cured in simulated pore solution.

- The apparent diffusion coefficients fit to the field surface chloride profiles were much lower than those fit to lab chloride profiles. This is likely because the concrete in the piles was only partially saturated in the field.
- It was seen that results from samples cored from the piles lined up with the experimental results that were collected in laboratory conditions, validating the laboratory tests performed.
- The following mixes, two binary and nine ternary, were found to meet the extremely aggressive exposure durability requirements for resistance to chloride and sulfate attack. Total cementitious material content and w/cm were 700 lb/ft^3 and 0.35, respectively.
    - 40% Type I/II PC – 60% Slag
    - 92% Type I/II PC – 8% SF
    - 45% Type I/II PC – 10% FFA – 45% Slag
    - 30% Type I/II PC - 10% FFA – 60% Slag
    - 76% Type I/II PC – 20% FFA – 4% SF
    - 74% Type I/II PC – 20% FFA – 6% SF
    - 72% Type I/II PC – 20% FFA – 8% SF
    - 37% Type I/II PC – 55% Slag – 8% SF
    - 35% Type I/II PC – 55% Slag – 10% MK
    - 30% Type IL PC – 10% FFA – 60% Slag
    - 72% Type IL PC – 20% FFA – 8% SF

  where PC is portland cement, SF is silica fume, FFA is Class F fly ash, Slag is ground granulated blast furnace slag, and MK is metakaolin.
- Meeting the extremely aggressive exposure durability requirements for resistance to chloride attack for a particular mix design does not guarantee that the mix design will meet the extremely aggressive exposure durability requirements for resistance to sulfate attack.

1.4 Recommendations

Project recommendation can be summarized as follows:

- Given the complexity and uncertainty in quantifying the concrete pore solution required to calculate the formation factor from resistivity measurements, added laboratory complexity of curing samples in individualized simulated pore solutions, and the correlations seen between

bulk resistivity and apparent diffusion coefficient for Florida materials, it is recommended to continue using resistivity measurements in specifications.

- Given that the difference in correlation was marginal, the excellent correlation for samples cured in the moist room between bulk resistivity and RCMT, and practical issues related to curing samples in SPS, it is recommended to adopt a bulk resistivity instead of surface resistivity and use an acceptance criteria of 18 kΩ-cm at 56 or 91 days with moist-room-cured samples.
- Reduce silica fume dosage requirements in ternary blends from 7-9% to 6%.

1.5 Future Work

Future work should investigate the possibility of using accelerated curing methods to obtain a reliable estimation of long-term concrete transport properties in 28 days. It should also develop better methods to predict the pore solution resistivity and alternative curing methods to prevent leaching in concrete samples. Additional SCM combinations and total cementitious material contents that are representative of currently used FDOT concrete mix designs should be evaluated for long-term durability.

TABLE OF CONTENTS

LIST OF TABLES

LIST OF FIGURES

CHAPTER 1. INTRODUCTION

1.1 Background

Chloride-induced reinforcement corrosion is the largest cause of deterioration for reinforced concrete. In a study regarding the premature deterioration of concrete structures, it was reported that in 70 to 90% of the deteriorated structures, reinforcement corrosion was the dominant degradation mechanism [1–3]. A majority of the deterioration mechanisms in concrete are driven by the transport properties of concrete, particularly the chloride diffusivity. Supplementary cementitious materials (SCMs) have been shown to improve many aspects of concrete performance, especially the chloride transport properties. Rapid test methods are needed in order to quantify the benefits of these SCMs on transport properties.

Concrete mixtures can be made very resistant to chloride ingress, especially through the use of multiple types of SCMs. This durability needs to be verified however, through testing during the qualification process. Concrete resistivity has been used in recent years as a rapid measure of the concrete resistance to chloride ingress. There have been some concerns about the ability of resistivity measurements to be used to measure the durability of concrete containing ternary blends of supplementary cementitious materials. Concrete electrical resistivity measurements are known to be influenced by the pore solution composition, which can be significantly affected by the use of SCMs [4]. Formation factor has shown promise in its ability to correct for concrete pore solution effects on concrete resistivity [5]. In this research, the ability of electrical test methods and formation factor to determine the transport properties of concrete containing ternary blends were investigated.

1.2 Research Objectives

The research objective of this project is to determine if electrical resistivity and formation factor can be used to determine the transport properties for qualification testing of concrete containing multiple SCMs. In order to determine the suitability of electrical testing and the formation factor as an indication of concrete transport properties, this research seeks to determine the correlation between electrical and transport properties of concrete in mixtures of binary and ternary mix designs at different ages. A critical part of the research is to also link the laboratory testing to field performance of structures. This will be achieved by testing electrical properties and chloride

concentrations of concrete that has been exposed to marine conditions and compare their properties to similar mixtures in the lab condition. Additionally, concrete prisms were made for exposure to a 5% sulfate solution to determine if sulfate durability was related to transport properties.

1.3 Research Approach

To accomplish the research objectives of this project, a combined experimental and numerical approach was used:

- Measure concrete transport-related properties between 28 and 365 days using the following techniques:
  - Surface resistivity (AASHTO T 358)
  - Bulk resistivity (AASHTO TP 119)
  - Rapid Chloride Permeability Test (ASTM C1202)
  - Rapid Chloride Migration Test (NT Build 492)
  - Bulk Diffusion (ASTM C1556)
  - Length change due to sulfate exposure (ASTM C1012)
  - Water Permeability
  - Concrete Water Absorption Rate (ASTM C1585)
  - Concrete Pore System Using Mercury Intrusion Porosimetry
  - Concrete volume of permeable voids (ASTM C642)
  - Compare results of surface and bulk resistivity results to other commonly used transport results
- Measure the following properties of the cementitious systems for use in numerical simulations:
  - Chloride binding isotherms
  - Pore solution resistivity
- Simulate chloride transport in concrete using:
  - Concrete bulk or surface resistivity
  - Pore solution resistivity
  - Chloride binding isotherms
  - Concrete volume of permeable voids (ASTM C642)
  - Concrete density
- Measure chloride profiles for samples exposed to 16.5% NaCl solution for 6 months and 12 months and compare to simulated chloride profile
- Measure concrete prism expansions and mass changes after exposure to 5% sodium sulfate solution for 18 months (ASTM C1012)

CHAPTER 2. MATERIAL CHARACTERIZATION AND MIXTURE PROPORTIONS

2.1 Aggregate Properties

The coarse aggregate used in this project was a Miami Oolite limestone. The coarse aggregate specific gravity and absorption were measured according to ASTM C127 [6] and are shown in Table 2-1. The coarse aggregate particle size distribution was measured according to ASTM C136 [7] and shown in Table 2-2.

Table 2-1: Coarse Aggregate Specific Gravity and Absorption [8]

Bulk specific gravity dry	2.29
Bulk specific gravity SSD	2.40
Apparent specific gravity	2.56
Absorption	4.66 %

Table 2-2: Coarse Aggregate Particle Size Distribution [8]

Sieve Size	**Percent Passing**	**FDOT Specs**
1 ½”	100	100
1”	99.8	95-100
¾”	92.7	---
½”	45.6	25-60
3/8”	19.1	---
No. 4	5.3	0-10
No. 8	4.7	0-5

The fine aggregate used in this project was a Georgia silica sand. The fine aggregate specific gravity and absorption were measured according to ASTM C128 [9] and are shown in Table 2-3, and the sieve analysis gradation was performed according to ASTM C 136 [7] and shown in Table 2-4.

Table 2-3: Fine Aggregate Specific Gravity and Absorption [8]

Relative Density (Specific Gravity) (Oven Dry)	2.599
Relative Density (Specific Gravity) (Saturated Surface Dry)	2.605
Apparent Relative Density (Specific Gravity)	2.614
Absorption	0.22 %

Table 2-4: Fine Aggregate Particle Size Distribution [8]

Sieve Size	Percent Passing	FDOT Specs
No.4	99.9	95-100
No. 8	98.8	85-100
No. 16	89.9	65-97
No. 30	66.8	25-70
No. 50	32.3	5-35
No. 100	6.0	0-7
No. 200	0.1	Max 4

2.2 Cementitious Materials

A locally available ASTM C150 [10] Type I/II cement, an ASTM C150 [10] Type V cement, an ASTM C150 [10] Type I cement with a high alkali content, and a locally available ASTM C595 [11] Type IL cement were selected for the project. Four different cements, one ASTM C618 [12] Class F fly ash, one ASTM C989 [13] slag cement, one ASTM C1240 [14] silica fume, and an ASTM C618 [12] Class N metakaolin were procured for this project. The cement and fly ash chemical compositions were measured by x-ray fluorescence at the University of Florida (UF) using a Rigaku Supermini x-ray fluorescence (XRF) machine. The XRF was calibrated using ten cements from the Cement and Concrete Reference Laboratory (CCRL). The cement and supplementary cementitious material compositions are shown in Table 2-5.

Table 2-5: Cement and Supplementary Cementitious Material Composition as Measured by XRF [8]

Material	SiO_2 wt%	TiO_2 wt%	Al_2O_3 wt%	Fe_2O_3 wt%	MnO wt%	MgO wt%	CaO wt%	Na_2O wt%	K_2O wt%	P_2O_5 wt%	LOI wt%
Cement IL(11)	19.93	0.39	4.47	3.63	0.02	0.86	64.03	0.07	0.33	0.10	5.21
Cement type V	20.83	0.21	4.12	3.88	0.16	0.87	66.24	0.02	0.62	0.11	2.86
Cement type I/II	21.00	0.23	5.06	3.28	0.08	0.68	66.74	0.10	0.24	0.15	3.02
High alkali cement	20.56	0.21	4.55	3.78	0.09	3.06	63.65	0.29	0.87	0.12	2.68
Class F Fly Ash	48.59	1.00	19.49	19.68	0.04	0.84	5.08	0.83	2.09	0.12	1.88
Slag	34.1	0.58	14.04	0.59	0.25	5.45	41.27	0.23	0.24	0.01	0.47
Silica fume	87.67	<0.01	0.34	0.89	0.09	6.71	0.63	0.75	0.99	0.10	3.12
Metakaolin	52.53	1.8	42.96	1.49	<0.01	0.18	<0.01	0.05	0.14	0.15	1.46

The cement crystalline compositions were analyzed using x-ray diffraction and Rietveld refinement. The x-ray diffraction patterns were collected using a 0.008 2θ step size, 10 seconds per step, and Cu K_α. radiation. The open-source software Profex 3.11.1 was used to perform the Rietveld refinement. The resolved cement compositions are shown in Table 2-6.

Table 2-6: Cement Composition Analyzed by X-Ray Diffraction and Rietveld Refinement [8]

Phase	Type I/II	Type V	IL(11)	High Alkali Type I/II
Alite	49.87	59.80	49.98	53.29
Belite	18.34	11.52	14.78	19.27
Orthorhombic Aluminate	5.27	2.21	2.46	2.02
Cubic Aluminate	4.46	0.00	1.95	1.77
Ferrite	10.33	15.36	13.93	14.52
Anhydrite	0.55	0.41	0.37	0.56
Bassanite	0.00	2.53	3.11	0.64
Gypsum	5.22	1.25	0.77	3.47
Arcanite	0.87	0.40	0.51	1.39
Calcite	3.97	5.78	10.73	0.98
Free Lime	0.79	0.00	0.39	0.19
MgO	0.32	0.74	0.05	1.90
Quartz	0.00	0.00	0.96	0.00

2.3 Concrete Mixture proportions

There has been a concern about the ability of electrical resistivity to provide an indirect measure of concrete transport and durability properties in binary and ternary mixtures commonly used in extremely aggressive exposure environments in Florida. Concrete mixture proportions used in this project were selected to represent mixture proportions similar to those used in Florida or with slightly varying compositions from FDOT requirements to evaluate specific criteria. Concrete mixture proportions used in this study are presented in Table 2-7.

Table 2-7: Concrete mixture proportions (CA and FA are coarse and fine aggregate, Cem is cement, FFA is class F fly ash, SF is silica fume, SL is slag, MK is metakaolin, Type A is water-reducer, Type F is high-range water-reducer, and AEA is air-entraining admixture

Mix No.	Mix ID	CA lb/yd^3	FA lb/yd^3	Cem lb/yd^3	FFA lb/yd^3	SF lb/yd^3	SL lb/yd^3	MK lb/yd^3	Water lb/yd^3	Type A oz/cwt	Type F oz/cwt	AEA oz/cwt
1	C-100	1680	1184	700	0	0	0	0	245	4.3	3.1	0.3
2	C-100h	1552	1190	700	0	0	0	0	308	0.1	0.0	0.1
3	C-F10	1680	1167	630	70	0	0	0	245	4.3	2.7	0.3
4	C-F20	1680	1150	560	140	0	0	0	245	4.3	2.7	0.3
5	C-F10h	1552	1145	630	70	0	0	0	308	0.1	0.0	0.1
6	C-F20h	1552	1130	560	140	0	0	0	308	0.1	0.0	0.1
7	C-G60	1680	1175	280	0	0	420	0	245	4.3	5.0	0.3
8	C-S8	1680	1188	644	0	56	0	0	245	4.3	3.1	0.3
9	C-M10	1680	1193	630	0	0	0	70	245	4.3	3.1	0.3
10	C-F10G30	1680	1172	420	70	0	210	0	245	4.3	3.1	0.3
11	C-F10G45	1680	1164	315	70	0	315	0	245	4.3	3.1	0.3
12	C-F10G60	1680	1156	210	70	0	420	0	245	4.3	4.4	0.3
13	C-F10G60h	1552	1140	210	70	0	420	0	308	0.1	1.2	0.1
14	C-F20S4	1680	1161	532	140	28	0	0	245	4.3	3.1	0.3
15	C-F20S6	1680	1157	518	140	42	0	0	245	4.3	5.0	0.3
16	C-F20S8	1680	1152	504	140	56	0	0	245	5.0	5.0	0.3
17	C-F20S8h	1680	989	504	140	56	0	0	308	4.3	0.0	0.3
18	C-F20M6	1680	1161	518	140	0	0	42	245	4.3	5.0	0.3
19	C-F20M8	1680	1159	504	140	0	0	56	245	5.0	5.7	0.2
20	C-F20M10	1680	1155	490	140	0	0	70	245	5.0	6.6	0.1
21	C-F20M10h	1680	995	490	140	0	0	70	308	2.1	2.4	0.3
22	C-G55S8	1680	1160	259	0	56	385	0	245	4.3	4.7	0.3
23	C-G55M10	1680	1164	245	0	0	385	70	245	4.3	5.0	0.3
24	CV-100	1680	1185	700	0	0	0	0	245	4.3	3.1	0.3
25	CV-100h	1552	1190	700	0	0	0	0	308	0.1	0.0	0.1
26	CV-F10G60	1680	1156	210	70	0	420	0	245	4.3	3.1	0.3
27	CV-F20S8	1680	1153	504	140	56	0	0	245	4.3	3.1	0.3
28	CV-M10	1680	1193	630	0	0	0	70	245	4.3	3.1	0.3
29	CL-100	1680	1184	700	0	0	0	0	245	4.3	3.1	0.3
30	CL-100h	1552	1165	700	0	0	0	0	308	0.1	0.0	0.1
31	CL-F10G60	1680	1156	210	70	0	420	0	245	4.3	3.1	0.3
32	CL-F20S8	1680	1152	504	140	56	0	0	245	4.3	3.1	0.3
33	CL-M10	1680	1192	630	0	0	0	70	245	4.3	5.7	0.3
34	CHA-100	1680	1184	700	0	0	0	0	245	4.3	3.1	0.3
35	CHA-100h	1552	1165	700	0	0	0	0	308	0.1	0.0	0.1
36	CHA-F10G60	1680	1156	210	70	0	420	0	245	4.3	3.1	0.3
37	CHA-F20S8	1680	1152	504	140	56	0	0	245	4.3	3.1	0.3
38	CHA-M10	1680	1192	630	0	0	0	70	245	4.3	5.7	0.3
39	C-100SS*	1680	1225	700	0	0	0	0	245	4.3	8.9	0.2
40	C-F20S8SS*	1680	1194	504	140	56	0	0	245	5.9	12.1	0.2

*ASTM C33 [15] #89 Miami Oolite limestone was used in mixtures 39 and 40.

2.4 Concrete Samples Fabrication and Quality Control Testing

Concrete samples were made as part of a previous project for testing in this project [8]. Cylinders used for measuring concrete transport and electrical properties were made according to ASTM C192 "Standard Practice for Making and Curing Concrete Test Specimens in the Laboratory"[16]. All concrete batches were made in the concrete mixing facilities at the University of Florida (UF). Concrete slump was measured according to ASTM C143 "Standard Test Method for Slump of Hydraulic-Cement Concrete" [17]. The unit weight test is used to verify the density of fresh concrete for quality control purposes and can help pick up problems with incorrect ingredients or air content. This test was performed according to ASTM C138 "Standard Test Method for Density (Unit Weight), Yield, and Air Content (Gravimetric) of Concrete" [18]. For the majority of the mixes, the unit weight values were 139 to 144 lb/ft^3 (2227 to 2307 kg/m^3). The concrete air content was measured using the ASTM C231 "Standard Test Method for Air Content of Freshly Mixed Concrete by the Pressure Method" [19]. The concrete fresh temperature was measured according to ASTM C1064 "Standard Test Method for Temperature of Freshly Mixed Hydraulic-Cement Concrete" [20]. Since the concrete mixtures were all mixed in a temperature-controlled laboratory, the concrete temperature measured was between 71.6 and 75.6°F (22 and 24.2°C). Table 2-8 shows the measured concrete fresh properties. Mix 39 and 40 are repeated mixtures with No. 89 coarse aggregate. Table 2-9 shows the concrete 28 day compressive strength results as measured according to ASTM C39 [21].

Table 2-8: Measured concrete fresh properties [22]

Mix No	Mix ID	Slump, in (mm)	Air (%)	Unit weight, lb/ft^3 (kg/m^3)	Mix Temp, °F (°C)
1	C-100	6 (152)	3.0%	144 (2310)	74.3 (23.5)
2	C-100h	7 (165)	2.0%	142 (2280)	74.5 (23.6)
3	C-F10	4 (102)	3.0%	144 (2303)	74.5 (23.6)
4	C-F20	6 (140)	4.0%	141 (2259)	75.2 (24)
5	C-F10h	8 (191)	3.0%	142 (2272)	72.5 (22.5)
6	C-F20h	8 (203)	3.5%	142 (2269)	72.7 (22.6)
7	C-G60	5 (127)	2.0%	146 (2331)	72.1 (22.3)
8	C-S8	2 (51)	3.8%	142 (2277)	72.3 (22.4)
9	C-M10	3 (64)	2.8%	144 (2302)	72.7 (22.6)
10	C-F10G30	5 (127)	4.5%	141 (2266)	73.4 (23)
11	C-F10G45	6 (140)	3.1%	142 (2271)	72 (22.2)
12	C-F10G60	8 (203)	2.5%	142 (2276)	71.8 (22.1)
13	C-F10G60h	6 (152)	2.8%	140 (2249)	72.7 (22.6)
14	C-F20S4	2 (51)	3.0%	143 (2284)	74.8 (23.8)
15	C-F20S6	3 (64)	3.4%	142 (2282)	75.4 (24.1)
16	C-F20S8	6 (152)	5.0%	141 (2262)	74.1 (23.4)
17	C-F20S8h	6 (152)	1.6%	140 (2244)	72.1 (22.3)
18	C-F20M6	4 (102)	3.4%	141 (2252)	73.8 (23.2)
19	C-F20M8	2 (51)	4.0%	144 (2305)	73.8 (23.2)
20	C-F20M10	2 (51)	2.5%	145 (2316)	73.6 (23.1)
21	C-F20M10h	6 (152)	2.0%	141 (2261)	73.9 (23.3)
22	C-G55S8	3 (64)	3.5%	140 (2240)	72.5 (22.5)
23	C-G55M10	2 (51)	2.5%	140 (2240)	72.7 (22.6)
24	CV-100	3 (64)	2.75%	144 (2309)	74.7 (23.7)
25	CV-100h	6 (152)	1.5%	140 (2249)	75.4 (24.1)
26	CV-F10G60	7 (178)	3.0%	142 (2278)	71.8 (22.1)
27	CV-F20S8	4 (89)	4.5%	140 (2240)	73 (22.8)
28	CV-M10	3 (70)	3.1%	142 (2267)	72.7 (22.6)
29	CL-100	4 (108)	3.5%	141 (2258)	76.5 (24.7)
30	CL-100h	5 (114)	4.0%	140 (2239)	76.8 (24.9)
31	CL-F10G60	5 (127)	3.2%	142 (2277)	71.6 (22)
32	CL-F20S8	3 (64)	4.0%	139 (2228)	75.6 (24.2)
33	CL-M10	2 (38)	2.7%	144 (2307)	75.2 (24)
34	CHA-100	3 (83)	3.0%	143 (2284)	75 (23.9)
35	CHA-100h	7 (184)	2.8%	142 (2269)	75.6 (24.2)
36	CHA-F10G60	5 (114)	3.2%	141 (2255)	71.8 (22.1)
37	CHA-F20S8	3 (64)	4.0%	140 (2239)	74.8 (23.8)
38	CHA-M10	2 (51)	2.5%	140 (2239)	74.7 (23.7)
39	C-100	1 (25)	2.5%	145 (2323)	74.7 (23.7)
40	C-F20S8	1 (25)	2.0 %	141 (2264)	75.2 (24)

Table 2-9: Concrete 28 Day Compressive Strength [8]

Mix No	Mix ID	w/cm	Compressive strength, psi (MPa)			
			1	2	3	Average
1	C-100	0.35	5150 (35.5)	5110 (35.2)	4920 (33.9)	5060 (34.9)
2	C-100h	0.44	5490 (37.8)	6030 (41.6)	6570 (45.3)	6030 (41.6)
3	C-F10	0.35	7760 (53.5)	7840 (54)	7990 (55.1)	7860 (54.2)
4	C-F20	0.35	8050 (55.5)	7420 (51.2)	8000 (55.1)	7820 (53.9)
5	C-F10h	0.44	6130 (42.3)	5760 (39.7)	6230 (42.9)	6040 (41.6)
6	C-F20h	0.44	5440 (37.5)	5560 (38.3)	5290 (36.4)	5430 (37.4)
7	C-G60	0.35	9170 (63.3)	9140 (63)	9180 (63.3)	9160 (63.2)
8	C-S8	0.35	8190 (56.5)	8370 (57.7)	8060 (55.6)	8200 (56.6)
9	C-M10	0.35	9460 (65.2)	8920 (61.5)	7990 (55.1)	8790 (60.6)
10	C-F10G30	0.35	8310 (57.3)	8060 (55.6)	7000 (48.2)	7790 (53.7)
11	C-F10G45	0.35	7680 (53)	8440 (58.2)	7880 (54.3)	8000 (55.2)
12	C-F10G60	0.35	7620 (52.5)	8380 (57.8)	7790 (53.7)	7930 (54.7)
13	C-F10G60h	0.44	6300 (43.4)	6290 (43.4)	6310 (43.5)	6300 (43.5)
14	C-F20S4	0.35	8800 (60.7)	7770 (53.6)	7570 (52.2)	8050 (55.5)
15	C-F20S6	0.35	8530 (58.8)	8890 (61.3)	7040 (48.5)	8160 (56.2)
16	C-F20S8	0.35	8630 (59.5)	7910 (54.6)	7610 (52.5)	8050 (55.5)
17	C-F20S8h	0.44	5930 (40.9)	7070 (48.7)	6440 (44.4)	6480 (44.7)
18	C-F20M6	0.35	7980 (55.1)	8810 (60.7)	8900 (61.4)	8560 (59)
19	C-F20M8	0.35	9190 (63.3)	7540 (52)	9550 (65.9)	8760 (60.4)
20	C-F20M10	0.35	9160 (63.2)	8880 (61.2)	9690 (66.8)	9240 (63.7)
21	C-F20M10h	0.44	5950 (41)	7380 (50.9)	7030 (48.5)	6790 (46.8)
22	C-G55S8	0.35	7600 (52.4)	9070 (62.6)	8950 (61.7)	8540 (58.9)
23	C-G55M10	0.35	8480 (58.5)	8500 (58.6)	7800 (53.8)	8260 (57)
24	CV-100	0.35	7380 (50.9)	8400 (57.9)	8000 (55.2)	7930 (54.7)
25	CV-100h	0.44	6540 (45.1)	6600 (45.5)	6460 (44.5)	6530 (45)
26	CV-F10G60	0.35	8390 (57.8)	7280 (50.2)	8070 (55.6)	7910 (54.6)
27	CV-F20S8	0.35	6890 (47.5)	7300 (50.3)	6190 (42.7)	6790 (46.8)
28	CV-M10	0.35	9010 (62.1)	9530 (65.7)	8580 (59.2)	9040 (62.3)
29	CL-100	0.35	7200 (49.6)	8200 (56.5)	8260 (56.9)	7890 (54.4)
30	CL-100h	0.44	5920 (40.8)	6390 (44.1)	6720 (46.4)	6350 (43.8)
31	CL-F10G60	0.35	7070 (48.7)	7680 (52.9)	6870 (47.4)	7200 (49.7)
32	CL-F20S8	0.35	6860 (47.3)	7600 (52.4)	8360 (57.6)	7600 (52.4)
33	CL-M10	0.35	8710 (60)	9640 (66.5)	9670 (66.7)	9340 (64.4)
34	CHA-100	0.35	6690 (46.1)	6260 (43.2)	6440 (44.4)	6460 (44.6)
35	CHA-100h	0.44	4430 (30.6)	5900 (40.7)	5380 (37.1)	5240 (36.1)
36	CHA-F10G60	0.35	7680 (52.9)	6110 (42.1)	8290 (57.1)	7360 (50.7)
37	CHA-F20S8	0.35	6700 (46.2)	5820 (40.1)	6870 (47.3)	6460 (44.5)
38	CHA-M10	0.35	7640 (52.6)	6760 (46.6)	8190 (56.5)	7530 (51.9)

CHAPTER 3. CHLORIDE BINDING

3.1 Introduction

In this project, cement paste samples were made to measure the chloride binding isotherms. The chloride binding results will be used to help separate the binding and diffusion portions of the chloride transport in the bulk diffusion testing done as part of this project to calculate an effective diffusion coefficient for each concrete mixture made. Table 3-1 summarizes the cement paste mixture proportions that the research team used to measure chloride binding. These mixture proportions were chosen to match the cementitious systems used in the concrete mixtures made for bulk diffusion testing according to ASTM 1556 [23] in phase I [8] of the project [24].

Table 3-1: Cement paste mixture proportions [8]

Mix #	Mix ID	Cement (%)				SCM Type (%)				w/cm
		Type I/II	Type V	Type IL	Type I HA	Fly Ash	Slag Cement	Silica Fume	Metakaolin	
1	C-100	100								0.35
2	C-100h	100								0.44
3	C-F10	90				10				0.35
4	C-F20	80				20				0.35
5	C-F10h	90				10				0.44
6	C-F20h	80				20				0.44
7	C-G60	40					60			0.35
8	C-S8	92						8		0.35
9	C-M10	90							10	0.35
10	C-F10G30	60				10	30			0.35
11	C-F10G45	45				10	45			0.35
12	C-F10G60	30				10	60			0.35
13	C-F10G60h	30				10	60			0.44
14	C-F20S4	76				20		4		0.35
15	C-F20S6	74				20		6		0.35
16	C-F20S8	72				20		8		0.35
17	C-F20S8h	72				20		8		0.44
18	C-F20M6	74				20			6	0.35
19	C-F20M8	72				20			8	0.35
20	C-F20M10	70				20			10	0.35
21	C-F20M10h	70				20			10	0.44
22	C-G55M8	37					55	8		0.35
23	C-G55M10	35					55		10	0.35
24	0.35CV-100		100							0.35
25	CV-100h		100							0.44
26	CV-F10G60		30			10	60			0.35
27	CV-F20S8		72			20		8		0.35
28	CV-M10		90						10	0.35
29	CL-100			100						0.35
30	CL-100h			100						0.44
31	CL-F10G60			30		10	60			0.35
32	CL-F20S8			72		20		8		0.35
33	CL-M10			90					10	0.35
34	CHA-100				100					0.35
35	CHA-100h				100					0.44
36	CHA-[illegible]				30	10	60			0.35
37	CHA-F20S8				72	20		8		0.35
38	CHA-M10				90				10	0.35

3.2 Methodology

Cement paste samples were made and tested based on the principles outlined by Tang and Nilsson [25]. After the cement paste samples were made and cured, they were crushed, dried, and exposed to solutions of different chloride concentrations. The chloride concentrations were measured after the samples came to an equilibrium allowing for the chloride binding isotherm data to be fit to the measured free and bound chloride concentrations.

Sample Preparation

Paste samples were prepared using a Model 7000 constant speed mixer made by Cement Test Equipment Tulsa, Oklahoma USA according to ASTM C1738 [26]. Figure 3-1 shows the high-shear mixer in use. After connecting the water bath shown in Figure 3-2 to the cooled-base high shear mixer, the mixing water was placed inside the mixer. The water bath was set to 61°F (16°C), or 12.6°F (7°C) below the target mixing temperature in order to cool the mixing water. After cooling the mixing water, the cementitious materials were placed in the mixer while the mixer was running at 4000 rpm through the feeder lid shown in Figure 3-3. Cementitious material feeding was done to ensure uniform distribution of materials and was completed within 60 seconds. After adding the cementitious materials, the feeder lid was replaced with the high shear lid as shown in Figure 3-1. The paste was mixed at 10,000 rpm for 30 seconds, followed by a rest period of 150 seconds, and a final mixing at 10,000 rpm for 30 seconds. During the first 15 seconds of the rest period, the temperature was checked, and the sides of the mixer were scraped using a scraper.

Figure 3-1: High shear cement paste mixer [8]

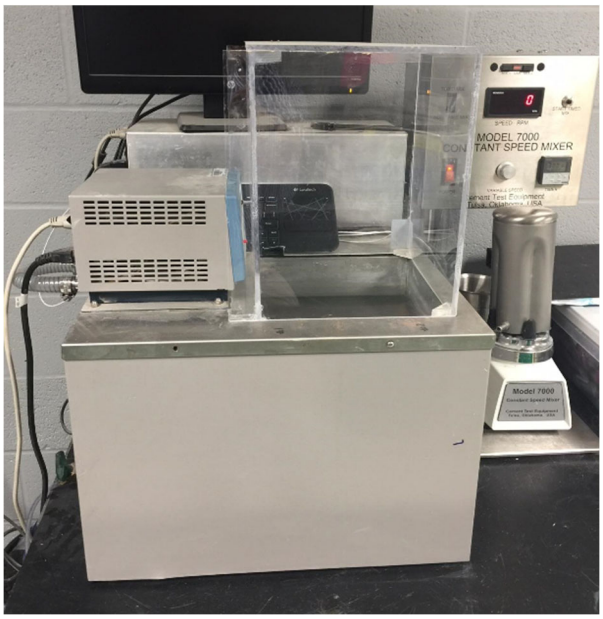

Figure 3-2: Water bath to control the paste temperature [8]

Figure 3-3: Cooled based mixer with the feeder lid [8]

After the paste mixing was completed, centrifuge tubes were filled with paste, sealed, and labeled. The tubes were attached to a rotating wheel at a speed of 6 rpm for the first 24 hours to avoid bleeding, as shown in Figure 3-4 . After 24 hours, the paste samples and containers were placed in a sealed container with soda lime to avoid carbonation at room temperature for 28 days.

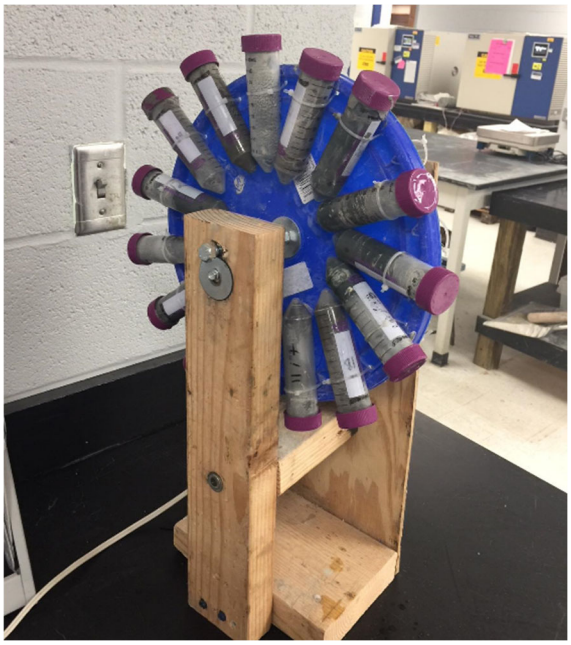

Figure 3-4: Paste rotation instrument

Sample Conditioning

After the curing period, the samples were demolded and crushed to increase the surface area and accelerate the chloride binding process. The crushed samples were sieved to control the particle size. The crushed particles were sieved using the #8 and #100 sieve to obtain cement paste particles between 0.0929 inches (2.36 mm) and 0.0063 inches (0.15 mm) in diameter. The graded crushed paste was dried in a room temperature vacuum desiccator with silica gel for 24 hours. To control the relative humidity at 11% and produce a carbon dioxide-free environment to avoid carbonation of the crushed paste, the paste was placed on a rack in a room-temperature desiccator containing soda lime and supported above a saturated lithium chloride solution for 3 days.

Crushed paste samples were placed in five different chloride solutions. Approximately 0.88 oz (25 g) of paste was placed in each container, which was filled with 3.38 fl oz (100 mL) of chloride solution, as shown in Figure 3-5. Chloride concentrations of 0.1, 0.3, 0.5, 1.0 and 3.0 M were used.

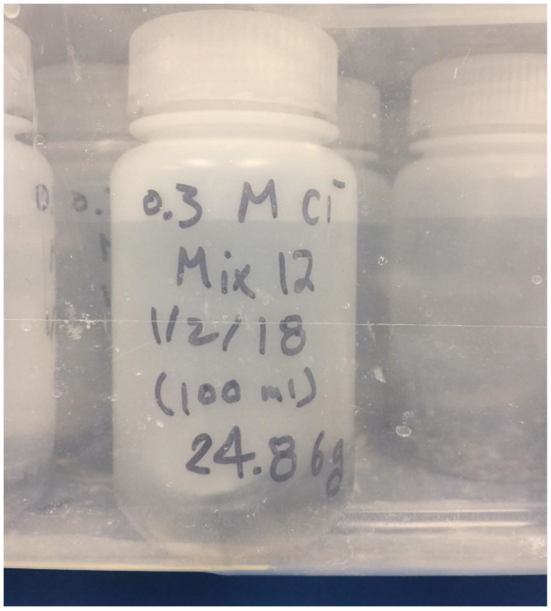

Figure 3-5: Paste samples placed in chloride solution [8]

Chloride Concentration Measurement

Chloride binding for each sample at each solution concentration was measured after completion of the ponding. The chloride concentration was measured using an autotitrator. Silver nitrate (0.1 N) was used as the titrant. The chloride solution was placed in a 3.38 fl oz (100 ml) container using the solution amount for each concentration shown in Table 3-2.

Table 3-2: Chloride solution volume used during autotitration

Expected chloride concentration (M)	Volume of solution used (ml)
0.1	50
0.3	20
0.5	10
1.0	10
3.0	5

One milliliter (0.0338 fl oz) of nitric acid was added to the sample solution for every 0.338 fl oz (10 ml) of chloride solution, stirred using a glass stirring rod, and washed with distilled water into the beaker. The beaker was covered with a watch glass and left for an hour. An equivalent amount of sodium acetate, 0.0338 fl oz (1 ml) for every 0.338 fl oz (10 ml) of chloride solution, was added to the solution and stirred. Distilled water was added until the 3.38 fl oz (100 ml) mark was reached.

The Mettler Toledo Easy Cl Titrator shown in Figure 3-6, was used to measure the solution chloride concentration. The change in molarity (M) of the solution was used to calculate the bound chloride concentration using Equation 3-1 [27]:

$$C_b = \frac{35.45\ V\ (\ c_0 - c_1)}{w} \qquad \text{Equation 3-1}$$

Where C_b is the bound chloride content (mg/g), $(c_0\text{-}c_1)$ is the change in chloride concentration (M or mol/l), V is the volume of solution (ml), and w is the dry weight of sample (g).

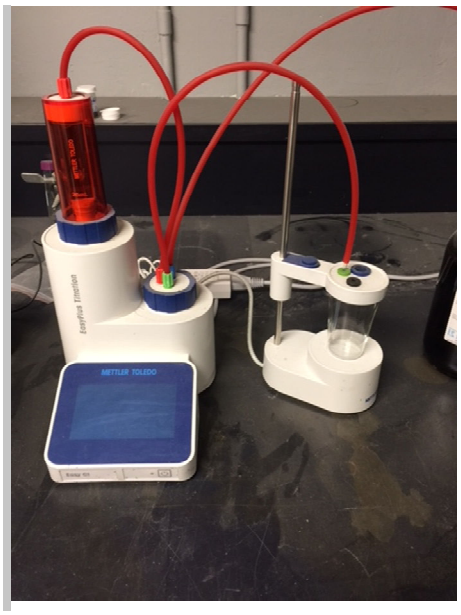

Figure 3-6: The autotitrator used in this project [8]

3.3 Results

The chloride binding test results are shown in Table 3-3. A Freundlich binding isotherm was used to model the relationship between the free chloride concentration and bound chloride concentration in cement paste. The Freundlich binding isotherm is shown in Equation 2-2.

$$C_b = \alpha\, C_f^{\beta} \qquad \text{Equation 2-2}$$

Where α and β are unit-less coefficients. The α and β values fitted to the measured chloride values along with the fitted coefficients of determination (R^2) are shown in Table 3-4.

Table 3-3: Chloride binding test results

Mix	0.1 (M)	0.3 (M)	0.5 (M)	1.0 (M)	3.0 (M)
1	3.590	6.629	7.126	10.189	16.082
2	3.897	5.538	7.537	11.119	17.030
3	4.580	6.615	6.907	10.032	16.750
4	4.180	6.203	7.592	10.029	17.345
5	3.882	6.205	7.757	10.946	17.934
6	3.669	6.636	8.353	10.434	17.036
7	3.745	6.827	9.842	13.791	20.729
8	3.989	5.441	6.324	8.460	14.053
9	5.764	8.361	9.795	11.940	17.354
10	5.161	7.635	7.799	11.058	17.818
11	4.277	7.878	8.146	11.125	18.314
12	4.011	7.372	10.139	14.162	21.317
13	3.811	7.109	10.783	12.678	21.462
14	3.860	5.636	7.489	9.563	13.956
15	3.688	5.525	6.649	8.718	13.477
16	3.563	4.811	5.590	8.445	12.373
17	3.556	4.673	6.310	7.698	12.730
18	4.976	7.788	9.070	11.966	19.121
19	5.018	6.623	9.001	12.638	20.340
20	4.015	7.038	9.008	13.818	19.854
21	4.602	8.451	10.826	14.498	20.505
22	3.997	5.970	8.273	11.297	19.603
23	3.070	6.795	9.231	12.401	22.636
24	3.710	5.656	6.855	9.025	12.539
25	3.446	5.833	7.145	9.662	12.753
26	3.109	5.055	7.093	10.837	20.487
27	2.835	4.498	4.895	6.790	10.018
28	4.567	7.271	9.009	10.938	16.826
29	4.279	6.588	7.017	9.186	13.647
30	3.724	6.016	8.125	10.209	14.018
31	2.717	5.316	6.551	10.747	21.572
32	3.180	5.054	6.223	6.920	10.719
33	4.360	7.172	8.781	12.226	16.671
34	3.437	6.706	7.459	10.470	14.316
35	3.619	6.334	7.157	10.447	14.833
36	2.619	5.168	8.193	11.689	19.727
37	3.213	4.965	6.446	7.245	11.197
38	3.632	5.894	8.274	10.717	15.905

Table 3-4: Freundlich isotherm coefficients

Mix	α	β	R^2
1	10.50	0.40	0.99
2	10.87	0.41	0.98
3	10.59	0.34	0.96
4	10.84	0.38	0.99
5	11.31	0.41	1.00
6	11.21	0.41	1.00
7	13.60	0.48	0.99
8	9.00	0.34	0.97
9	12.57	0.28	1.00
10	11.70	0.31	0.96
11	11.99	0.38	0.98
12	14.09	0.45	0.99
13	13.81	0.46	0.98
14	9.65	0.35	0.99
15	9.03	0.35	1.00
16	8.19	0.35	0.97
17	8.24	0.35	0.98
18	12.73	0.35	0.99
19	12.91	0.38	0.97
20	13.21	0.44	0.99
21	14.52	0.40	0.99
22	11.90	0.44	0.99
23	13.46	0.54	0.99
24	8.96	0.33	1.00
25	9.30	0.36	0.99
26	11.26	0.53	0.99
27	6.83	0.35	0.99
28	11.65	0.34	1.00
29	9.58	0.30	0.99
30	10.10	0.36	0.99
31	11.38	0.58	1.00
32	7.55	0.32	0.99
33	11.88	0.36	0.99
34	10.23	0.38	0.98
35	10.20	0.39	0.99
36	11.68	0.57	0.99
37	7.80	0.34	0.99
38	10.77	0.41	0.99

Effect of water to cement ratio

The effect of w/c was noticed in the chloride binding results. As w/c increased the chloride binding slightly increased, as shown in Figure 3-7 for the Type I/II cement. The effect was minimal due to the limited and small range of w/c (0.35 – 0.44) tested. The effect of w/c on chloride binding is caused by the increase of porosity and permeability which produces more surface area for chloride binding.

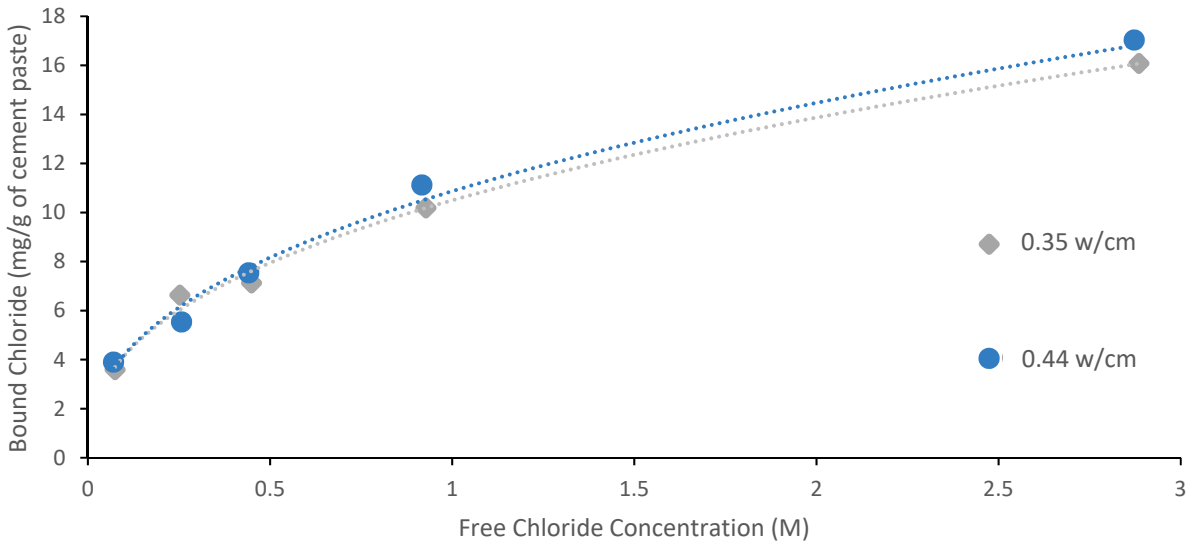

Figure 3-7: Effect of w/c on chloride binding for Type I/II portland cement

Effect of type of cement

As shown in Figure 3-8, the Type I/II cement had the highest chloride binding compared to the other cement types, whereas the Type V cement had the lowest. Chloride binding in cement is generally attributed to the aluminate (C_3A) content. The Type I/II cement used in this research had around 9.73% C_3A content, Type IL cement had 4.41% C_3A content, high alkali Type I cement had 3.79% C_3A content and Type V cement had 2.21% C_3A content, as measured by X-ray diffraction with Rietveld refinement. The bound chloride content was found to be directly proportional to the C_3A content as shown in Figure 3-9.

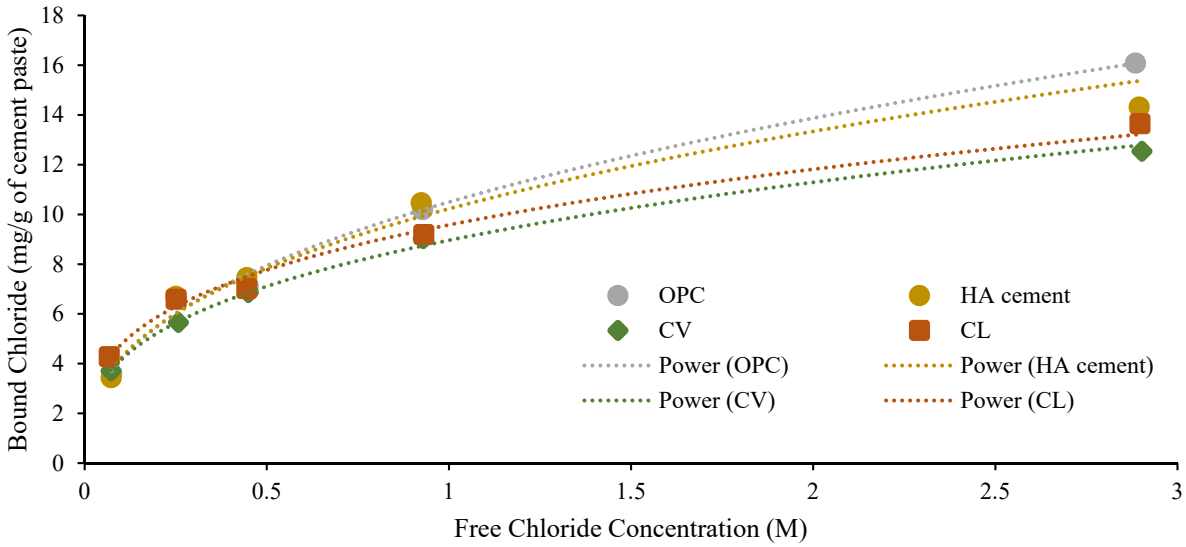

Figure 3-8: Effect of type of cement on free chloride binding

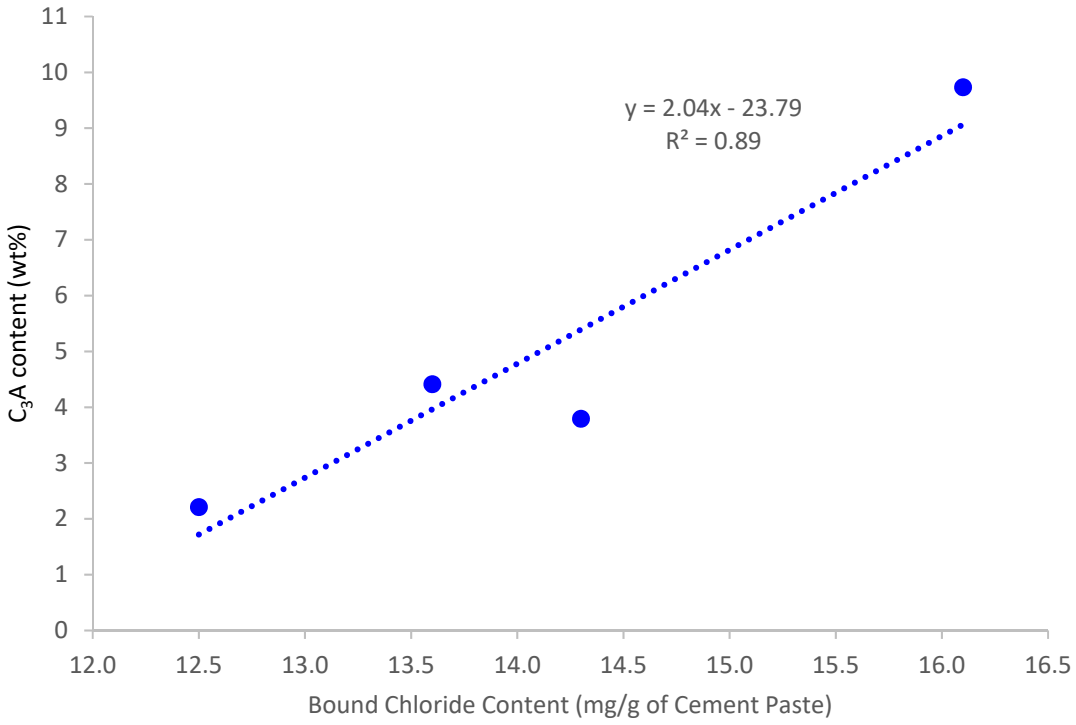

Figure 3-9: Effect of C_3A content of cement on the bound chloride content at 2.9 M free chloride concentration

Effect of slag

Slag cement increased the chloride binding significantly, as shown in Figure 3-10. This was mainly caused by the high alumina content in the slag cement, which was 14.04% by mass. This amount of alumina would increase the chemical chloride binding of the paste, with binding increasing with slag cement dosage.

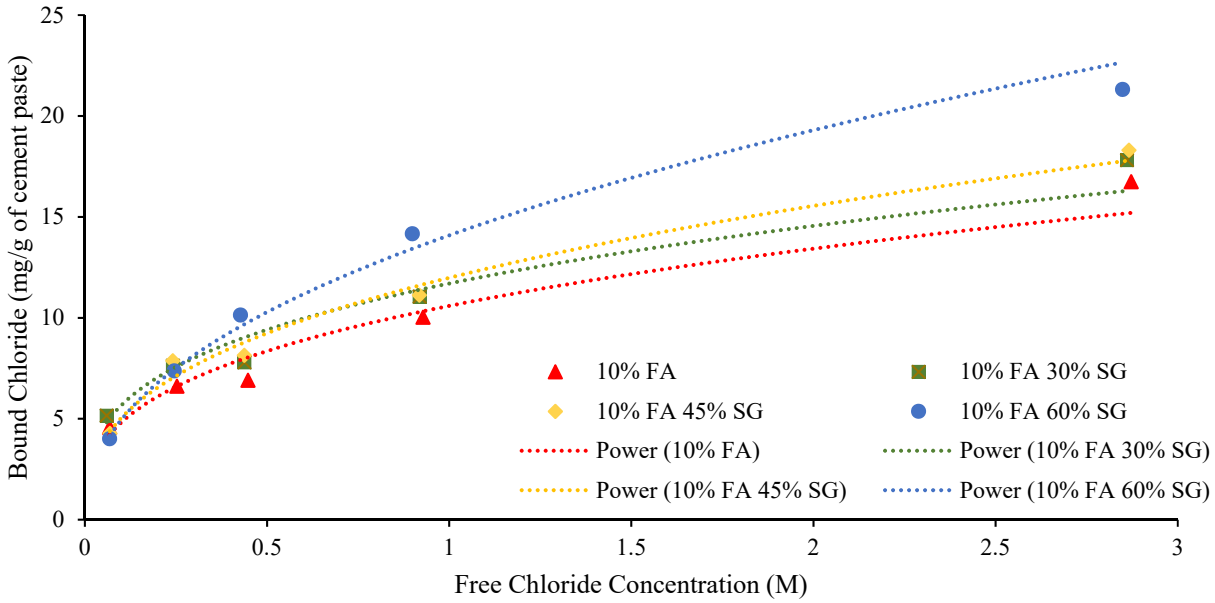

Figure 3-10: Effect of slag content on free chloride binding

Effect of fly ash

As shown in Figure 3-11, the effect of fly ash was weak due to the limited dosages of fly ash used in this research. The limited increase in chloride binding could be because of a low fly ash degree of hydration after 28 days of curing prior to exposure to the chloride solution and the reduction in the calcium-to-silica ratio (C/S).

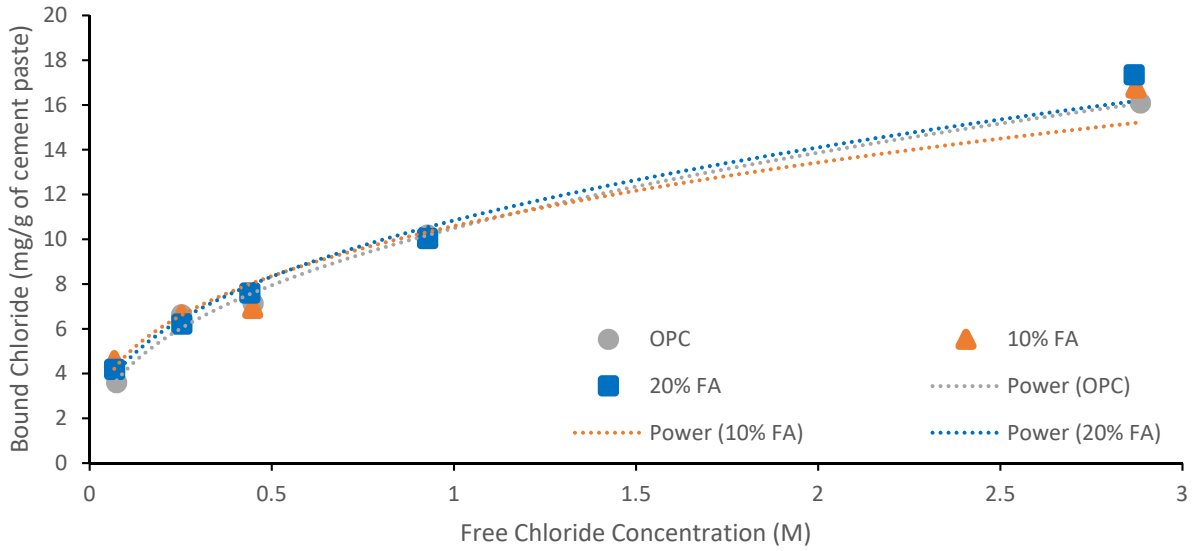

Figure 3-11: Effect of fly ash content on free chloride binding

Effect of silica fume

The use of silica fume as an SCM decreased chloride binding as shown in Figure 3-12. As silica fume content increased, the chloride binding decreased. This decrease was mainly caused by the reduction of C/S, which would affect the formation of C-S-H and the chloride binding capacity of that C-S-H.

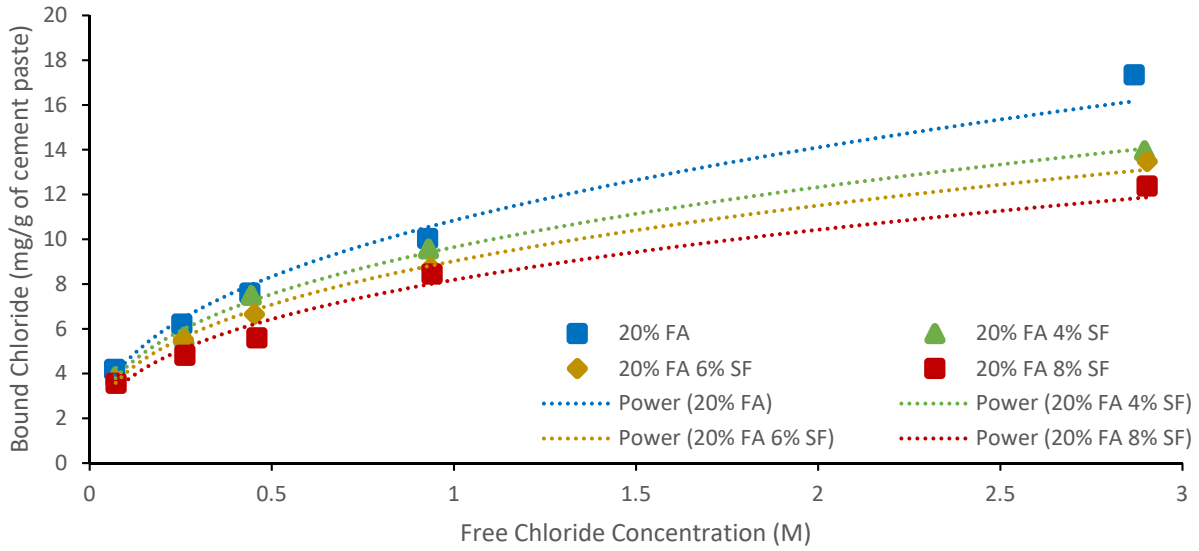

Figure 3-12: Effect of silica fume content on free chloride binding

Effect of metakaolin

Figure 3-13 shows the noticeable effect of metakaolin on chloride binding. The use of metakaolin as an SCM increased the chloride binding capacity, even though the metakaolin content did not exceed 10%. The additional binding provided by the metakaolin was likely because of its high alumina content and potential to form Friedel's salt.

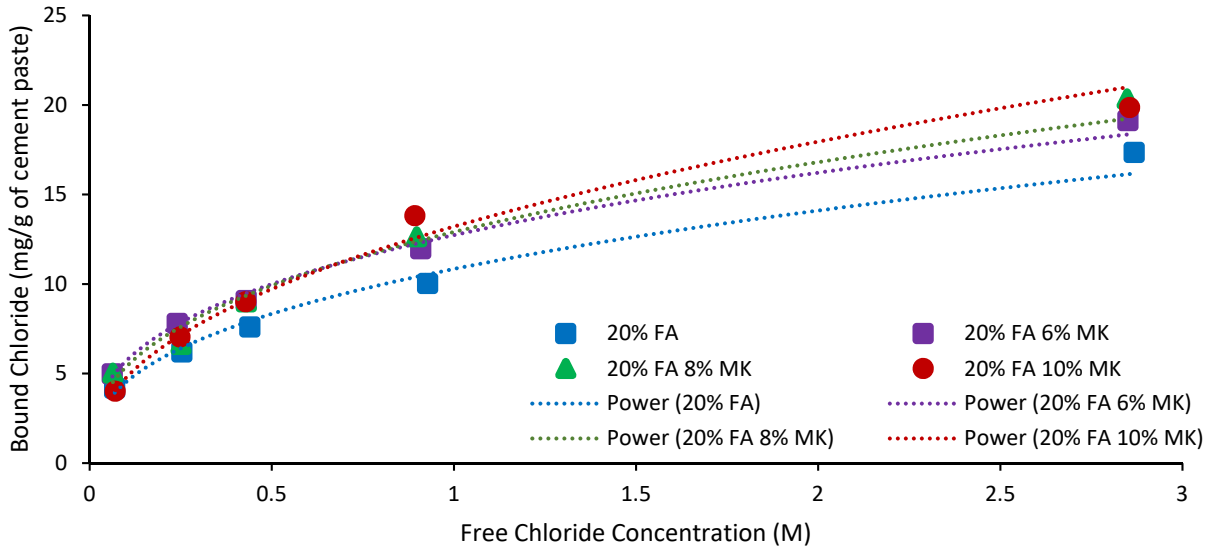

Figure 3-13: Effect of metakaolin content of free chloride binding

3.4 Summary

Chloride binding isotherms were measured after 28 days of curing on paste samples made with the same cementitious systems as the concrete samples made in phase I of this study. A comparison of chloride binding isotherms for cementitious systems tested in this study found the following:

- w/cm had only a very minor effect on chloride binding
- C_3A content correlated with an increase in chloride binding, with higher C_3A levels showing higher amounts of binding
- Slag cement caused a large increase in binding with increased dosage
- The fly ash used in this study showed very little change in chloride binding, possibly because of a low degree of hydration at 28 days and a reduction in C/S
- Silica fume showed a slight decrease in chloride binding, probably from a dilutional effect on the alumina content in the system
- Metakaolin showed a small increase in chloride binding with increased dosage

CHAPTER 4. PORE SOLUTION RESISTIVITY

4.1 Introduction

The formation factor is an empirical parameter that describes the ionic transport properties of concrete. Formation factor was originally developed to relate hydraulic conductivity of rock formations to electrical measurements in the oil industry [28]. In order to relate the concrete electrical properties to the concrete transport properties using the formation factor, the pore solution conductivity must be known [29]. As a porous material, formation factor *F* can be applied to concrete to calculate the concrete effective diffusion coefficient using Equation 4-1:

$$F = \frac{\rho_t}{\rho_0} = \frac{D_0}{D_e} \qquad \text{Equation 4-1}$$

Where ρ_t is the concrete resistivity (kΩ.cm) and ρ_0 is the pore solution resistivity (kΩ.cm), D_e is the effective diffusion coefficient. For chlorides, the self-diffusion D_0 coefficient is 20.3×10^{-10} m^2/s at 25 °C [30].

In order to better characterize the concrete formation factor and assess the ability of the NIST pore solution calculator to estimate the pore solution resistivity for ternary blend mixtures, pore solution was extracted from cement paste samples made to represent the cementitious systems used. The pore solution resistivity was then measured.

4.2 Methodology

Cement paste mixtures were made to measure the pore solution resistivity. After curing, pore solutions were expressed from the samples. The sample pore solution resistivity were measured using several methods and compared.

Sample Preparation

Cement paste samples were made to match the cementitious systems used in the concrete mixtures tested in this study. Cement paste samples were used because pore solution extraction on ternary concrete mixtures used in this study did not produce enough pore solution for electrical measurements. Table 3-1 shows the cement paste mixture proportions used.

The paste mixtures were prepared using a high shear mixer according to ASTM C1738/C1738M-19 [26] and shown in Figure 3-1. In order to remove the excessive heat generated by mixing, a mixing container with a cooling reservoir under the sample and attached to a refrigerating and circulating water bath was used. After mixing, the cement paste was placed into 2 × 4 in. (50 × 100 mm) cylinder molds. To avoid segregation of the paste, the molds were sealed and rotated at a speed of 10 rpm for 24 hours. The samples inside the sealed containers were then put in a secondary sealed container with relative humidity of more than 90% at 23ºC. Soda lime was placed in the secondary sealed container to eliminate carbonation. The specimens were cured until 28 days of age.

Ten mixtures, numbers 2, 4, 5, 6, 13, 17, 21, 25, 30, and 35, were selected for additional testing to compare the electrical resistivity at different ages and curing conditions. These samples were cured using three different methods. Samples were cured for 7 days at 23ºC, cured using accelerated curing for 7 days at 23ºC followed by 21 days at 38ºC, or for 15 months at 23ºC, after which the pore solution resistivity and composition were measured.

Pore Solution Resistivity Estimation

Several methods were used to obtain the cement paste pore solution resistivity and were compared. The cement paste pore solution and resistivity were first estimated to prepare the simulated pore solutions used to cure the concrete samples. The National Institute for Standards and Technology (NIST) developed an online calculator [31] that estimates the pore solution composition and then calculates its corresponding electrical resistivity [32]. Several assumptions required to estimate the pore solution composition are built into the model, while another was assumed in this study [31]:

1) The cementitious materials were assumed by the research team to have a degree of hydration of 75%.
2) Alkalis present in the slag will contribute to hydration but have no influence on the pore solution composition.
3) Silica fume percentage will affect the alkali composition by absorbing alkalis.
4) To maintain the electro-neutrality in the pore solution, the sum of Na+ and K+ ion concentrations is equal to the concentration of OH-.

The calculator is useful in that it provides a simple method of estimating the pore solution. There are some limitations, however. Knowledge of the degree of hydration at 28 days is limited and the calculator does not include options for some SCMs such as metakaolin. Consequently, when metakaolin was used it was instead entered as silica fume in the calculator.

Pore Solution Extraction

To extract the pore solution, a hydraulic compression machine that could provide up to 500,000 lb of force was used, as shown in Figure 4-1a. The pore solution extraction setup was built to extract solution from the concrete as shown in Figure 4-1b.

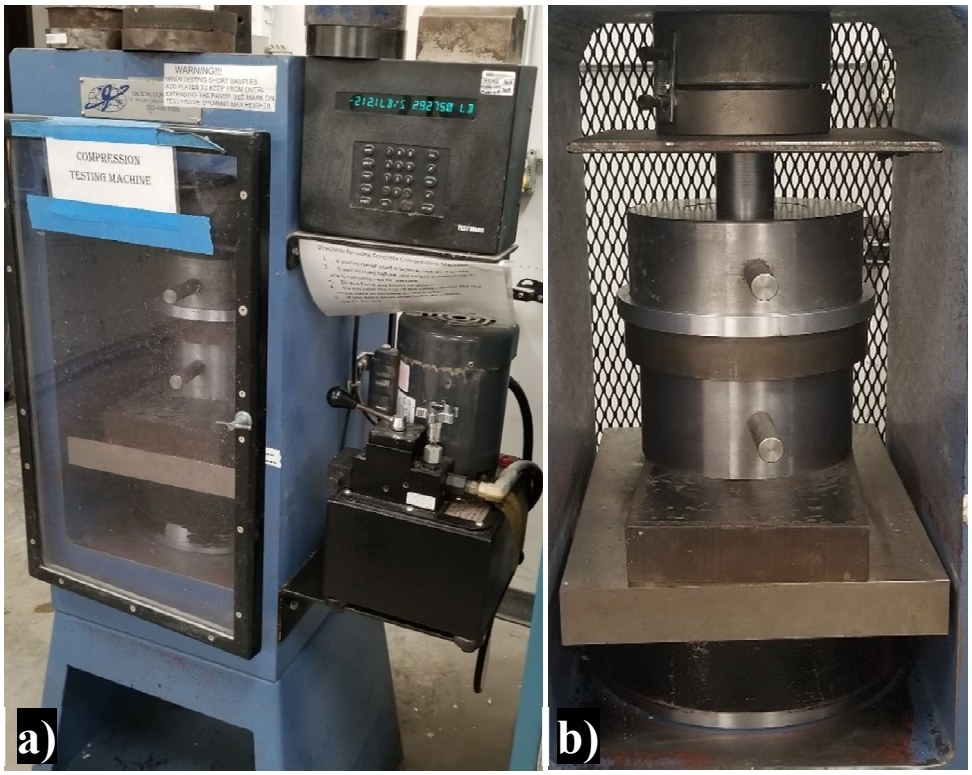

Figure 4-1: a) Hydraulic compressing machine used for pore solution extraction. b) Custom-built extraction set up

Pore solution extraction followed the general procedures used in previous studies [33]. Figure 4-2 shows a schematic of the pore solution extraction apparatus and process. A plastic container was placed in an opening under the sample cavity to receive the pore solution during extraction. The specimens were crushed into small pieces prior to testing and placed in the center of the press. A

metal piston was then placed on top of the cement paste inside the press to apply force to the sample. A force was increased at a rate of 500 to 700 lb/sec until reaching 300,000 lb. After reaching the maximum load, the machine was held at a constant load for two minutes to make sure enough solution was extracted from the paste.

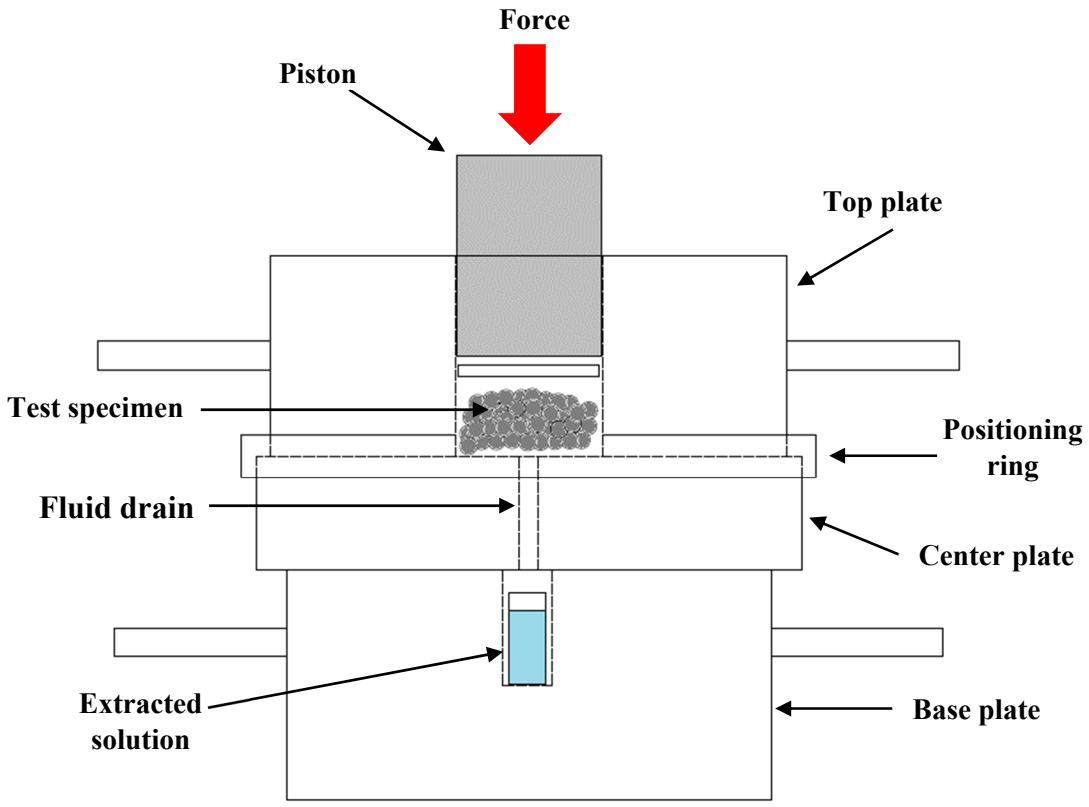

Figure 4-2: Pore solution extraction apparatus

After the sample was unloaded, the pore solution in the plastic containers was removed from the press, as shown in Figure 4-3. The amount of extracted materials varied based on mixture type, testing age, the amount of pressure applied, rate of pressure and other factors. Based on the previous experiments an optimum range was found for all the parameters mentioned to obtain enough solution. In case that there was not enough solution extracted, more solution was collected from additional specimens made. Immediately after expressing the solutions the vials were sealed to avoid contamination and evaporation.

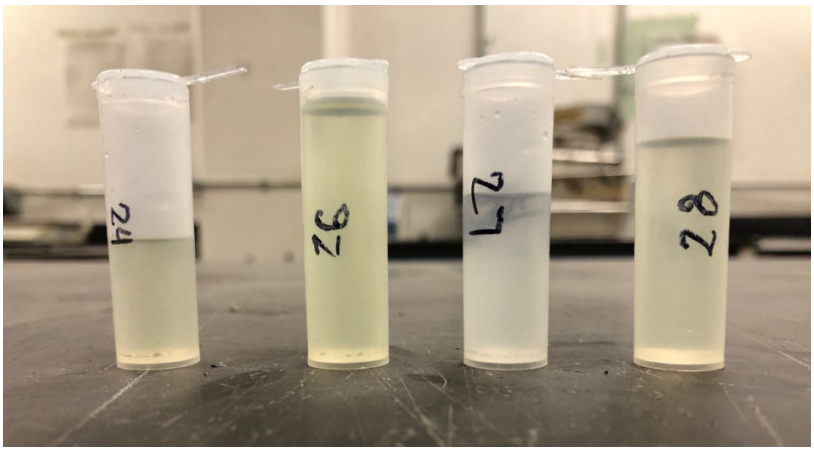

Figure 4-3: Extracted solution from the mixtures

The resistivity of the solutions were measured by electrochemical impedance spectroscopy (EIS) using a GAMRY reference 600 and a solution cell as shown in Figure 4-4. The EIS testing cell was a polycarbonate tube with an inner cross-sectional area of 0.265 cm^2 and a length of 4.823 cm as shown in Figure 4-4. Two conductive steel sheets were placed on each of the testing cell ends and secured. The testing cell had two openings pointed upward. One opening was used to insert the solution and the other one was used to allow air to escape the testing cell. After inserting the solution into the testing cell, the cell was inspected to make sure that no air bubbles were present that would interfere with the EIS testing. The EIS initial testing frequency was 200,000 Hz and the final frequency was 1 Hz. The software selected 55 points between the programmed minimum and maximum frequencies to plot the EIS response curve. The electrical resistivity was reported at two frequencies of 40 Hz and 100 kHz. 40 Hz is the frequency that is used in the Proceq Resipod used in testing electrical resistivity, and 100 kHz was selected because the resistivity was found to have converged to a stable value at that frequency. EIS testing showed that the resistivity of the pore solution does not change significantly between 1k Hz to 100k Hz. For a solution placed in a container with area of A and length l, the resistivity is defined in Equation 4-2 [34]:

$$\rho_0 = R\frac{A}{l} \qquad \text{Equation 4-2}$$

Where ρ is the resistivity and R is the resistance. The conductivity is the inverse of the resistivity. Accordingly, the conductivity of solution is determined using Equation 4-3:

$$\sigma_0 = \frac{1}{\rho_0}$$ Equation 4-3

Where σ_0 is the conductivity of the solution (S/m) for ρ_0 measured in Ohm-m (Ω-m).

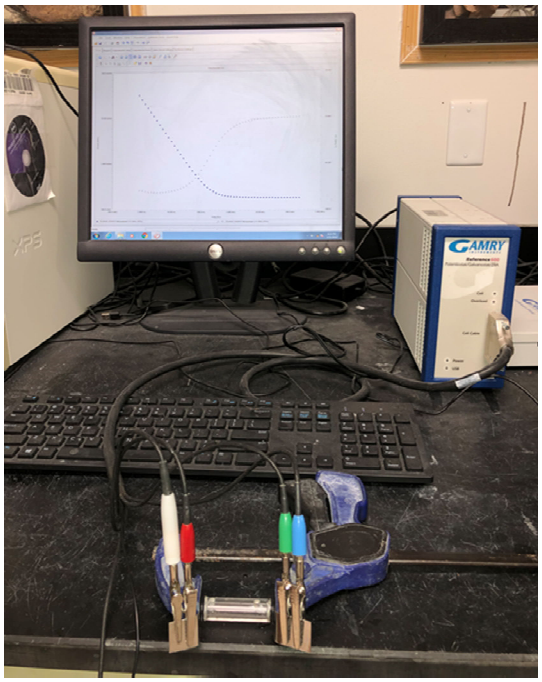

Figure 4-4: Gamry reference 600 and the pore solution testing cell.

After EIS measurements, the composition of the pore solution extracted from the ten paste mixtures cured using different methods was measured. The sodium and potassium concentrations were measured using ion chromatography.

Figure 4-5 shows the conductivity measurement setup used to analyze the simulated pore solution. An Oakton PC700 Conductivity meter was used to measure the conductivity of the simulated pore solution. The resistivity was determined using Equation 4-3.

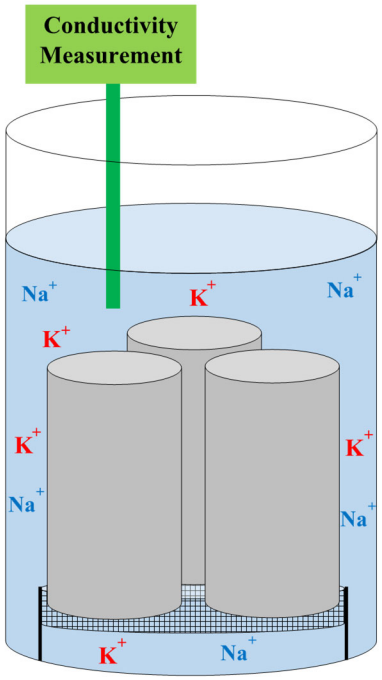

Figure 4-5: Conductivity measurement on the simulated pore solution (SPS)

4.3 Results

Table 4-1 shows the electrical resistivity results from EIS on the extracted pore solution at 28 days of age. The EIS results are shown at frequencies of 40 and 100 kHz. Table 4-2 shows the pore solution resistivity results for cement paste samples cured using conditions other than standard lab curing at 23°C for 28 days. Table 4-3 shows the sodium and potassium concentrations for the ten cement paste mixtures tested.

Table 4-1: Electrical resistivity results from EIS at 40 Hz and 100 kHz (cured 28d at 23°C).

Mix No	Mix ID	Extracted Pore Solution Resistivity (Ω.cm)	
		EIS	
		(40 Hz)	(100 kHz)
1	C-100	12.2	7.8
2	C-100h	16.9	10.2
3	C-F10	12.2	8.1
4	C-F20	17.1	10.0
5	C-F10h	16.3	10.3
6	C-F20h	16.1	11.3
7	C-G60	23.5	18.8
8	C-S8	12.1	8.3
9	C-M10	20.8	16.4
10	C-F10G30	14.7	10.6
11	C-F10G45	19.5	15.2
12	C-F10G60	27.0	22.1
13	C-F10G60h	33.2	27.3
14	C-F20S4	30.9	24.9
15	C-F20S6	48.8	42.9
16	C-F20S8	46.1	40.7
17	C-F20S8h	60.0	54.1
18	C-F20M6	21.0	16.5
19	C-F20M8	21.4	16.9
20	C-F20M10	25.2	20.9
21	C-F20M10h	28.5	23.9
22	C-G55S8	75.3	67.8
23	C-G55M10	38.5	32.6
24	CV-100	13.9	7.2
25	CV-100h	13.4	9.2
26	CV-F10G60	37.6	24.7
27	CV-F20S8	45.7	35.5
28	CV-M10	23.6	16.1
29	CL-100	15.1	7.4
30	CL-100h	16.5	11.7
31	CL-F10G60	31.4	26.3
32	CL-F20S8	68.3	57.9
33	CL-M10	24.3	20.4
34	CHA-100	9.7	5.8
35	CHA-100h	9.3	5.7
36	CHA-F10G60	23.1	18.9
37	CHA-F20S8	33.3	28.1
38	CHA-M10	13.9	10.6

Table 4-2: Pore solution resistivity values measured using EIS at 100 kHz on extracted pore solution for samples cured under the indicated non-standard conditions

Mix #	Mix ID	Resistivity (Ω.cm)		
		7 days	28 days Accelerated curing	15 months
2	C-100h	12.23	9.84	---
4	C-F20	10.89	9.64	----
5	C-F10h	12.40	10.47	13.41
6	C-F20h	12.96	11.26	15.62
13	C-F10G60h	31.28	27.31	35.92
17	C-F20S8h	51.50	51.71	75.39
21	C-F20M10h	26.38	23.30	25.28
25	CV-100h	10.00	9.60	10.05
30	CL-100h	14.04	11.46	12.30
35	CHA-100h	7.27	5.50	----

Table 4-3: Ion chromatography results for extracted pore solution at 7 days, 28 days, 28 days accelerated curing (AC), and 15 months

Mix #	Mix ID	IC (g/L)							
		7 days		28 days		28 days AC		15 months	
		Na^+	K^+	Na^+	K^+	Na^+	K^+	Na^+	K^+
2	C-100h	4.60	4.59	3.53	8.26	3.61	8.88	4.28	4.52
4	C-F20	4.26	6.69	3.68	9.49	3.58	9.16	3.04	6.77
5	C-F10h	6.26	2.59	3.39	8.46	3.34	8.35	3.16	7.01
6	C-F20h	4.66	3.61	3.05	7.46	2.93	7.46	3.30	4.56
13	C-F10G60h	1.61	3.03	1.46	2.51	1.54	2.51	2.01	2.53
17	C-F20S8h	0.94	1.51	0.72	1.18	0.73	1.13	0.66	1.26
21	C-F20M10h	2.21	4.01	1.51	3.51	1.38	3.90	2.15	3.37
25	CV-100h	1.55	10.67	1.33	13.20	1.28	13.20	2.07	11.73
30	CL-100h	3.10	5.40	2.50	7.53	2.83	8.49	3.23	7.12
35	CHA-100h	6.33	13.05	6.23	18.04	6.64	19.06	6.67	14.20

A comparison of the pore solution resistivity at 40 Hz and 100k Hz is shown in Figure 4-6 shows a linear relationship between two frequencies for OPC, binary and ternary mixtures at w/cm of 0.35 and 0.44.

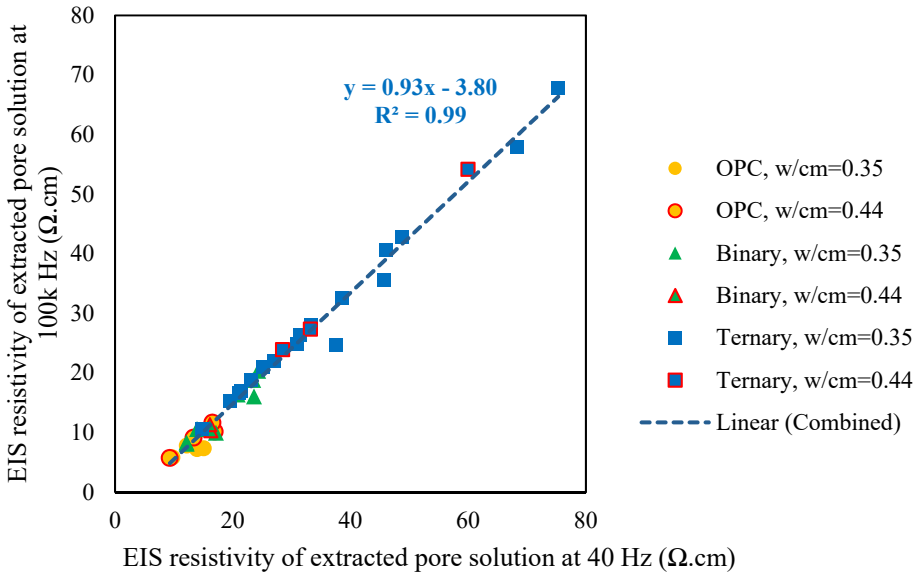

Figure 4-6: EIS resistivity of extracted pore solution at 40 Hz and 100 kHz

A comparison of the extracted pore solution sodium equivalent alkali concentration and the extracted pore solution conductivity measured using EIS at 100 kHz in Figure 4-7 shows a linear relationship independent of curing used. This shows that the pore solution conductivity is principally a function of the alkali concentration of the pore solution, even for ternary blends.

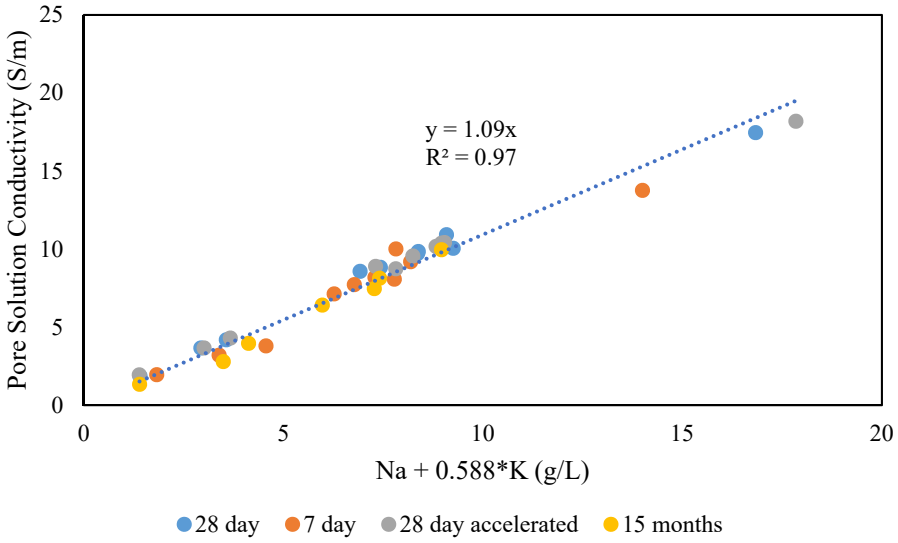

Figure 4-7: Relationship between extracted pore solution conductivity measured using EIS at 100 kHz and extracted pore solution equivalent alkali concentration

Figure 4-8 shows the effect of slag on the electrical resistivity of the extracted pore solution measured at 100 kHz. As the slag content increased, the resistivity of the pore solution increased for both w/cm used. However, the electrical resistivity also increased as the water content increased, likely from the dilution effect.

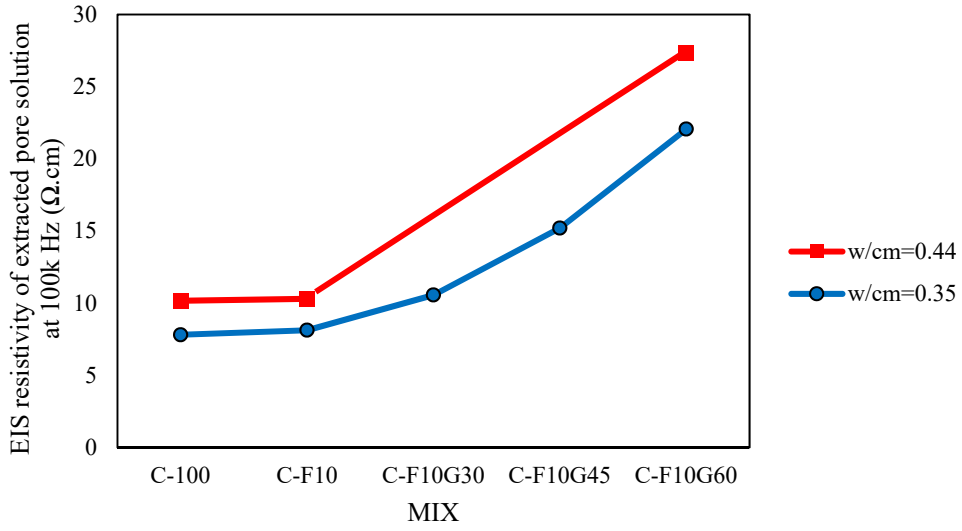

Figure 4-8: Effect of slag on the resistivity of the pore solution

Figure 4-9 shows the effect of silica fume on the electrical resistivity of the pore solution. As the replacement percentage of silica fume increased, the electrical resistivity increased. For partial portland cement replacement by silica fume, the electrical resistivity of the pore solution did not increase above a 6% replacement. Figure 4-10 shows the effect of metakaolin on the electrical resistivity of the pore solution. As the replacement percentage of metakaolin increased, the electrical resistivity increased. Figure 4-11 shows the effect of cement type on electrical resistivity of extracted pore solution of different mix types including OPC, binary, and ternary mixtures.

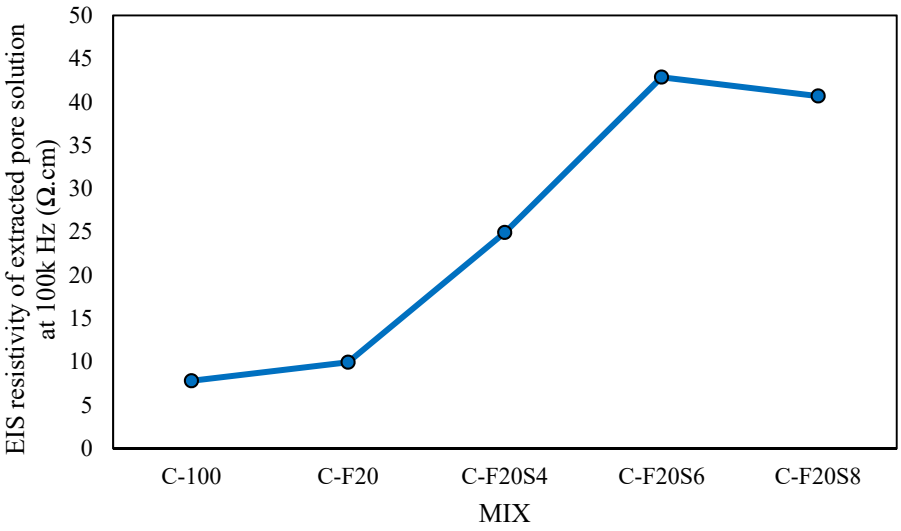

Figure 4-9: Effect of silica fume on the resistivity of pore solution

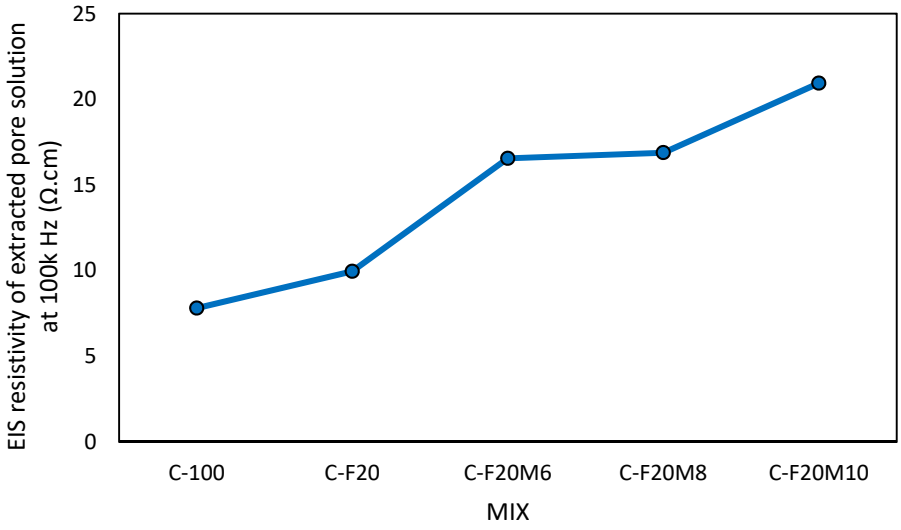

Figure 4-10: Effect of metakaolin on the resistivity of pore solution

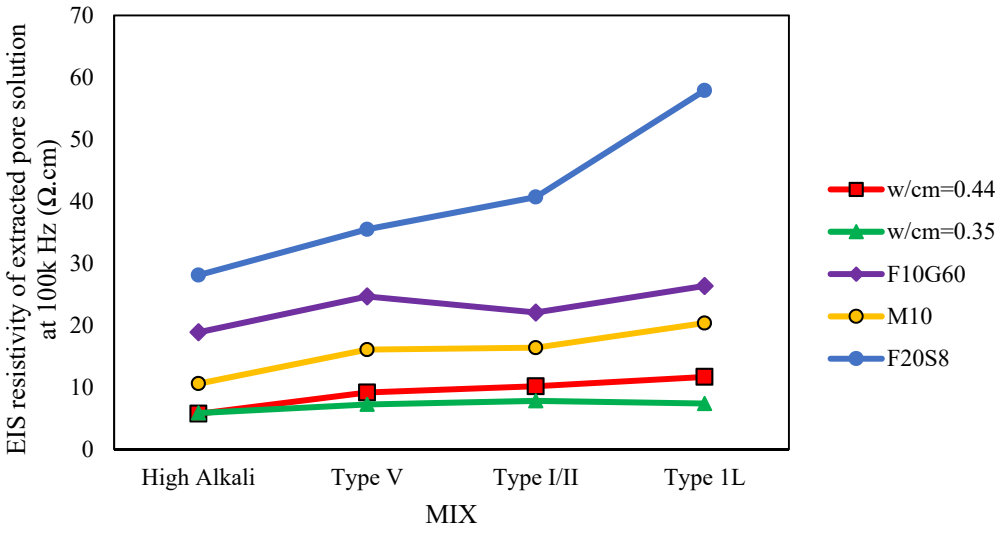

Figure 4-11: Effect of cement type on the resistivity of pore solution

The electrical resistivity of the pore solution in the SPS curing was measured using a conductivity meter at 28, 56, 91, 182, and 365 days as shown in Table 4-4. Sample pore solution resistivity values estimated using the NIST calculator and assuming sealed curing are shown in Table 4-4. A problem occurred while making the SPS for mixture 7, leading to a large difference between that measured in the SPS and the target composition estimated using the NIST calculator. Figure 4-12 shows the resistivity of SPS at 28 days compared to the estimated value by the NIST calculator. This shows that there is little change in the simulated pore solution resistivity during the 27 days the concrete cylinders were in the simulated pore solution, with the possible exception of two mixtures containing fly ash at a 0.35 w/cm. Figure 4-13 shows a comparison of the estimated pore solution resistivity by the NIST calculator and the measured extracted pore solution resistivity using EIS at 100 kHz. The NIST calculator with the assumptions used in this analysis did not provide a reliable estimate of the pore solution resistivity.

Table 4-4: Pore solution resistivity results in SPS curing and NIST calculator

Mix No.	Mix ID	Resistivity (Ω.cm)					
		Simulated pore solution					NIST calculator
		28 Days	56 Days	91 Days	182 Days	365 Days	
1	C-100	14.3	14.4	14.4	14.9	16.4	14.4
2	C-100h	18.9	18.9	18.8	19.3	20.3	20.5
3	C-F10	13.6	13.9	14.1	16.4	18.1	8.6
4	C-F20	13.8	14.1	14.1	17.5	20.0	6.3
5	C-F10h	12.9	12.9	13.0	13.1	14.2	12.2
6	C-F20h	9.0	9.2	9.8	10.4	11.1	8.9
7	C-G60	11.8	11.7	11.8	11.8	12.7	33.6
8	C-S8	13.9	14.1	12.0	12.0	13.0	13.3
9	C-M10	16.2	16.6	17.0	17.7	19.0	15.8
10	C-F10G30	10.3	10.3	10.4	10.5	11.2	10.2
11	C-F10G45	11.5	11.5	11.5	11.5	12.4	11.2
12	C-F10G60	11.3	11.4	11.5	11.7	12.5	12.5
13	C-F10G60h	18.1	18.5	12.4	12.5	13.5	17.8
14	C-F20S4	7.1	7.2	7.4	7.8	9.2	6.6
15	C-F20S6	7.2	7.2	7.4	7.8	8.9	6.7
16	C-F20S8	7.3	7.3	7.4	7.9	8.4	6.9
17	C-F20S8h	11.0	11.6	12.1	13.9	15.7	9.7
18	C-F20M6	8.4	8.6	9.0	9.9	10.8	6.4
19	C-F20M8	6.9	6.9	7.0	7.5	8.2	6.5
20	C-F20M10	7.0	7.0	7.1	7.7	7.9	6.5
21	C-F20M10h	9.7	10.8	11.0	11.7	12.3	9.2
22	C-G55S8	22.3	22.7	22.6	23.2	24.6	20.7
23	C-G55M10	36.9	37.2	36.8	37.6	39.4	38.0
24	CV-100	9.0	9.0	9.2	9.8	10.7	8.8
25	CV-100h	12.7	12.7	12.7	13.2	13.6	12.4
26	CV-F10G60	10.9	11.0	11.3	11.3	11.9	10.7
27	CV-F20S8	6.3	6.4	6.6	7.1	7.9	6.0
28	CV-M10	10.0	10.4	10.9	11.0	11.9	9.6
29	CL-100	12.7	12.6	12.6	12.6	13.5	12.9
30	CL-100h	18.7	18.6	18.7	20.5	22.8	18.4
31	CL-F10G60	12.4	12.3	12.4	12.7	13.4	12.2
32	CL-F20S8	7.2	7.5	7.3	7.6	8.3	6.7
33	CL-M10	14.5	15.1	14.6	15.0	16.2	14.2
34	CHA-100	5.6	5.4	5.5	4.8	4.9	4.9
35	CHA-100h	6.9	6.9	6.9	7.6	8.4	6.8
36	CHA-	8.3	8.3	8.3	8.6	9.0	8.1
37	CHA-F20S8	5.2	5.4	5.7	6.3	8.5	4.6
38	CHA-M10	5.6	5.7	5.7	5.9	6.6	5.3
39	C-100 (#89)	14.3	14.3	14.6	15.2	20.4	14.4
40	C-F20S8	7.6	8.2	8.7	9.7	11.0	6.9

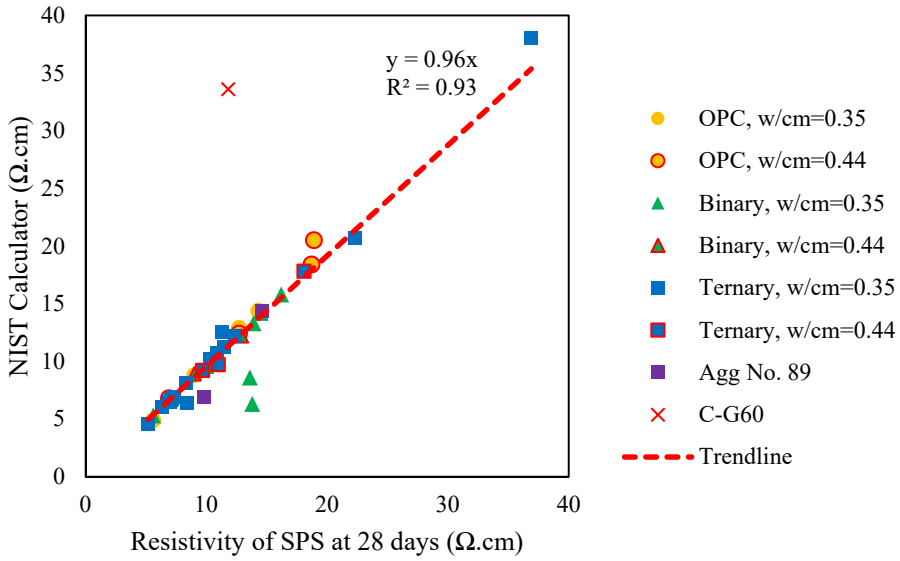

Figure 4-12: SPS resistivity at 28 days compared to NIST calculator

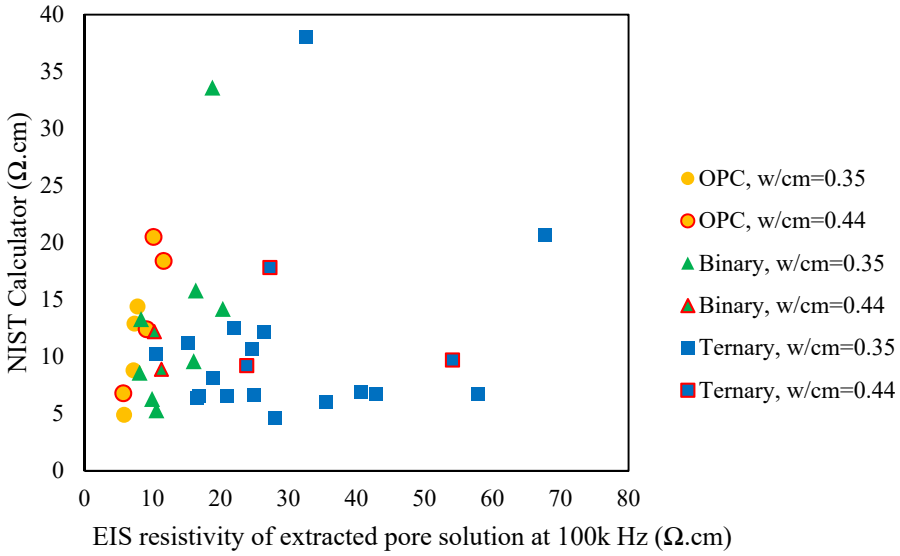

Figure 4-13: Comparison of estimated pore solution resistivity from NIST calculator and measured extracted pore solution resistivity

A closer look at the NIST calculator-predicted alkali concentrations for different mixture proportions can shed further light on its utility. Figure 4-14 shows the sodium equivalent alkali concentrations estimated by the NIST calculator for different mixtures made with the four different cements used in this study. The NIST calculator estimates that the high alkali cement at 0.44 w/cm

will have a pore solution concentration over 3.3 times that of the Type I/II cement mixture (Figure 4-14). However, for the measured resistivity of the pore solutions at 0.44 w/cm (Figure 4-11), the resistivity of the Type I/II cement was only 1.8 times that of the high alkali cement. Another example of how the NIST calculator with the assumptions used estimates the pore solution composition incorrectly is for fly ash and slag cement. Figure 4-15 shows the estimated sodium equivalent alkali concentration for ternary blend mixtures containing fly ash and slag. While the slag cement was shown to slightly lower the alkali concentration, fly ash was predicted to increase it substantially; however, fly ash showed a slight decrease in measured alkali concentration of the extracted pore solution.

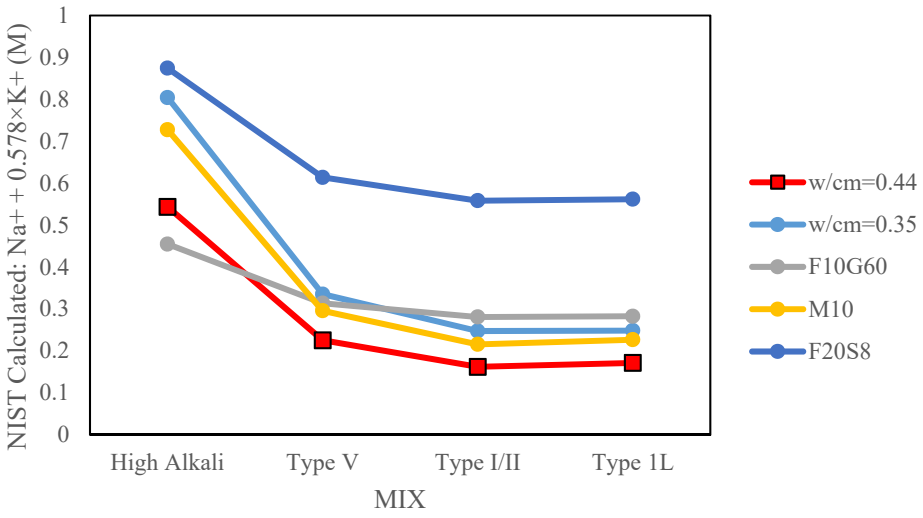

Figure 4-14: Alkali concentration estimated for pore solutions by NIST calculator for different portland cement types studied

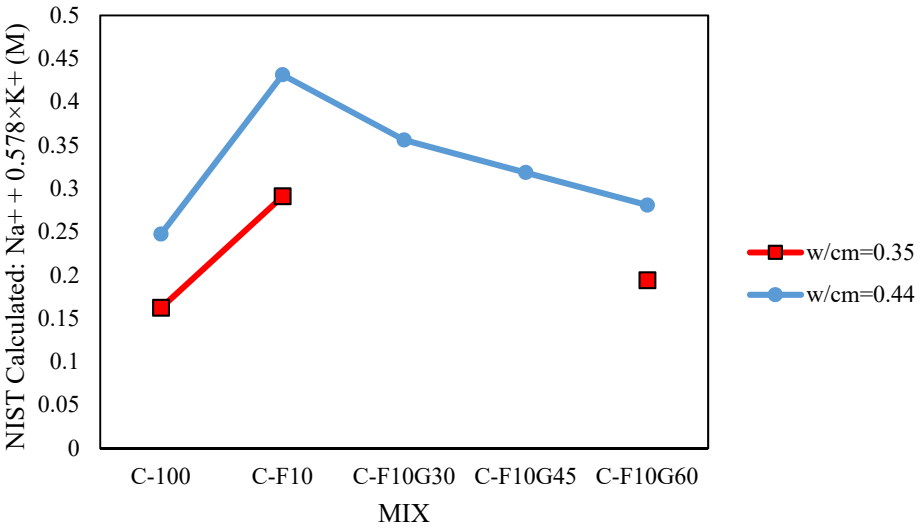

Figure 4-15: Predicted alkali concentrations for ternary mixtures containing fly ash and slag cement

The measured pore solution concentration was compared against an equation to predict the pore solution concentration developed by Thomas [4]. It was shown that the hydroxyl concentration of the pore solution was proportional to the composite cementitious material composition, as shown in Equation 4-4 [4]:

$$OH^- = 6.03\frac{Na_2O_e \times CaO}{(SiO_2)^2} \qquad \text{Equation 4-4}$$

where OH^- is the hydroxyl concentration of the pore solution, Na_2O_e is the sodium equivalent alkali concentration of the composite cementitious system, CaO is the calcium oxide content of the composite cementitious system, and SiO_2 is the silicon dioxide content of the composite cementitious system. This equation was developed for cement paste mixtures made with a w/cm of 0.50. It was assumed that the hydroxyl concentration was equal to the sum of the potassium and sodium concentrations for 10 cement pastes with measured sodium and potassium concentrations on a molar basis. Figure 4-16 shows the measured data from this study plotted with the data reported by Thomas [4]. Even though the mixtures tested in this study were at 0.35 and 0.44 w/cm, all but two were within 15% of the estimated value calculated by Equation 4-4.

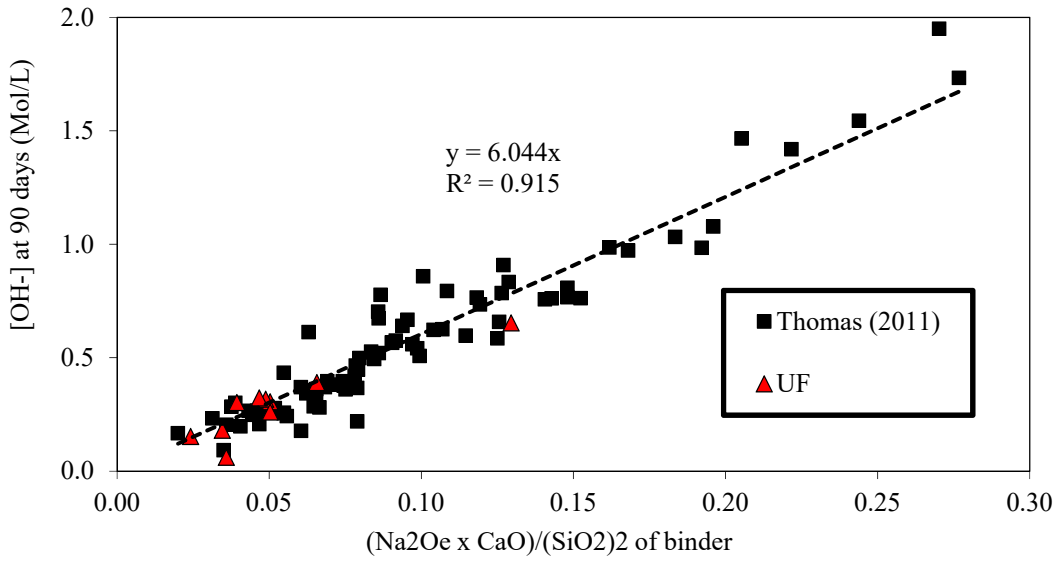

Figure 4-16: Comparison of fit of UF (Current study) to Equation 4-4 and the values reported in [4]

A comparison of the pore solution resistivity for the same cementitious materials at 0.35 and 0.44 w/cm showed a linear relationship between the two w/cm, as shown in Figure 4-17. The lower resistivity at a lower w/cm is expected because the cement degree of hydration at each w/cm is likely similar giving similar amounts of alkalis in less water. Using the 28% increase in pore solution resistivity with an increase in the w/cm from 0.35 to 0.44 and assuming a linear relationship between w/cm and pore solution resistivity, an adjustment to Equation 4-4 is proposed in Equation 4-5:

$$OH^- = \frac{3.015}{\frac{w}{cm}} \frac{Na_2O_e \times CaO}{(SiO_2)^2} \qquad \text{Equation 4-5}$$

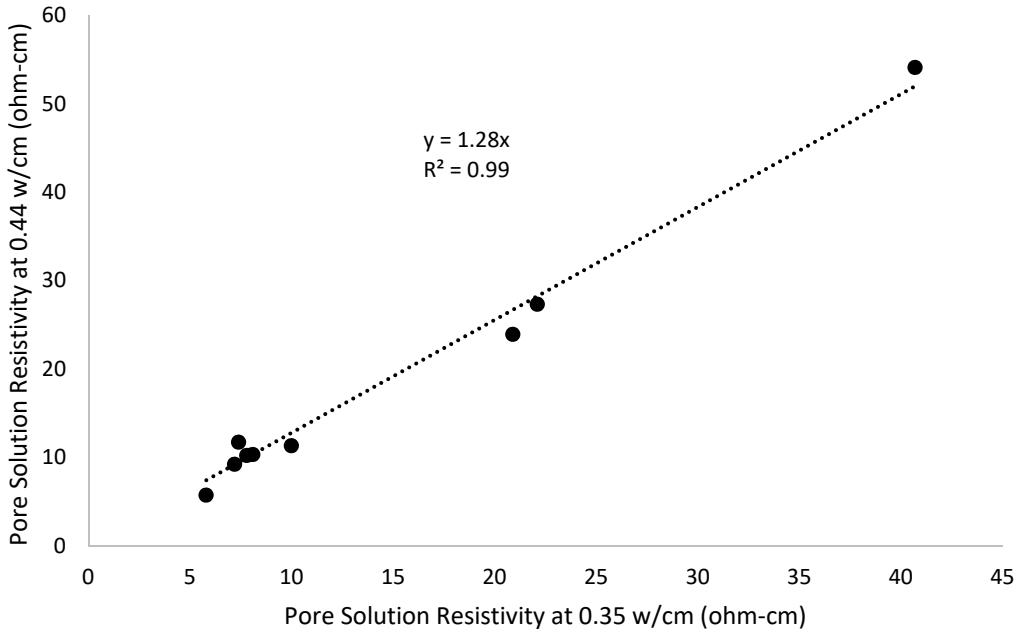

Figure 4-17: Comparison of pore solution resistivity for the same cementitious materials at 0.35 and 0.44 w/cm

The OH^- concentration was calculated using the pore solution conductivity, the relationship between pore solution resistivity and sodium equivalent alkalis shown in Figure 4-7, and the assumption that OH^- concentration balances with the alkali concentration for the 38 mixtures measured. The calculated OH^- concentration from the pore solution resistivity is shown versus the calculated OH^- concentration using Equation 4-5 in Figure 4-18. The average absolute error between the OH^- concentration calculated from the pore solution resistivity and that calculated using Equation 4-5 for the measurements performed at the University of Florida is 0.118 Mol/L, with a maximum difference of 0.434 Mol/L.

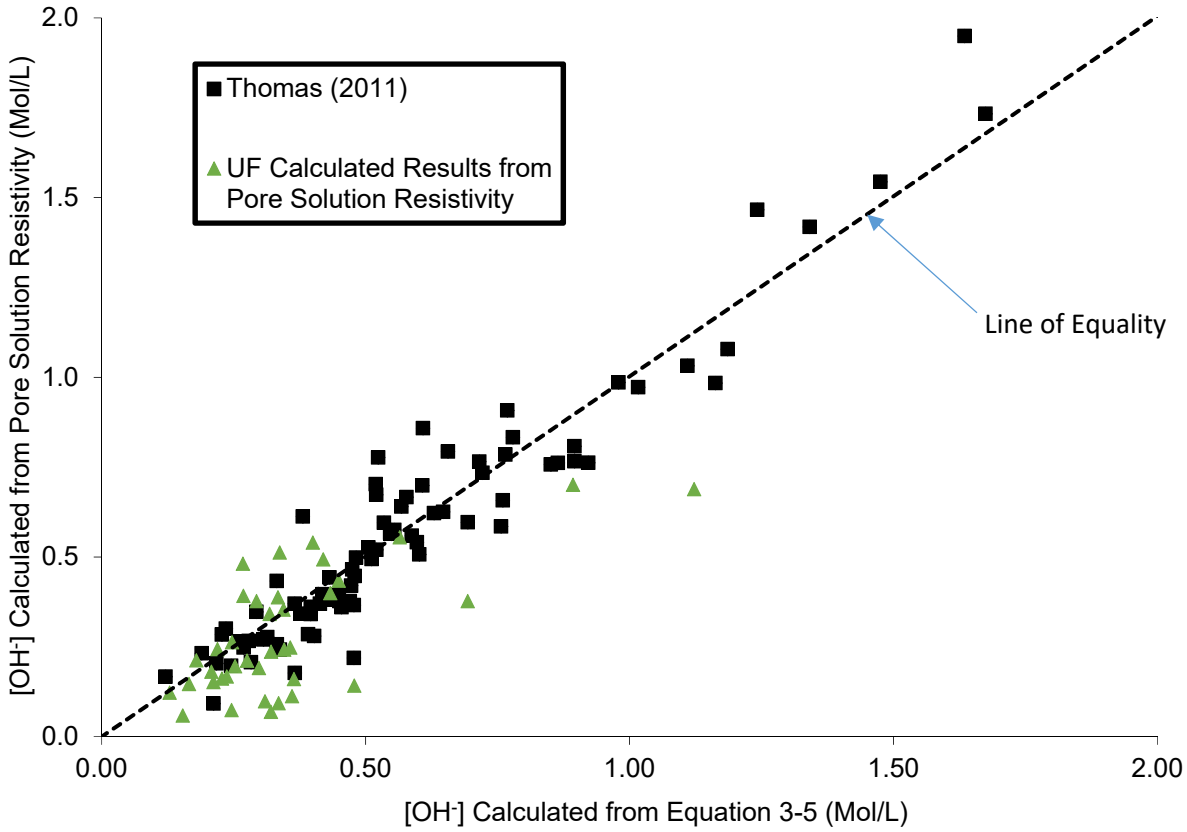

Figure 4-18: Comparison of OH- calculated from pore solution resistivity and from Equation 3-5

The relationship between pore solution conductivity and sodium equivalent alkalis shown in Figure 4-7, the assumption that OH^- concentration balances with the sodium equivalent alkali concentration, and Equation 4-5 can be combined to solve for the pore solution resistivity in Ω•cm as shown in Equation 4-6:

$$\rho = \frac{1.325\left(\frac{w}{cm}\right)(SiO_2)^2}{(Na_2O_e \times CaO)} \qquad \text{Equation 4-6}$$

4.4 Summary

Cement paste mixtures were made to measure the pore solution resistivity. After curing, pore solutions were expressed from the samples. The sample pore solution resistivities were measured using EIS at 40 Hz and 100 kHz. 100 kHz was used for comparing the pore solution resistivity

with the electrical resistivity estimated by the NIST calculator. It was seen from the pore solution extraction experiments that the NIST calculator did not correctly estimate the pore solution resistivity with the assumptions used. An equation has been proposed to estimate the pore solution resistivity based on the w/cm and cementitious material composition.

CHAPTER 5. ACCELERATED LABORATORY CONCRETE TRANSPORT TESTS

5.1 Introduction

In order to determine the suitability of concrete electrical test methods for measuring concrete transport properties, concrete electrical and transport property measurements were performed for comparison to surface resistivity measurements for concrete mixtures used in several different classes of concrete. Cementitious materials, water-cementitious materials ratio (w/cm), and supplementary cementitious material (SCM) replacement levels were selected to give a wide range of concrete transport and electrical properties measured to ensure that the results are applicable to the wide range materials and mixture proportions approved for use in extremely aggressive environments. Concrete mixture proportions used in this project are presented at Table 2-7.

Concrete samples were made according to ASTM C192/C192M [35] and were cured in a fog room according to ASTM C511 [36] until the time required for testing. Water absorption was measured according to ASTM C1585 [37], volume of permeable voids was measured using ASTM C642 [38]. Water permeability testing was performed to determine the water penetration rate using a method developed at the University of Florida [39]. ASTM C1202 [40] was used to measure the concrete charge passed in the rapid chloride permeability test (RCPT) and NT Build 492 [41] rapid chloride migration test (RCMT) was used to measure the concrete non-steady state diffusion coefficient. Samples were tested for bulk resistivity according to AASHTO TP 119 [42] and surface resistivity according to AASHTO T358-15 [43] at each age required and returned to the fog room for further testing at additional ages. Additional samples were made for surface resistivity and bulk resistivity and were cured in simulated pore solutions (SPS) in sealed buckets stored in the fog room for temperature control. Alkali concentrations in the pore solution contribute significantly to the concrete pore solution resistivity and any electrical measurements taken to determine the effects of leaching on resistivity measurements. Samples were cured in the simulated pore solution to reduce the concentration difference between the concrete and curing solution and to limit alkali leaching.

The simulated pore solution was made for each mixture based on the mixture composition. The solution was made of NaOH and KOH and water. The concentration of NaOH and KOH was

determined using the NIST pore solution calculator [31]. The solution was also saturated with $Ca(OH)_2$ [44].

The formation factor was determined for the SPS-cured specimens at each age using the bulk resistivity measurements and the conductivity measurements of the solution measured using a conductivity meter. For the moist-cured specimens, the formation factor was determined using the NIST calculator and the bulk resistivity measurement of the moist-cured specimens [31].

Mercury intrusion porosimetry (MIP) was also performed on select concrete mixtures made with smaller #89 aggregates. All concrete transport properties were measured at concrete ages of 28, 56 and 365 days. Because surface and bulk electrical resistivity measurements are simple and quick to perform and are non-destructive, additional measurements were made at 91 and 180 days. MIP samples were only measured at 28 and 56 days. This chapter summarizes the results of the concrete transport testing performed and describes any correlations found between values measured.

5.2 Results

Concrete electrical and transport properties were measured to determine the ability of concrete surface resistivity to predict concrete transport. The initial and secondary absorption rates ($mm/s^{0.5}$) along with absorptions (mm) at 28, 56 and 365 days after concrete mixing are presented in Table 5-1. Table 5-2 shows the concrete volume of permeable voids (%) and absorption after immersion (%) for mixtures at 28, 56 and 365 days of curing in the moist room. Table 5-3 shows the water permeability results of the concrete mixtures at 28, 56 and 365 days. The charges passed through specimens with age, when tested according to ASTM C1202 (Rapid Chloride Penetration Test, RCPT), are presented at Table 5-4. Accordingly, the non-steady state migration coefficients were determined. Table 5-5 shows the non-steady state migration coefficients determined when tested according to NT Build 492 (Rapid Chloride Migration Test, RCMT) at ages of 28, 56 and 365 days.

Table 5-1: Rate of water absorption at 28, 56 and 365 days

Mix No	Mix ID	28 Days			56 Days			365 Days		
		Int.	Sec.	Abs.	Int.	Sec.	Abs.	Int.	Sec.	Abs.
1	C-100	0.00167	0.00101	0.93	0.00197	0.00090	0.97	0.00216	0.00079	1.13
2	C-100h	0.00561	0.00169	2.93	0.00192	0.00122	1.17	0.00208	0.00090	1.13
3	C-F10	0.00187	0.00080	0.98	0.00167	0.00107	1.03	0.00153	0.00112	1.03
4	C-F20	0.00124	0.00071	0.80	0.00122	0.00060	0.70	0.00121	0.00041	0.51
5	C-F10h	0.00404	0.00181	2.09	0.00248	0.00159	1.23	0.00253	0.00090	1.22
6	C-F20h	0.00245	0.00129	1.34	0.00206	0.00076	0.92	0.00157	0.00066	0.84
7	C-G60	0.00122	0.00044	0.58	0.00113	0.00029	0.44	0.00093	0.00047	0.56
8	C-S8	0.00104	0.00040	0.52	0.00071	0.00049	0.49	0.00080	0.00036	0.50
9	C-M10	0.00102	0.00060	0.59	0.00177	0.00071	0.82	0.00100	0.00040	0.50
10	C-F10G30	0.00142	0.00051	0.59	0.00111	0.00030	0.47	0.00088	0.00043	0.50
11	C-F10G45	0.00095	0.00042	0.43	0.00091	0.00022	0.38	0.00106	0.00044	0.53
12	C-F10G60	0.00105	0.00025	0.44	0.00101	0.00051	0.56	0.00116	0.00030	0.48
13	C-F10G60h	0.00179	0.00043	0.70	0.00134	0.00038	0.60	0.00149	0.00050	0.68
14	C-F20S4	0.00145	0.00053	0.71	0.00203	0.00049	0.88	0.00166	0.00045	0.61
15	C-F20S6	0.00140	0.00056	0.73	0.00136	0.00038	0.64	0.00149	0.00032	0.50
16	C-F20S8	0.00238	0.00043	0.87	0.00088	0.00023	0.48	0.00147	0.00048	0.70
17	C-F20S8h	0.00200	0.00069	0.95	0.00103	0.00038	0.61	0.00183	0.00045	0.69
18	C-F20M6	0.00296	0.00052	1.04	0.00136	0.00048	0.69	0.00168	0.00062	0.86
19	C-F20M8	0.00241	0.00064	1.02	0.00125	0.00046	0.68	0.00154	0.00046	0.64
20	C-F20M10	0.00101	0.00026	0.48	0.00256	0.00062	0.96	0.00170	0.00043	0.58
21	C-F20M10h	0.00200	0.00059	0.93	0.00155	0.00043	0.67	0.00239	0.00040	0.76
22	C-G55S8	0.00121	0.00042	0.56	0.00154	0.00029	0.58	0.00103	0.00032	0.48
23	C-G55M10	0.00111	0.00047	0.67	0.00114	0.00026	0.48	0.00120	0.00038	0.52
24	CV-100	0.00129	0.00070	0.77	0.00150	0.00076	0.76	0.00186	0.00098	1.08
25	CV-100h	0.00390	0.00237	2.29	0.00223	0.00158	1.47	0.00205	0.00067	0.89
26	CV-F10G60	0.00093	0.00024	0.41	0.00117	0.00029	0.50	0.00111	0.00032	0.48
27	CV-F20S8	0.00106	0.00045	0.36	0.00147	0.00062	0.40	0.00119	0.00037	0.51
28	CV-M10	0.00146	0.00054	0.59	0.00173	0.00064	0.82	0.00175	0.00052	0.73
29	CL-100	0.00479	0.00222	2.40	0.00101	.000930	0.90	0.00159	0.00081	0.85
30	CL-100h	0.00336	0.00174	1.92	0.00165	0.00098	0.93	0.00169	0.00138	1.21
31	CL-F10G60	0.00105	0.00020	0.39	0.00180	0.00057	0.82	0.00113	0.00029	0.43
32	CL-F20S8	0.00113	0.00061	0.69	0.00126	0.00043	0.64	0.00135	0.00035	0.55
33	CL-M10	0.00159	0.00049	0.75	0.00245	0.00064	0.99	0.00119	0.00047	0.62
34	CHA-100	0.00407	0.00150	1.90	0.00198	0.00101	1.00	0.00170	0.00052	0.77
35	CHA-100h	0.00368	0.00165	1.95	0.00157	0.00099	0.99	0.00190	0.00076	1.03
36	CHA-F10G60	0.00156	0.00040	0.67	0.00177	0.00052	0.79	0.00148	0.00024	0.48
37	CHA-F20S8	0.00152	0.00041	0.58	0.00120	0.00033	0.56	0.00137	0.00035	0.56
38	CHA-M10	0.00142	0.00051	0.68	0.00142	0.00048	0.69	0.00142	0.00070	0.79
39	C-100SS	0.00162	0.00065	0.76	0.00150	0.00079	0.88	0.00147	0.00072	0.73
40	C-F20S8SS	0.00086	0.00030	0.37	0.00068	0.00030	0.41	0.00080	0.00025	0.31

Table 5-2: Volume of permeable voids and absorption

Mix No	Mix ID	Voids (%)			Absorption (%)		
		28 Days	56 Days	365 Days	28 Days	56 Days	365 Days
1	C-100	13.89	13.78	13.37	6.15	6.04	5.34
2	C-100h	17.13	16.02	16.15	7.79	7.11	7.01
3	C-F10	15.03	15.01	14.24	6.12	6.25	6.27
4	C-F20	15.01	14.45	14.31	6.47	6.31	6.36
5	C-F10h	19.21	18.21	17.72	8.50	8.02	7.78
6	C-F20h	18.51	18.97	17.80	8.16	8.60	7.90
7	C-G60	14.74	15.77	15.39	6.52	6.80	6.56
8	C-S8	13.04	13.35	13.11	5.91	5.92	5.83
9	C-M10	13.74	14.35	13.59	6.09	6.38	5.98
10	C-F10G30	14.73	14.45	14.46	6.48	6.45	6.33
11	C-F10G45	16.04	15.05	13.07	7.09	6.55	6.42
12	C-F10G60	16.85	16.38	15.86	7.15	6.94	6.58
13	C-F10G60h	19.10	20.62	19.80	8.32	8.85	8.58
14	C-F20S4	14.23	13.73	13.89	6.10	6.15	6.22
15	C-F20S6	14.59	14.20	14.16	6.02	6.26	6.31
16	C-F20S8	14.37	14.91	15.43	6.63	6.81	7.19
17	C-F20S8h	18.16	17.61	19.52	8.22	8.03	8.89
18	C-F20M6	14.69	14.92	14.96	6.43	6.74	6.60
19	C-F20M8	13.76	14.27	16.50	5.91	6.12	7.09
20	C-F20M10	14.13	13.92	15.81	6.22	5.92	6.89
21	C-F20M10h	19.23	19.04	19.10	8.16	8.29	8.45
22	C-G55S8	14.89	13.00	16.25	6.64	5.86	7.09
23	C-G55M10	15.31	13.57	16.94	6.52	5.88	7.32
24	CV-100	13.74	13.99	13.36	5.87	5.91	5.44
25	CV-100h	16.53	16.70	16.24	7.58	7.55	7.21
26	CV-F10G60	16.21	16.00	15.49	6.94	6.65	6.45
27	CV-F20S8	15.50	15.01	14.87	7.02	6.82	6.89
28	CV-M10	14.99	14.75	13.92	6.62	6.47	6.89
29	CL-100	13.81	12.84	12.98	5.82	5.52	5.72
30	CL-100h	16.17	16.55	15.78	7.11	7.36	7.07
31	CL-F10G60	17.09	17.13	16.46	7.12	7.11	6.98
32	CL-F20S8	15.34	15.36	16.23	6.95	6.94	7.24
33	CL-M10	13.82	13.44	12.96	6.03	5.87	5.66
34	CHA-100	16.07	14.79	14.52	6.46	6.18	5.86
35	CHA-100h	17.91	17.59	18.16	7.65	7.73	7.85
36	CHA-F10G60	17.28	16.81	16.42	7.19	7.00	7.08
37	CHA-F20S8	16.26	16.86	17.64	6.90	7.19	7.21
38	CHA-M10	15.80	15.64	16.47	6.40	6.41	6.71
39	C-100SS	11.14	10.98	11.07	4.92	4.77	4.91
40	C-F20S8SS	11.41	11.36	11.41	5.14	5.15	5.10

Table 5-3: Water permeability at 28, 56 and 365 days

Mix No	Mix ID	Water permeability (m/s) × 10^{-14}		
		28 Days	56 Days	365 Days
1	C-100	33	22	17
2	C-100h	35	31	26
3	C-F10	16	10	6
4	C-F20	15	7	3
5	C-F10h	30	30	11
6	C-F20h	29	29	9
7	C-G60	3.7	4	4
8	C-S8	5.6	7	6
9	C-M10	9.6	12	10
10	C-F10G30	2.2	2	2
11	C-F10G45	3.4	3	3
12	C-F10G60	3.4	3	2
13	C-F10G60h	7.0	6	5
14	C-F20S4	6.0	8	4
15	C-F20S6	7.9	4	4
16	C-F20S8	7.9	5	4
17	C-F20S8h	9.2	9	5
18	C-F20M6	11	6	6
19	C-F20M8	5.5	6	5
20	C-F20M10	6.6	5	4
21	C-F20M10h	6.7	6	5
22	C-G55S8	4.7	4	3
23	C-G55M10	3.9	4	4
24	CV-100	17	16	10
25	CV-100h	36	34	23
26	CV-F10G60	2.8	3	3
27	CV-F20S8	12	12	4
28	CV-M10	7.0	7	6
29	CL-100	17	15	14
30	CL-100h	20	23	22
31	CL-F10G60	2.7	6	4
32	CL-F20S8	2.7	2	2
33	CL-M10	5.7	6	6
34	CHA-100	16	20	15
35	CHA-100h	21	20	21
36	CHA-F10G60	4.6	4	4
37	CHA-F20S8	5.9	3	4
38	CHA-M10	5.0	5	5
39	C-100SS	12	8	7
40	C-F20S8SS	5.3	10	5

Table 5-4: Amount of charge passed according to ASTM C1202 at 28, 56 and 365 days

Mix No	Mix ID	RCPT (Coulombs)		
		28 Days	56 Days	365 Days
1	C-100	2630	2567	2554
2	C-100h	4666	5296	4475
3	C-F10	3730	2866	1218
4	C-F20	3407	1981	738
5	C-F10h	5966	3493	1875
6	C-F20h	5427	2664	1063
7	C-G60	807	715	412
8	C-S8	1061	691	591
9	C-M10	932	736	715
10	C-F10G30	1520	1037	464
11	C-F10G45	1042	780	394
12	C-F10G60	809	540	339
13	C-F10G60h	699	533	371
14	C-F20S4	1458	943	399
15	C-F20S6	1101	684	286
16	C-F20S8	1073	655	329
17	C-F20S8h	1445	1096	415
18	C-F20M6	1360	882	328
19	C-F20M8	1158	849	275
20	C-F20M10	940	656	254
21	C-F20M10h	1279	955	396
22	C-G55S8	585	409	134
23	C-G55M10	529	425	164
24	CV-100	4336	3612	2914
25	CV-100h	6858	5852	5236
26	CV-F10G60	750	546	330
27	CV-F20S8	876	546	284
28	CV-M10	1075	729	581
29	CL-100	2960	3058	2633
30	CL-100h	5250	5410	4734
31	CL-F10G60	656	388	321
32	CL-F20S8	1194	629	278
33	CL-M10	644	649	552
34	CHA-100	3384	3431	2541
35	CHA-100h	5553	5383	4397
36	CHA-F10G60	707	504	328
37	CHA-F20S8	805	505	303
38	CHA-M10	656	661	527
39	C-100SS	2447	2084	1580
40	C-F20S8SS	799	459	257

Table 5-5: Non-steady-state migration coefficient measured according to NT Build 492

Mix No	Mix ID	Diffusion Coefficient (m^2/s) × 10^{-12}		
		28 Days	56 Days	365 Days
1	C-100	12.7	8.8	9.9
2	C-100h	17.8	17.5	13.3
3	C-F10	13.6	10.3	5.3
4	C-F20	16.4	9.0	4.4
5	C-F10h	22.0	16.0	10.6
6	C-F20h	24.5	15.3	6.0
7	C-G60	2.8	2.9	1.5
8	C-S8	5.2	3.1	2.9
9	C-M10	4.1	3.4	2.9
10	C-F10G30	5.5	4.0	3.0
11	C-F10G45	4.3	2.6	2.2
12	C-F10G60	3.0	2.5	1.5
13	C-F10G60h	3.1	2.1	1.6
14	C-F20S4	7.2	4.2	2.5
15	C-F20S6	6.1	2.5	2.2
16	C-F20S8	6.2	3.5	2.1
17	C-F20S8h	11.1	4.8	1.9
18	C-F20M6	8.8	5.3	2.4
19	C-F20M8	5.2	4.5	2.6
20	C-F20M10	3.3	3.3	1.8
21	C-F20M10h	6.8	4.4	1.7
22	C-G55S8	3.1	1.5	0.9
23	C-G55M10	2.8	1.5	1.0
24	CV-100	17.4	10.9	12.2
25	CV-100h	17.4	17.0	14.3
26	CV-F10G60	2.8	2.7	1.9
27	CV-F20S8	6.4	3.3	1.8
28	CV-M10	5.7	3.6	2.8
29	CL-100	12.7	10.5	10.4
30	CL-100h	20.6	17.7	17.3
31	CL-F10G60	3.5	2.4	1.7
32	CL-F20S8	5.4	4.0	2.1
33	CL-M10	3.0	3.3	2.5
34	CHA-100	11.4	11.4	11.1
35	CHA-100h	21.4	17.4	17.1
36	CHA-F10G60	3.7	2.0	1.8
37	CHA-F20S8	3.4	2.8	1.1
38	CHA-M10	2.7	4.1	2.1
39	C-100SS	9.6	6.9	5.2
40	C-F20S8SS	4.2	2.3	1.4

Specimens for the bulk resistivity were fabricated and tested. Two curing environments were used. Bulk resistivity measurements were made 28, 56, 91, 182 and 365 days after concrete mixing. Table 5-6 and Table 5-7 show the bulk resistivity and surface resistivity results, respectively, for the two curing methods versus testing age. MIP was performed on mixtures 39 and 40. After the required curing age, samples were cut using water jetting to 1-in. × 1-in. cylinders. After saw cutting, samples were oven-dried, and the pore system was measured using MIP. The total volume of cumulative porosity is presented at Table 5-8.

Table 5-6: Bulk resistivity (kΩ-cm) at 28, 56, 91, 182 and 365 days for SPS and moist curing

Mix No	Mix ID	Moist Room curing					SPS curing				
		28 Days	56 Days	91 Days	182 Days	365 Days	28 Days	56 Days	91 Days	182 Days	365 Days
1	C-100	8.5	12.1	11.9	15.0	14.6	5.1	5.6	6.8	7.1	5.3
2	C-100h	4.3	5.7	7.8	8.8	9.6	2.9	3.5	3.5	3.9	3.1
3	C-F10	6.4	9.7	12.5	17.8	23.7	4.0	5.6	7.4	9.8	12.1
4	C-F20	6.7	11.8	15.4	24.7	34.9	4.3	7.2	10.2	14.1	19.0
5	C-F10h	5.3	6.2	8.9	12.4	13.1	2.9	3.6	4.5	5.5	6.4
6	C-F20h	5.0	7.9	14.0	20.4	21.8	3.0	4.7	7.4	9.1	11.6
7	C-G60	22.7	32.8	39.4	42.4	52.3	11.4	17.2	18.0	15.8	19.0
8	C-S8	18.9	30.5	34.6	35.4	38.4	11.4	17.2	18.9	17.2	17.7
9	C-M10	21.8	28.0	31.9	34.1	43.4	13.8	15.7	18.7	17.4	19.4
10	C-F10G30	13.4	19.2	23.0	29.7	36.4	7.3	11.2	13.6	14.1	17.2
11	C-F10G45	20.5	25.8	30.2	37.6	48.6	9.3	13.0	17.1	15.8	22.2
12	C-F10G60	23.3	32.3	37.0	45.6	61.0	15.4	15.5	17.3	19.5	20.5
13	C-F10G60h	23.8	32.2	41.9	46.8	58.0	11.1	18.4	18.5	16.9	18.6
14	C-F20S4	16.0	25.0	32.9	48.7	66.9	9.0	10.4	14.5	9.7	17.9
15	C-F20S6	23.0	33.4	42.7	57.0	82.2	11.0	13.4	17.0	9.2	18.0
16	C-F20S8	19.0	33.3	43.2	55.9	80.6	9.0	11.8	15.1	18.1	16.9
17	C-F20S8h	14.1	22.9	29.4	42.6	55.9	7.4	11.2	13.0	13.3	18.5
18	C-F20M6	15.2	24.3	30.1	43.8	75.2	7.8	10.2	13.9	16.1	19.8
19	C-F20M8	19.2	25.5	31.4	40.3	83.1	9.5	9.1	11.7	24.2	21.8
20	C-F20M10	21.6	31.5	33.5	41.1	84.6	10.6	9.8	10.9	20.3	18.3
21	C-F20M10h	17.1	23.4	32.2	43.8	70.0	8.1	11.5	12.6	17.1	21.2
22	C-G55S8	28.3	50.8	69.7	110.0	149.5	22.9	30.4	33.4	38.5	48.8
23	C-G55M10	32.4	52.0	64.9	85.0	118.0	25.7	32.1	34.1	35.1	47.6
24	CV-100	6.1	9.2	7.4	10.0	9.1	3.1	3.3	3.7	4.1	2.2
25	CV-100h	4.1	5.5	6.1	7.8	8.5	2.4	3.1	2.8	3.1	2.3
26	CV-F10G60	21.8	34.9	36.8	45.8	58.2	14.1	16.3	16.3	17.5	19.8
27	CV-F20S8	23.5	32.7	47.6	59.0	71.5	11.5	13.4	14.2	14.7	19.0
28	CV-M10	22.1	24.0	31.6	37.6	40.5	9.4	10.4	12.0	12.2	13.9
29	CL-100	6.9	9.2	10.9	11.3	12.1	3.6	4.5	4.5	4.8	5.0
30	CL-100h	4.0	6.0	7.4	8.4	8.7	2.2	3.0	3.3	3.1	2.8
31	CL-F10G60	34.7	49.7	51.4	64.1	79.9	14.5	17.9	18.5	19.4	23.6
32	CL-F20S8	19.1	31.9	40.6	48.5	71.5	10.8	16.6	15.0	10.8	24.9
33	CL-M10	25.1	28.7	32.3	31.8	48.1	17.1	15.0	15.3	16.3	16.2
34	CHA-100	5.4	7.7	10.4	11.0	10.6	2.4	3.6	3.2	4.0	4.2
35	CHA-100h	3.4	5.0	6.6	8.9	7.3	1.9	2.8	2.9	2.8	2.4
36	CHA-F10G60	23.1	32.6	38.0	46.3	60.5	10.7	15.0	14.6	15.8	17.2
37	CHA-F20S8	24.1	36.5	43.1	49.8	73.9	9.4	12.1	11.5	12.2	21.6
38	CHA-M10	24.3	26.5	30.7	32.1	45.6	11.8	9.6	8.9	9.0	9.5
39	C-100SS	7.5	11.3	12.9	8.6	19.5	4.3	5.0	5.2	6.1	6.7
40	C-F20S8SS	23.3	42.5	53.6	55.9	89.7	12.4	14.3	15.0	27.4	22.6

Table 5-7: Surface resistivity (kΩ-cm) at 28, 56, 91, 182 and 365 days for SPS and moist curing

Mix No	Mix ID	Moist Room curing					SPS curing				
		28 Days	56 Days	91 Days	182 Days	365 Days	28 Days	56 Days	91 Days	182 Days	365 Days
1	C-100	12.9	15.8	17.8	19.5	18.5	9.0	9.6	10.6	10.5	10.4
2	C-100h	6.8	7.4	8.3	8.2	8.3	5.6	5.8	6.1	6.2	5.8
3	C-F10	9.5	13.2	16.1	23.7	28.1	7.8	9.3	11.1	14.1	15.6
4	C-F20	10.3	16.7	23.1	35.1	43.7	8.2	12.1	14.2	18.3	20.9
5	C-F10h	6.9	8.4	10.7	14.3	16.2	4.6	5.6	6.7	8.3	9.1
6	C-F20h	6.6	10.0	15.1	22.6	28.2	4.7	6.6	9.5	11.3	13.4
7	C-G60	40.6	51.0	60.0	62.9	67.7	16.9	16.3	16.3	16.6	16.3
8	C-S8	32.6	48.4	54.1	50.2	51.1	15.3	19.5	17.7	16.2	18.3
9	C-M10	38.3	46.6	49.4	49.6	55.2	20.0	20.0	20.4	20.1	21.9
10	C-F10G30	22.2	29.5	35.4	43.6	55.4	10.0	11.8	11.3	12.1	14.3
11	C-F10G45	30.7	40.1	48.5	56.9	69.3	13.0	13.6	13.7	14.6	16.0
12	C-F10G60	42.2	54.4	59.2	66.2	87.3	16.2	16.8	17.5	15.4	15.9
13	C-F10G60h	37.5	48.6	57.2	64.5	73.1	15.2	16.1	17.3	17.7	17.2
14	C-F20S4	25.0	39.3	49.7	71.0	99.9	7.8	10.2	11.2	10.4	15.9
15	C-F20S6	36.5	54.7	68.7	91.3	122.9	9.8	11.2	12.1	10.1	12.4
16	C-F20S8	33.3	52.7	69.6	86.9	120.7	9.5	10.7	9.8	11.8	12.0
17	C-F20S8h	22.5	32.8	43.1	55.3	74.6	10.1	13.0	14.4	15.0	19.0
18	C-F20M6	27.8	36.9	47.4	69.2	108.4	9.6	11.5	12.6	15.2	15.3
19	C-F20M8	32.3	40.3	50.1	75.4	126.1	8.2	9.4	9.8	9.2	11.3
20	C-F20M10	36.6	44.6	51.0	72.0	116.0	8.6	9.7	9.7	9.7	11.1
21	C-F20M10h	27.5	33.4	42.3	59.0	94.1	9.1	13.2	13.9	15.2	17.6
22	C-G55S8	55.3	90.9	121.9	188.7	245.7	27.1	30.0	33.6	34.5	34.4
23	C-G55M10	59.6	89.0	106.5	135.5	186.4	34.3	38.0	40.9	40.3	45.1
24	CV-100	8.0	9.2	10.0	10.8	10.6	5.3	5.6	6.0	6.2	5.9
25	CV-100h	6.6	6.9	7.7	7.6	7.5	4.8	5.0	5.0	5.0	4.7
26	CV-F10G60	40.6	52.3	56.8	66.1	89.4	15.4	15.5	17.0	15.2	16.8
27	CV-F20S8	41.6	61.4	74.8	86.2	109.8	10.8	8.8	9.6	11.1	11.6
28	CV-M10	38.3	43.0	48.2	48.9	56.6	12.0	12.1	13.0	13.0	14.8
29	CL-100	10.6	11.7	12.0	13.2	13.5	8.0	7.4	7.4	7.4	7.2
30	CL-100h	6.7	7.0	7.5	7.8	7.9	5.3	5.4	5.7	5.8	5.3
31	CL-F10G60	61.1	81.3	84.3	102.1	132.7	16.0	16.2	17.6	16.0	18.7
32	CL-F20S8	29.7	47.8	61.0	73.2	102.2	9.5	11.1	12.9	11.2	11.6
33	CL-M10	45.0	48.2	51.0	47.8	55.7	18.9	17.2	17.7	19.1	18.0
34	CHA-100	8.6	10.1	10.7	11.8	11.9	5.7	5.3	5.0	5.0	4.7
35	CHA-100h	6.0	6.5	7.2	7.5	7.3	4.5	4.7	4.6	4.7	4.5
36	CHA-F10G60	38.4	49.3	53.8	66.7	85.8	11.7	11.8	12.8	12.1	14.4
37	CHA-F20S8	41.7	57.7	68.1	77.9	109.6	7.7	7.3	9.9	8.2	11.4
38	CHA-M10	45.3	45.8	48.3	47.3	56.6	7.9	8.0	7.7	7.9	7.9
39	C-100SS	10.9	13.1	13.7	15.0	17.8	7.3	7.9	8.5	8.8	10.6
40	C-F20S8SS	40.7	65.9	80.6	96.4	130.1	10.5	11.2	11.7	11.9	16.1

Table 5-8: MIP results

Mix No	Mix 39		Mix 40	
	28 Days	56 Days	28 Days	56 Days
Total Volume (cc)	1.08	1.14	1.20	1.09
Cumulative Porosity (%)	0.11	0.11	0.12	0.11

5.3 Correlations Between Test Methods

Figure 5-1 shows the bulk resistivity vs. surface resistivity at 28, 56, 91, 182 and 365 days. A linear relationship between the two tests was found because both tests are based on the same general mechanism of electrical resistivity with differences only in testing geometry and leaching. It is seen that the surface resistivity readings on average were 35% higher compared to the bulk resistivity. Figure 5-2 shows the bulk resistivity vs. surface resistivity using SPS curing at 28, 56, 91, 182, and 365 days. A linear relationship is observed between the two tests. It is seen that the results in the SPS curing were very close in both tests, even though there is slightly more variability because there were lower amounts of alkali leaching with the SPS curing. Equation 5-1 shows the relationship between bulk resistivity and surface resistivity found for moist room curing (R^2=0.98) for all ages, while Equation 5-2 shows the relationship for SPS curing (R^2=0.79):

$$BR = 0.619 \times SR + 2.116 \qquad \text{Equation 5-1}$$

$$BR = 1.040 \times SR - 0.741 \qquad \text{Equation 5-2}$$

Where *BR* is the bulk resistivity (kΩ-cm) and *SR* is the surface resistivity (kΩ-cm). Much of the difference between the BR and SR in the fog room samples can be attributed to the difference in geometry between the methods that requires the values to be corrected. The geometry of the specimen greatly influences the results of the electrical test and a geometry factor can be used to correct for this factor. For a 4-in. × 8-in. concrete cylinder, the bulk resistivity theoretically should be 0.54 times that of the surface resistivity, which compares favorably to the 0.535 geometry factor calculated using only the 28-day data [45,46]. The difference between the 0.54 theoretical value and the 0.62 value from all ages is likely from alkali leaching in the fog room. The lower correlation in the SPS-cured specimens could be due to differences in the compositions of the SPS

solutions. If the composition of the SPS is not the same as the pore solution in the specimen, there will be differences in the measured BR and SR values due to a concentration gradient in the pore solution from the edge to the center of the specimen. Using the relationship between the bulk and surface resistivity found in Figure 5-1, an equivalent bulk resistivity acceptance criteria to the FDOT 29 kΩ-cm surface resistivity requirement [47] would be 18 kΩ-cm. When using simulated pore solution to cure, a bulk resistivity value of 24 kΩ-cm would be equivalent to 29 kΩ-cm using surface resistivity at 28 days, while at 56 days the value would be 28 kΩ-cm.

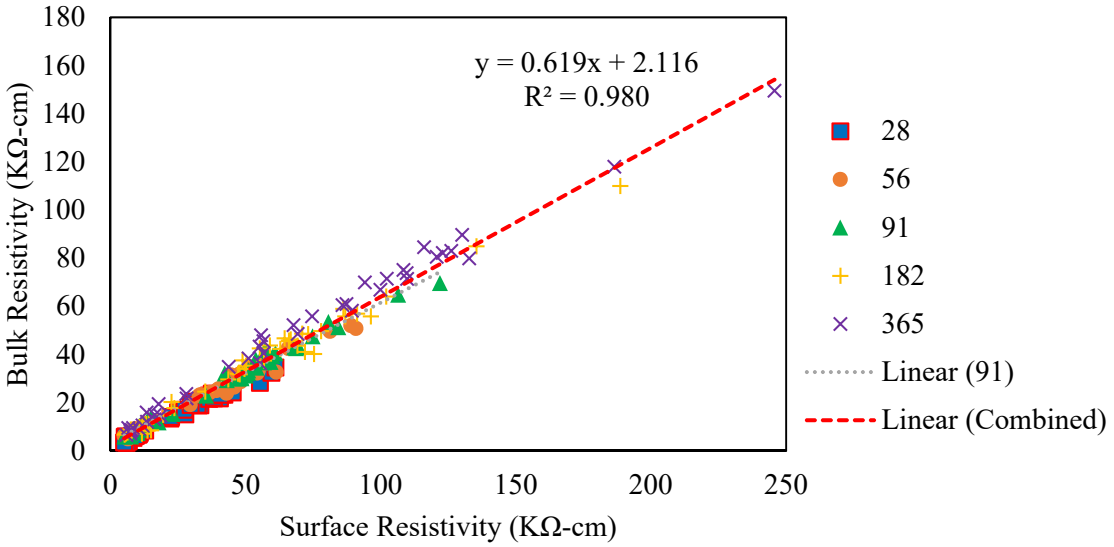

.

Figure 5-1: Bulk resistivity vs. surface resistivity measurements found for moist room curing

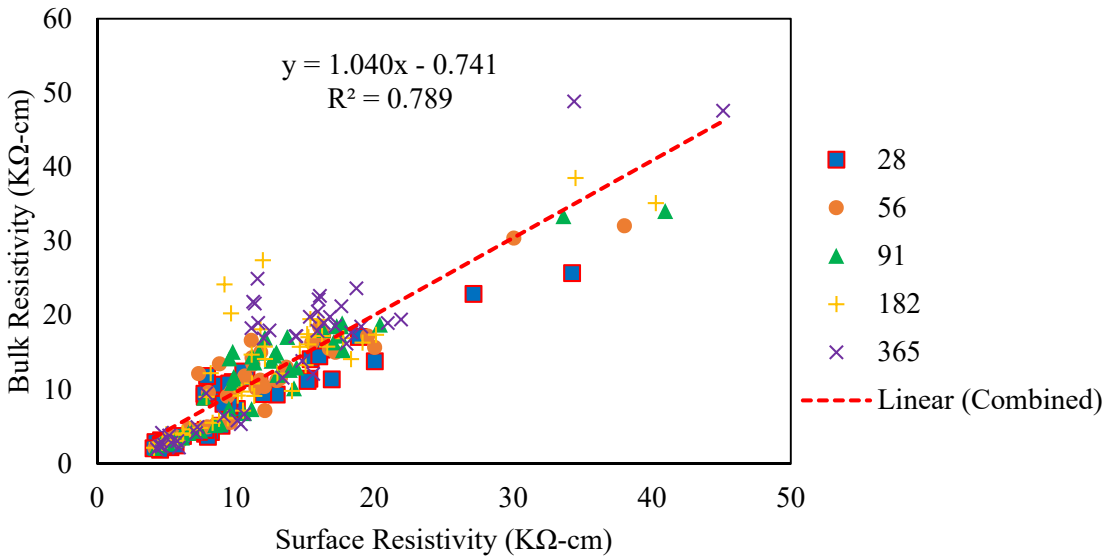

Figure 5-2: Bulk resistivity vs. surface resistivity measurements found for SPS curing

The bulk resistivity results were compared to the RCMT results for samples cured in the moist curing room and in SPS and are shown in Figure 5-3 and Figure 5-4, respectively. A power-based relationship was observed between the bulk resistivity and RCMT for both curing methods. The coefficient of determination (R^2) was above 0.90 for both tests, demonstrating high degrees of correlation. The high levels of correlation were expected since RCPT and surface resistivity measure essentially the same fundamental properties. Bulk resistivity measurements at 28, 56, and 91 days were compared to the non-steady state diffusion coefficient calculated from RCMT performed at 365 days in Figure 5-5 to determine which age better predicts the long-term concrete transport properties. It was seen that use of 56- or 91-day bulk resistivity measurements better predicted the 365-day non-steady state diffusion coefficient.

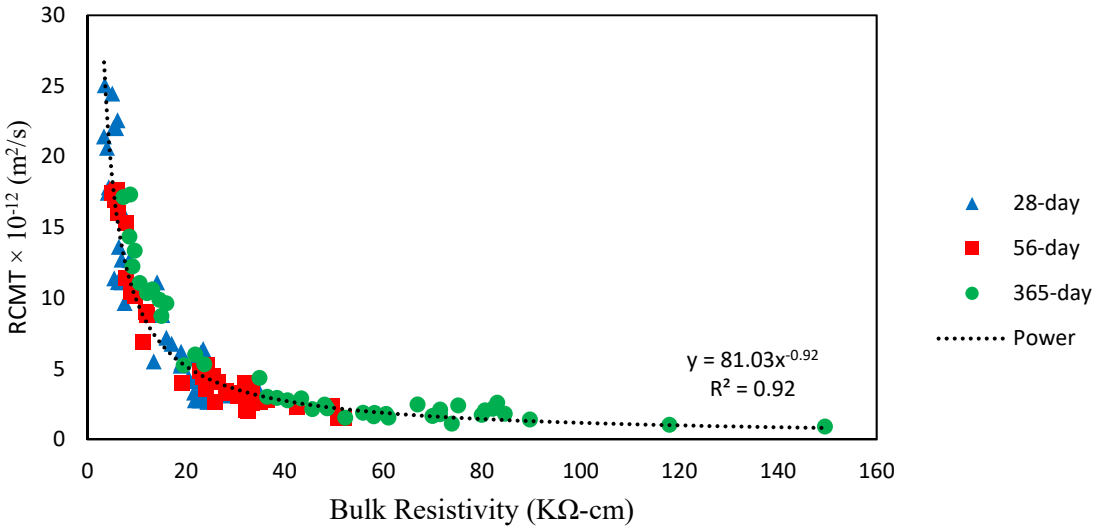

Figure 5-3: Diffusion coefficient from RCMT vs. bulk resistivity for samples cured in the moist room

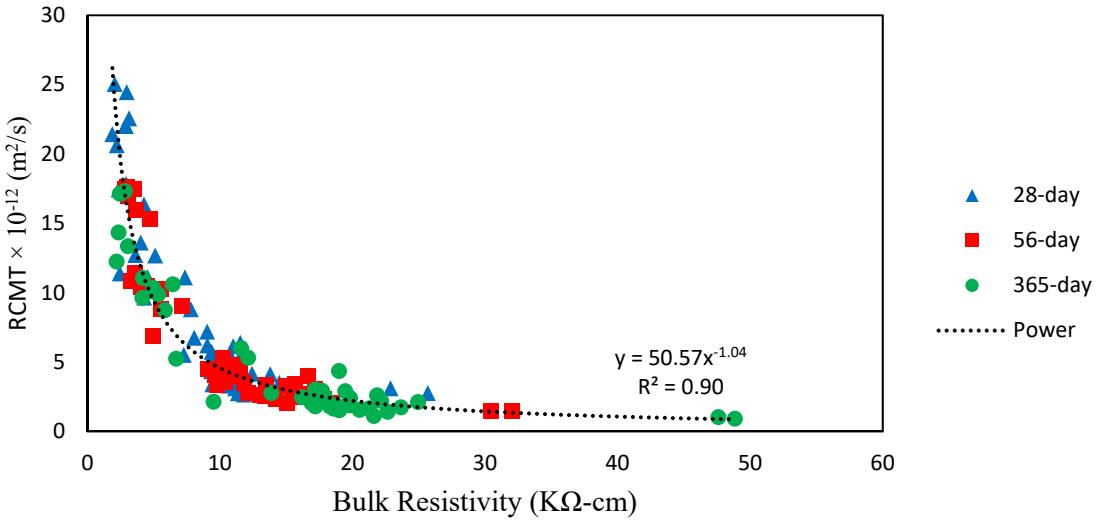

Figure 5-4: Diffusion coefficient from RCMT vs. bulk resistivity for samples cured in SPS

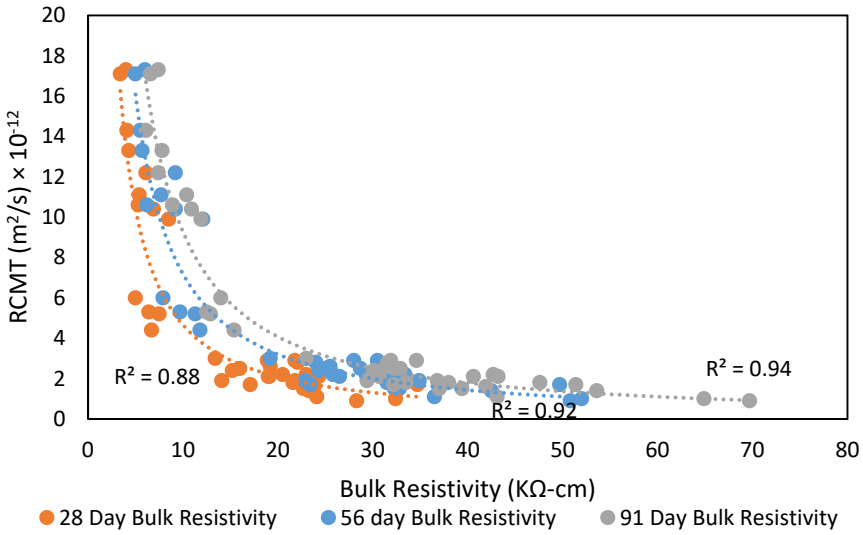

Figure 5-5: Comparison of bulk resistivity measurements at 28, 56, and 91 days with RCMT at 365 days

Figure 5-6 shows the relationship between rapid chloride migration and rapid chloride permeability test results at 28, 56 and 365 days. The RCMT is not a pure electrical test. It measures the diffusion of chloride ions in concrete exposed to an electrical potential. A strong correlation was found between these test methods. This demonstrates the relationship that exists between chloride migration through the interconnected concrete porosity and the electrical conductivity of the samples.

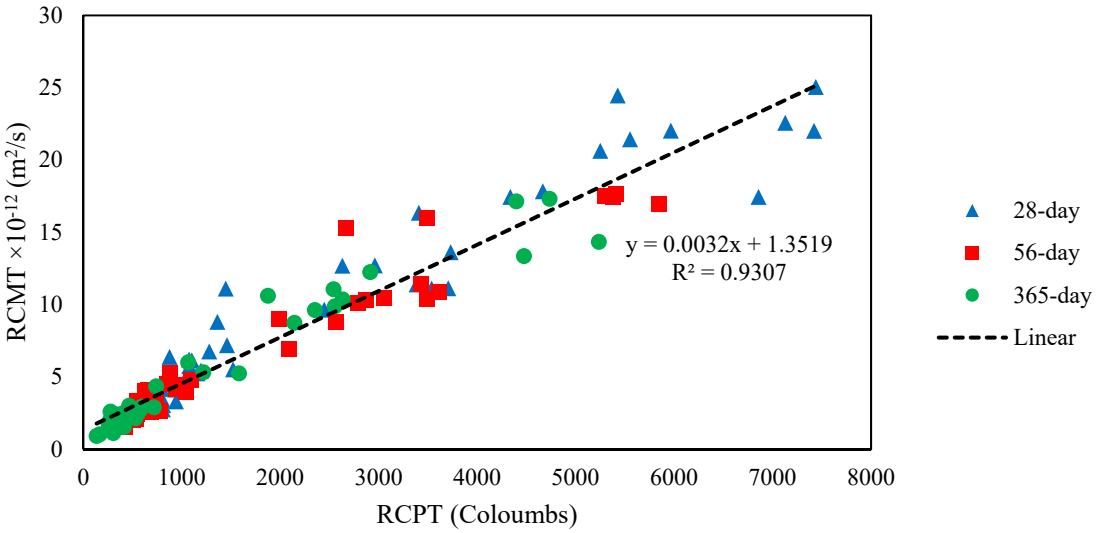

Figure 5-6: RCMT vs. RCPT at 28, 56 and 365 days

Figure 5-7 shows the water permeability versus the secondary absorption rate for 28, 56 and 365 days. The absorption rate increased as the water permeability increased. This was expected because they both depend on water transport through concrete. Both tests could have some experimental error, especially the water permeability for samples with low permeability.

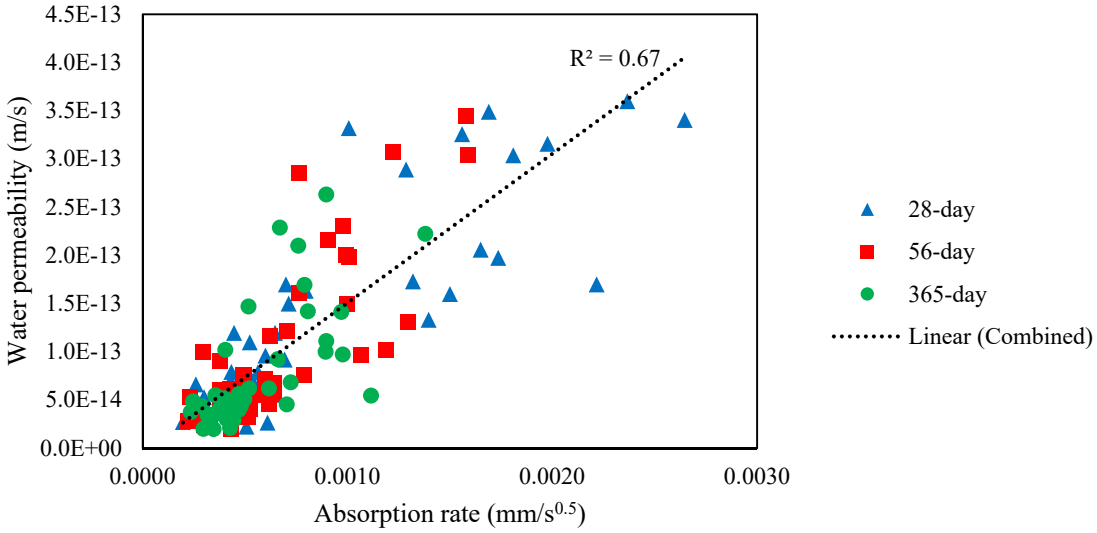

Figure 5-7: Water permeability vs. water absorption results at 28, 56 and 365 days

Figure 5-8 shows the secondary absorption rate vs. bulk resistivity for moist-cured specimens at 28, 56 and 365 days. It is seen that there is a power relationship between the two test methods. A

similar trend is observed for specimens with SPS curing as shown in Figure 5-9. The correlation between bulk resistivity and absorption results was found to be similar for both methods of curing. This is because the absorption results, unlike the RCPT results, are not dependent on the concrete pore solution conductivity.

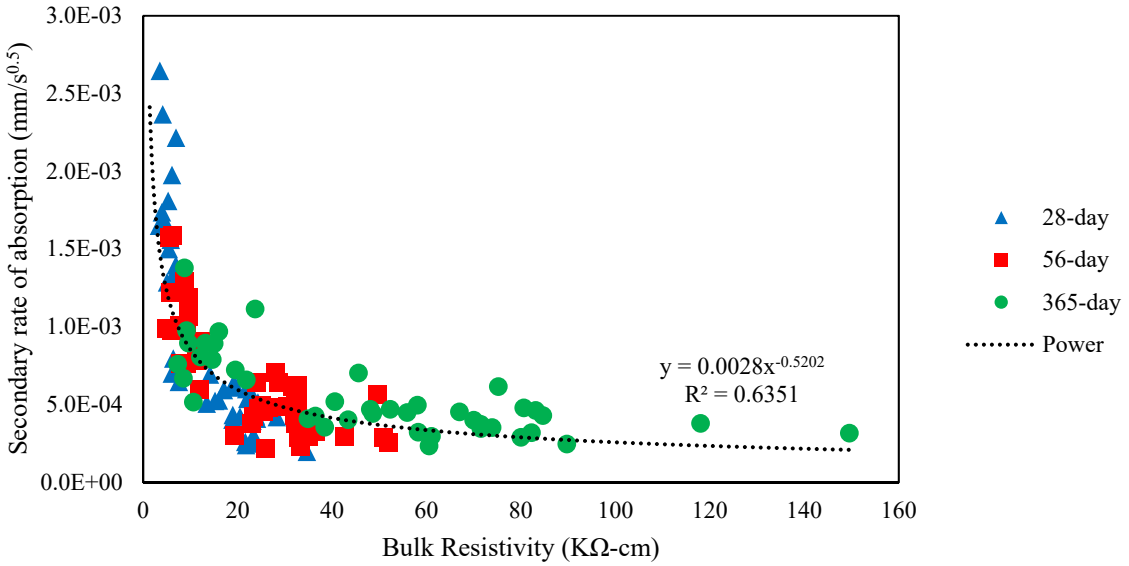

Figure 5-8: Water absorption vs. bulk resistivity measurements for bulk resistivity samples cured in the moist room

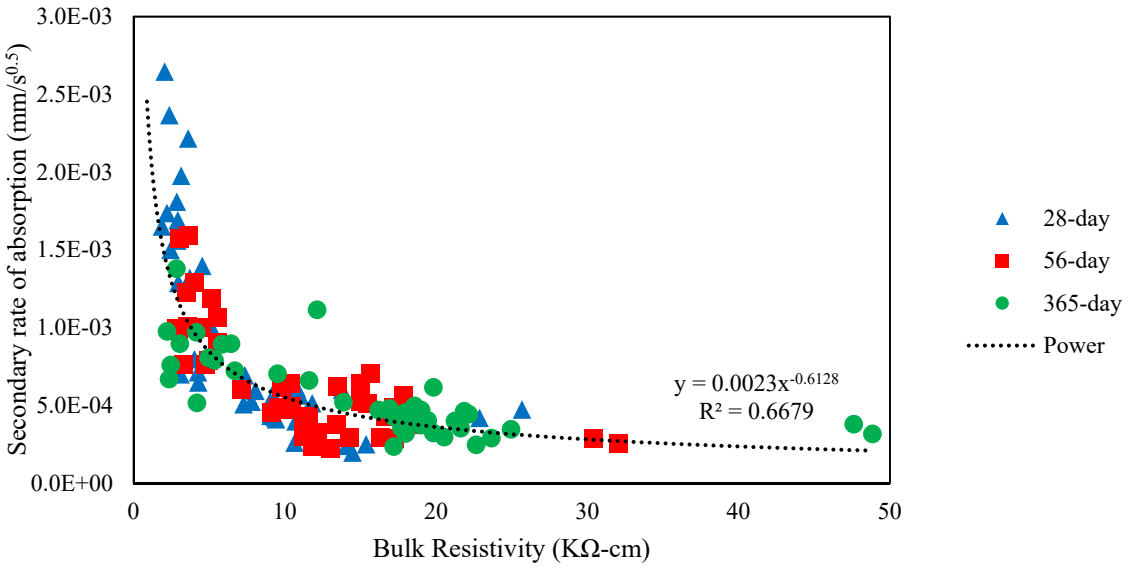

Figure 5-9: Water absorption vs. bulk resistivity for bulk resistivity samples cured using SPS

The correlations between RCMT and formation factor are presented in Figure 5-10 and Figure 5-11 for moist and SPS curing respectively. The formation factors for the SPS-cured specimens were determined from the bulk resistivity readings. A better correlation is observed for the SPS curing compared to the moist curing. This is likely because the SPS provided a better estimate of the pore solution composition for a more accurate calculated formation factor.

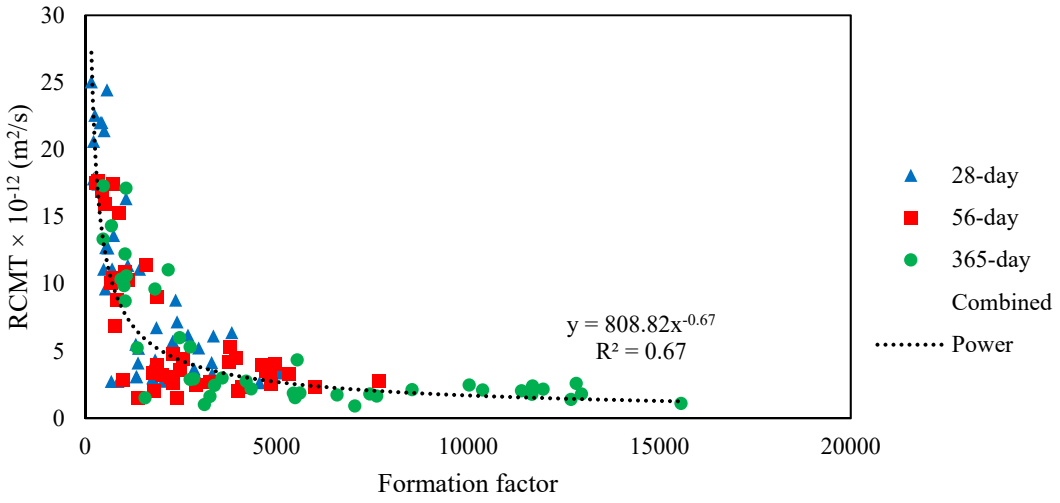

Figure 5-10: RCMT vs. formation factor for formation factor samples cured using moist room

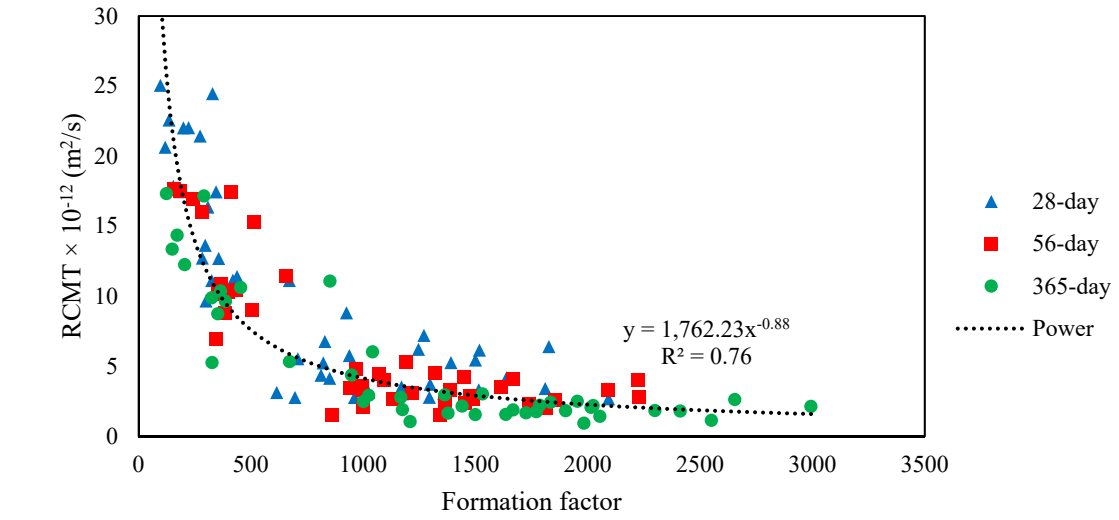

Figure 5-11: RCMT vs formation factor for formation factor samples cured using SPS

The correlations between water permeability and bulk resistivity are presented at Figure 5-12 and Figure 5-13 for moist and SPS curing respectively. Although a trend was found between water permeability and bulk resistivity, the relationship had a low correlation and was less reliable than that found for the other methods. This is likely due to the limitation in pressure of 85 psi for the water permeability test. For the specimens with lower permeability, a high amount of variability was seen because the water flow rate measured was quite low and difficult to measure.

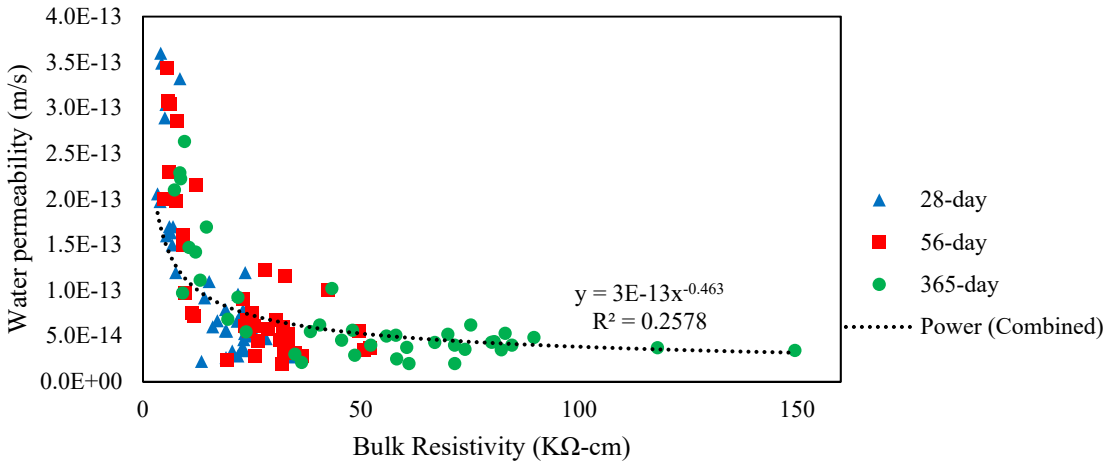

Figure 5-12: Water permeability vs. bulk resistivity for bulk resistivity samples cured using moist room

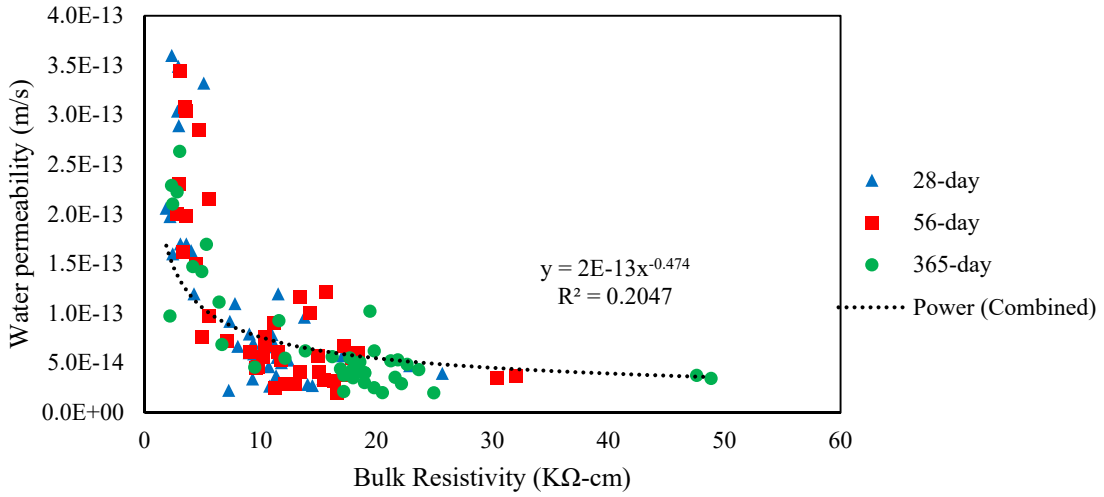

Figure 5-13: Water permeability vs. bulk resistivity for bulk resistivity samples cured using SPS

The correlation between water permeability and formation factor determined from bulk resistivity is presented in Figure 5-14 and Figure 5-15 for moist room and SPS curing, respectively. A better correlation is observed for the SPS curing compared to the moist curing. For the water permeability, a better correlation was found with the formation factor than with the bulk resistivity. When a power-law relationship is used, the formation factor has better correlation than the plain electrical reading such as bulk resistivity. The effect of air content on the water permeability-formation factor correlation was investigated [48]. There was a small effect from air content found on the relationship seen between formation factor and water permeability. The concrete mixtures with air contents 4% or higher were removed from the analysis. This increased the correlation coefficient to 0.69 for samples cured in SPS, however no increase was seen for the samples cured in the moist room.

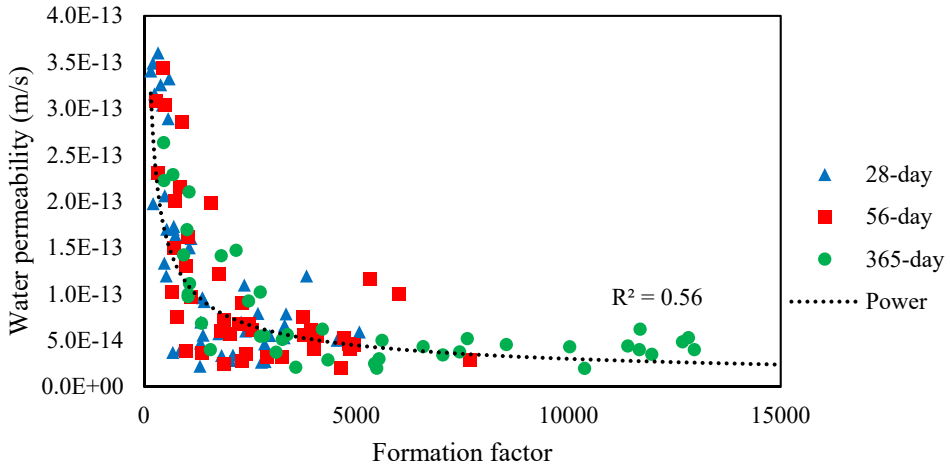

Figure 5-14: Water permeability vs. formation factor for formation factor samples cured using moist room

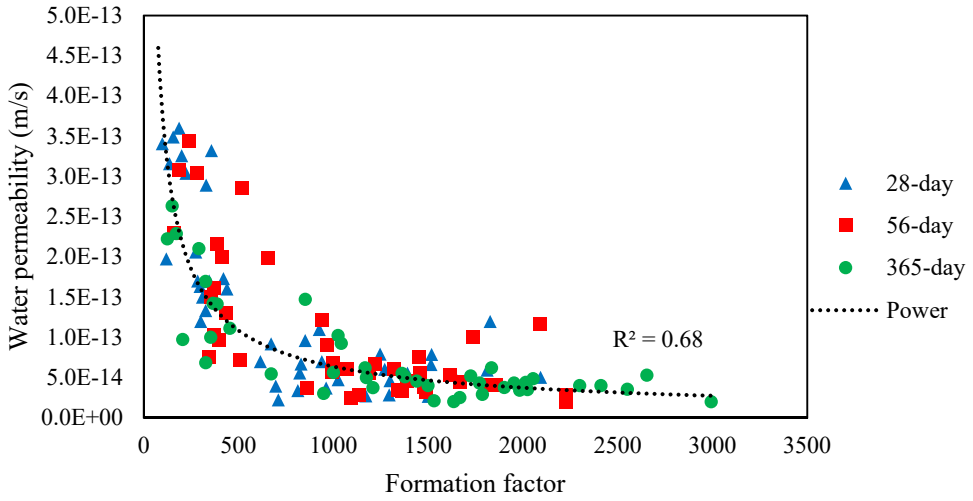

Figure 5-15: Water permeability vs. formation factor for formation factor samples cured using SPS

The correlation between water absorption and formation factor is presented in Figure 5-16 and Figure 5-17 for moist and SPS curing, respectively. A better correlation was observed for the SPS curing compared to the moist curing.

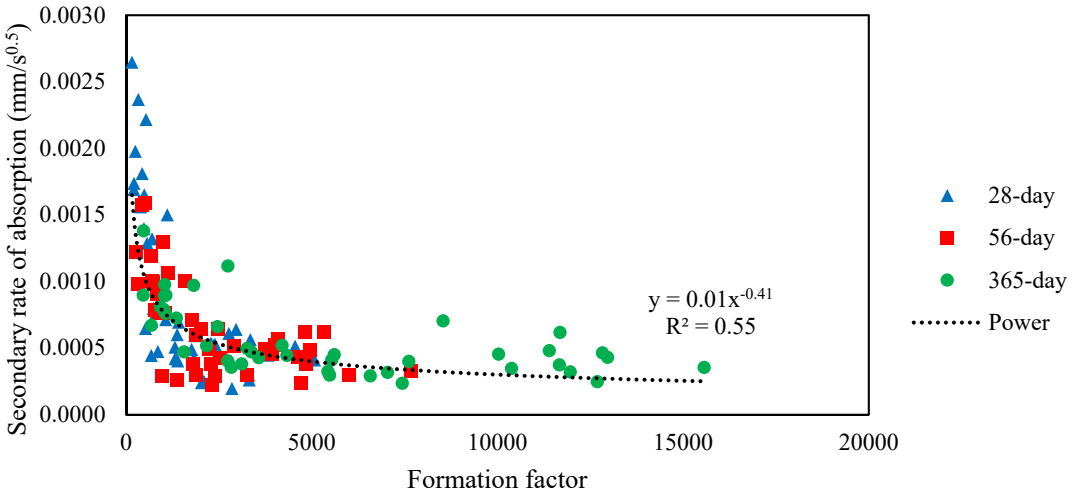

Figure 5-16: Water absorption vs. formation factor for formation factor samples cured using moist room

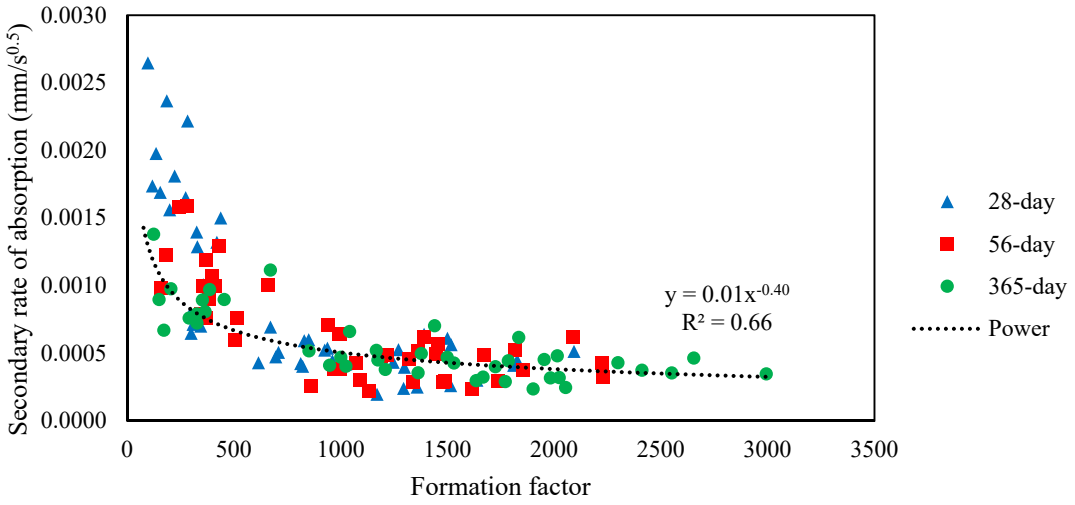

Figure 5-17: Water absorption vs. formation factor for formation factor samples cured using SPS

The effects of silica fume and metakaolin dosage in ternary blends on transport properties was examined. Figure 5-18 and Figure 5-19 show the effects of silica fume dosage on RCMT and bulk resistivity, respectively. Figure 5-20 and Figure 5-21 show the effects of metakaolin dosage on RCMT and bulk resistivity, respectively. Little benefit was seen in increasing the silica fume dosage above 6% in RCMT and bulk resistivity tests, while improvements were only seen in

RCMT when metakaolin dosage was increased up to 10%. A change in silica fume dosage requirements from 7-9% to 6% in ternary blends would give similar durability with a lower cost.

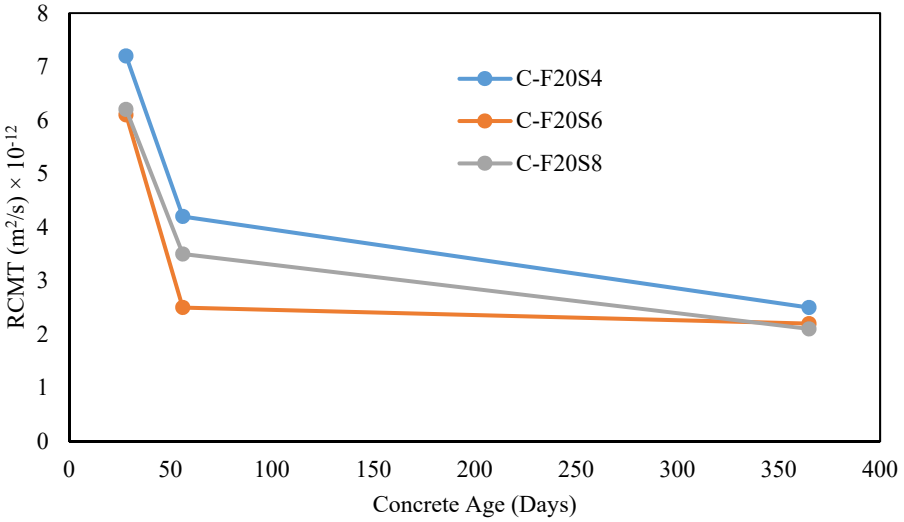

Figure 5-18: Effect of silica fume dosage in ternary blends on RCMT

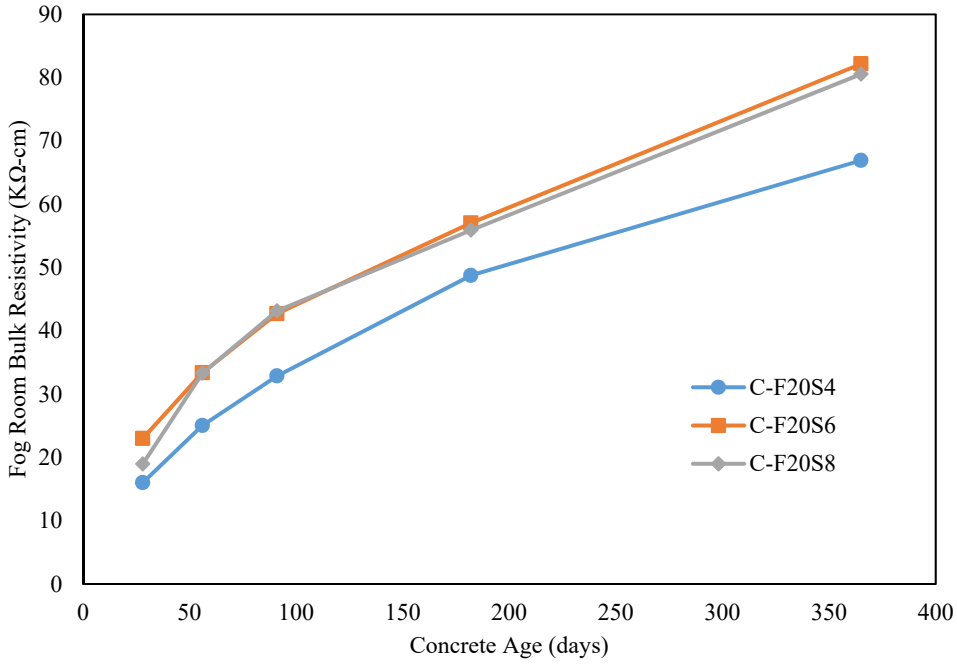

Figure 5-19: Effect of silica fume dosage in ternary blends on bulk resistivity

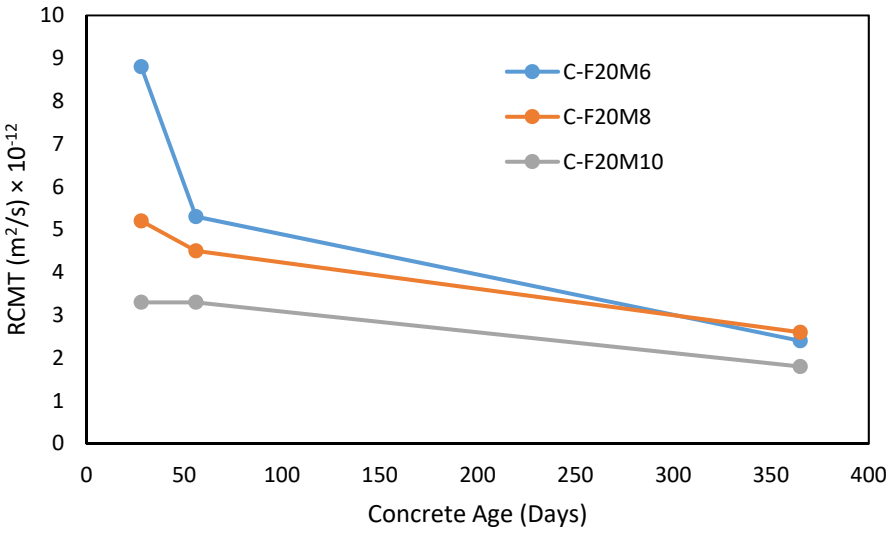

Figure 5-20: Effect of metakaolin dosage in ternary blends on RCMT

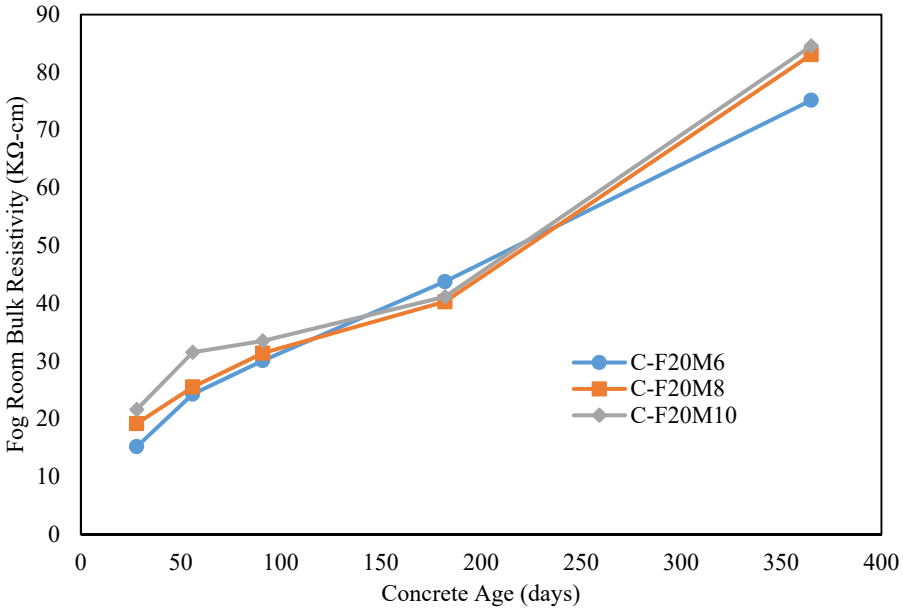

Figure 5-21: Effect of metakaolin dosage in ternary blends on bulk resistivity

5.4 Summary

The results of transport tests including the water absorption, volume of permeable voids, and water permeability were presented along with electrical-based test methods including rapid chloride migration, rapid chloride permeability, surface resistivity, and bulk resistivity measurements.

While there was a strong correlation between surface and bulk resistivity measurements, bulk resistivity measurements showed less variability than surface resistivity. Samples cured in SPS showed better correlations to secondary absorption rate and water permeability than samples cured in the fog room. Formation factor showed a marginally better correlation for SPS-cured samples against secondary absorption rate than bulk resistivity. Given that the difference in correlation was marginal, the excellent correlation for samples cured in the moist room between bulk resistivity and RCMT, and practical issues related to curing samples in SPS, it is recommended to adopt a bulk resistivity acceptance criteria of 18 kΩ-cm at 56 or 91 days with moist-room-cured samples using the average relationship obtained between surface and bulk resistivity. Little benefit was seen in increasing the silica fume dosage above 6% in RCMT and bulk resistivity tests, potentially allowing FDOT to reduce silica fume dosage requirements in ternary blends to 6%.

CHAPTER 6. BULK DIFFUSION EXPERIMENTS

6.1 Introduction

The corrosion of steel in reinforced concrete is often caused by chlorides penetrating through the concrete cover to the level of the reinforcement. Diffusion is a prominent mass transport mechanism in concrete in marine conditions and follows Fick's second law shown in Equation 6-1 [49].

$$\frac{dC}{dt} = D\frac{d^2C}{dx^2} \qquad \text{Equation 6-1}$$

Where, C is the concentration (%), t is time (s), x is distance (m), and D is the diffusion coefficient (m^2/s). A portion of the chlorides that penetrate into the concrete will be chemically bound or absorbed by the cement hydration products, while the rest will remain in the pore solution free to continue penetrating inwards. The concrete effective diffusion coefficient is the diffusion coefficient that describes the free chloride transport into the concrete through diffusion with binding being explicitly accounted for separately in the analysis [50]. The concrete apparent diffusion coefficient is a term that is a composite of the diffusion and chloride binding effects on transport. When the apparent diffusion coefficient is used in Fick's second law as the diffusion coefficient, no additional consideration of chloride binding is used [23,51].

ASTM C1556 "Standard Test Method for Determining the Apparent Chloride Diffusion Coefficient of Cementitious Mixtures by Bulk Diffusion" is a commonly used method to measure the ability of concrete to resist chloride penetration [23]. In this test, a concrete sample is immersed in a chloride solution for a minimum of 35 days. When this test is conducted by the Florida Department of Transportation (FDOT), samples are immersed for one year. At the end of that time period, the sample is removed from the solution and profile ground by layer or sliced into sections that are then ground. The concrete powder is then analyzed to determine the chloride content with depth [52]. The concrete diffusion coefficient is then fit to the measured chloride profile. If the apparent concrete diffusion coefficient is assumed to be constant with time, an analytical equation can be used to calculate the chloride concentration with depth as shown in Equation 6-2 [23]:

$$C(x,t) = C_s - (C_s - C_i) \cdot erf\left(\frac{x}{\sqrt{4 \cdot D_a \cdot t}}\right) \quad \text{Equation 6-2}$$

Where *C(x,t)* is the concrete chloride concentration by mass (%) measured at depth x (in.) and time exposed to chlorides (days), C_s is the concrete surface concentration by mass (%) at the concrete-liquid interface, C_i is the initial concrete chloride concentration by mass (%), D_a is the apparent chloride diffusion coefficient (in.^{2}/s), and erf is the error function.

Alternatively, concrete transport properties can be determined using electrical properties of concrete using the formation factor. The formation factor is shown in Equation 4-1 and is defined as the ratio of self-diffusion coefficient divided by the concrete effective diffusion coefficient. The self-diffusion coefficient for different ionic species at different temperatures is shown in shown in Table 6-1.

Table 6-1: Self-diffusion coefficients of ionic species [30]

Ionic species	Self-diffusion coefficient, D_0 (m^2/s) × 10^{-10}		
	0°C	18°C	25°C
Na^+	6.3	11.3	13.3
K^+	9.9	16.7	19.6
Mg^{2+}	3.6	5.9	7.1
OH^-	25.6	44.9	52.7
Cl^-	10.1	17.1	20.3
SO_4^{2-}	5	8.9	10.7

While electrical methods have many advantages over other tests methods because of method simplicity and cost, their ability to measure concrete transport properties needs to be validated. In this section, the apparent diffusion coefficients of 40 concrete mixtures were determined using chloride profile measurements from bulk diffusion experiments at 6 and 12 months. In addition, the effective chloride diffusion coefficients were determined by modeling the chloride profile through finite difference simulation that takes into account the chloride binding of the concrete specimen.

6.2 Sample Fabrication and Testing Procedure

Concrete cylinders were made for bulk diffusion testing from 40 mixtures used to also make samples for other transport property tests. Table 2-7 summarizes the concrete mixture proportions

used. For mixtures 1 to 38, #57 limestone aggregates were used and for mix 39 and 40, #89 limestone aggregates were used as coarse aggregate. The cylinders were cured in the moist room until 28 days of age and then saw cut into three sections, as shown in Figure 6-1. The section with the finished surface was cut to a depth of at least 3 in. (75 mm) and was the section used in the salt-water exposure. The 1 in. (25 mm) thick slice below the sample used for salt-water exposure was used to determine the initial chloride concentration of the concrete mixture. The bottom concrete piece was discarded. Nine samples were cut for bulk diffusion testing from each mixture. Samples were labeled and stored for 24 hours at 72 ± 3.6°F (23 ± 2°C) and 50% RH with the cut-side facing up as shown in Figure 6-2.

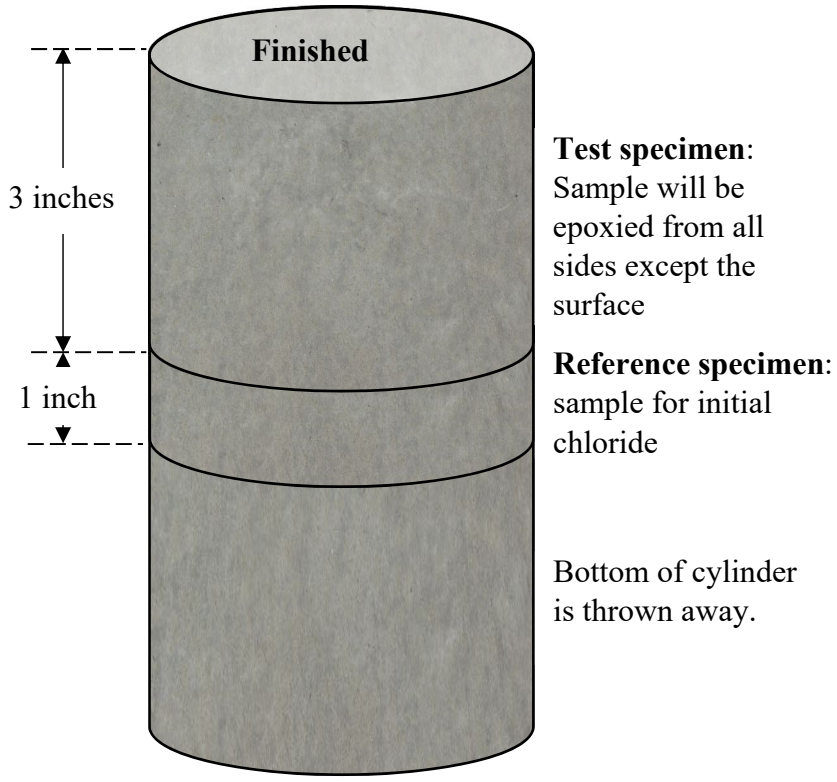

Figure 6-1: Schematic view of the test specimen and reference sample obtained from the cylinder

Figure 6-2: Bulk diffusion samples during storage at 23 ± 2ºC and 50% RH

After the concrete surface was dry, the sample bottom and sides were sealed with epoxy to force one-dimensional chloride ingress through the exposed surface. A two-component epoxy (Sikadur 32 Hi-Mod) was used as the sealant. After five hours, the specimens were coated with a second layer of epoxy. The epoxied samples were then cured overnight. The epoxied specimens were immersed in a saturated calcium hydroxide water bath for 48 hours prior to chloride exposure. The samples were soaked in the calcium hydroxide solution to reduce the effects of absorption on chloride ingress. After the calcium hydroxide soak period was finished, the samples were rinsed with tap water and placed in tanks containing 16.5% of Sodium chloride (NaCl) at the Florida Department of Transportation (FDOT) State Materials Office (SMO), as shown in Figure 6-3. The chloride solution is circulated throughout the tank to ensure uniform chloride concentration and exposure for all samples. Figure 6-4 illustrates the sample placement in the tank.

Figure 6-3: Tank containing 16.5% NaCl solution and bulk diffusion samples

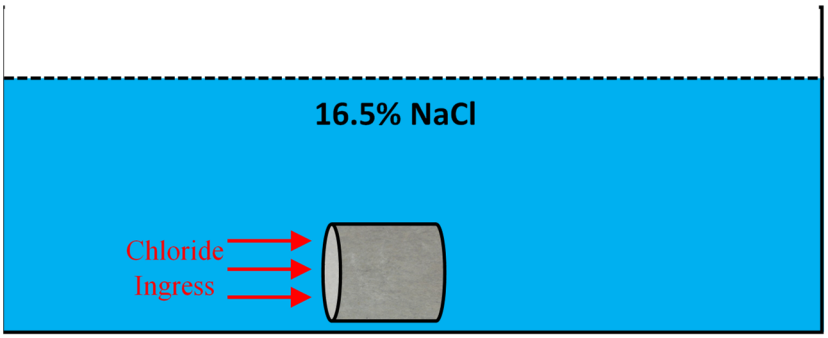

Figure 6-4: One dimensional chloride ingress in the tank

Samples made for bulk diffusion were removed from the NaCl solution after 6 months and 1 year of exposure. A third set of specimens were made for potential later-age testing. After the exposure period was complete, the sample edges were saw cut to remove the epoxy before profile grinding. The epoxy cutting process was performed by cutting the bottom part off and then saw cutting an

octagon shape to remove the side epoxy. The samples were profile ground in 12 layers as shown in Table 6-2. After grinding each layer, the powder was collected in a sealed Ziploc bag for testing.

Table 6-2: Layers and thickness of the chloride profiling.

Layer	Thickness (mm)	Depth (mm)
1	1	0-1
2	3	1-4
3	3	4-7
4	3	7-10
5	5	10-15
6	5	15-20
7	5	20-25
8	5	25-30
9	5	30-35
10	5	35-40
11	5	40-45
12	5	45-50

A Mettler Toledo EasyCl auto-titrator was used to measure the chloride content. The chloride content for samples exposed to chlorides for 6 months was determined according to ASTM C1152 [27], while the chloride content for samples exposed to chlorides for 12 months was determined according to [53]. The chloride concentration was measured twice for each layer on the 3 concrete samples placed in salt water. Each reported chloride concentration value is the average of 6 measurements.

6.3 Chloride Diffusion Coefficient Determination

The concrete effective and apparent diffusion coefficients were determined using a couple of different approaches. The apparent diffusion coefficients were determined using the methods specified in ASTM C1556. The first method used to find the effective diffusion coefficients was to simulate the concrete chloride concentration with depth using a fully explicit finite difference scheme, the chloride binding coefficients, and volume of permeable voids for the mixture. The effective diffusion coefficient was determined by using non-linear regression to fit the simulated chloride concentration to the measured chloride concentration with depth. The second approach was to use measured concrete bulk resistivity and pore solution resistivity in Equation 4-1 to calculate the effective diffusion coefficient.

Apparent Diffusion Coefficient

The surface concentration and apparent chloride diffusion coefficient were determined by fitting Equation 6-2 to the measured chloride contents using a non-linear regression analysis. To fit the apparent diffusion coefficient, the sum of the squares of the difference between the measured and calculated chloride concentrations with depth were minimized. The chloride surface concentration value was determined from the fit to the measured data, while the measured top layer chloride concentration was not included in the analysis.

Effective Diffusion Coefficient Fit to Measured Data

The chloride binding isotherms and volume of permeable voids for each cementitious paste mixture were used to separate the bound from the free chlorides and were used in the simulations to find the effective chloride diffusion coefficient. This method incorporated the Freundlich binding isotherm described in Chapter 3 to model the relationship between the free chloride concentration and bound chloride concentration in cementitious paste.

The volume of permeable voids was determined by performing ASTM C642 [38]. This test was performed on each concrete mixture after 28 days of moist room curing.

The total chloride content C_{tc} (%) was modeled using the free chloride content C_{fc} (%), the concrete permeable voids ω_e (%), and concrete density CD (lb/yd^3) according to the Equation 6-3 [54]:

$$C_{tc} = \frac{\alpha\,(C_{fc})^{\beta} + [(C_{fc}) \times \omega_e]}{CD \times 100} \qquad \text{Equation 6-3}$$

Where α is a Freundlich binding isotherm coefficient (lb/yd^3 of concrete), β is a Freundlich binding isotherm (unitless).

The effective chloride diffusion coefficient was determined by analyzing the chloride profiles after including the chloride binding effect through a finite difference model applying Fick's second law of diffusion and by incorporating the Freundlich chloride binding isotherm the equation is modified as shown in Equation 6-4 [54].

$$D_a = \frac{D_e}{1 + \frac{1}{\omega_e}\alpha\beta C_{fc}^{\beta-1}} \qquad \text{Equation 6-4}$$

Finite difference modeling of Fick's second law of diffusion was used to simulate chloride diffusion through the concrete specimens during the time of exposure. The model calculated the change in chloride concentration at selected time and depth steps. The diffusion coefficient decrease with age was accounted for using Equation 6-5 and Equation 6-6 [51].

$$D_e(t) = D_{28}(\frac{28}{t})^m + D_{ult}(1 - \left(\frac{28}{t}\right)^m) \quad \text{Equation 6-5}$$

$$D_{ult} = D_{28}(\frac{28}{36{,}500})^m \quad \text{Equation 6-6}$$

Where $D_e(t)$ is the effective chloride diffusion at time t (m^2/day), D_{28} is the effective chloride diffusion at the age of 28 days (m^2/day), D_{ult} is the ultimate effective chloride diffusion coefficient (m^2/day), which is assumed to be the effective diffusion coefficient at 100 years, t is exposure time (days) and m is the aging factor.

The aging factor was determined using four methods. Riding et al. [51,55] presented an aging factor based on the replacement ratio of the supplementary cementitious materials as shown in Equation 6-7:

$$m_1 = 0.26 + 0.4 \cdot (\frac{FA}{50} + \frac{SG}{70}) \quad \text{Equation 6-7}$$

Where m_1 is the aging factor, FA is fly ash replacement (mass %) and SG is slag replacement (mass %). A time step of 0.01 day with a depth of 0.5 mm were used in the analysis. The calculated chloride profiles from the model were compared to the measure chloride profiles from the concrete specimens at the same exposure period. The effective diffusion coefficient and surface chloride concentration were selected by reaching the minimum error value between the calculated and measured chloride contents. The first 1 mm was excluded from the fitting between the calculated and measured chloride content.

The effective chloride diffusion profiles for 6 and 12 months of salt exposure were fit using three different methods for determining the chloride surface concentrations and decreases in apparent diffusion coefficients with age:

1. The effective diffusion coefficient at 28 days (D_{28}) and surface chloride (C_s) were determined through fitting. The aging factor used was determined by Equation 6-7, hereafter referred to as m_1. Figure 6-5 shows a schematic view of the calculation procedure.

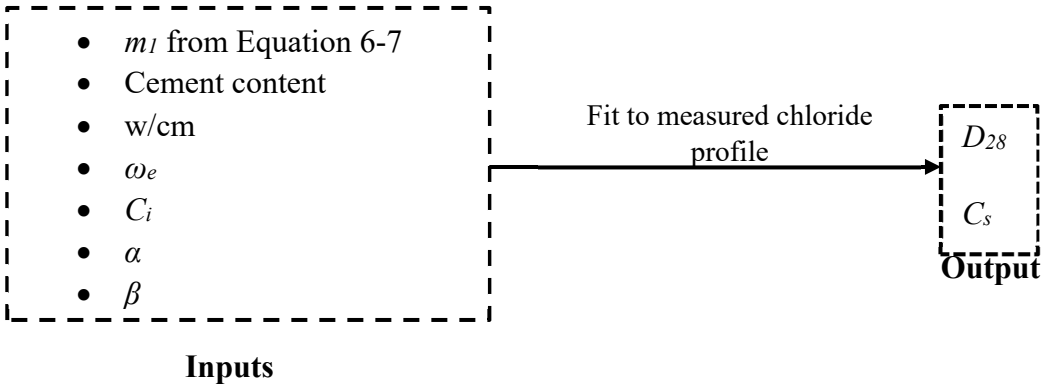

Figure 6-5: Fitting chloride profile from effective diffusion to measured chloride profile

2. The effective diffusion coefficient at 28 days (D_{28}) were determined through fitting. The aging factor used was determined by Equation 6-7. The chloride concentration in the pore solution at the surface layer was assumed to come to equilibrium immediately at the chloride concentration used in the salt water exposure tank of 100 kg/m^3. Figure 6-6 shows a schematic view of the calculation procedure.

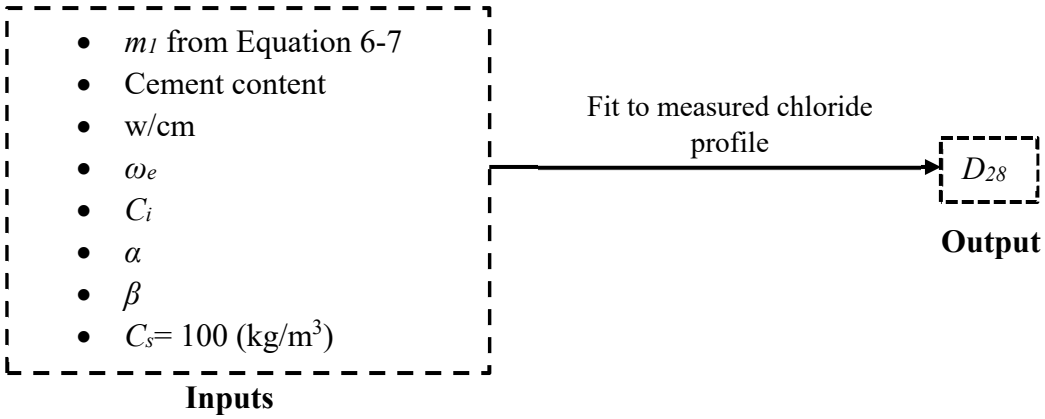

Figure 6-6: Fitting chloride profile from effective diffusion to measured chloride profile assuming that the surface concentration is 100 kg.cl/m^3

3. The effective diffusion coefficient at 28 days (D_{28}) was determined through fitting. The aging factor used hereafter referred to as m_2 was determined from fitting the aging coefficient to the measured decrease of rapid chloride migration (RCMT) values with age [55]. The chloride concentration in the pore solution at the surface layer was assumed to come to equilibrium immediately at 100 kg/m^3 which is the chloride concentration used in the salt water exposure tank. Figure 6-7 shows a schematic view of the calculation procedure.

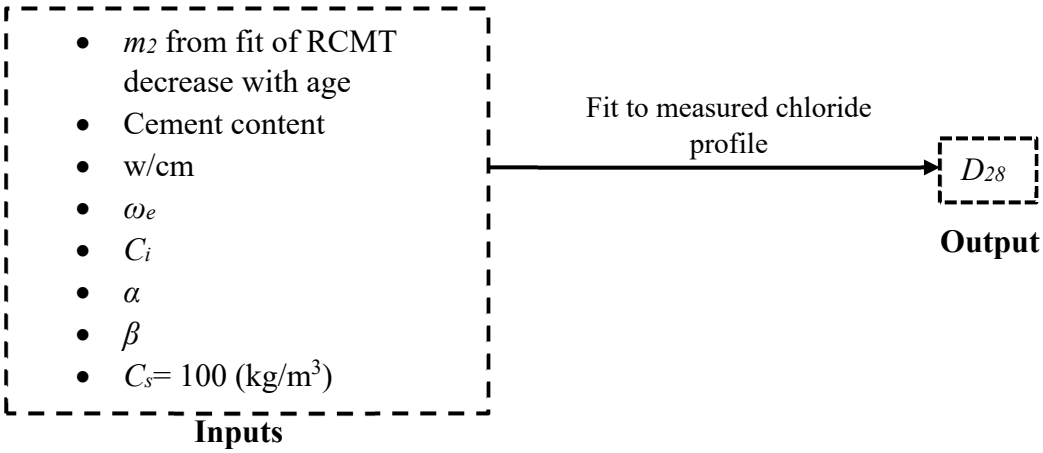

Figure 6-7: Fitting chloride profile from effective diffusion to measured chloride profile assuming that the surface concentration is 100 kg.cl/m^3

Effective Diffusion Coefficient from Formation Factor

The formation factors calculated from bulk resistivity measurements, pore solution resistivity values, and D_0 were used to first calculate the effective diffusion coefficients at 28 56, 91, 180, and 365 days and then fit D_{28} and m values as described in Equation 6-5. These coefficients were then used in simulations to calculate the chloride profile and compare it to the measured chloride profiles at 6 and 12 months of chloride exposure. Figure 6-8 shows a schematic of the process used to simulate the chloride profile using the calculated formation factor values.

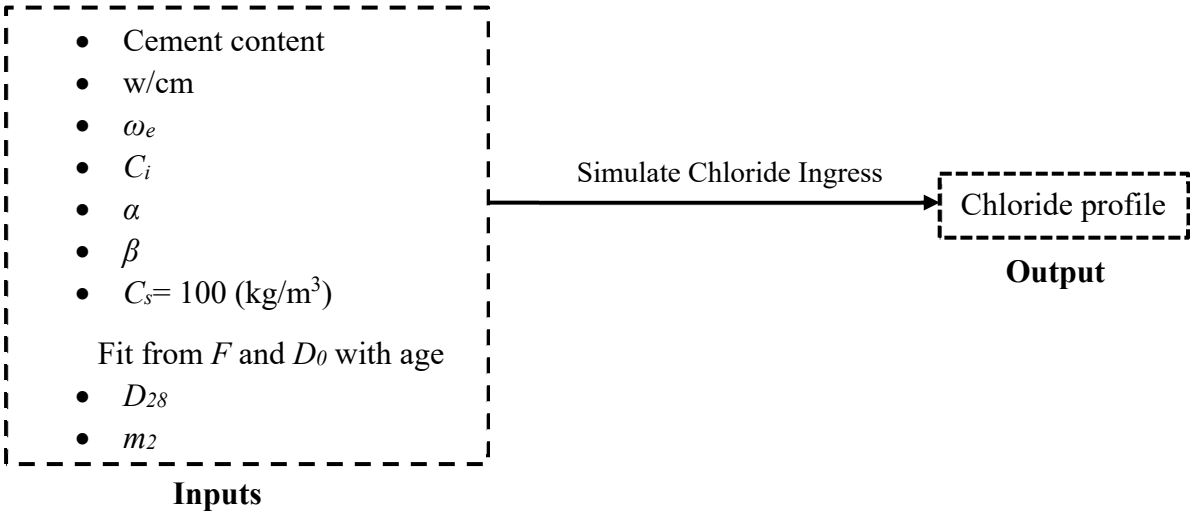

Figure 6-8: Chloride profile calculated using D_{28} and m fit to effective diffusion coefficient calculated from formation factor according to Equation 4-1 to measured chloride profile assuming that the surface concentration is 100 kg/m^3

The formation factor values used to calculate the effective diffusion coefficients were calculated using measured bulk resistivity values from samples cured using moist and SPS curing. The pore solution resistivity values were determined using the NIST calculator, the SPS resistivities were measured using a conductivity meter, and the resistivities of the extracted pore solutions obtained from cement paste were measured and are presented in Chapters 3 and 4.

The three combinations of bulk resistivity and pore solution resistivity values used are as follows:

1. **Moist-NIST**: concrete resistivity at moist curing / pore solution resistivity from NIST calculator
2. **Moist-EIS**: Concrete resistivity at moist curing / pore solution resistivity from EIS
3. **Bucket-conductivity meter:** Concrete resistivity for bucket curing (SPS) / pore solution resistivity of the bucket using conductivity meter. Figure 6-9 shows the steps used to calculate the aging factor for bucket-conductivity meter specimens.

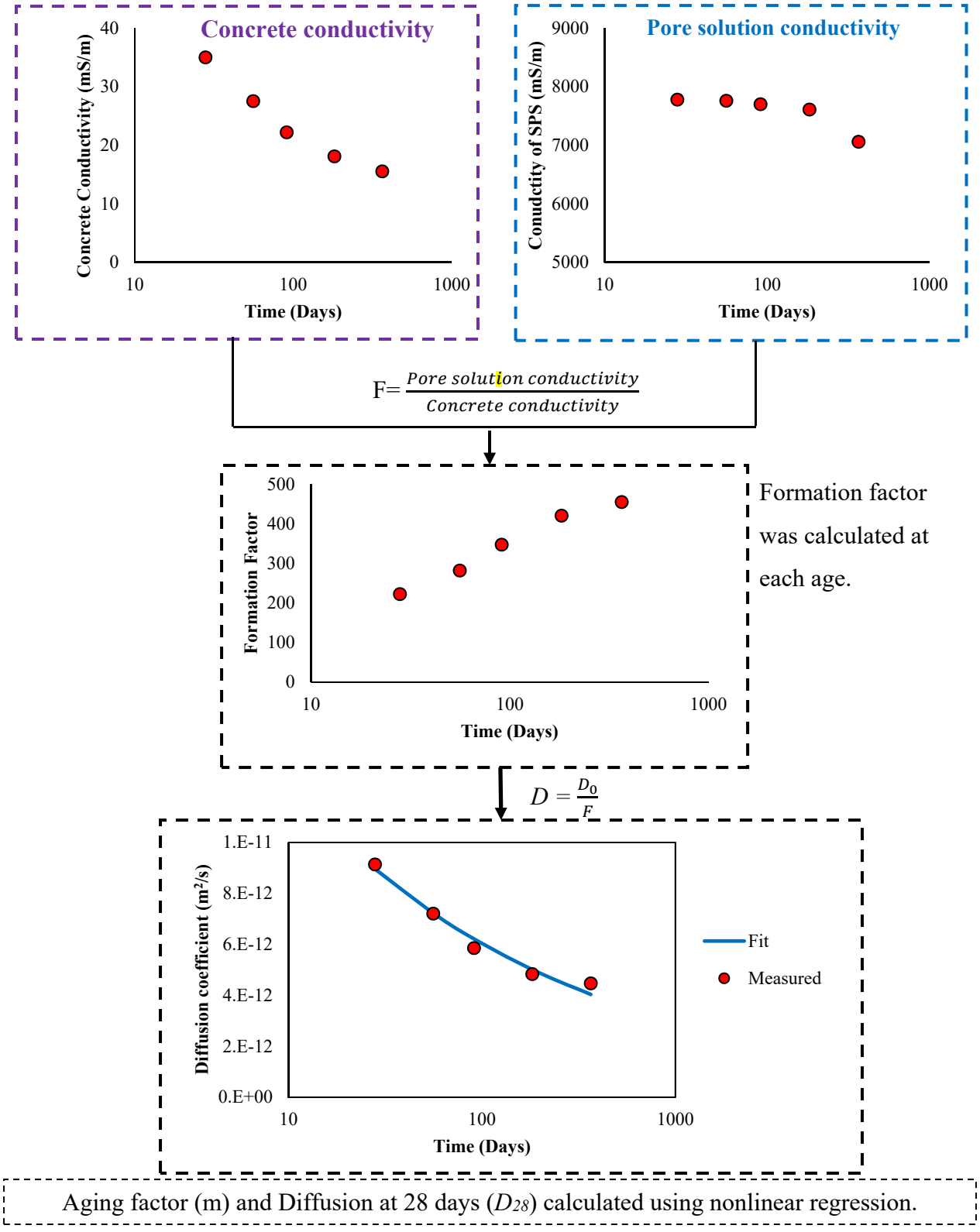

Figure 6-9: Steps in calculation of aging factor and D_{28}

Figure 6-10 shows a chart summarizing the different ways that the formation factor was calculated, and Table 6-3 shows the aging factors used in the effective diffusion calculations.

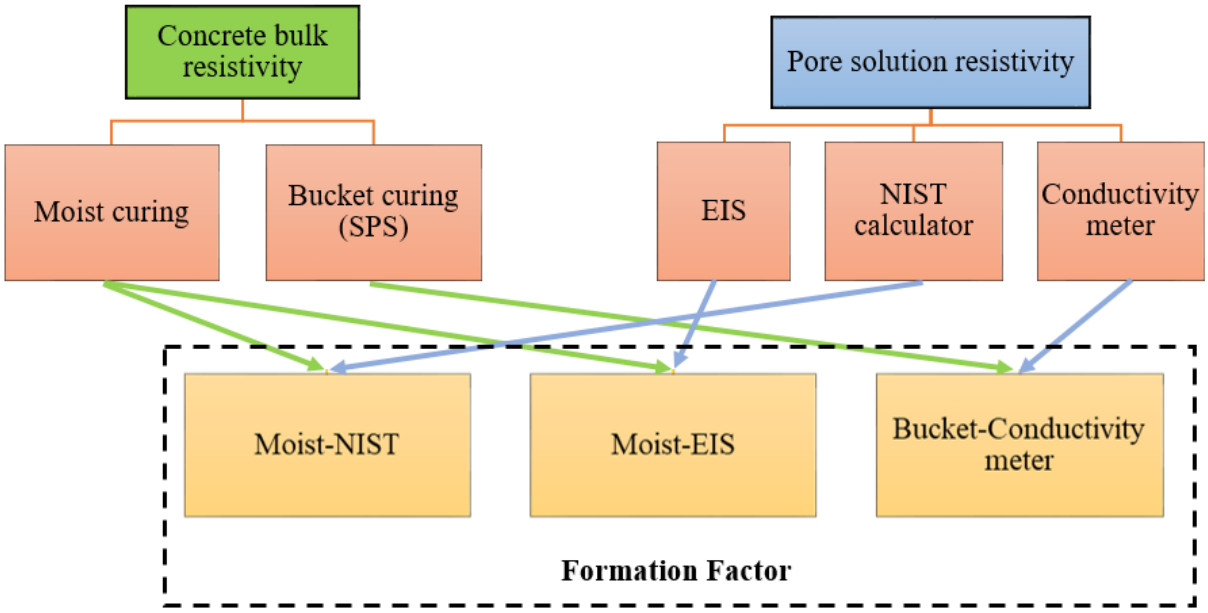

Figure 6-10: Formation factor calculation chart

Table 6-3: Aging factor used in the effective diffusion coefficient

Mix No	Mix ID	Aging factor (m)			
		m_1	Moist NIST & Moist EIS	Bucket conductivity meter	RCMT (m_2)
1	C-100	0.260	0.235	0.042	0.137
2	C-100h	0.260	0.359	0.000	0.104
3	C-F10	0.340	0.543	0.360	0.374
4	C-F20	0.420	0.697	0.532	0.652
5	C-F10h	0.340	0.404	0.310	0.316
6	C-F20h	0.420	0.716	0.539	0.597
7	C-G60	0.603	0.342	0.158	0.186
8	C-S8	0.260	0.314	0.242	0.304
9	C-M10	0.260	0.259	0.068	0.152
10	C-F10G30	0.511	0.413	0.337	0.272
11	C-F10G45	0.597	0.331	0.314	0.344
12	C-F10G60	0.683	0.370	0.089	0.270
13	C-F10G60h	0.683	0.370	0.416	0.305
14	C-F20S4	0.420	0.590	0.103	0.521
15	C-F20S6	0.420	0.500	0.005	0.731
16	C-F20S8	0.420	0.621	0.242	0.550
17	C-F20S8h	0.420	0.586	0.203	1.040
18	C-F20M6	0.420	0.595	0.293	0.588
19	C-F20M8	0.420	0.465	0.313	0.265
20	C-F20M10	0.420	0.425	0.210	0.198
21	C-F20M10h	0.420	0.525	0.288	0.570
22	C-G55S8	0.574	0.733	0.257	0.703
23	C-G55M10	0.574	0.534	0.190	0.518
24	CV-100	0.260	0.168	0.000	0.196
25	CV-100h	0.260	0.305	0.000	0.073
26	CV-F10G60	0.683	0.398	0.089	0.140
27	CV-F20S8	0.420	0.488	0.088	0.674
28	CV-M10	0.260	0.266	0.086	0.358
29	CL-100	0.260	0.236	0.104	0.098
30	CL-100h	0.260	0.366	0.005	0.081
31	CL-F10G60	0.683	0.323	0.146	0.326
32	CL-F20S8	0.420	0.548	0.126	0.383
33	CL-M10	0.260	0.206	0.000	0.062
34	CHA-100	0.260	0.331	0.273	0.010
35	CHA-100h	0.260	0.418	0.004	0.106
36	CHA-F10G60	0.683	0.380	0.144	0.387
37	CHA-F20S8	0.420	0.430	0.085	0.396
38	CHA-M10	0.260	0.213	0.000	0.017
39	C-100SS	0.260	0.238	0.052	0.275
40	C-F20S8SS	0.420	0.559	0.146	0.552

6.4 Results

The apparent chloride diffusion coefficients calculated for all mixtures at 6 months and 12 months are shown in Table 6-4. The chloride profiles and apparent diffusion coefficients for all mixtures are presented in Appendix A and Appendix B for 6- and 12-month exposures, respectively.

Table 6-4: Apparent diffusion coefficients and calculated surface concentrations at 6 and 12 months

Mix No	Mix ID	6 Months		12 Months	
		D_{app} (m^2/s) × 10^{-12}	C_s (%)	D_{app} (m^2/s) × 10^{-12}	C_s (%)
1	C-100	2.12	0.638	2.15	0.654
2	C-100h	3.15	0.607	3.54	0.918
3	C-F10	2.51	0.627	1.18	1.055
4	C-F20	1.07	0.655	1.38	0.945
5	C-F10h	2.74	0.990	3.03	1.155
6	C-F20h	3.67	0.482	1.85	1.143
7	C-G60	0.63	0.734	0.75	1.283
8	C-S8	0.93	0.668	0.77	0.984
9	C-M10	1.60	0.554	0.49	0.916
10	C-F10G30	0.84	0.643	0.87	0.873
11	C-F10G45	1.21	0.915	0.78	1.143
12	C-F10G60	0.42	0.713	0.58	1.064
13	C-F10G60h	2.08	0.589	0.55	1.130
14	C-F20S4	1.36	0.443	0.92	0.581
15	C-F20S6	1.23	0.570	0.62	0.883
16	C-F20S8	0.67	0.678	0.63	0.833
17	C-F20S8h	0.74	0.544	1.42	0.927
18	C-F20M6	1.24	0.852	0.91	0.998
19	C-F20M8	0.79	1.111	0.98	1.275
20	C-F20M10	0.50	0.869	0.54	1.044
21	C-F20M10h	1.11	1.097	1.04	1.168
22	C-G55S8	0.35	1.014	0.51	0.983
23	C-G55M10	0.64	0.340	0.20	0.837
24	CV-100	1.66	0.355	1.70	0.436
25	CV-100h	2.03	0.450	3.80	1.267
26	CV-F10G60	0.43	1.174	0.32	1.379
27	CV-F20S8	0.92	0.436	0.42	0.778
28	CV-M10	0.93	0.564	1.31	0.910
29	CL-100	2.85	0.751	1.75	0.624
30	CL-100h	5.33	0.933	9.19	1.253
31	CL-F10G60	0.54	0.682	0.61	0.955
32	CL-F20S8	0.89	0.777	0.62	0.759
33	CL-M10	0.91	1.879	1.22	1.538
34	CHA-100	3.30	0.702	3.06	0.613
35	CHA-100h	8.33	0.569	5.28	0.896
36	CHA-F10G60	0.55	1.253	0.48	1.031
37	CHA-F20S8	0.83	1.308	1.12	1.269
38	CHA-M10	0.71	0.745	0.58	0.469
39	C-100SS	1.46	0.610	1.91	0.544
40	C-F20S8SS	1.17	0.693	0.50	0.525

The effective diffusion coefficients at 28 days that were fit to the measured chloride profiles at 6 months is shown in Table 6-5 and at 12 months in Table 6-6. The average values of C_s for 6 and 12 months were 69.6 kg/m^3 and 88.0 kg/m^3, respectively. As the exposure period increased, the surface chloride was seen to increase. Fit chloride profiles compared to the measured chloride profiles are presented in Appendix C and Appendix D for 6 and 12 months, respectively.

Table 6-5: Effective chloride diffusion coefficients at 28 days acquired from 6 months of exposure

Mix No	Mix ID	C_s	D_{28} (m^2/s) × 10^{-12}		
		(kg/m^3)	m_1 C_s (fit)	m_1 C_s=100	RCMT (m_2) C_s=100
1	C-100	76.2	1.19	0.92	0.75
2	C-100h	37.8	3.57	1.03	0.85
3	C-F10	50.8	3.05	1.02	1.07
4	C-F20	51.0	1.63	0.95	1.27
5	C-F10h	74.9	2.60	2.07	2.00
6	C-F20h	49.7	1.42	0.80	0.36
7	C-G60	64.1	0.79	0.84	0.25
8	C-S8	75.6	0.66	0.70	0.75
9	C-M10	95.0	0.50	0.62	0.89
10	C-F10G30	50.0	1.20	0.78	0.57
11	C-F10G45	135.0	1.25	1.61	1.16
12	C-F10G60	36.0	1.09	0.33	0.19
13	C-F10G60h	45.0	2.05	0.41	0.50
14	C-F20S4	70.0	1.02	0.25	0.91
15	C-F20S6	59.6	0.93	0.74	1.09
16	C-F20S8	72.0	0.68	0.69	0.81
17	C-F20S8h	44.6	0.66	0.24	0.48
18	C-F20M6	62.3	1.81	1.09	1.35
19	C-F20M8	86.4	1.69	1.05	0.85
20	C-F20M10	50.0	1.00	0.68	0.50
21	C-F20M10h	80.0	1.02	0.87	1.06
22	C-G55S8	110.0	0.44	0.50	0.58
23	C-G55M10	75.0	0.27	0.30	0.21
24	CV-100	22.0	1.84	0.47	0.10
25	CV-100h	27.1	2.09	0.40	0.15
26	CV-F10G60	85.0	1.17	0.93	0.46
27	CV-F20S8	34.1	1.41	0.30	0.33
28	CV-M10	32.1	1.48	0.50	0.24
29	CL-100	82.4	1.96	1.67	1.09
30	CL-100h	84.0	4.74	4.11	2.25
31	CL-F10G60	39.1	2.21	0.47	0.30
32	CL-F20S8	80.0	1.00	0.81	0.77
33	CL-M10	220.0	0.96	2.01	1.57
34	CHA-100	65.0	2.53	1.76	0.76
35	CHA-100h	33.7	9.88	1.95	0.90
36	CHA-F10G60	102.6	1.08	1.23	0.85
37	CHA-F20S8	137.9	1.07	1.41	1.37
38	CHA-M10	48.2	1.15	0.55	0.42
39	C-100SS	56.4	1.93	0.92	0.94
40	C-F20S8SS	85.0	1.45	1.24	1.47

Table 6-6: Effective chloride diffusion coefficients at 28 days acquired from 12 months of exposure

Mix No	Mix ID	C_s	D_{28} (m^2/s) × 10^{-12}		
		(kg/m^3)	m_1 C_s (fit)	m_1 C_s=100	RCMT (m_2) C_s=100
1	C-100	35.5	5.45	0.70	0.91
2	C-100h	78.0	5.37	3.38	2.57
3	C-F10	108.0	1.45	1.54	1.65
4	C-F20	95.0	2.30	2.12	3.21
5	C-F10h	89.0	4.99	4.37	4.18
6	C-F20h	98.0	2.78	2.64	3.57
7	C-G60	112.0	1.70	1.97	0.94
8	C-S8	152.9	0.99	1.35	1.48
9	C-M10	92.0	0.43	0.40	0.33
10	C-F10G30	86.6	1.42	1.20	0.78
11	C-F10G45	116.0	1.49	2.08	1.34
12	C-F10G60	87.0	1.30	1.14	0.56
13	C-F10G60h	72.0	1.48	1.09	0.57
14	C-F20S4	53.0	1.59	0.64	0.77
15	C-F20S6	87.0	1.18	0.94	1.56
16	C-F20S8	93.5	0.86	0.81	1.01
17	C-F20S8h	84.0	2.50	2.05	5.21
18	C-F20M6	85.8	1.48	1.16	1.54
19	C-F20M8	110.0	1.94	3.59	1.75
20	C-F20M10	90.0	1.10	0.80	0.53
21	C-F20M10h	79.1	1.78	1.48	1.41
22	C-G55S8	86.8	1.43	1.33	1.63
23	C-G55M10	54.8	0.79	0.32	0.53
24	CV-100	42.5	1.37	0.42	0.30
25	CV-100h	146.0	2.80	5.68	4.15
26	CV-F10G60	98.0	1.58	1.56	0.61
27	CV-F20S8	99.2	0.58	0.57	0.87
28	CV-M10	87.8	1.35	1.21	1.45
29	CL-100	64.9	1.63	1.11	0.84
30	CL-100h	114.0	10.03	13.02	9.61
31	CL-F10G60	73.7	2.04	1.40	0.76
32	CL-F20S8	79.4	1.00	0.69	0.65
33	CL-M10	192.0	1.26	2.62	1.89
34	CHA-100	39.0	5.24	1.26	0.88
35	CHA-100h	82.0	6.82	5.65	4.31
36	CHA-F10G60	83.0	1.49	1.13	0.69
37	CHA-F20S8	124.0	2.15	2.89	2.77
38	CHA-M10	28.3	1.04	0.31	0.08
39	C-100SS	48.5	3.07	0.73	0.75
40	C-F20S8SS	52.0	0.98	0.57	0.72

The chloride profiles were calculated independently using the effective diffusion coefficients found from the formation factor results in order to compare the results to the measured chloride profiles. Table 6-7 shows the effective diffusion coefficients at 28 days fit to the formation factor results. Appendices E and F show the comparison of measured profiles and chloride profiles simulated using the effective diffusion coefficients taken from the formation factors at 6 and 12 months, respectively.

Table 6-7: Effective diffusion coefficient at 28 days from formation factor

Mix No	Mix ID	D_{28} (m^2/s) × 10^{-12}		
		Moist NIST C_s=100	Moist EIS C_s=100	Bucket conductivity meter C_s=100
1	C-100	3.22	1.75	5.88
2	C-100h	9.34	4.64	11.71
3	C-F10	2.72	2.55	6.64
4	C-F20	1.87	2.97	6.27
5	C-F10h	4.80	4.04	8.96
6	C-F20h	3.56	4.54	5.96
7	C-G60	2.84	1.60	1.85
8	C-S8	1.32	0.81	2.20
9	C-M10	1.43	1.48	2.27
10	C-F10G30	1.50	1.56	2.65
11	C-F10G45	1.11	1.51	2.36
12	C-F10G60	0.95	1.89	1.52
13	C-F10G60h	1.48	2.27	3.02
14	C-F20S4	0.84	3.12	1.52
15	C-F20S6	0.60	3.76	1.22
16	C-F20S8	0.73	4.22	1.53
17	C-F20S8h	1.40	7.62	2.76
18	C-F20M6	0.85	2.18	2.11
19	C-F20M8	0.70	1.82	1.60
20	C-F20M10	0.61	1.95	1.48
21	C-F20M10h	1.10	2.87	2.41
22	C-G55S8	1.50	4.78	1.92
23	C-G55M10	2.31	1.99	2.84
24	CV-100	2.69	2.21	6.23
25	CV-100h	5.98	4.43	9.78
26	CV-F10G60	0.95	2.18	1.53
27	CV-F20S8	0.52	3.04	1.08
28	CV-M10	0.90	1.51	2.14
29	CL-100	3.56	2.04	6.69
30	CL-100h	8.83	5.61	14.34
31	CL-F10G60	0.69	1.49	1.66
32	CL-F20S8	0.71	5.94	1.25
33	CL-M10	1.16	1.67	1.92
34	CHA-100	1.71	2.03	4.39
35	CHA-100h	3.92	3.27	5.98
36	CHA-F10G60	0.70	1.62	1.43
37	CHA-F20S8	0.39	2.29	1.08
38	CHA-M10	0.46	0.91	1.25
39	C-100SS	3.59	3.59	6.32
40	C-F20S8SS	0.58	0.58	1.26

The average R-squared values for the fit models for each mixture type are shown in Figure 6-11. When the surface concentration is removed from the analysis, the fits competently model the rate of ingress with depth. Additionally, the better fits seen with ternary blends could be indicative of lower uncertainties because of lower pore volumes.

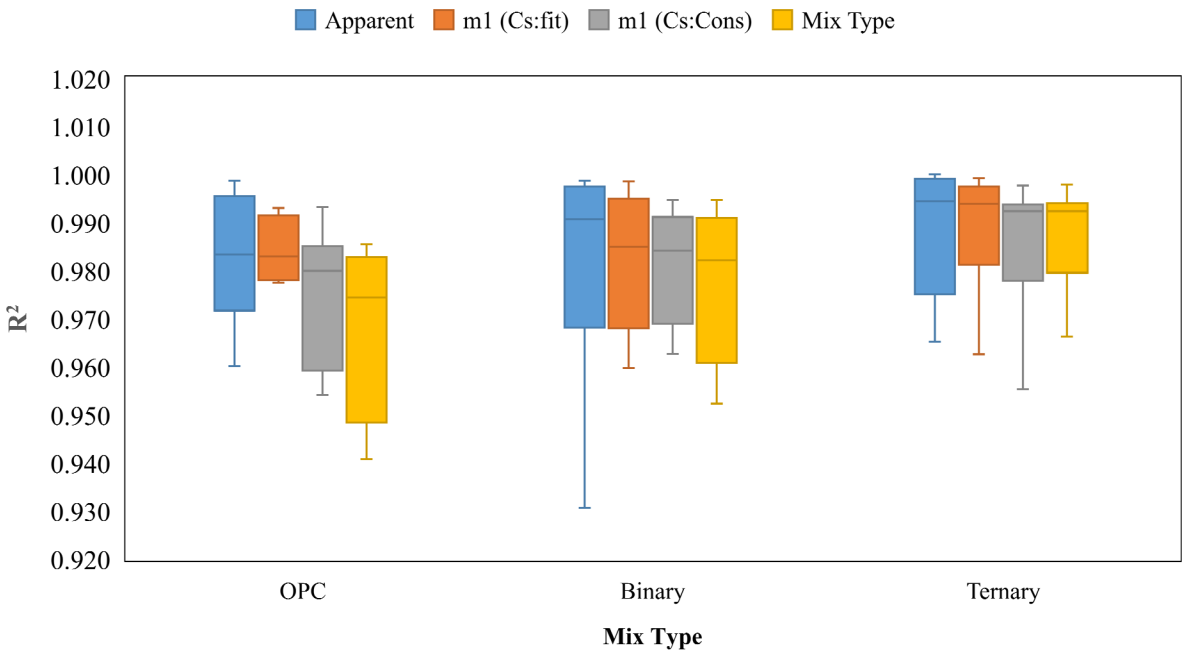

Figure 6-11: Average R-squared value for fit models

Figure 6-12 shows the average R-squared values obtained from comparing the chloride profiles from the effective diffusion coefficients calculated from formation factor and the measured chloride profiles. The simulations based on measurements from samples cured in the fog room appear to have a better fit to the measured chloride profiles. This could be due to the unusual decrease in the resistivity at later ages for the bucket-cured specimens, which added error to the formation factor calculations.

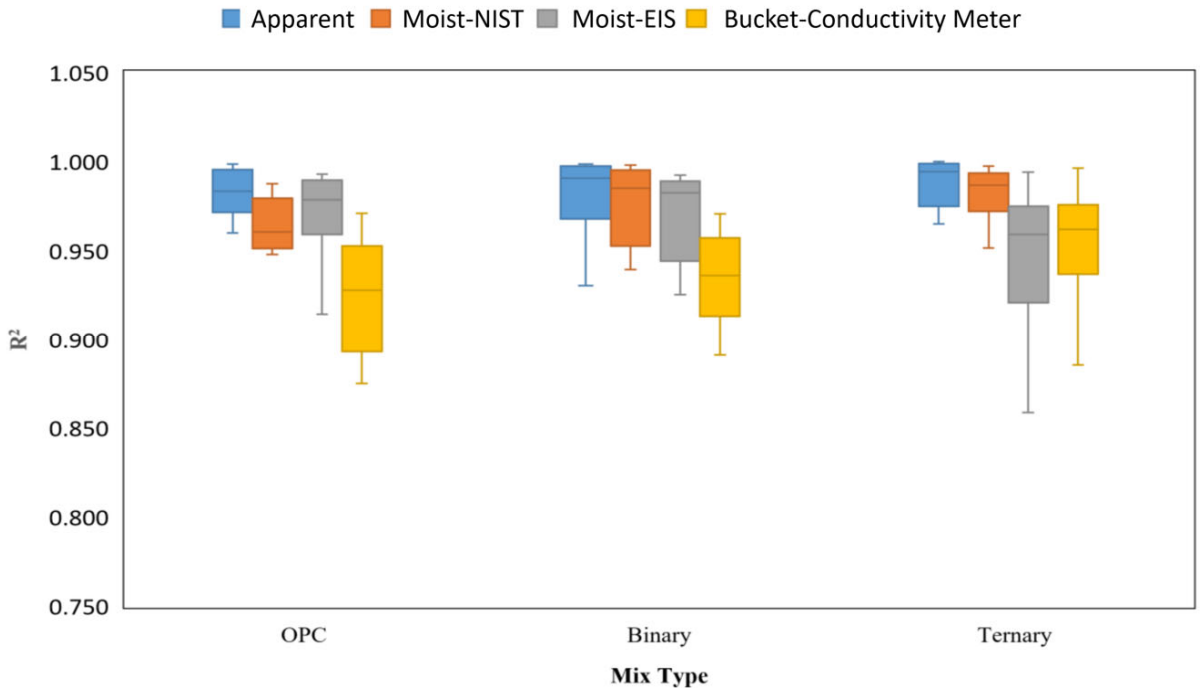

Figure 6-12: Average R-squared value for prediction models

The Moist-EIS model worked excellently for OPC mixtures; however, the Moist-NIST model performed better in binary and ternary mixtures. This could be due to the fact that formation factors for ternary and some binary mixtures for Moist-EIS were really high.

The correlation between the apparent diffusion coefficient at 6 and 12 months is shown in Figure 6-13. On average, the one-year diffusion coefficient is 10% lower than that calculated for 6 months of exposure. Because Equation 6-2 assumes a constant apparent diffusion coefficient and therefore calculates an average diffusion coefficient over the exposure period considered, the samples exposed to chlorides for 12 months would be expected to have a larger decrease in the diffusion coefficient from 6 months to 12 months than 10%. Most of the decrease in permeability occurs in the first 1 to 2 months, so this is also the time period when the diffusion coefficient decreases most.

The correlation between apparent diffusion and water permeability is shown at Figure 6-14. There were two outliers in the result which were Mix 30 and 35. When those two points are excluded, there is a strong correlation between water permeability and diffusion coefficient.

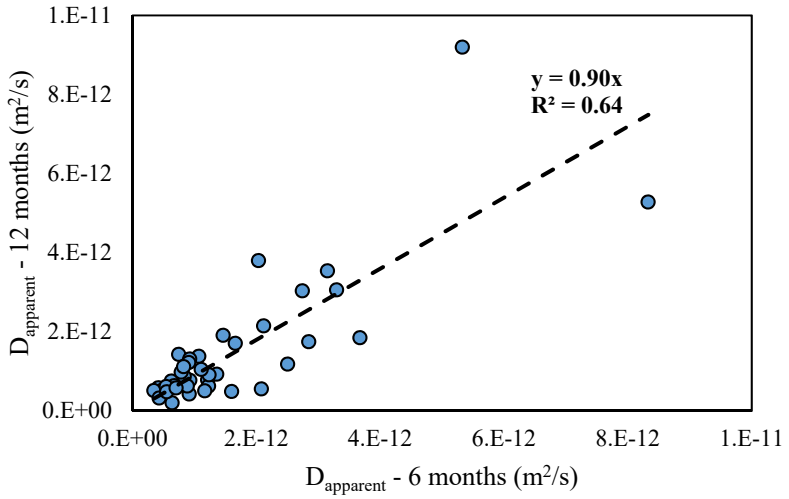

Figure 6-13: Apparent chloride diffusion coefficient at 6 and 12 months

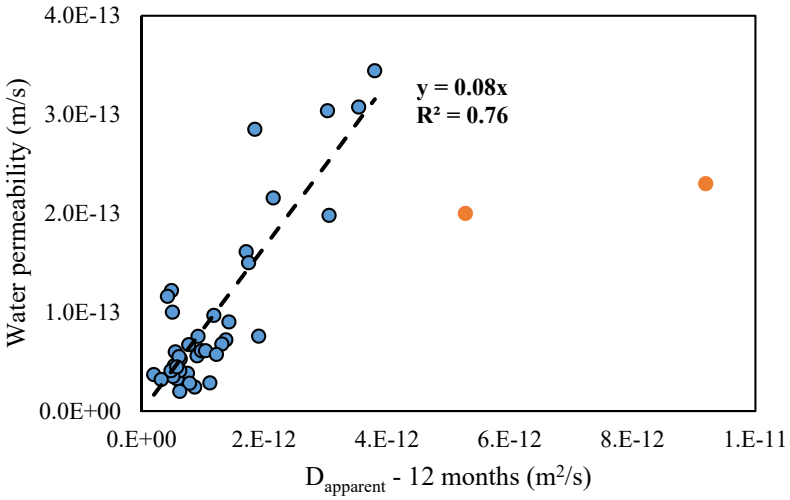

Figure 6-14: Correlation between apparent diffusion coefficient at 12 months and water permeability

The apparent diffusion coefficients at 12 months exposure were compared to the moist-room-cured bulk resistivity measurements at 28 and 56 days and after mixing as shown in Figure 6-15. A power law models well the relationship between bulk resistivity and apparent diffusion with the 56-day measurement showing a higher R-squared value of 0.81. This correlation value is high considering the variation expected with each method.

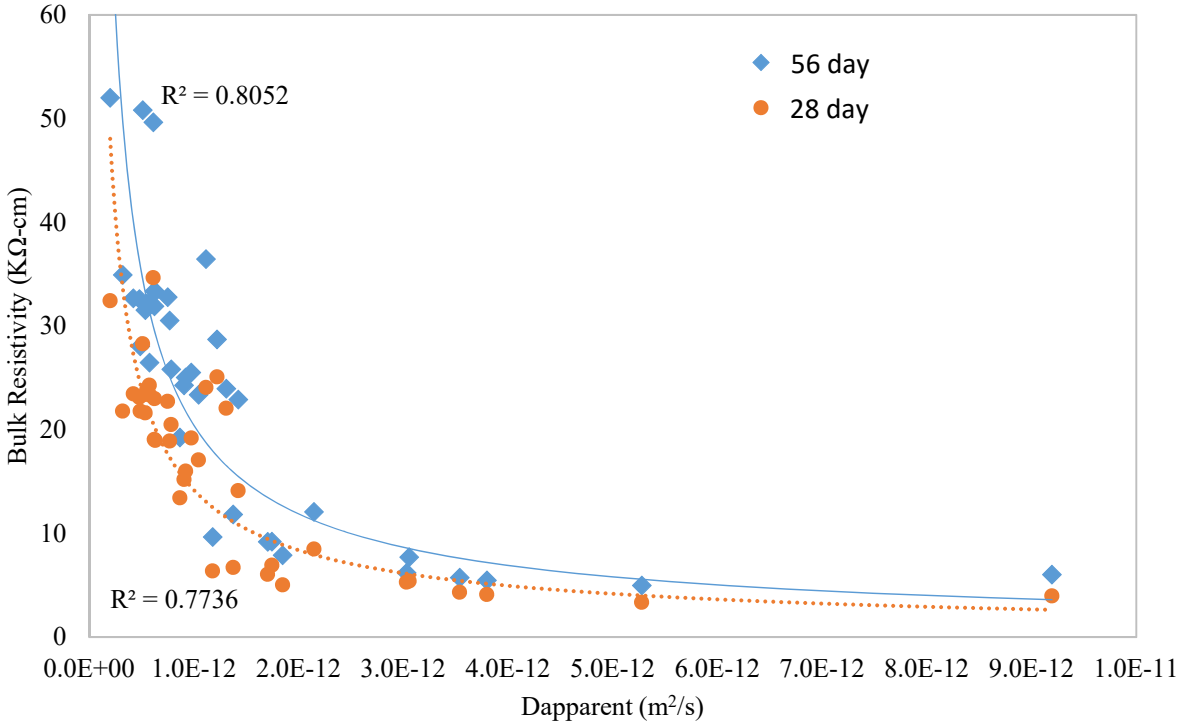

Figure 6-15: Correlation between apparent diffusion coefficient at 12 months to the moist-room-cured bulk resistivity at 28 and 56 days

Figure 6-16 shows the correlation between apparent diffusion coefficient and secondary water absorption rate. Two outlier data points were excluded from the trend-line. There is a strong correlation between diffusion and absorption, this could be because both tests are based on penetration of a fluid into the concrete.

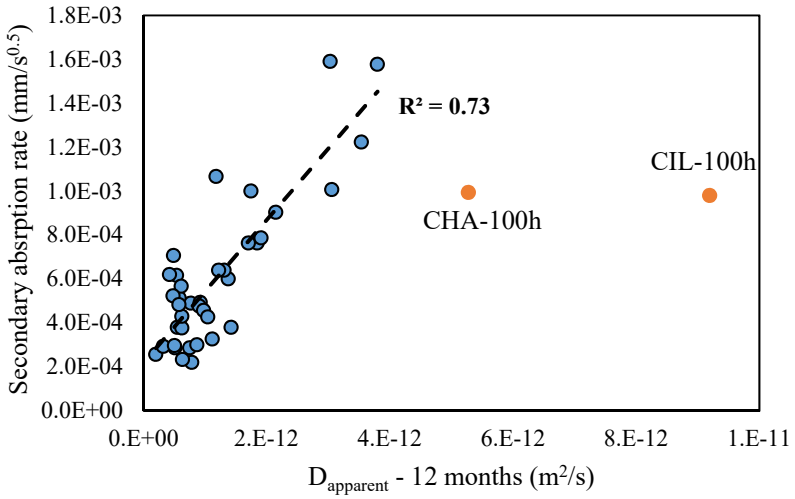

Figure 6-16: Correlation between apparent diffusion coefficient at 12 months and water absorption

Figure 6-17 shows the correlation between apparent diffusion coefficient and rapid chloride permeability test when the two outliers are excluded. A strong correlation with R-squared value of 0.85 is seen excluding the two outliers.

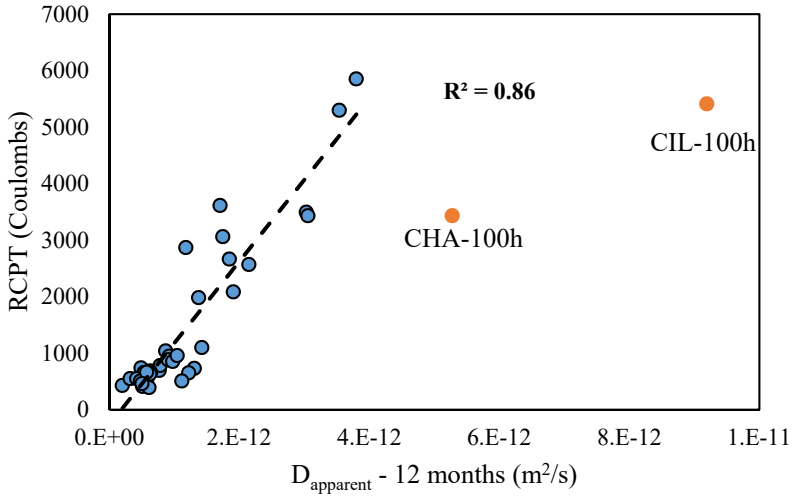

Figure 6-17: Correlation between apparent diffusion coefficient at 12 months and rapid chloride permeability

The diffusion coefficients calculated from rapid chloride migration tests also showed a strong correlation with the apparent diffusion coefficient as shown in Figure 6-18. The correlation is linear with R-squared value 0.82. Two outlier data points were excluded from the trend-line.

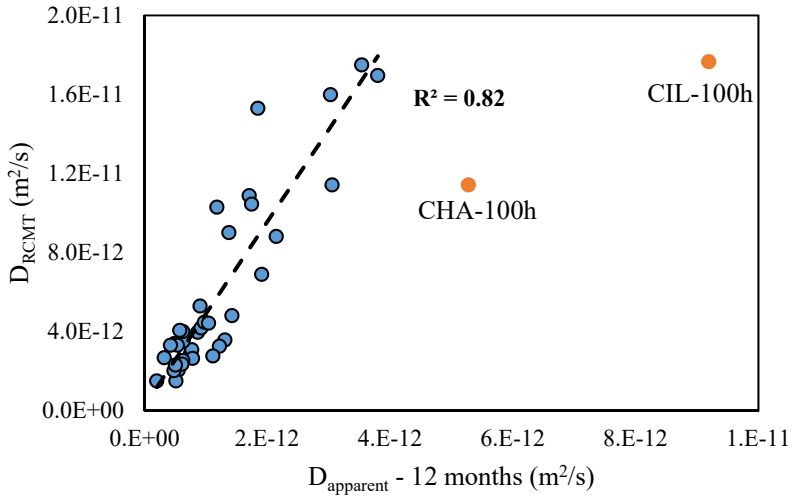

Figure 6-18: Correlation between apparent diffusion coefficient and non-steady state diffusion coefficient from chloride migration test

The diffusion coefficient calculated from bulk resistivity measurements has the potential to be used to determine the chloride profile. The differences seen between the simulated chloride profiles, calculated using effective diffusion coefficients determined from the formation factors, likely arises because the simulations use values for the porosity (volume of permeable voids), chloride binding (chloride binding capacity), effective diffusion coefficient, and density of the concrete, and each of those measurements has its own measurement error. When used together the combined error could diminish the usefulness of the simulation. However, the results simulated were conservative for most of the mixtures when there was a significant deviation between simulated and measured results, reducing the likelihood that issues with the use of the formation factor would lead to poor durability in the field. The samples cured in simulated pore solution consistently showed that the effective diffusion coefficients were too high. This was likely because increased sample saturation caused the samples to have lower resistivity values at later ages.

6.5 Summary

The chloride diffusion coefficients were determined in several ways from the measured chloride profiles after 6 and 12 months of salt water exposure in the bulk diffusion test. The apparent diffusion coefficients were calculated according to the procedures outlined in ASTM C1556, while the effective diffusion coefficients were fit to the chloride profiles with different aging coefficients and chloride surface concentrations. The effective diffusion coefficients were also calculated from

the concrete formation factor as a function of time and used to simulate the chloride profile for comparison against the measured chloride profiles. Bulk resistivity was shown to correlate well to the concrete apparent diffusion coefficient. Chloride ingress calculations performed using effective diffusion coefficients calculated from formation factor were shown to conservatively simulate measured profiles. Formation factor from moist-room-cured samples were shown to be closer to the measured profiles than samples cured in simulated pore solution. Given the complexity and uncertainty in quantifying the concrete pore solution required to calculate the formation factor from resistivity measurements, and the correlations seen between bulk resistivity and apparent diffusion coefficient for Florida materials, it is recommended to use 56-day bulk resistivity measurements in specifications.

CHAPTER 7. FIELD SITE DATA

7.1 Introduction

In this chapter, samples were taken from piles in marine exposure to validate the laboratory results performed as part of this project. The Key Royal Bridge site was selected for validation of the results. The Key Royal Bridge was constructed in 2006 and 2007, giving more than 12 years of chloride exposure between placement and coring. Fender piles were made from six different mixture designs. Cores taken from these concrete piles will provide useful information about the long-term durability performance of concrete with supplementary cementitious materials. The bulk resistivity and water absorption of the specimens were measured. Chloride content was measured at the outer surfaces of the piles where they were exposed to the marine environment. Three cored samples per pile were placed in chloride exposure tanks at the Florida Department of Transportation (FDOT) State Materials Office (SMO) to evaluate the concrete chloride penetration resistance.

7.2 Background

Concrete cores were taken from piles adjacent to the Key Royale Bridge, located on Anna Maria Island in Manatee Country, Florida to be used to validate the laboratory results. A satellite view of the bridge is shown in Figure 7-1. The 18-in. square fender piles cored were made from six different concrete mixture designs including a cement-only control mixture, a binary mixture containing fly ash, and ternary blends containing fly ash and ultrafine fly ash, slag, silica fume, or metakaolin. These piles were intended to serve as a concrete durability test bed for periodic sampling. The fender piles were fabricated with the same concrete and at the same time as the bridge piles [56]. Figure 7-2 shows a site plan of the Key Royal Bridge along with the location of the piles cored. Phase I fender piles were fabricated between June 8 and June 16 and placed in August 2006, while the Phase II fender piles were fabricated between September 28 and October 6 and placed in January, 2007.

Figure 7-1: Satellite view of the Key Royale Bridge (Source: Google & Apple)

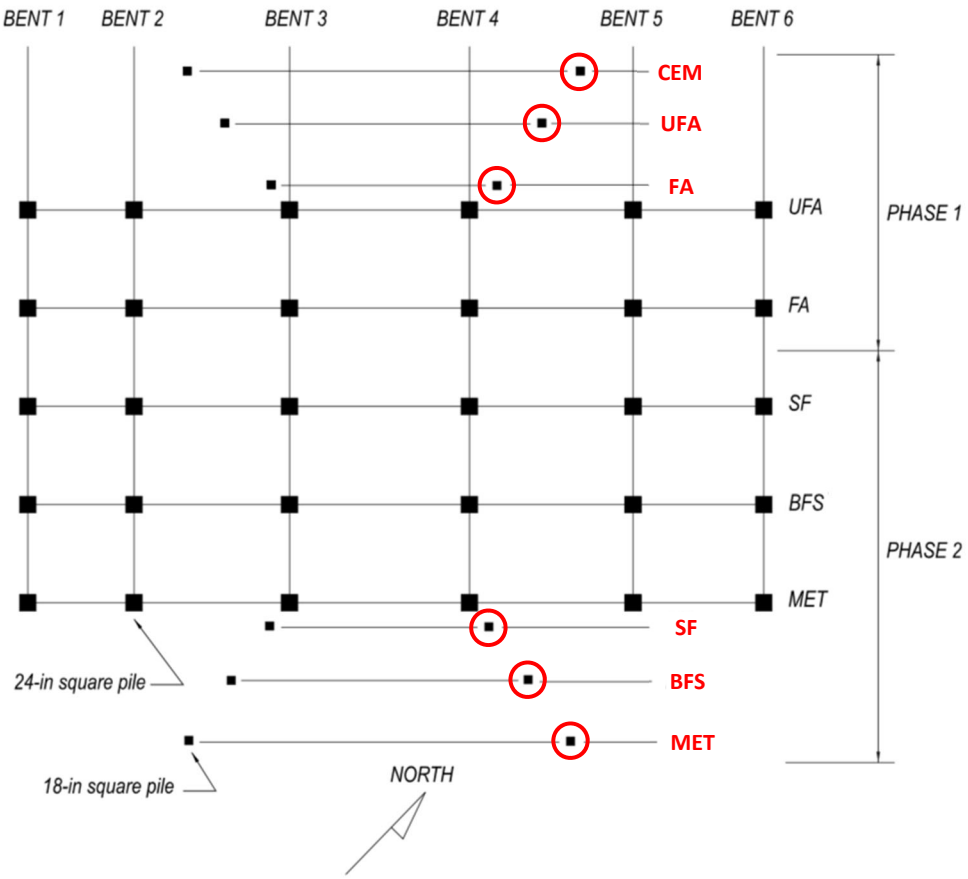

Figure 7-2: View of the site and selected piles for the extracting cores [56]

Table 7-1 shows the mixture composition used to produce concrete for the piles. All of the mixtures except for the control portland cement-only (CEM) mixture contained fly ash. All of the fly ash containing mixtures had 18% by mass of fly ash except the mixture with slag. That mixture contained only 15% fly ash by mass of cementitous materials because the total cementitious content was higher. The mixture proportions do not appear to have been adjusted to account for the different specific gravities of the supplementary cementitious materials. When portland cement is partially replaced with a supplementary cementitious material (SCM) by mass, the lower density SCM will occupy more volume per cubic yard of concrete than the portland cement. To account for this additional volume, the aggregate content is typically reduced. The mixture proportions

shown in Table 7-1 do not adjust the aggregate content for the additional cementitious material volume.

Table 7-1: Mixture composition for the Key Royal Bridge piles [56]

Material	Type	CEM	UFA	FA	SF	BFS	MET
Coarse Aggregate	#67	1840	1840	1840	1840	1840	1840
Fine Aggregate	Silica	806	806	806	806	806	806
Cement	Type II	970	670	795	715	670	695
Fly Ash	Type F	0	175	175	175	175	175
Slag	Grade 100	0	0	0	0	300	0
Ultrafine Fly Ash	Type F	0	125	0	0	0	0
Metakaolin	Type N	0	0	0	0	0	100
Silica Fume	Densified	0	0	0	80	0	0
Total Cementitious Material		970	970	970	970	1145	970
Water		330	333	333	333	333	333
w/cm		0.34	0.34	0.34	0.34	0.29	0.34
Air Entrainment Admixture	AEA	5	5	5	5	5	5
1st Admixture	Type D	28.6	28.6	28.6	28.6	28.6	28.6
2nd Admixture	Type F	42.9	42.9	42.9	42.9	42.9	42.9

7.3 Methodology

Overall, 18 4-in. diameter cores were collected as shown in Figure 7-3. The cores were roughly 7 in. in length. Three cores were taken from each pile at three elevations to evaluate the effects of elevation on chloride penetration. Figure 7-4 shows the labels assigned to the cores based on elevation.

shows the core elevation measured downward from the top of each pile and the distance from the pile side. The cores were labeled and placed in sealed bags for transport to and later testing at the University of Florida.

Figure 7-3: Getting core from the piles

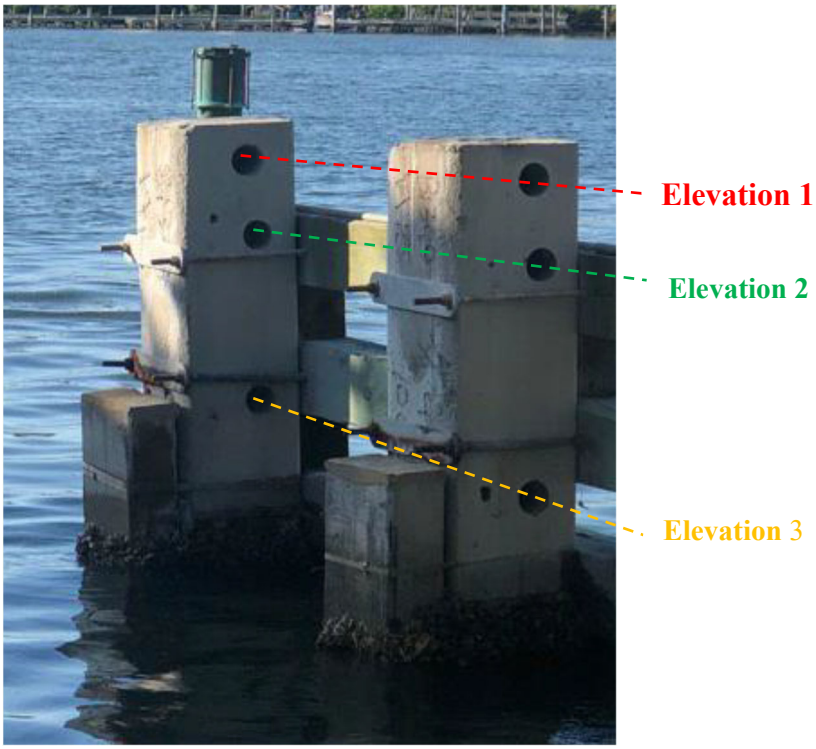

Figure 7-4: Cores were taken at three elevations

Table 7-2: Core locations

Pile No	Mix ID	Elevation ID	Distance from the top (in.)	Distance from the side (in.)
1	CEM	1	13.5	7
		2	21	7.5
		3	35	6.5
2	UFA	1	18	7.5
		2	27.5	7.5
		3	36	7
3	FA	1	15	6
		2	20	7
		3	36	6.5
4	SF	1	13	6
		2	25	6
		3	40	6
5	BFS	1	7	6.5
		2	15	5.5
		3	44	7
6	MET	1	5.5	7.5
		2	16	6
		3	40	7

After transferring the cores from the bridge location for testing to the University of Florida, the cores were cut into several pieces. Figure 7-5 shows the schematic of the core and test specimens. The top (exposed surface) 2-in. layer of each core was used to perform profile grinding and measure the field chloride profile from which an apparent diffusion coefficient was calculated. It was assumed that all intruded chlorides were contained within this section. Two interior 2-in. specimens were cut to measure the water absorption and bulk resistivity of the specimens. For the bulk resistivity, specimens were placed in a water tank for one week to condition the samples. The bottom 3-in. layer for each sample was used to calculate the concrete apparent diffusion coefficient from the measured lab chloride profile using procedures given in ASTM C1556 [23]. The samples were sawcut, after which the sides and one end were sealed with epoxy. After soaking the epoxied samples in saturated limewater for 2 days, they were placed in a 16.5% NaCl exposure tank at the SMO for 6 months. After the samples were removed from the saltwater tank, they were profile

ground. The acid soluble chloride concentrations of the concrete powder samples were measured according to FM 5-516 [53].

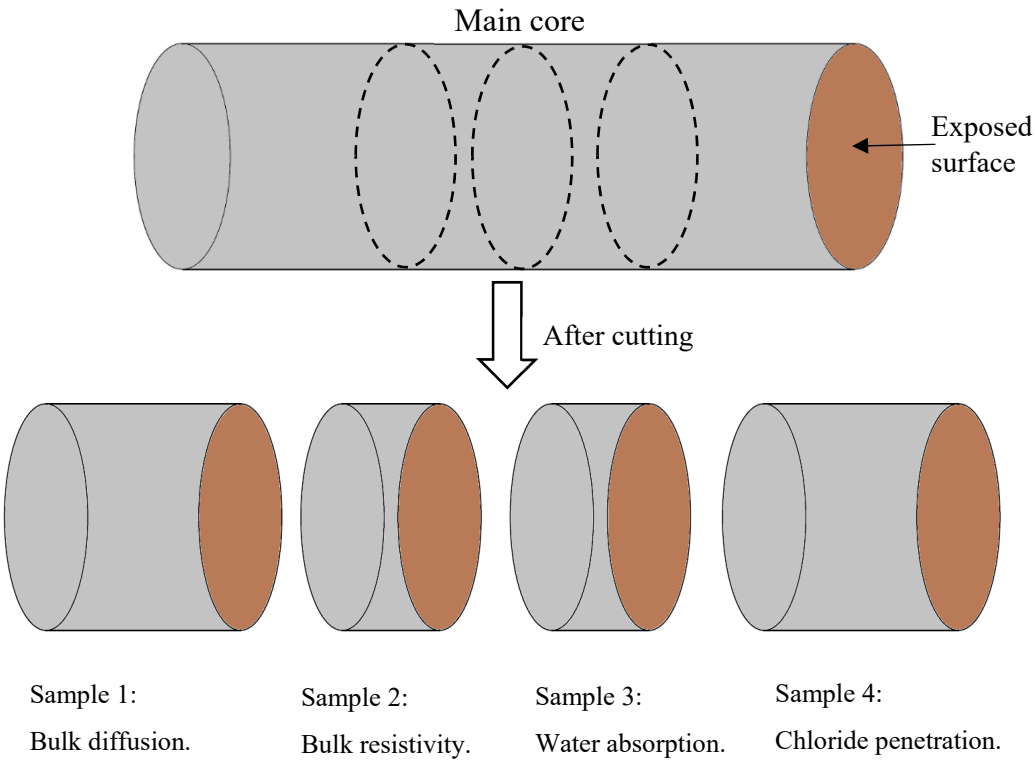

Figure 7-5: Schematic view of the cores and testing specimens

7.4 Results

Table 7-3 shows the diffusion coefficient results for the outer portions of the cores that were taken at the tidal and atmospheric zone. Elevation 1 could be considered as atmospheric zone and elevation 2 and 3 could be considered as splash zones. Appendix G shows the chloride profile results from the core surface and after saltwater exposure (ASTM C1556) for 6 months in the laboratory. The chloride surface concentration varied as the distance from the core location to the water level increased. In the first sample of pile No. 3, the amount of chloride was insignificant as marked in the table. A significant increase in chloride penetration was seen as the distance to the tidal zone decreased. The samples closest to the pile top had low chloride contents with depth and had varying levels of chloride surface concentrations. The apparent diffusion coefficient at

elevation 3 for the control mixture was between 3.7 and 7.8 times that calculated for the ternary blend mixtures, and 2.1 times that of the binary mixture containing fly ash. This illustrates the large benefits of SCMs in concrete.

Table 7-3: Apparent diffusion coefficients and surface chloride concentrations of the outer 2 in. of cores from the piles exposed for 12 to 13 years to intermittent splash/spray of seawater.

Pile No	MIX ID	Elevation ID	Distance from top of column (in.)	D_a (m^2/s) $\times 10^{-12}$	C_s (%)
1	CEM	1	13.5	0.198	0.295
		2	21	0.260	0.351
		3	35	1.11	0.482
2	UFA	1	18	0.062	0.273
		2	27.5	0.072	0.660
		3	36	0.300	1.033
3	FA	1	15	-	-
		2	20	0.150	0.305
		3	36	0.538	0.891
4	SF	1	13	0.069	0.217
		2	25	0.161	0.209
		3	40	0.142	0.505
5	BFS	1	7	0.093	0.403
		2	15	0.138	0.535
		3	44	0.204	0.862
6	MET	1	5.5	0.230	0.232
		2	16	0.436	0.164
		3	40	0.267	0.413

The diffusion coefficients were calculated for core sections that were exposed to sodium chloride in a saltwater tank at the FDOT for 6 months, as explained in the previous chapter. Table 7-4 shows the apparent chloride diffusion coefficients calculated from the chloride profiles obtained after 6 months of exposure. Figure 7-6 shows the apparent diffusion coefficients after 6 months of laboratory chloride exposure (ASTM C1556) compared to the chloride diffusion coefficients calculated from the 23- to 24-year field exposures to seawater splash and spray. The apparent diffusion coefficients measured in the saltwater tank were higher than those measured in the field because the samples in the field were likely only partially saturated because of the tidal action. Some similarities in relative performance between mixtures were seen between the measurements from the field and laboratory samples. Two of the mixtures – silica fume and slag – had the lowest

apparent diffusion coefficients in both the field and laboratory testing. Slag likely performed so well because of the lower w/cm than the other mixtures. Ultrafine fly ash performed better than the binary fly ash mixture, but not as well as the silica fume mixture and the slag mixture. Metakaolin had the highest apparent diffusion coefficient of the mixes with SCMs and showed the biggest difference between field and lab performance. Since metakaolin is a highly reactive pozzolan, this result was not expected. The source of this anomalous behavior is unknown.

Table 7-4: Apparent diffusion coefficient and surface chloride concentration of the inner (bottom) 3-inch section of one core from each pile; 12 to 13 years of service with negligible penetration of chlorides followed by 6 months of laboratory chloride exposure for ASTM C1556 bulk diffusion testing.

Column No	Mix ID	D_a (m^2/s) × 10^{-12}	C_s (%)
1	CEM	3.21	0.738
2	UFA	1.00	0.654
3	FA	1.42	1.380
4	SF	0.725	0.467
5	BFS	0.296	0.821
6	MET	2.56	0.855

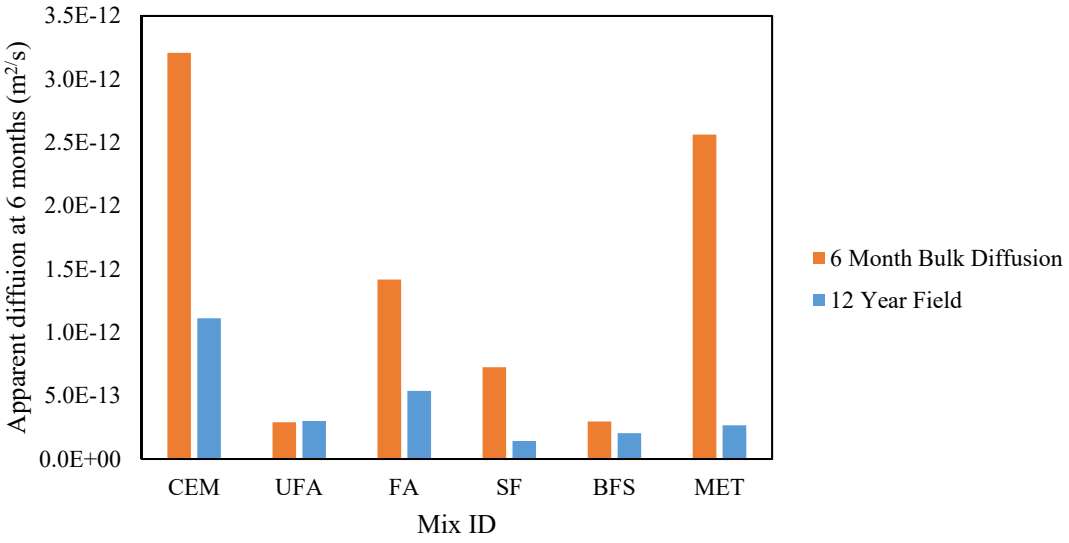

Figure 7-6: Apparent diffusion coefficient at 6 months of exposure

The electrical resistivity and secondary absorption rate of the cores that were taken from the pile were determined, as shown in Table 7-5. The bulk resistivity results shown were significantly lower than surface resistivity results measured at 365 days [56]. This could be partly explained by the geometrical correction factor [57] not being applied to the surface resistivity values reported. The different curing temperatures and moisture conditions that small cylinders and piles experience during curing could also lead to different results.

Table 7-5: Electrical resistivity and water absorption of the mixtures

Pile No	Mix ID	Bulk Resistivity (kΩ·cm)	Secondary absorption rate ($mm/s^{0.5}$)
1	CEM	15.0	9.23E-04
2	UFA	61.9	2.50E-04
3	FA	25.9	3.20E-04
4	SF	55.4	2.70E-04
5	BFS	72.1	2.80E-04
6	MET	36.4	6.97E-04

Similar to the diffusion results, there was a significant difference between the control mixture and mixtures incorporating SCMs. All of the mixtures with highly reactive pozzolans showed high resistivity values and low secondary absorption rates, with the exception of the metakaolin secondary absorption rate. It is possible that the concrete in the pile center where the concrete sample for secondary absorption was taken had different properties than the outer 2 in., leading to differences between the concrete apparent diffusion coefficient from over 12 years of field exposure and the 6 month lab saltwater exposure.

Figure 7-7 shows the relationship between bulk resistivity and apparent diffusion coefficient after exposure to 16.5% NaCl solution for 6 months for the samples taken from the Key Royal Bridge piles. Those data points are shown with the bulk resistivity and apparent diffusion coefficient test results from laboratory made samples. In this comparison the 6-month bulk resistivity measurements were compared to apparent diffusion coefficients from 6 months of chloride exposure, while the 12-month bulk resistivity measurements were compared to the apparent

diffusion coefficients from 12 months of chloride exposure. The measurements from the Key Royal Bridge piles validate the trends seen from the laboratory-made samples.

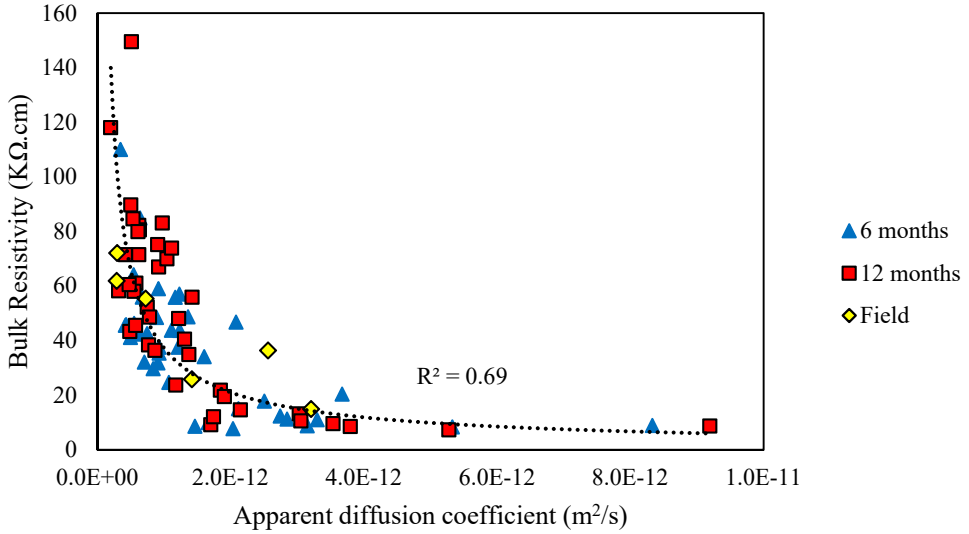

Figure 7-7: Relationship between and bulk electrical resistivity and apparent diffusion coefficient

Figure 7-8 shows the correlation between secondary absorption rate and electrical resistivity for all laboratory-made samples tested at 28, 56, and 365 days along with the data from the field samples. The results from field specimens lined up with lab results described in chapters 5 and 6.

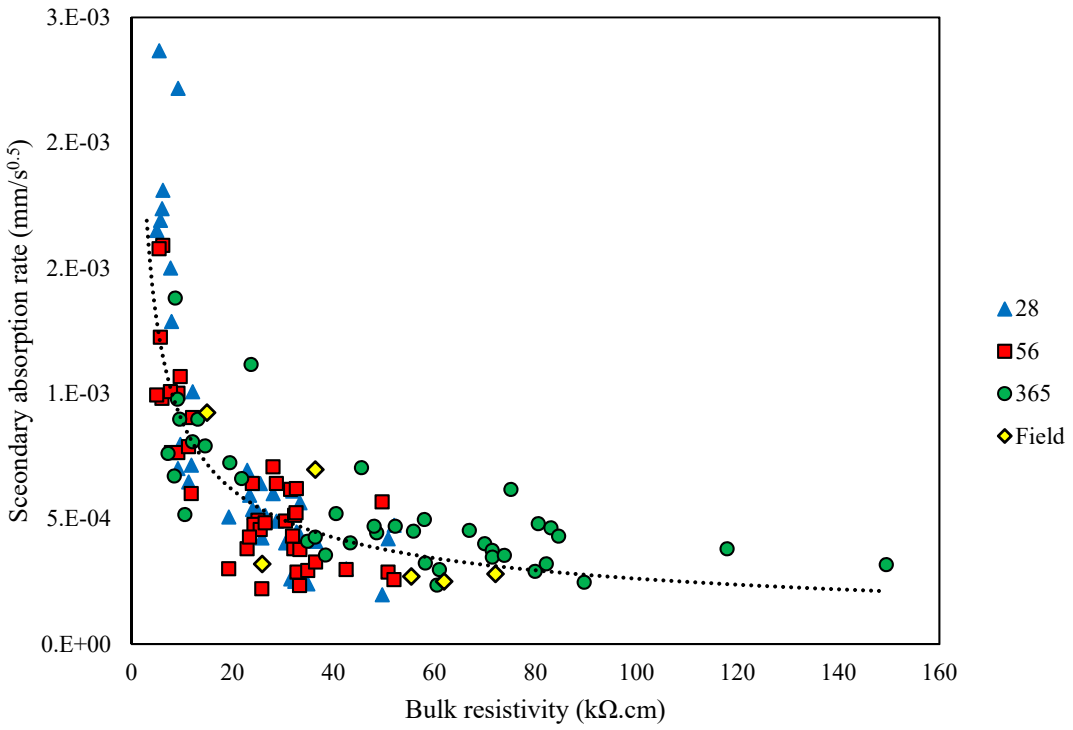

Figure 7-8: Relationship between secondary absorption rate and bulk electrical resistivity

7.5 Summary

Concrete cores were collected from 6 piles placed next to the Key Royale Bridge in Manatee County to validate the laboratory results. The piles were made from 6 different concrete mixtures including a control portland cement-only mixture, a binary mixture containing fly ash, and ternary blend mixtures containing fly ash and slag, silica fume, ultrafine fly ash, or metakaolin. The samples were tested for electrical resistivity, water absorption, and chloride bulk diffusion. Also, a set of samples from the cores were placed in a chloride tank to measure the chloride penetration in lab condition. It was found that the apparent diffusion coefficients fit to the field surface chloride profiles were much lower than those from the salt water tanks. This is likely because the concrete in the piles was only partially saturated in the field. The mixtures containing silica fume or slag cement were found to have the lowest apparent diffusion coefficients. It was seen that field results lined up with the experimental results that were collected in laboratory conditions, validating the laboratory tests performed.

CHAPTER 8. SULFATE ATTACK DURABILITY

8.1 Introduction

External sulfate attack of concrete occurs because of sulfate ions transported into the concrete from water in contact with the structure. Concrete prisms were made for sulfate exposure testing from the same mixtures used to test the concrete transport properties. The concrete prism were made and exposed to a sulfate solution using a method similar to that prescribed for ASTM C1012 [58] to compare the expansion results to the concrete transport properties. Because ASTM C1012 does not account for variations in water-cementitious material ratio (w/cm) on the durability, Drimalas modified ASTM C1012 to use 3 x 3 x 11.25 in. concrete prisms instead of the standard mortar prisms [59]. To accommodate larger aggregates used in this study, 4 x 4 x 11.25 in. concrete prisms were used. Results from this comparison can be used to quantify the benefits of a low water-cementitious materials ratio (w/cm) and use of supplementary cementitious materials (SCMs) in mitigating sulfate attack.

8.2 Methodology

Thirty-eight concrete mixtures were made to measure the concrete sulfate resistance [60,61]. Four cements with oxide compositions shown in Table 2-5 were used. Table 2-6 shows the cement phase compositions as measured by x-ray diffraction with Rietveld refinement. Grade 120 ASTM C989 slag cement, ASTM C618 class F fly ash, ASTM C618 metakaolin, and ASTM C1240 silica fume were also used with compositions shown in Table 2-5. Table 2-6 shows the concrete mixture designs used. For every mix, three steel prism molds were assembled with gauge studs attached to each inner mold end in accordance with ASTM C490 [24]. An example of prism molds ready for use is shown in Figure 8-1. The steel molds were oiled with 5W-20 engine oil to facilitate concrete removal. After mixing the concrete following ASTM C192 [35], concrete was placed in the molds using a scoop in two layers, as shown in Figure 8-2. After the first layer of concrete was placed, the prism mold was vibrated on a vibrating table as shown in Figure 8-2, before the second layer was added. The mold was vibrated again and finished using a trowel as seen in Figure 8-3. The prisms were covered with a plastic sheet at the concrete mixing laboratory for the first 24 hours of curing after mixing, as shown in as shown in Figure 8-4. They were then demolded as shown in

Figure 8-5, and cured until 28-days old in a moist room in accordance with the requirements of ASTM C511 [36], as shown in Figure 8-6.

Figure 8-1: Prism molds assembled and ready for use

Figure 8-2: Concrete placement in mold

Figure 8-3: Prism being finished

Figure 8-4: Sample after finishing

Figure 8-5: Prism demolding after initial curing

Figure 8-6: Samples placed in moist curing room for curing prior to sulfate exposure

After curing for 28 days, initial lengths of the three concrete prisms from each mixture were measured. As shown in Figure 8-7, the readings were made using a length-change comparator as specified in ASTM C490. After the initial reading, the three prisms were put in a sealable container that contained 3.5 to 4.5 times their volumes in a 5% sodium sulfate solution. The solution was made at least 24 hours before submerging the prisms as required by ASTM C1012 section 5.4. After the initial readings, readings were taken at weeks 1, 2, 3, 4, 8, 13, and 15. After week 15, the subsequent length measurements were taken at 4, 6, 9, 12, 15, and 18 months. Length changes were calculated according to ASTM C1012 and Equation 8-1:

$$L = \frac{(L_x - L_i)}{G} \times 100 \qquad \text{Equation 8-1}$$

Where, L is the change in length (%), L_x is the comparator reading of specimen at x age minus the comparator reading of the reference bar at x age (in.), L_i is the initial comparator reading of the specimen minus the comparator reading of the reference bar at that same time (in.), and G is the nominal gauge length, (10 in.).

Figure 8-7: Concrete prism in length comparator

The prisms were returned to the 5% sodium sulfate solution in the sealed container after every reading, as shown in Figure 8-8. The solution was replaced with new sodium sulfate solution at the time of each measurement age.

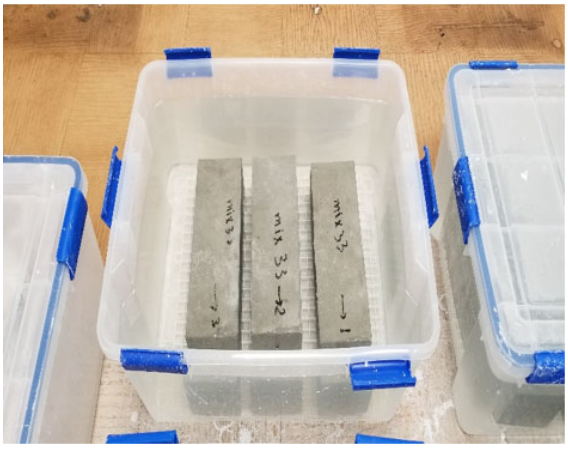

Figure 8-8: Prisms stored in 5% sodium sulfate solution

8.3 Results

Prisms for all 38 mixtures have been exposed to a 5% sodium sulfate solution for at least 18 months. Some of the mixtures have now reached 24 months of exposure. Table 8-1 shows the expansion results by age for each mixture, while Table 8-2 shows the mass gain for each mixture. Dashes are given in Table 8-1 and Table 8-2 for measurements that have not been taken yet. Figure 8-9 and Figure 8-10 show the expansion results for the portland cement (OPC) and binary blend mixtures, respectively. Figure 8-11 shows the expansion results for the ternary blend mixtures containing 10% fly ash, Figure 8-12 shows the expansion results for the ternary blend mixtures containing 20% fly ash, and Figure 8-13 shows the expansion results for the ternary blend mixtures containing metakaolin. For the OPC mixtures at 0.44 w/cm, only the IL cement was below 0.04% expansion at 2 years. The Type I/II cement at 0.44 w/cm (mix 2) and high alkali cement at 0.44 (mix 35) showed the highest expansions at 2 years as expected, because they had the highest C_3A contents. Lower w/cm improved the performance of the OPC mixtures significantly. The SCMs and lower w/cm improved the performance of the concrete mixtures. None of the binary or ternary mixtures showed expansion greater than 0.04% during the time period tested. A comparison of the expansion at 18 months with the 28-day formation factor was made, as shown in Figure 8-14. Sulfate durability of concrete involves several mechanisms, only one of which is sulfate ion diffusion, giving this comparison only marginal benefit. A slight correlation was seen between sulfate durability and transport properties. It is not expected that a good correlation will be found because sulfate durability is reliant on chemical composition and sulfate transport, however the correlation found does give some credence to the idea that a principal mechanism of sulfate durability improvement by SCMs is reduction in transport. More time is needed to further differentiate mixture performance, however, because expansion had just started on some prisms at exposures greater than 1 year.

Table 8-1: Concrete prism length change results after exposure to 5% sodium sulfate solution

Mix #	Mix ID	Length Change (%)													
		Weeks of Exposure to 5% Sodium Sulfate Solution													
		1	2	3	4	8	13	15	17	26	39	52	65	78	104
1	I/II-100	0.001	0.002	-0.001	-0.005	-0.002	0.002	-0.002	0.001	-0.003	-0.001	-0.001	0.002	0.010	0.011
2	I/II-100h	0.003	0.001	0.001	0.001	0.002	0.001	-0.001	0.013	0.007	0.008	0.013	0.023	0.032	0.072
3	I/II-F10	0.001	-0.002	-0.004	0.002	0.002	0.002	0.000	-0.002	0.001	-0.001	-0.002	0.001	0.011	0.016
4	I/II-F20	0.004	-0.004	0.005	0.004	0.003	0.004	0.004	0.003	0.009	0.002	0.002	0.003	0.013	0.019
5	I/II-F10h	0.002	-0.002	0.001	0.002	-0.006	-0.001	0.001	0.003	0.001	0.006	0.006	0.012	0.018	0.027
6	I/II-F20h	0.001	-0.003	-0.001	-0.001	-0.004	-0.002	0.005	-0.005	0.003	0.005	0.006	0.010	0.018	0.030
7	I/II-G60	0.007	0.007	0.009	0.007	0.014	0.016	0.018	0.001	0.010	0.012	0.011	0.018	0.022	0.027
8	I/II-S8	0.006	0.009	0.005	0.012	0.017	0.006	0.004	0.008	0.010	0.009	0.012	0.015	0.025	-
9	I/II-M10	0.006	0.010	0.003	0.011	0.012	0.008	0.005	0.010	0.008	0.007	0.009	0.017	0.022	-
10	I/II-F10G30	0.004	0.004	0.001	0.004	0.005	0.007	0.015	0.004	0.005	0.006	0.014	0.014	0.018	-
11	I/II-F10G45	0.006	0.004	0.003	0.003	0.006	0.006	0.006	0.002	0.005	0.005	0.010	0.014	0.017	-
12	I/II-F10G60	0.004	-0.005	0.000	0.005	0.001	0.014	0.003	0.002	-0.001	0.004	0.006	0.008	0.010	-
13	I/II-F10G60h	-0.001	0.000	-0.006	-0.003	0.003	0.003	0.006	-0.002	-0.004	-0.001	-0.003	0.003	0.008	0.011
14	I/II-F20S4	0.005	0.005	0.019	0.003	0.003	-0.006	-0.005	-0.006	-0.003	-0.002	0.000	0.008	0.007	-
15	I/II-F20S6	0.008	0.003	0.018	0.004	0.002	0.000	0.001	0.000	0.003	0.003	0.006	0.014	0.016	-
16	I/II-F20S8	-0.004	0.013	-0.005	0.016	-0.004	-0.004	-0.005	-0.004	-0.003	-0.004	0.002	0.007	0.009	-
17	I/II-F20S8h	0.001	0.004	0.003	0.005	0.006	0.000	0.000	-0.001	0.001	0.002	0.006	0.014	0.015	-
18	I/II-F20M6	-0.004	0.013	-0.007	0.021	-0.004	-0.005	-0.006	-0.007	-0.004	-0.006	0.001	0.006	0.007	-
19	I/II-F20M8	0.018	-0.002	0.005	0.002	-0.004	-0.003	-0.001	-0.003	-0.002	-0.002	0.004	0.009	0.013	-
20	I/II-F20M10	0.017	-0.003	0.006	0.001	-0.005	-0.003	-0.001	-0.003	-0.001	-0.001	0.004	0.009	0.014	-
21	I/II-F20M10h	0.004	0.004	0.001	0.001	0.004	-0.002	-0.003	-0.005	-0.003	-0.003	0.002	0.008	0.007	-
22	I/II-G55S8	0.004	0.010	0.007	0.009	0.004	0.005	0.008	0.004	0.005	0.002	0.005	0.014	0.017	-
23	I/II-G55M10	0.001	0.006	0.003	0.005	0.003	0.005	0.003	0.000	0.001	-0.003	0.001	0.009	0.013	-
24	V-100	0.001	0.003	0.002	0.000	0.003	0.006	-0.002	0.003	0.001	0.001	0.004	0.007	0.015	0.016
25	V-100h	0.011	0.012	0.010	0.003	0.009	0.014	0.015	0.022	0.014	0.017	0.018	0.024	0.031	0.041
26	V-F10G60	-0.001	0.001	0.001	0.007	0.006	0.007	0.007	0.006	0.002	0.001	0.005	0.011	0.014	-

Mix #	Mix ID	Length Change (%)													
		Weeks of Exposure to 5% Sodium Sulfate Solution													
		1	2	3	4	8	13	15	17	26	39	52	65	78	104
27	V-F20S8	-0.001	0.000	0.000	-0.002	0.003	0.007	0.001	0.003	0.001	0.001	0.002	0.008	0.014	-
28	V-M10	-0.003	-0.002	-0.002	-0.007	0.003	0.006	0.005	0.002	-0.003	-0.003	-0.002	0.007	0.013	-
29	IL-100	-0.010	0.000	0.000	-0.004	-0.001	0.000	-0.001	0.001	0.003	-0.005	-0.003	0.004	0.010	0.019
30	IL-100h	0.006	0.006	0.005	0.002	0.006	0.003	0.008	0.007	0.008	0.006	0.010	0.011	0.022	0.036
31	IL-F10G60	-0.003	0.003	0.005	0.003	0.002	-0.003	0.005	-0.002	-0.003	-0.004	0.004	0.009	0.012	-
32	IL-F20S8	-0.002	0.001	-0.009	-0.004	-0.002	-0.003	-0.006	-0.006	-0.004	-0.005	-0.002	0.006	0.008	-
33	IL-M10	0.000	-0.010	-0.003	-0.001	0.013	-0.004	-0.006	-0.005	-0.005	-0.006	-0.004	0.008	0.011	-
34	IHA-100	-0.001	0.005	0.004	0.005	0.006	0.008	0.011	0.011	0.011	0.006	0.008	0.018	0.025	0.035
35	IHA-100h	0.003	0.004	0.000	0.002	0.008	-0.002	0.010	0.009	0.012	0.010	0.015	0.020	0.035	0.063
36	IHA-F10G60	-0.003	-0.002	0.003	0.001	0.001	-0.001	0.002	-0.004	-0.002	-0.004	0.003	0.009	0.012	-
37	IHA-F20S8	-0.002	0.001	-0.009	-0.002	-0.001	-0.002	-0.004	-0.003	0.000	-0.001	0.001	0.009	0.013	-
38	IHA-M10	0.001	-0.007	-0.007	0.001	0.017	-0.004	-0.004	-0.003	-0.001	0.000	0.004	0.013	0.016	-

Table 8-2: Concrete prism weight change results after exposure to 5% sodium sulfate solution

Mix#	Mix ID	Weight Change (g)														
		Weeks of Exposure to 5% Sodium Sulfate Solution														
		0	1	2	3	4	8	13	15	17	26	39	52	65	78	104
1	I/II-100	0.0	-1.8	-1.8	-0.5	4.2	11.9	16.0	17.8	19.2	27.2	34.8	41.4	48.7	51.3	65.5
2	I/II-100h	0.0	-1.5	-0.8	-0.8	-0.5	2.0	5.9	7.9	8.5	17.8	28.4	41.9	59.0	73.8	132.1
3	I/II-F10	0.0	0.0	0.0	0.0	-0.3	3.6	6.7	8.2	8.6	13.6	19.7	22.5	27.1	28.1	36.9
4	I/II-F20	0.0	0.0	0.0	0.0	-1.2	3.5	6.5	7.6	8.6	13.9	18.3	21.3	26.0	26.6	35.4
5	I/II-F10h	0.0	-2.9	-3.5	-2.0	-0.5	4.4	9.8	11.2	12.2	20.3	28.7	36.1	42.8	47.2	65.0
6	I/II-F20h	0.0	-4.8	-6.7	-5.0	-5.0	-3.8	0.0	0.8	0.9	7.4	12.1	15.0	18.9	19.8	29.5
7	I/II-G60	0.0	1.2	0.5	0.6	-0.2	0.6	0.5	0.0	0.6	3.9	5.3	8.3	10.7	13.8	19.5
8	I/II-S8	0.0	-0.8	-1.1	-2.0	-3.0	-2.9	-3.0	-3.9	-3.9	-1.4	0.8	3.8	6.5	12.9	-
9	I/II-M10	0.0	-1.7	-2.1	-3.0	-2.9	-3.9	-3.9	-5.0	-5.3	-3.0	-2.1	0.5	1.2	6.5	-

Mix#	Mix ID	Weight Change (g)														
		Weeks of Exposure to 5% Sodium Sulfate Solution														
		0	1	2	3	4	8	13	15	17	26	39	52	65	78	104
10	I/II-F10G30	0.0	0.3	-2.3	-1.8	-1.1	0.3	2.1	3.8	4.1	7.7	10.1	12.2	12.1	15.7	-
11	I/II-F10G45	0.0	-1.7	-2.6	-3.5	-3.2	-3.0	-1.8	-3.0	-3.0	-1.4	-0.3	1.5	2.4	7.0	-
12	I/II-F10G60	0.0	0.2	-1.5	-1.5	-1.5	-2.9	-2.6	-2.6	-2.4	-0.2	0.9	2.0	2.0	7.1	-
13	I/II-F10G60h	0.0	0.6	1.4	-0.6	-1.5	-2.6	-3.5	-4.4	-4.1	-3.2	-3.5	-2.7	-1.1	0.3	2.7
14	I/II-F20S4	0.0	-0.3	-1.4	-2.6	-2.7	-3.6	-2.9	-2.6	-3.6	-1.5	1.2	5.4	6.7	10.0	-
15	I/II-F20S6	0.0	-0.6	-2.1	-3.3	-3.6	-4.8	-4.1	-3.3	-5.4	-3.6	-1.5	2.4	4.2	8.8	-
16	I/II-F20S8	0.0	-0.5	-0.3	-0.3	-0.5	3.0	5.9	5.6	6.8	13.5	21.0	25.9	30.2	34.5	-
17	I/II-F20S8h	0.0	0.3	-1.5	-2.0	-3.5	-3.6	-2.4	-2.6	-2.3	2.0	7.3	12.4	14.7	19.5	-
18	I/II-F20M6	0.0	2.9	3.5	4.5	4.8	8.3	12.4	12.4	13.3	19.1	24.9	28.7	31.4	34.6	-
19	I/II-F20M8	0.0	0.0	0.0	-1.2	-1.2	-0.2	1.2	0.3	0.8	4.2	8.2	9.4	15.4	17.8	-
20	I/II-F20M10	0.0	0.2	-0.9	-2.4	-3.0	-2.4	-2.1	-2.6	-2.7	-0.8	2.0	2.1	5.4	7.0	-
21	I/II-F20M10h	0.0	2.3	1.2	1.5	0.9	4.2	6.7	7.1	7.1	10.3	14.7	17.5	18.0	21.3	-
22	I/II-G55S8	0.0	-1.7	-2.6	-3.0	-3.8	-5.7	-7.1	-7.9	-8.5	-8.3	-8.5	-7.0	-8.5	-5.9	-
23	I/II-G55M10	0.0	-2.6	-3.5	-4.5	-5.4	-6.8	-7.7	-7.7	-7.7	-6.0	-5.0	-3.0	-4.4	-1.7	-
24	V-100	0.0	-1.4	-2.3	-2.6	-1.2	1.7	5.4	7.0	8.0	15.0	21.0	25.1	30.7	31.6	45.2
25	V-100h	0.0	-3.9	-3.5	-3.8	-3.0	1.8	7.3	9.5	11.2	20.6	29.0	37.2	46.0	51.6	73.6
26	V-F10G60	0.0	0.8	-1.2	-1.7	-2.1	-3.0	-3.9	-4.7	-3.8	-1.8	-0.9	1.1	0.8	5.4	-
27	V-F20S8	0.0	1.4	0.8	0.5	0.2	2.0	3.0	4.5	5.3	11.9	20.3	26.2	29.6	36.6	-
28	V-M10	0.0	0.0	-0.5	-0.2	0.5	5.0	8.5	8.6	9.7	16.0	20.7	26.2	28.7	35.1	-
29	IL-100	0.0	0.0	0.0	0.0	0.0	0.0	4.8	4.8	5.7	11.0	17.5	22.4	25.7	27.5	39.6
30	IL-100h	0.0	0.0	0.0	0.0	0.0	-0.3	-0.6	0.3	1.5	7.4	15.6	21.6	32.1	41.3	66.8
31	IL-F10G60	0.0	-1.1	-1.7	-2.6	-3.3	-5.3	-6.4	-7.1	-5.9	-5.9	-5.7	3.6	3.3	5.9	-
32	IL-F20S8	0.0	-0.8	-2.4	-4.4	-5.0	-5.9	-6.5	-7.3	-6.8	-3.3	-0.2	5.0	5.9	8.9	-
33	IL-M10	0.0	-1.2	-1.8	-2.3	-3.0	-3.5	-2.0	-2.4	-1.5	0.9	3.9	7.3	8.2	13.2	-
34	IHA-100	0.0	0.0	0.0	0.0	0.0	0.0	3.8	4.4	4.4	8.9	14.5	18.0	20.4	21.2	33.0
35	IHA-100h	0.0	0.0	0.0	0.0	0.0	6.4	12.5	15.9	16.5	24.2	33.9	41.7	52.5	62.4	92.2

Mix#	Mix ID	Weight Change (g)														
		Weeks of Exposure to 5% Sodium Sulfate Solution														
		0	1	2	3	4	8	13	15	17	26	39	52	65	78	104
36	IHA-F10G60	0.0	-1.1	-1.8	-2.1	-3.0	-5.6	-5.7	-7.4	-6.8	-6.4	-6.5	-6.4	-7.4	-3.5	-
37	IHA-F20S8	0.0	-2.7	-2.6	-4.7	-5.1	-6.0	-5.6	-5.9	-6.5	-2.3	1.2	6.4	7.7	12.9	-
38	IHA-M10	0.0	-1.1	-3.0	-1.8	-3.9	-4.7	-2.9	-4.2	-5.3	-4.5	-2.6	0.8	1.1	4.7	-

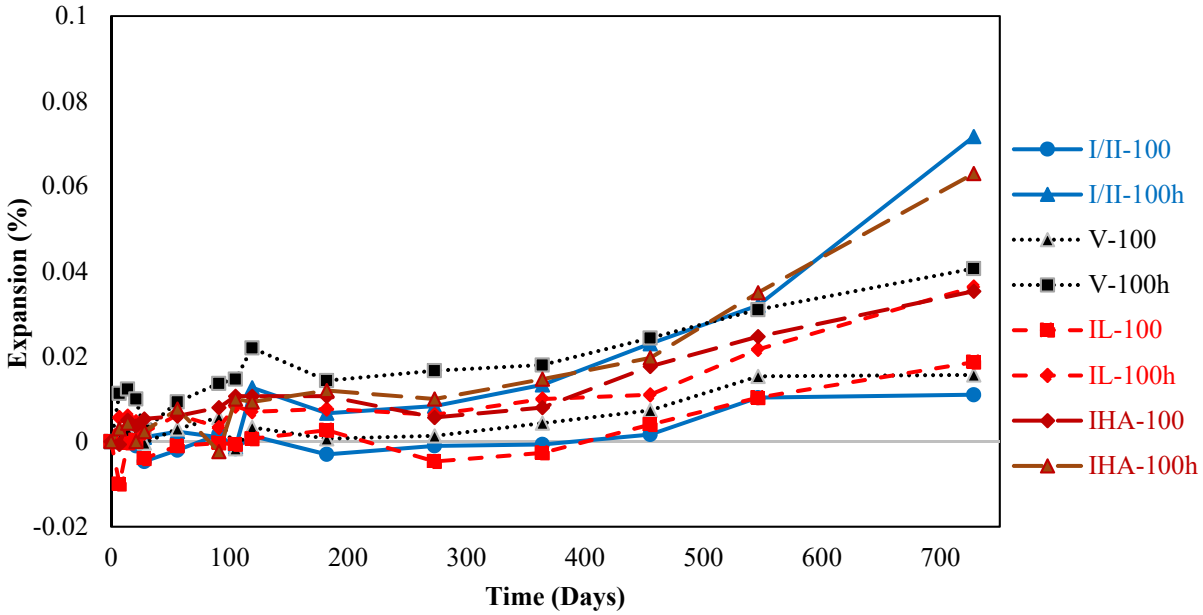

Figure 8-9: OPC concrete mixes expansion results

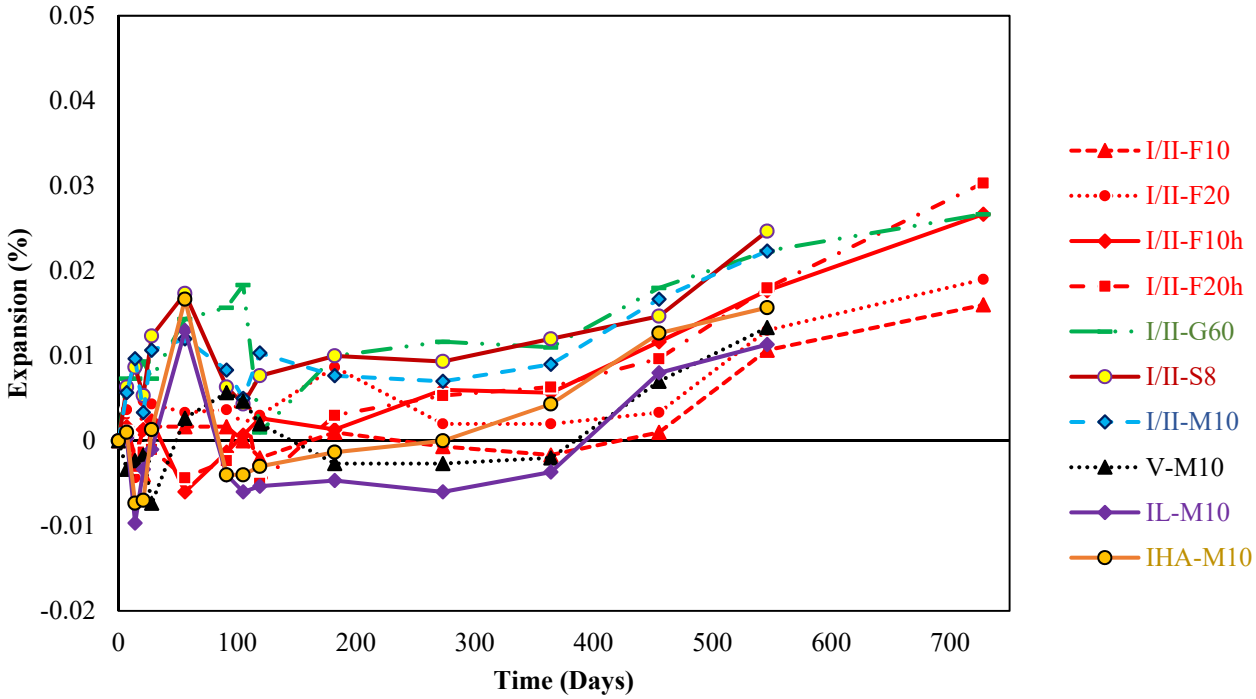

Figure 8-10: Binary concrete mixes expansion results

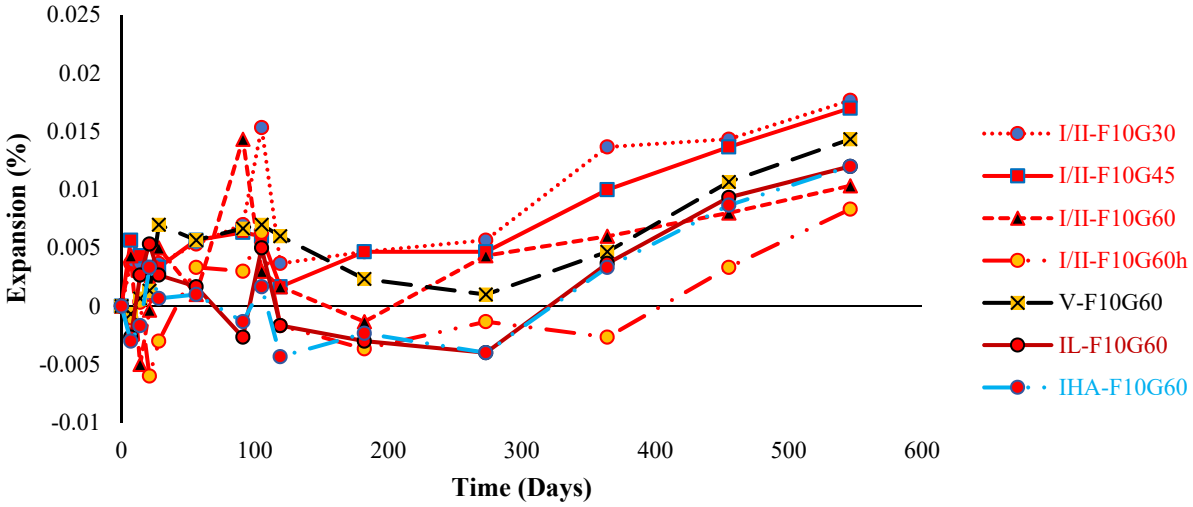

Figure 8-11: Expansion of ternary mixtures with 10% fly ash

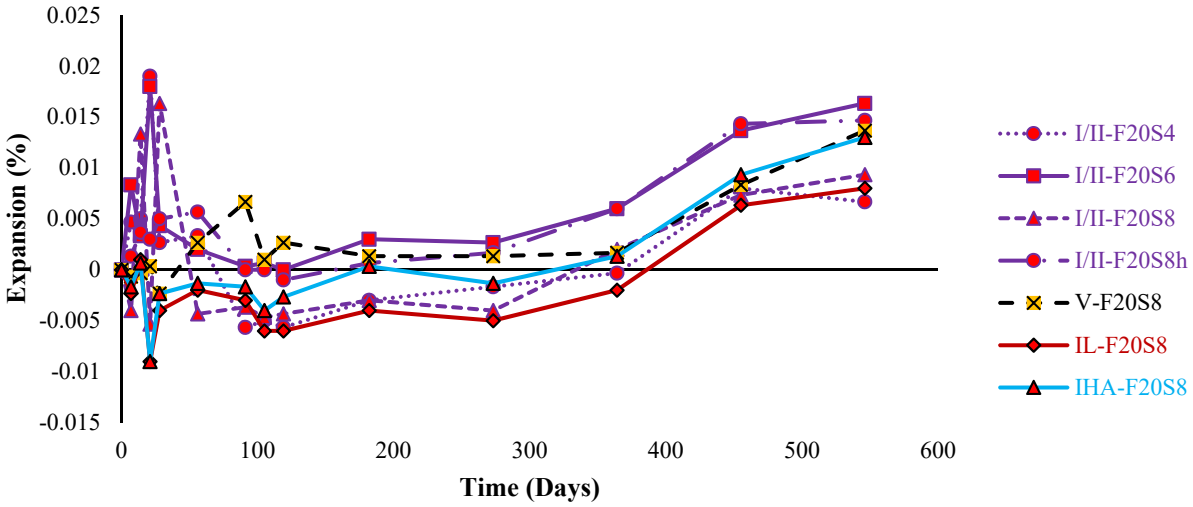

Figure 8-12: Expansion of ternary mixtures with 20% fly ash

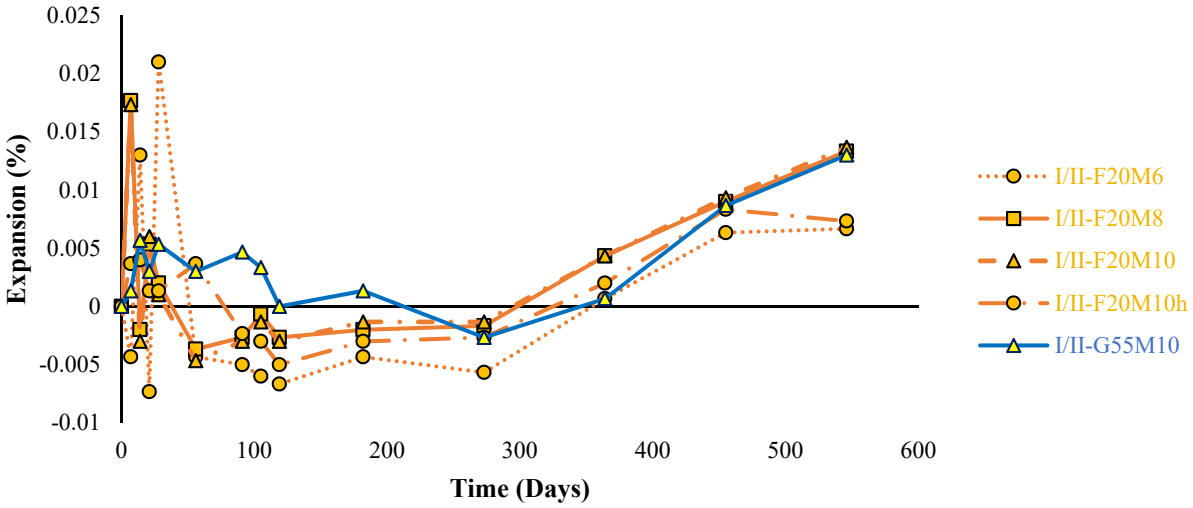

Figure 8-13: Expansion of ternary mixtures including metakaolin

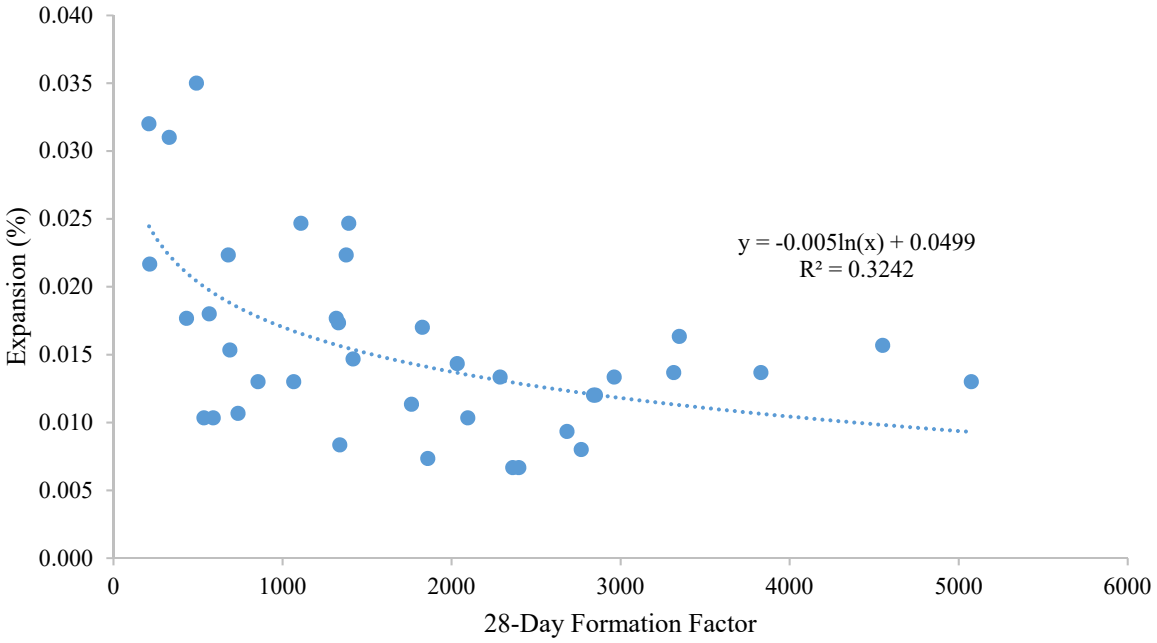

Figure 8-14: Concrete expansion after 18 months exposure to 5% sodium sulfate solution compared with 28-day formation factor

8.4 Summary

Concrete prisms were made for sulfate attack experiments and monitored for expansion up to 18 months, and 2 years for some prisms. Samples made with portland cement at 0.44 w/cm began to show some expansion at 2 years, with only the Type IL cement mixture showing less than 0.04% expansion at that point. None of the OPC mixtures showed more than 0.04% expansion when made with a 0.35 w/cm, demonstrating the value of a reduced w/cm. A comparison of 18-month expansion with 28-day formation factor showed a weak correlation, indicating at least some of the improved behavior is a result of improved transport properties, assuming that formation factor was a good measure of ion penetration resistance. These results indicate that marginally acceptable cementitious materials may still be used in Florida concrete by control of the transport properties with a low risk of sulfate durability problems. It is recommended to continue monitoring the expansion of the prisms made to further differentiate the performance of ternary blend mixtures.

CHAPTER 9. CONCLUSIONS AND RECOMMENDATIONS

9.1 Conclusions

40 concrete mixtures with different w/cm, portland cement types, and combinations of SCMs were made and tested to determine if resistivity tests are applicable to low w/cm concrete made with ternary blends. Concrete transport properties were tested using surface resistivity, bulk resistivity, ASTM C1202, rapid chloride migration (NT Build 492), water absorption (ASTM C1585), water permeability, and volume of permeable voids at ages between 28 days and 1 year. Concrete pore solution resistivity was measured along with the resistivity measurements to calculate the concrete formation factor. Concrete samples were tested using the bulk diffusion test ASTM C1556 with 6 and 12 months of ponding to calculate the concrete apparent and effective chloride diffusion coefficients. Based on the testing performed in this study, the following conclusions are made:

- An empirical equation has been developed to estimate the pore solution resistivity from the w/cm and oxide composition.
- Samples cured in SPS showed better correlations to secondary absorption rate and water permeability than samples cured in the fog room.
- Formation factor showed a marginally better correlation for SPS-cured samples against secondary absorption rate than bulk resistivity.
- Little benefit was seen in increasing the silica fume dosage above 6% in RCMT and bulk resistivity tests.
- Bulk resistivity was shown to correlate adequately (R^2 = 0.76 to 0.80) with the concrete apparent diffusion coefficient.
- Chloride ingress calculations performed using effective diffusion coefficients calculated from formation factor were shown to conservatively simulate measured profiles. Formation factor from moist-room-cured samples were shown to be closer to the measured profiles than samples cured in simulated pore solution.
- The apparent diffusion coefficients fit to the field surface chloride profiles were much lower than those fit to lab chloride profiles. This is likely because the concrete in the piles was only partially saturated in the field.

- The mixtures containing silica fume or slag were found to have the lowest apparent diffusion coefficients of those taken from the concrete piles. It was seen that results from samples cored from the piles lined up with the experimental results that were collected in laboratory conditions, validating the laboratory tests performed.
- The following mixes, two binary and nine ternary, were found to meet the extremely aggressive exposure durability requirements for resistance to chloride and sulfate attack. Total cementitious material content and w/cm were 700 lb/ft^3 and 0.35, respectively.
    - 40% Type I/II PC – 60% Slag
    - 92% Type I/II PC – 8% SF
    - 45% Type I/II PC – 10% FFA – 45% Slag
    - 30% Type I/II PC - 10% FFA – 60% Slag
    - 76% Type I/II PC – 20% FFA – 4% SF
    - 74% Type I/II PC – 20% FFA – 6% SF
    - 72% Type I/II PC – 20% FFA – 8% SF
    - 37% Type I/II PC – 55% Slag – 8% SF
    - 35% Type I/II PC – 55% Slag – 10% MK
    - 30% Type IL PC – 10% FFA – 60% Slag
    - 72% Type IL PC – 20% FFA – 8% SF

  Where PC is portland cement, SF is silica fume, FFA is Class F fly ash, Slag is ground granulated blast furnace slag, and MK is metakaolin.
- Meeting the extremely aggressive exposure durability requirements for resistance to chloride attack for a particular mix design does not guarantee that the mix design will meet the extremely aggressive exposure durability requirements for resistance to sulfate attack.

9.2 Recommendations

Based on the experimental results obtained and conclusions drawn, the following recommendations are made:

- Given the complexity and uncertainty in quantifying the concrete pore solution required to calculate the formation factor from resistivity measurements, the added complexity of

laboratory operations to implement SPS curing with individualized SPS concentrations for each mixture, and the correlations seen between bulk resistivity and apparent diffusion coefficient for Florida materials, it is recommended to continue using resistivity measurements in specifications until these complexities are simplified.

- Given that the difference in correlation was marginal, the excellent correlation for samples cured in the moist room between bulk resistivity and RCMT, and practical issues related to curing samples in SPS, it is recommended to adopt a bulk resistivity acceptance criteria of 18 kΩ-cm at 56 or 91 days with moist-room-cured samples.
- Reduce silica fume dosage requirements in ternary blends from 7-9% to 6%.

9.3 Future Research

While this research project showed the correlation that exists between resistivity measurements and other concrete transport properties, future research could include:

- Develop more accurate method of predicting pore solution composition and curing methods to prevent pore solution composition changes from leaching.
- Investigate the possibility of using accelerated curing methods to obtain long-term day concrete transport properties in 28 days.
- Investigate alternative curing methods to prevent leaching in concrete samples.
- Evaluate the long-term durability of additional SCM combinations and total cementitious material contents that are representative of currently used FDOT concrete mix designs.

REFERENCES

[1] FIB, Condition Control and Assessment of Reinforced Concrete Structures Exposed to Corrosive Environments (carbonation/chlorides), 2011.

[2] U.M. Angst, Challenges and opportunities in corrosion of steel in concrete, Mater. Struct. Constr. 51 (2018) 1–20. https://doi.org/10.1617/s11527-017-1131-6.

[3] A.E.K. Jones, Development of an holistic approach to ensure the durability of new concrete construction, Crowthorne, United Kingdom, 1997.

[4] M. Thomas, The effect of supplementary cementing materials on alkali-silica reaction: A review, Cem. Concr. Res. 41 (2011) 1224–1231. https://doi.org/10.1016/j.cemconres.2010.11.003.

[5] C. Qiao, A.T. Coyle, O.B. Isgor, W.J. Weiss, Prediction of Chloride Ingress in Saturated Concrete Using Formation Factor and Chloride Binding Isotherm, Adv. Civ. Eng. Mater. 7 (2018) 20170141. https://doi.org/10.1520/acem20170141.

[6] ASTM, C127-15 Standard Test Method for Relative Density (Specific Gravity) and Absorption of Coarse Aggregate, 2015.

[7] ASTM, C136/C136M-14 Standard Test Method for Sieve Analysis of Fine and Coarse Aggregates, 2014.

[8] K.A. Riding, C.C. Ferraro, M. Almarshoud, H. Mosavi, R. Alrashidi, M.H. Alyami, Durability Evaluation of Ternary Mix Designs for Extremely Aggressive Exposures, Fla. Dep. Transp. (2018). https://doi.org/10.13140/RG.2.2.29094.47687.

[9] ASTM, C128-15 Standard Test Method for Relative Density (Specific Gravity) and Absorption of Fine Aggregate, 15.

[10] ASTM, C150/C150M-18 Standard Specification for Portland Cement, 2018.

[11] ASTM, C595/C595M-19 Standard Specification for Blended Hydraulic Cements. West Conshohocken, PA; ASTM International, 2019. doi: https://doi.org/10.1520/C0595_C0595M-19, n.d.

[12] ASTM, C618-17a Standard Specification for Coal Fly Ash and Raw or Calcined Natural Pozzolan for Use in Concrete.

[13] ASTM, C989/C989M-18 Standard Specification for Slag Cement for Use in Concrete and Mortars, 18.

[14] ASTM, C1240-15 Standard Specification for Silica Fume Used in Cementitious Mixtures, 15.

[15] ASTM, C33/C33M - 18 Standard Specification for Concrete Aggregates, 18.

[16] ASTM, C192/C192M-16a Standard Practice for Making and Curing Concrete Test Specimens in the Laboratory, 2016.

[17] ASTM, C143/C143M-15a Standard Test Method for Slump of Hydraulic-Cement Concrete.

[18] ASTM, C138/C138M-17a Standard Test Method for Density (Unit Weight), Yield, and Air Content (Gravimetric) of Concrete.

[19] ASTM, C231/C231M-17a Standard Test Method for Air Content of Freshly Mixed Concrete by the Pressure Method.

[20] ASTM, C1064/C1064M-17 Standard Test Method for Temperature of Freshly Mixed Hydraulic-Cement Concrete, 17.

[21] ASTM C39, Standard Test Method for Compressive Strength of Cylindrical Concrete Specimens, ASTM International, West Conshohocken, PA, 2018. https://compass.astm.org/download/C39C39M.6829.pdf (accessed August 6, 2018).
[22] ASTM, C39/C39M-18 Standard Test Method for Compressive Strength of Cylindrical Concrete Specimens, 18.
[23] ASTM C1556, Standard Test Method for Determining the Apparent Chloride Diffusion Coefficient of Cementitious Mixtures by Bulk Diffusion, (2016) 1–7. https://doi.org/10.1520/C1556-11AR16.2.
[24] ASTM C490, Standard Practice for Use of Apparatus for the Determination of Length Change of Hardened Cement Paste, Mortar, and Concrete, (2017) 1–5.
[25] T. Luping, L.O. Nilsson, Chloride binding capacity and binding isotherms of OPC pastes and mortars, Cem. Concr. Res. 23 (1993) 247–253. https://doi.org/10.1016/0008-8846(93)90089-R.
[26] ASTM C1738, Standard Practice for High-Shear Mixing of Hydraulic Cement Pastes, (2019) 1–3. https://doi.org/10.1520/C1738-13.2.
[27] ASTM C1152, Standard Test Method for Acid-Soluble Chloride in Mortar and Concrete, (2020) 4. https://doi.org/10.1520/C1152.
[28] G.E. Archie, The Electrical Resistivity Log as an Aid in Determining Some Reservoir Characteristics, Trans. AIME. 146 (1942) 54–62. https://doi.org/10.2118/942054-G.
[29] R. Spragg, C. Qiao, J. Barrett, J. Weiss, Assessing a concrete's resistance to chloride ion ingress using the formation factor, in: Corros. Steel Concr. Struct., 2016: pp. 211–238.
[30] L. Yuan-Hui, S. Gregory, Diffusion of Ions in Sea Water and in Deep-Sea Sediments, Geochim. Cosmochim. Acta. 38 (1974) 703–714.
[31] D.P. Bentz, A virtual rapid chloride permeability test, Cem. Concr. Compos. 29 (2007) 723–731. https://doi.org/10.1016/j.cemconcomp.2007.06.006.
[32] H.F.W. Taylor, A method for predicting alkali ion concentrations in cement pore solutions, Adv. Cem. Res. 1 (1987) 5–17.
[33] D. Trejo, M. Shakouri, N.P. Vaddey, O.B. Isgor, Development of empirical models for chloride binding in cementitious systems containing admixed chlorides, Constr. Build. Mater. 189 (2018) 157–169. https://doi.org/10.1016/j.conbuildmat.2018.08.197.
[34] E. Barsoukov, J.R. Macdonald, Impedance Spectroscopy: Theory, Experiment, and Applications, John Wiley & Sons, 2018.
[35] ASTM C192, Standard Practice for Making and Curing Concrete Test Specimens in the Laboratory, (2019) 1–8. https://doi.org/10.1520/C0192.
[36] ASTM C511-03, Standard Specification for Mixing Rooms, Moist Cabinets, Moist Rooms, and Water Storage Tanks Used in the Testing of Hydraulic Cements and Concretes, (2003) 1–3. https://doi.org/10.1520/C0511-09.2.
[37] ASTM C1585, Standard Test Method for Measurement of Rate of Absorption of Water by Hydraulic Cement Concretes, (2013) 6. https://doi.org/10.1520/C1585-13.2.
[38] ASTM C642-13, Standard test method for density, absorption, and voids in hardened concrete, ASTM International, ASTM Int. (2013) 1–3. https://doi.org/10.1520/C0642-13.
[39] P. Soongswang, M. Tia, D.G. Bloomquist, C. Meletiou, L.M. Sessions, Efficient test setup for determining the water-permeability of concrete, Transp. Res. Rec. 1204 (1988) 77–82.

[40] ASTM C1202, Standard Test Method for Electrical Indication of Concrete's Ability to Resist Chloride Ion Penetration, Am. Soc. Test. Mater. (2019) 8. https://doi.org/10.1520/C1202-12.2.
[41] NT Build 492, Concrete, mortar and cement-based repair materials: Chloride migration coefficient from non-steady-state migration experiments, Measurement. (1999) 1–8. https://doi.org/UDC 691.32/691.53/691.54.
[42] AASHTO TP 119-15, Standard Method of Test for Electrical Resistivity of a Concrete Cylinder Tested in a Uniaxial Resistance Test, Am. Assoc. State Highw. Transp. Off. (2015) 1–11.
[43] AASHTO T358, Standard Method of Test for Surface Resistivity Indication of Concrete's Ability to Resist Chloride Ion Penetration, (2015) 1–10.
[44] R. Spragg, C. Villani, K. Snyder, D. Bentz, J. Bullard, J. Weiss, Factors that influence electrical resistivity measurements in cementitious systems, Transp. Res. Rec. (2013) 90–98. https://doi.org/10.3141/2342-11.
[45] R.P. Spragg, J. Castro, T. Nantung, M. Paredes, J. Weiss, Variability Analysis of the Bulk Resistivity Measured Using Concrete Cylinders, Adv. Civ. Eng. Mater. 1 (2012) 104596. https://doi.org/10.1520/acem104596.
[46] A. Malakooti, M. Maguire, R.J. Thomas, Evaluating Electrical Resistivity as a Performance based Test for Utah Bridge Deck Concrete, Rutgers University. Center for Advanced Infrastructure and Transportation, 2018.
[47] FDOT, Standard Specifications for Road and Bridge Construction, (2020).
[48] C. Qiao, M.K. Moradllo, H. Hall, M.T. Ley, W.J. Weiss, Electrical Resistivity and Formation Factor of Air-Entrained Concrete, ACI Mater. J. 116 (2019) 85–93.
[49] M.D.A. Thomas, A. Scott, T. Bremner, A. Bilodeau, D. Day, Performance of slag concrete in marine environment, ACI Mater. J. 105 (2008) 628–634. https://doi.org/10.14359/20205.
[50] H. Zibara, Binding of External Chlorides By Cement Pastes, Toronto, Ontario, 2001.
[51] K.A. Riding, M.D.A. Thomas, K.J. Folliard, Apparent diffusivity model for concrete containing supplementary cementitious materials, ACI Mater. J. 110 (2013) 705–713. https://doi.org/10.14359/51686338.
[52] A.K. Suryavanshi, J.D. Scantlebury, S.B. Lyon, Corrosion of reinforcement steel embedded in high water-cement ratio concrete contaminated with chloride, Cem. Concr. Compos. 20 (1998) 263–281. https://doi.org/10.1016/S0958-9465(98)00018-3.
[53] FM 5-516, Florida Method of Test For Determining Low-Levels of Chloride in Concrete and Raw Materials, (2018) 1–11.
[54] B. Martın-Pérez, Service life modelling of RC higway structures exposed to chlorides, PhD Thesis, PhD thesis, university of Toronto, 1999.
[55] H. Mosavi, R. Alrashidi, M. Almarshoud, M.H. Alyami, K.A. Riding, C.C. Ferraro, Use of Electrical Test Method on Determination Aging Factor of Concrete Incorporating Supplementary Cementitious Materials, in: J. Martirena-Hernandez, A. Alujas-Díaz, M. Amador-Hernandez (Eds.), Proc. Int. Conf. Sustain. Prod. Use Cem. Concr., 2019: pp. 299–306. https://doi.org/10.1007/978-3-030-22034-1_34.
[56] J. Mccall, Y.C. Tasi, S. Szyniszewski, E. Roske, C. Ferraro, H.R. Hamilton, Key Royale Bridge Five Year Evaluation University of Florida Civil and Coastal Engineering, Gainesville, FL, 2013.

[57] R.P. Spragg, C. Villani, J. Weiss, A. Poursaee, S. Jones, D.P. Bentz, K.A. Snyder, Surface and uniaxial electrical measurements on layered cementitious composites having cylindrical and prismatic geometries, Proc. 4th Int. Conf. Durab. Concr. Struct. ICDCS 2014. (2014) 317–326. https://doi.org/10.5703/1288284315417.
[58] ASTM C1012/C1012M-15, Standard test method for length change of hydraulic-cement mortars exposed to a sulfate solution, (2018) 1–9. https://doi.org/10.1520/C1012.
[59] T. Drimalas, Laboratory and field evaluations of external sulfate attack, University of Texas at Austin, 2007.
[60] M.H. Alyami, R.S. Alrashidi, H. Mosavi, M.A. Almarshoud, K.A. Riding, Potential accelerated test methods for physical sulfate attack on concrete, Constr. Build. Mater. 229 (2019) 116920.
[61] M.H. Alyami, H. Mosavi, R.S. Alrashidi, M.A. Almarshoud, C.C. Ferraro, K.A. Riding, Lab and Field Study of Physical Sulfate Attack on Concrete Mixtures with Supplementary Cementitious Materials, J. Mater. Civ. Eng. 33 (2021) 04020397. https://doi.org/10.1061/(ASCE)MT.1943-5533.0003500.

APPENDIX A: APPARENT CHLORIDE DIFFUSION: 6 MONTHS EXPOSURE

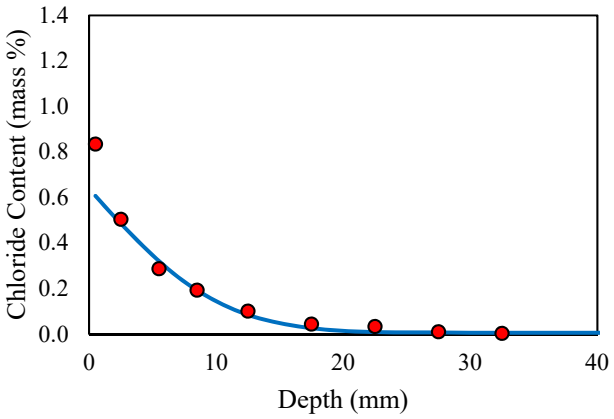

Mix No.	1
Mix ID	C-100
Exposure time (months)	6
Diffusion (m^2/s)	2.12×10^{-12}
Cs (mass %)	0.638
C_i (mass %)	0.006
R^2	0.989

Figure A-1: Chloride bulk diffusion results for Mix 1 at six months of exposure

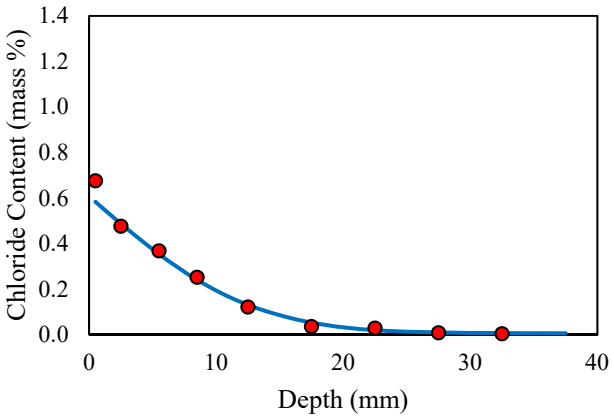

Mix No.	2
Mix ID	C-100h
Exposure time (months)	6
Diffusion (m^2/s)	3.15×10^{-12}
Cs (mass %)	0.607
C_i (mass %)	0.006
R^2	0.996

Figure A-2: Chloride bulk diffusion results for Mix 2 at six months of exposure

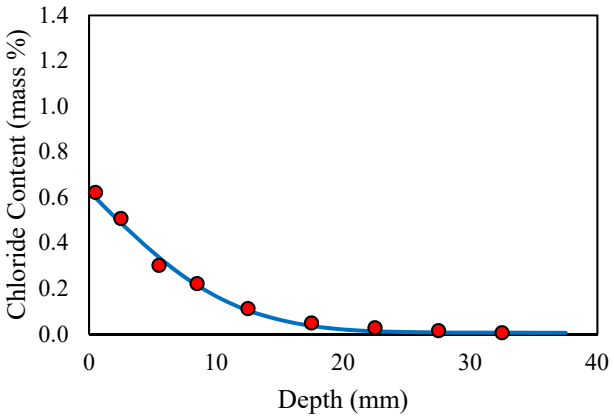

Mix No.	3
Mix ID	C-F10
Exposure time (months)	6
Diffusion (m^2/s)	2.51×10^{-12}
Cs (mass %)	0.627
C_i (mass %)	0.006
R^2	0.991

Figure A-3: Chloride bulk diffusion results for Mix 3 at six months of exposure

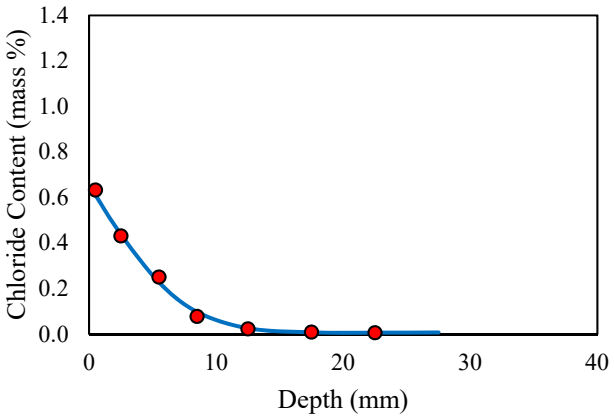

Mix No.	4
Mix ID	C-F20
Exposure time (months)	6
Diffusion (m^2/s)	1.07×10^{-12}
Cs (mass %)	0.655
C_i (mass %)	0.006
R^2	0.994

Figure A-4: Chloride bulk diffusion results for Mix 4 at six months of exposure

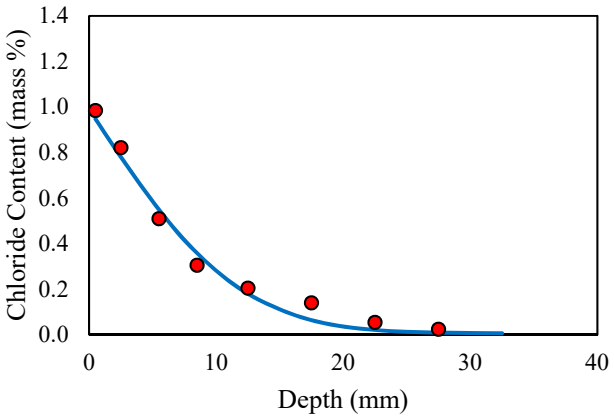

Mix No.	5
Mix ID	C-F10h
Exposure time (months)	6
Diffusion (m^2/s)	2.74×10^{-12}
Cs (mass %)	0.990
C_i (mass %)	0.006
R^2	0.977

Figure A-5: Chloride bulk diffusion results for Mix 5 at six months of exposure

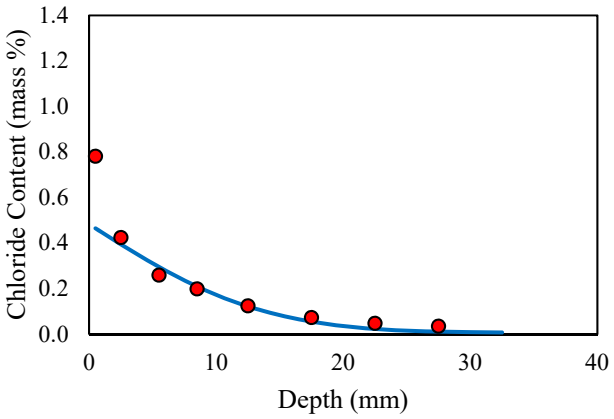

Mix No.	6
Mix ID	C-F20h
Exposure time (months)	6
Diffusion (m^2/s)	3.67×10^{-12}
Cs (mass %)	0.482
C_i (mass %)	0.006
R^2	0.974

Figure A-6: Chloride bulk diffusion results for Mix 6 at six months of exposure

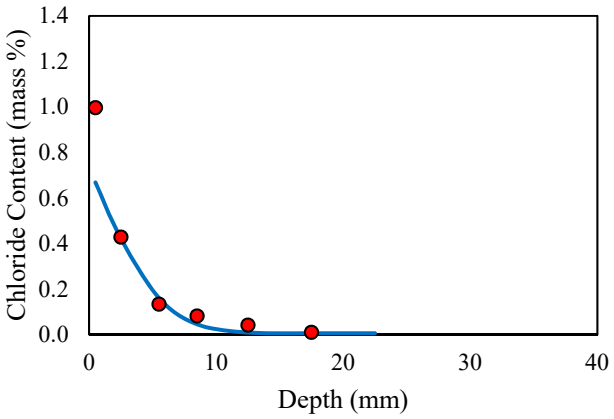

Mix No.	7
Mix ID	C-G60
Exposure time (months)	6
Diffusion (m^2/s)	0.63×10^{-12}
Cs (mass %)	0.734
C_i (mass %)	0.006
R^2	0.980

Figure A-7: Chloride bulk diffusion results for Mix 7 at six months of exposure

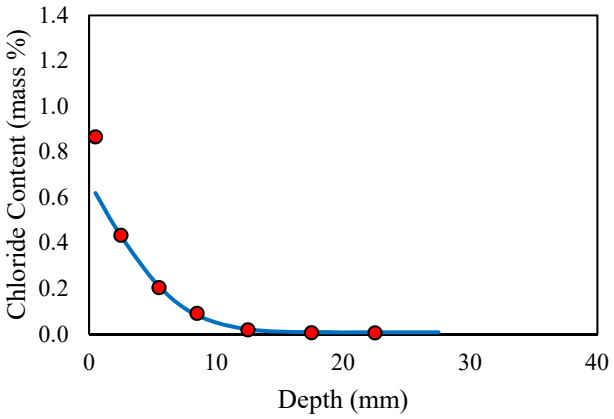

Mix No.	8
Mix ID	C-S8
Exposure time (months)	6
Diffusion (m^2/s)	0.93×10^{-12}
Cs (mass %)	0.668
C_i (mass %)	0.008
R^2	0.999

Figure A-8: Chloride bulk diffusion results for Mix 8 at six months of exposure

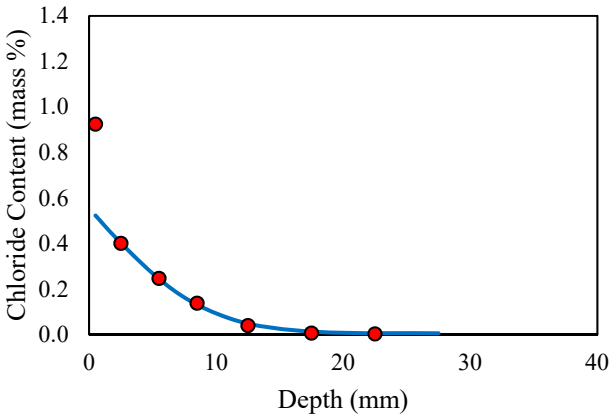

Mix No.	9
Mix ID	C-M10
Exposure time (months)	6
Diffusion (m^2/s)	1.60×10^{-12}
Cs (mass %)	0.554
C_i (mass %)	0.006
R^2	0.999

Figure A-9: Chloride bulk diffusion results for Mix 9 at six months of exposure

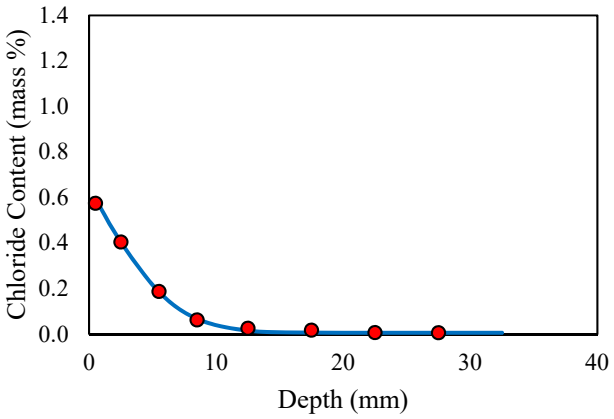

Mix No.	10
Mix ID	C-F10G30
Exposure time (months)	6
Diffusion (m^2/s)	0.84×10^{-12}
Cs (mass %)	0.643
C_i (mass %)	0.006
R^2	0.999

Figure A-10: Chloride bulk diffusion results for Mix 10 at six months of exposure

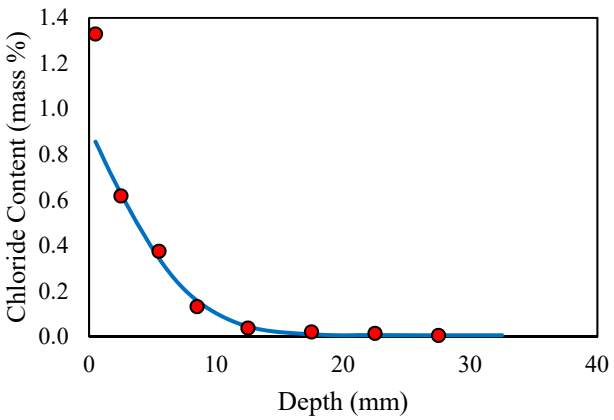

Mix No.	11
Mix ID	C-F10G45
Exposure time (months)	6
Diffusion (m^2/s)	1.21×10^{-12}
Cs (mass %)	0.915
C_i (mass %)	0.006
R^2	0.994

Figure A-11: Chloride bulk diffusion results for Mix 11 at six months of exposure

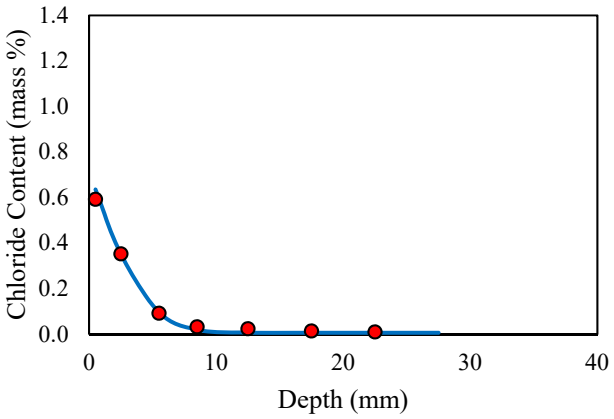

Mix No.	12
Mix ID	C-F10G60
Exposure time (months)	6
Diffusion (m^2/s)	0.42×10^{-12}
Cs (mass %)	0.713
C_i (mass %)	0.006
R^2	0.997

Figure A-12: Chloride bulk diffusion results for Mix 12 at six months of exposure

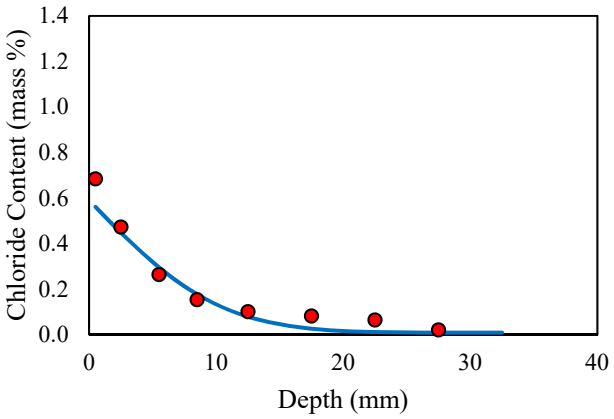

Mix No.	13
Mix ID	C-F10G60h
Exposure time (months)	6
Diffusion (m^2/s)	2.08×10^{-12}
Cs (mass %)	0.589
C_i (mass %)	0.008
R^2	0.962

Figure A-13: Chloride bulk diffusion results for Mix 13 at six months of exposure

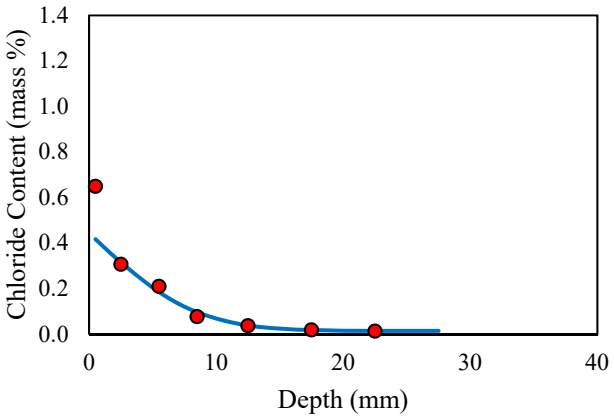

Mix No.	14
Mix ID	C-F20S4
Exposure time (months)	6
Diffusion (m^2/s)	1.361×10^{-12}
Cs (mass %)	0.443
C_i (mass %)	0.014
R^2	0.986

Figure A-14: Chloride bulk diffusion results for Mix 14 at six months of exposure

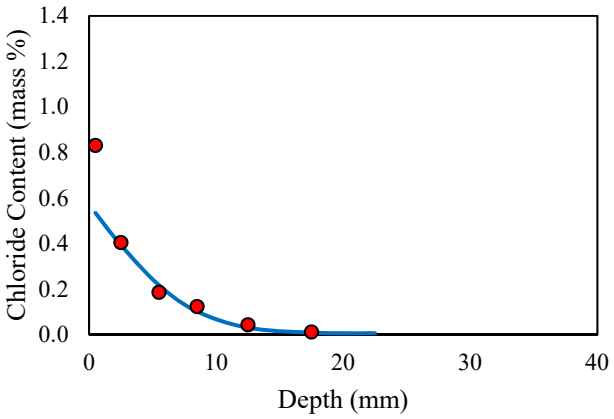

Mix No.	15
Mix ID	C-F20S6
Exposure time (months)	6
Diffusion (m^2/s)	1.23×10^{-12}
Cs (mass %)	0.570
C_i (mass %)	0.006
R^2	0.983

Figure A-15: Chloride bulk diffusion results for Mix 15 at six months of exposure

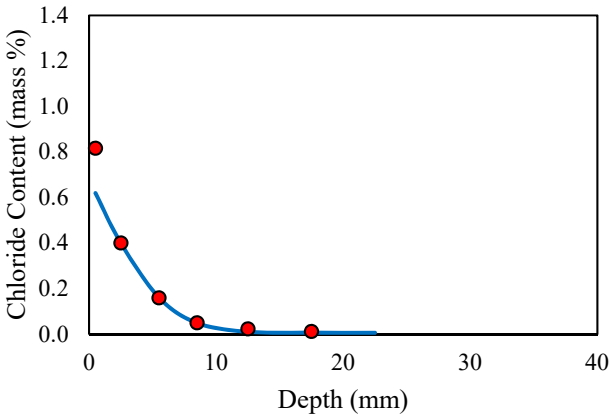

Mix No.	16
Mix ID	C-F20S8
Exposure time (months)	6
Diffusion (m^2/s)	0.67×10^{-12}
Cs (mass %)	0.678
C_i (mass %)	0.006
R^2	0.999

Figure A-16: Chloride bulk diffusion results for Mix 16 at six months of exposure

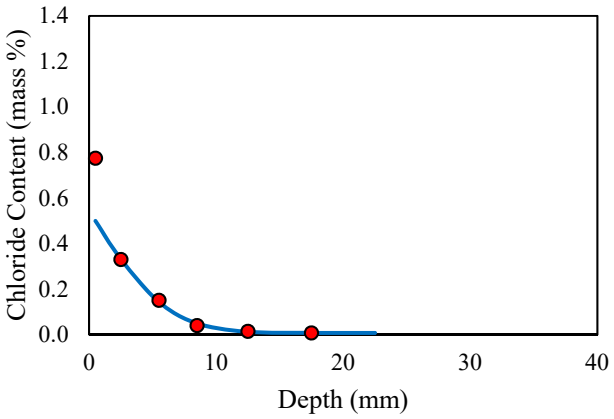

Mix No.	17
Mix ID	C-F20S8h
Exposure time (months)	6
Diffusion (m^2/s)	0.75×10^{-12}
Cs (mass %)	0.544
C_i (mass %)	0.007
R^2	0.998

Figure A-17: Chloride bulk diffusion results for Mix 17 at six months of exposure

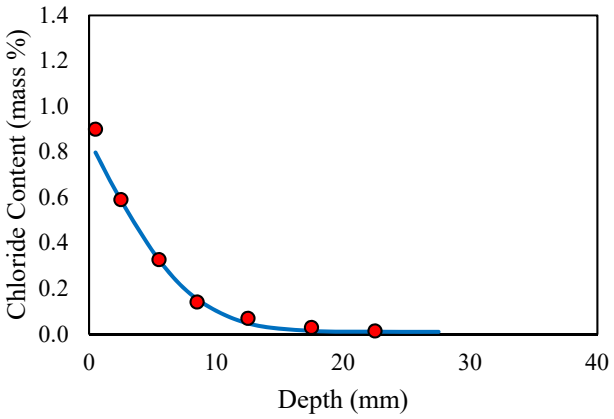

Mix No.	18
Mix ID	C-F20M6
Exposure time (months)	6
Diffusion (m^2/s)	1.24×10^{-12}
Cs (mass %)	0.852
C_i (mass %)	0.010
R^2	0.998

Figure A-18: Chloride bulk diffusion results for Mix 18 at six months of exposure

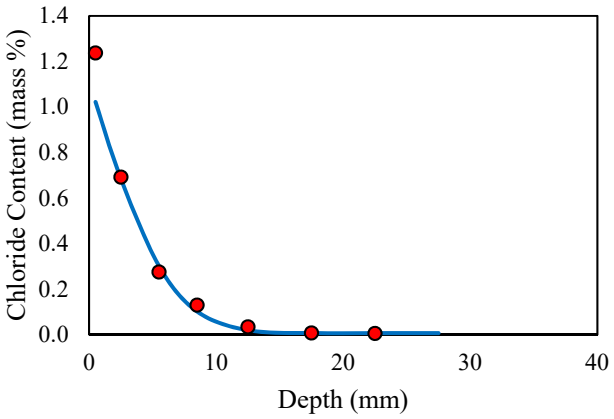

Mix No.	19
Mix ID	C-F20M8
Exposure time (months)	6
Diffusion (m^2/s)	0.79×10^{-12}
Cs (mass %)	1.111
C_i (mass %)	0.006
R^2	0.995

Figure A-19: Chloride bulk diffusion results for Mix 19 at six months of exposure

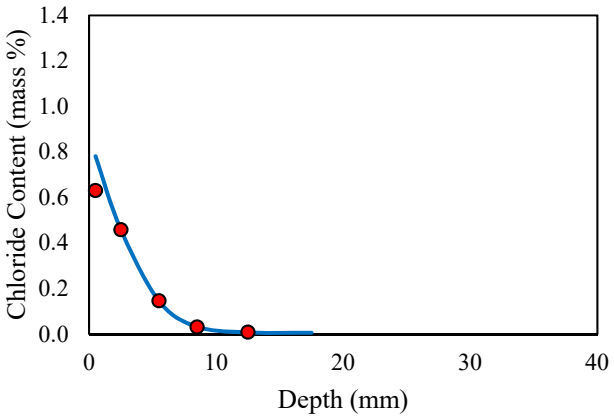

Mix No.	20
Mix ID	C-F20M10
Exposure time (months)	6
Diffusion (m^2/s)	0.50×10^{-12}
Cs (mass %)	0.869
C_i (mass %)	0.006
R^2	1.000

Figure A-20: Chloride bulk diffusion results for Mix 20 at six months of exposure

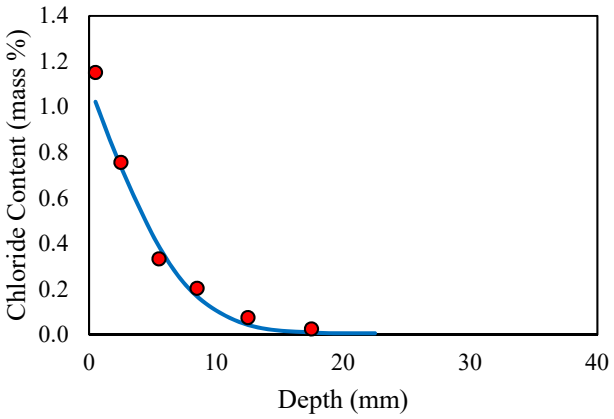

Mix No.	21
Mix ID	C-F20M10h
Exposure time (months)	6
Diffusion (m^2/s)	1.11×10^{-12}
Cs (mass %)	1.097
C_i (mass %)	0.006
R^2	0.985

Figure A-21: Chloride bulk diffusion results for Mix 21 at six months of exposure

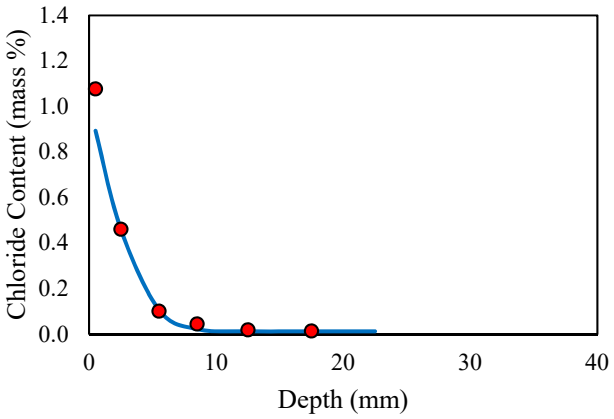

Mix No.	22
Mix ID	C-G55S8
Exposure time (months)	6
Diffusion (m^2/s)	0.35×10^{-12}
Cs (mass %)	1.015
C_i (mass %)	0.012
R^2	0.997

Figure A-22: Chloride bulk diffusion results for Mix 22 at six months of exposure

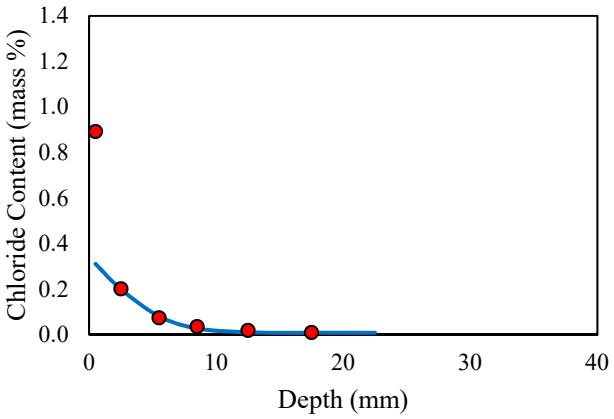

Mix No.	23
Mix ID	C-G55M10
Exposure time (months)	6
Diffusion (m^2/s)	0.64×10^{-12}
Cs (mass %)	0.340
C_i (mass %)	0.008
R^2	0.995

Figure A-23: Chloride bulk diffusion results for Mix 23 at six months of exposure

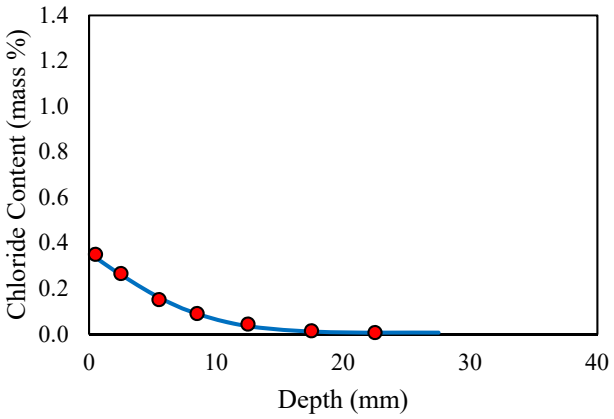

Mix No.	24
Mix ID	CV-100
Exposure time (months)	6
Diffusion (m^2/s)	1.66×10^{-12}
Cs (mass %)	0.355
C_i (mass %)	0.006
R^2	

Figure A-24: Chloride bulk diffusion results for Mix 24 at six months of exposure

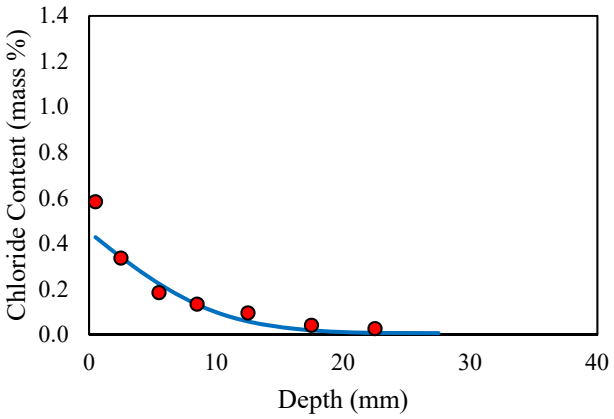

Mix No.	25
Mix ID	CV-100h
Exposure time (months)	6
Diffusion (m^2/s)	2.03×10^{-12}
Cs (mass %)	0.450
C_i (mass %)	0.006
R^2	0.972

Figure A-25: Chloride bulk diffusion results for Mix 25 at six months of exposure

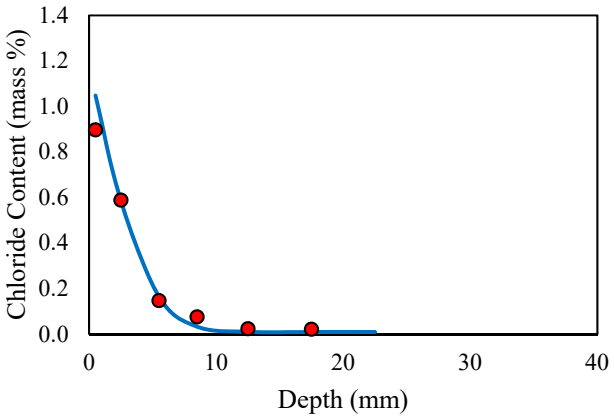

Mix No.	26
Mix ID	CV-F10G60
Exposure time (months)	6
Diffusion (m^2/s)	0.43×10^{-12}
Cs (mass %)	1.174
C_i (mass %)	0.009
R^2	0.993

Figure A-26: Chloride bulk diffusion results for Mix 26 at six months of exposure

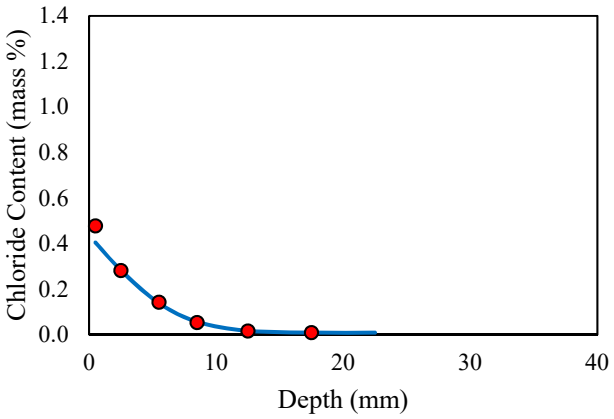

Mix No.	27
Mix ID	CV-F20S8
Exposure time (months)	6
Diffusion (m^2/s)	0.92×10^{-12}
Cs (mass %)	0.436
C_i (mass %)	0.008
R^2	0.999

Figure A-27: Chloride bulk diffusion results for Mix 27 at six months of exposure

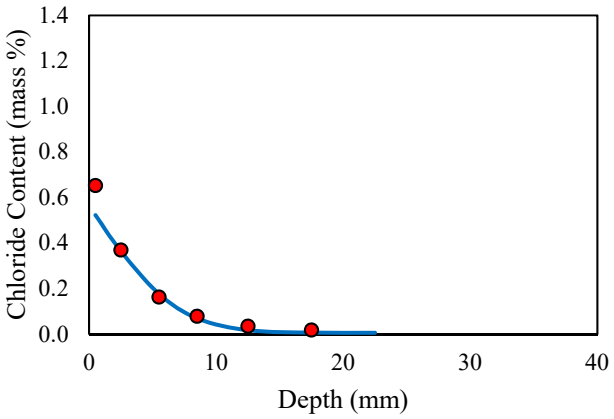

Mix No.	28
Mix ID	CV-M10
Exposure time (months)	6
Diffusion (m^2/s)	0.93×10^{-12}
Cs (mass %)	0.006
C_i (mass %)	0.564
R^2	0.995

Figure A-28: Chloride bulk diffusion results for Mix 28 at six months of exposure

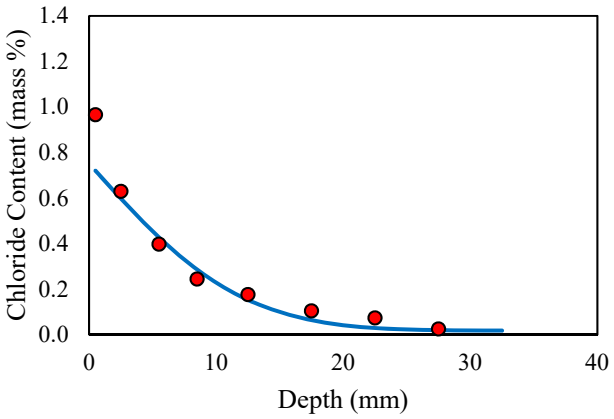

Mix No.	29
Mix ID	CL-100
Exposure time (months)	6
Diffusion (m^2/s)	2.85×10^{-12}
Cs (mass %)	0.751
C_i (mass %)	0.017
R^2	0.976

Figure A-29: Chloride bulk diffusion results for Mix 29 at six months of exposure

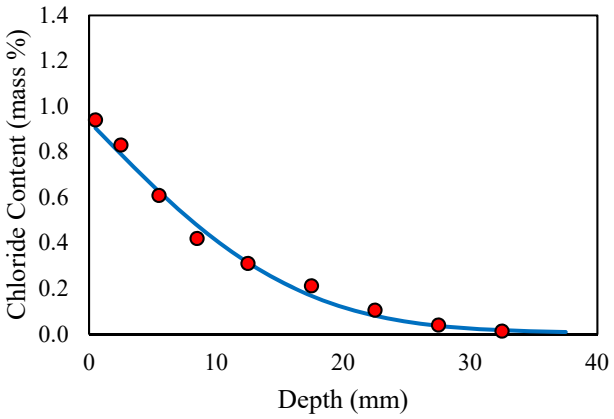

Mix No.	30
Mix ID	CL-100h
Exposure time (months)	6
Diffusion (m^2/s)	5.33×10^{-12}
Cs (mass %)	0.933
C_i (mass %)	0.006
R^2	0.987

Figure A-30: Chloride bulk diffusion results for Mix 30 at six months of exposure

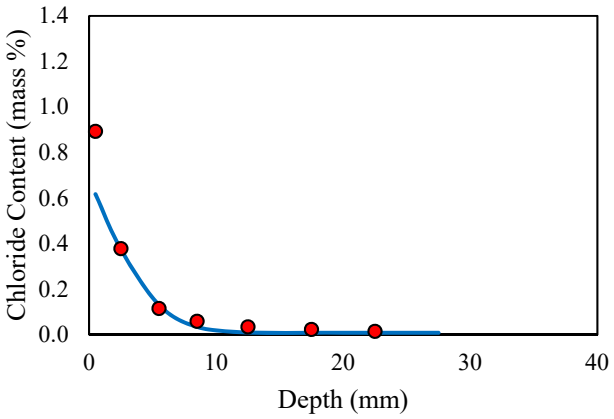

Mix No.	31
Mix ID	CL-F10G60
Exposure time (months)	6
Diffusion (m^2/s)	0.54×10^{-12}
Cs (mass %)	0.682
C_i (mass %)	0.007
R^2	0.991

Figure A-31: Chloride bulk diffusion results for Mix 31 at six months of exposure

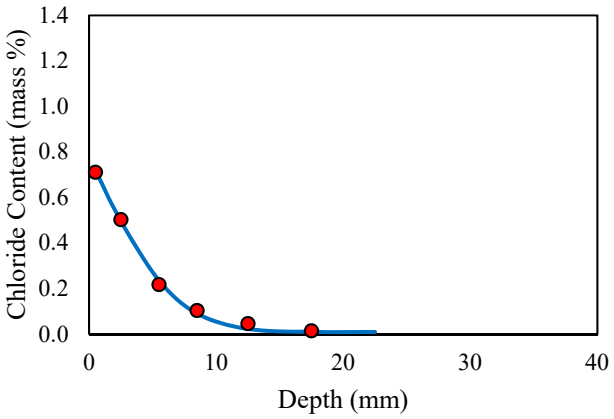

Mix No.	32
Mix ID	CL-F20S8
Exposure time (months)	6
Diffusion (m^2/s)	0.89×10^{-12}
Cs (mass %)	0.777
C_i (mass %)	0.009
R^2	0.995

Figure A-32: Chloride bulk diffusion results for Mix 32 at six months of exposure

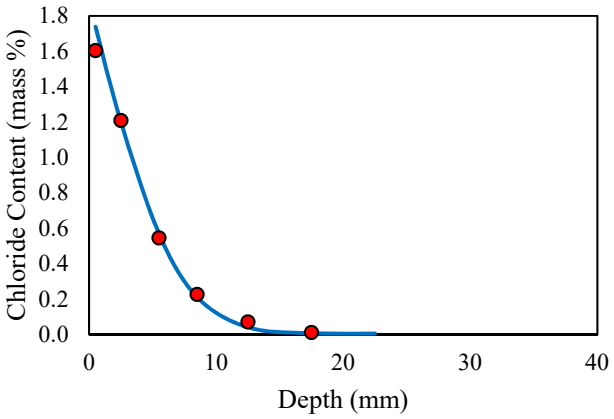

Mix No.	33
Mix ID	CL-M10
Exposure time (months)	6
Diffusion (m^2/s)	0.91×10^{-12}
Cs (mass %)	1.879
C_i (mass %)	0.006
R^2	0.999

Figure A-33: Chloride bulk diffusion results for Mix 33 at six months of exposure

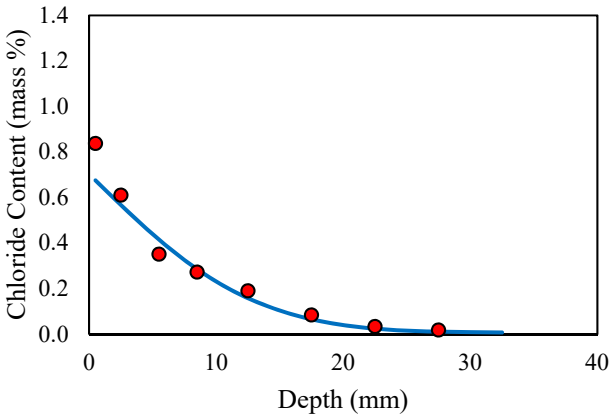

Mix No.	34
Mix ID	CHA-100
Exposure time (months)	6
Diffusion (m^2/s)	3.30×10^{-12}
Cs (mass %)	0.703
C_i (mass %)	0.006
R^2	0.972

Figure A-34: Chloride bulk diffusion results for Mix 34 at six months of exposure

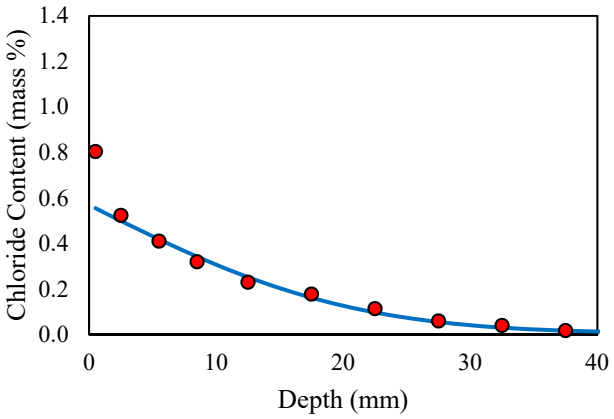

Mix No.	35
Mix ID	CHA-100h
Exposure time (months)	6
Diffusion (m^2/s)	8.33×10^{-12}
Cs (mass %)	0.569
C_i (mass %)	0.006
R^2	0.991

Figure A-35: Chloride bulk diffusion results for Mix 35 at six months of exposure

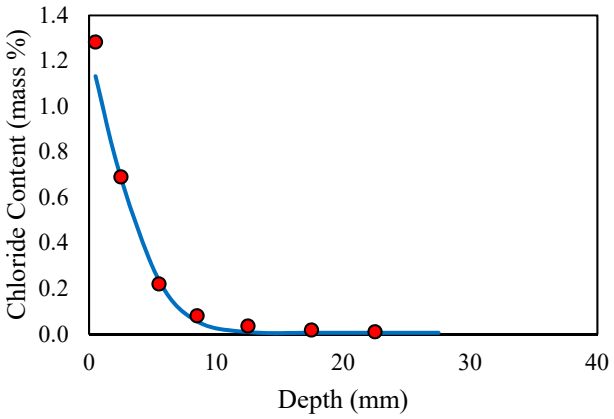

Mix No.	36
Mix ID	CHA-F10G60
Exposure time (months)	6
Diffusion (m^2/s)	0.55×10^{-12}
Cs (mass %)	1.253
C_i (mass %)	0.006
R^2	0.997

Figure A-36: Chloride bulk diffusion results for Mix 36 at six months of exposure

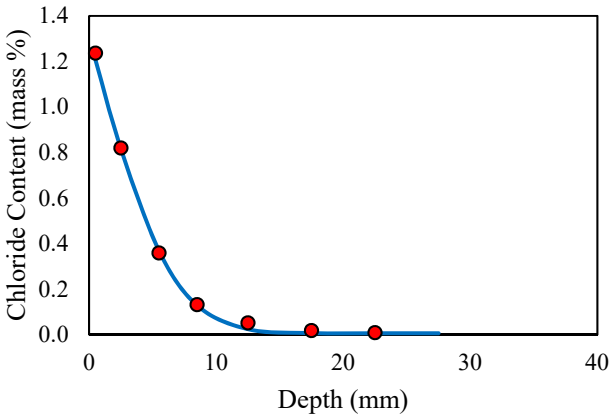

Mix No.	37
Mix ID	CHA-F20S8
Exposure time (months)	6
Diffusion (m^2/s)	0.83×10^{-12}
Cs (mass %)	1.308
C_i (mass %)	0.006
R^2	0.999

Figure A-37: Chloride bulk diffusion results for Mix 37 at six months of exposure

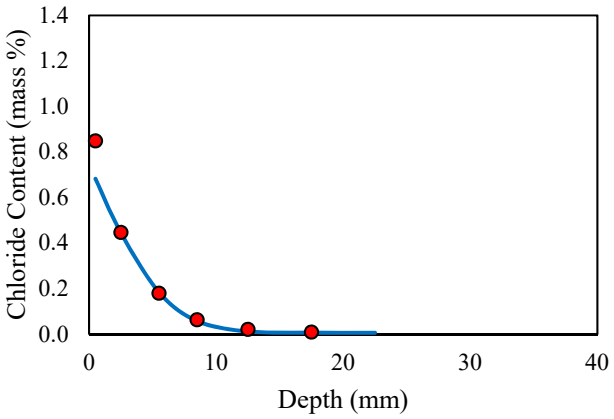

Mix No.	38
Mix ID	CHA-M10
Exposure time (months)	6
Diffusion (m^2/s)	0.71×10^{-12}
Cs (mass %)	0.745
C_i (mass %)	0.006
R^2	0.999

Figure A-38: Chloride bulk diffusion results for Mix 38 at six months of exposure

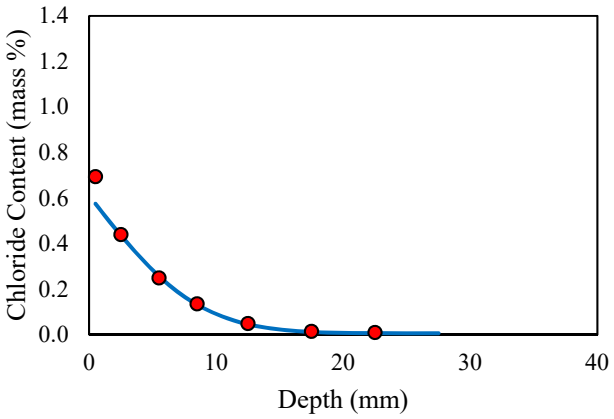

Mix No.	39
Mix ID	C-100SS
Exposure time (months)	6
Diffusion (m^2/s)	1.46×10^{-12}
Cs (mass %)	0.610
C_i (mass %)	0.006
R^2	0.999

Figure A-39: Chloride bulk diffusion results for Mix 39 at six months of exposure

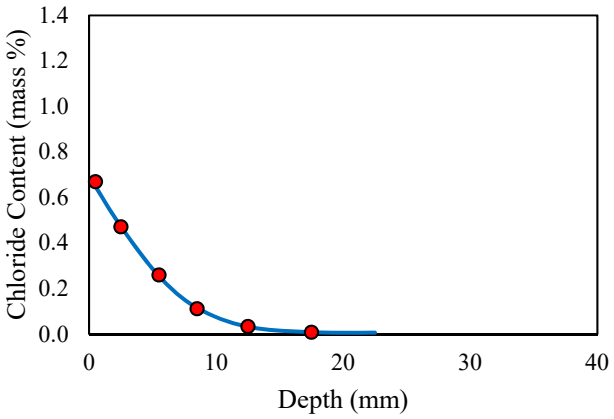

Mix No.	40
Mix ID	C-F20S8SS
Exposure time (months)	6
Diffusion (m^2/s)	1.17×10^{-12}
Cs (mass %)	0.694
C_i (mass %)	0.006
R^2	1.000

Figure A-40: Chloride bulk diffusion results for Mix 40 at six months of exposure

APPENDIX B: APPARENT CHLORIDE DIFFUSION: 12 MONTHS EXPOSURE

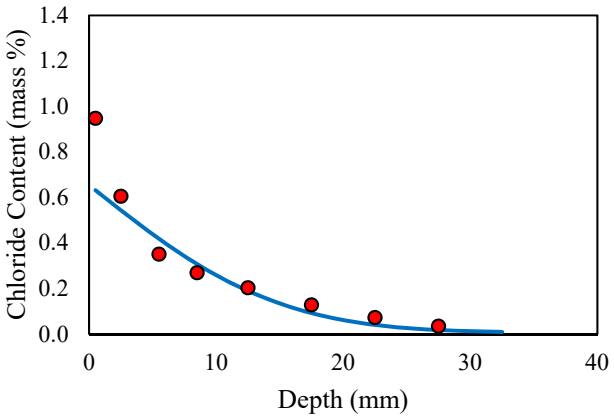

Mix No.	1
Mix ID	C-100
Exposure time (months)	12
Diffusion (m^2/s)	2.15×10^{-12}
Cs (mass %)	0.654
C_i (mass %)	0.01
R^2	0.950

Figure B-1: Chloride bulk diffusion results for Mix 1 at one year exposure

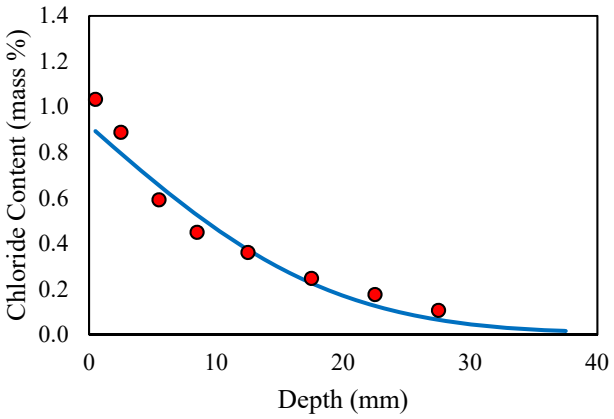

Mix No.	2
Mix ID	C-100h
Exposure time (months)	12
Diffusion (m^2/s)	2.15×10^{-12}
Cs (mass %)	0.918
C_i (mass %)	0.01
R^2	0.951

Figure B-2: Chloride bulk diffusion results for Mix 2 at one year exposure

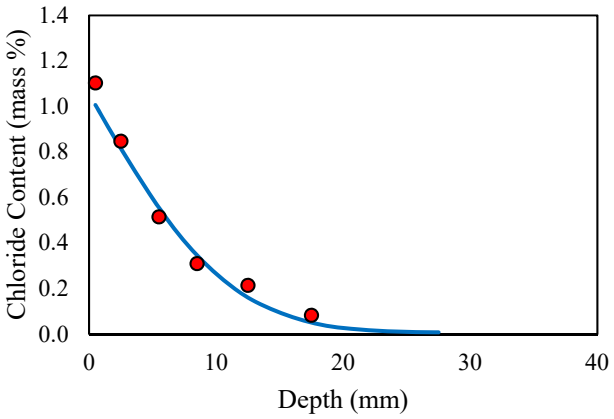

Mix No.	3
Mix ID	C-F10
Exposure time (months)	12
Diffusion (m^2/s)	1.18×10^{-12}
Cs (mass %)	1.055
C_i (mass %)	0.006
R^2	0.981

Figure B-3: Chloride bulk diffusion results for Mix 3 at one year exposure

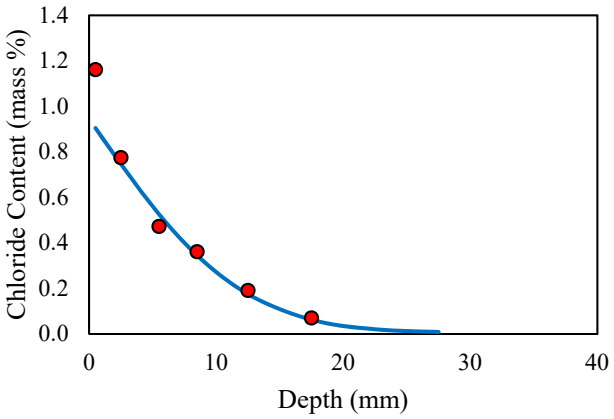

Mix No.	4
Mix ID	C-F20
Exposure time (months)	12
Diffusion (m^2/s)	1.38×10^{-12}
Cs (mass %)	0.945
C_i (mass %)	0.006
R^2	0.985

Figure B-4: Chloride bulk diffusion results for Mix 4 at one year exposure

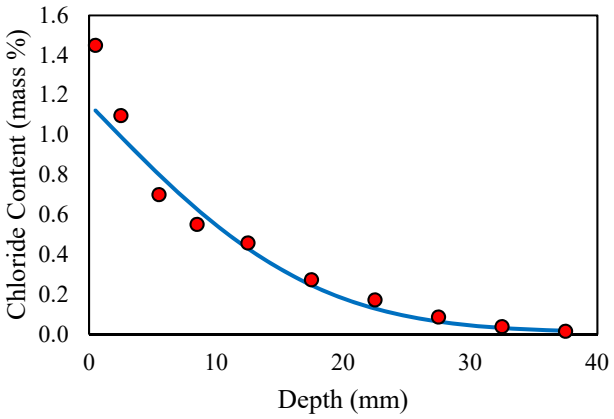

Mix No.	5
Mix ID	C-F10h
Exposure time (months)	12
Diffusion (m^2/s)	3.03×10^{-12}
Cs (mass %)	1.155
C_i (mass %)	0.009
R^2	0.971

Figure B-5: Chloride bulk diffusion results for Mix 5 at one year exposure

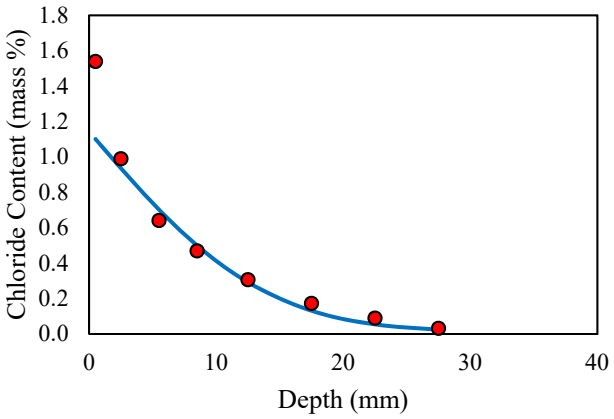

Mix No.	6
Mix ID	C-F20h
Exposure time (months)	12
Diffusion (m^2/s)	1.85×10^{-12}
Cs (mass %)	1.143
C_i (mass %)	.012
R^2	0.986

Figure B-6: Chloride bulk diffusion results for Mix 6 at one year exposure

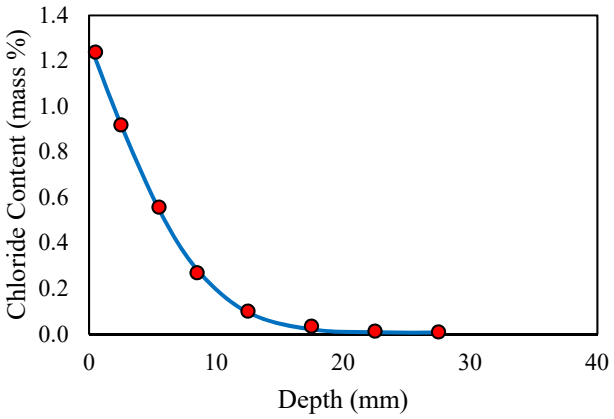

Mix No.	7
Mix ID	C-G60
Exposure time (months)	12
Diffusion (m^2/s)	0.75×10^{-12}
Cs (mass %)	1.283
C_i (mass %)	0.007
R^2	0.999

Figure B-7: Chloride bulk diffusion results for Mix 7 at one year exposure

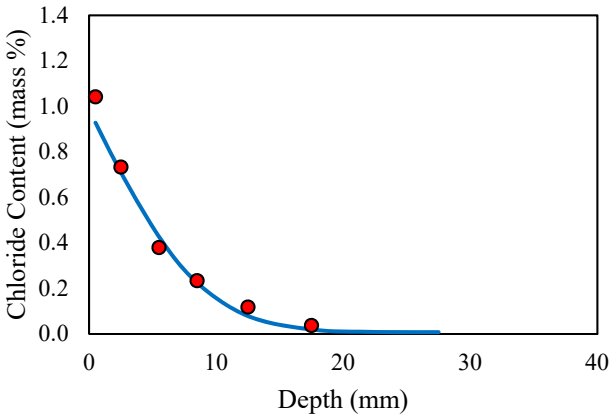

Mix No.	8
Mix ID	C-S8
Exposure time (months)	12
Diffusion (m^2/s)	0.77×10^{-12}
Cs (mass %)	0.984
C_i (mass %)	0.008
R^2	0.987

Figure B-8: Chloride bulk diffusion results for Mix 8 at one year exposure

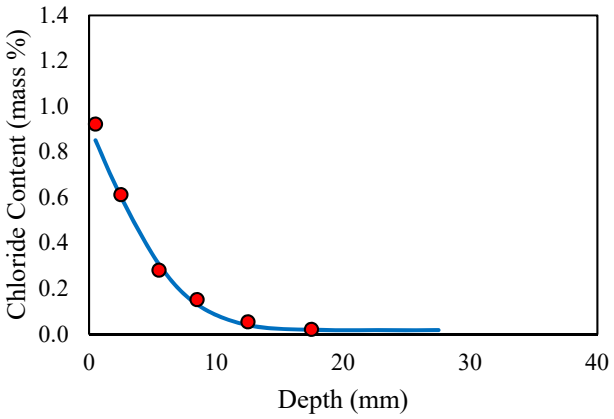

Mix No.	9
Mix ID	C-M10
Exposure time (months)	12
Diffusion (m^2/s)	0.49×10^{-12}
Cs (mass %)	0.916
C_i (mass %)	0.017
R^2	0.995

Figure B-9: Chloride bulk diffusion results for Mix 9 at one year exposure

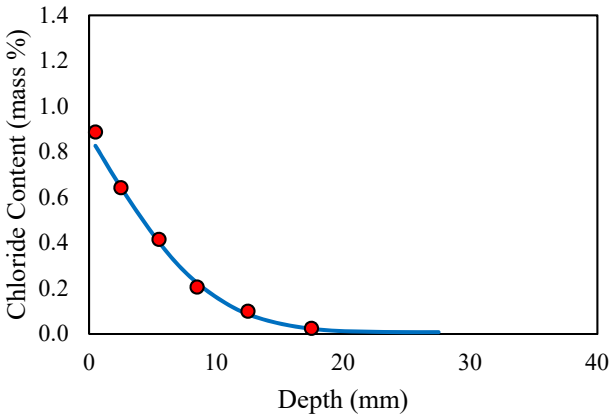

Mix No.	10
Mix ID	C-F10G30
Exposure time (months)	12
Diffusion (m^2/s)	0.87×10^{-12}
Cs (mass %)	0.873
C_i (mass %)	.008
R^2	0.997

Figure B-10: Chloride bulk diffusion results for Mix 10 at one year exposure

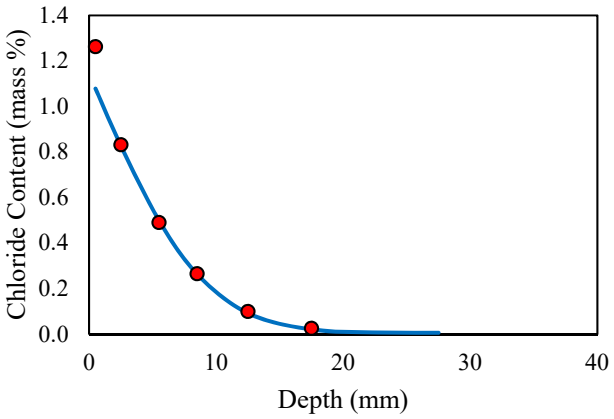

Mix No.	11
Mix ID	C-F10G45
Exposure time (months)	12
Diffusion (m^2/s)	0.78×10^{-12}
Cs (mass %)	1.143
C_i (mass %)	0.006
R^2	1.000

Figure B-11: Chloride bulk diffusion results for Mix 11 at one year exposure

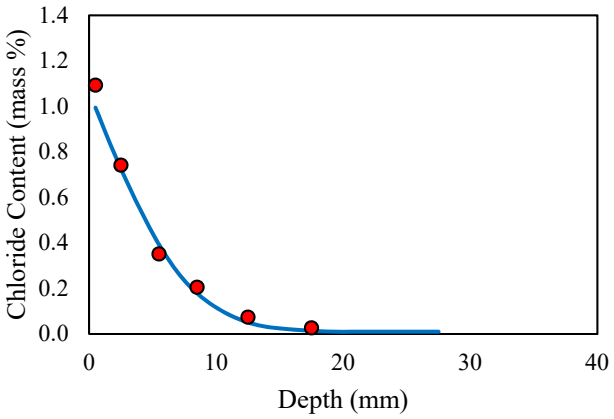

Mix No.	12
Mix ID	C-F10G60
Exposure time (months)	12
Diffusion (m^2/s)	0.58×10^{-12}
Cs (mass %)	1.064
C_i (mass %)	0.010
R^2	0.991

Figure B-12: Chloride bulk diffusion results for Mix 12 at one year exposure

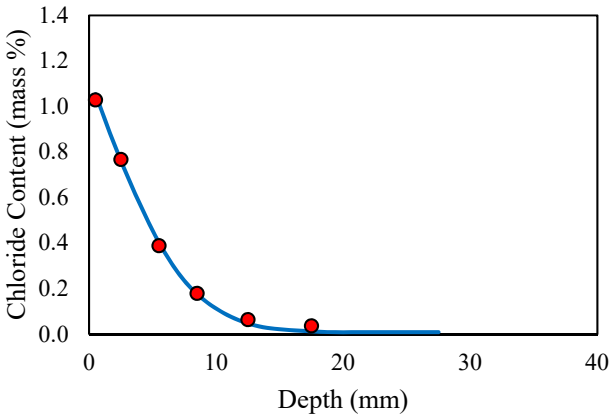

Mix No.	13
Mix ID	C-F10G60h
Exposure time (months)	12
Diffusion (m^2/s)	0.55×10^{-12}
Cs (mass %)	1.130
C_i (mass %)	0.008
R^2	0.998

Figure B-13: Chloride bulk diffusion results for Mix 13 at one year exposure

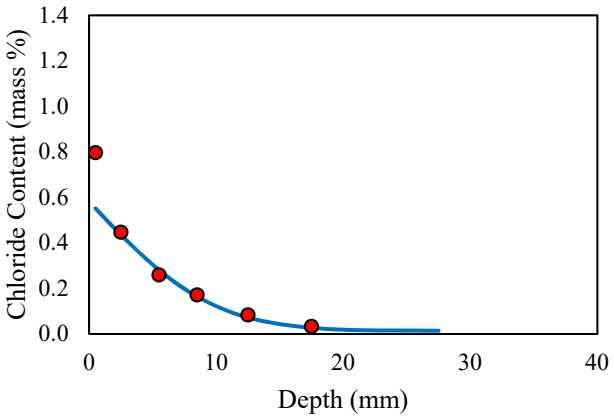

Mix No.	14
Mix ID	C-F20S4
Exposure time (months)	12
Diffusion (m^2/s)	0.92×10^{-12}
Cs (mass %)	0.581
C_i (mass %)	0.014
R^2	0.993

Figure B-14: Chloride bulk diffusion results for Mix 14 at one year exposure

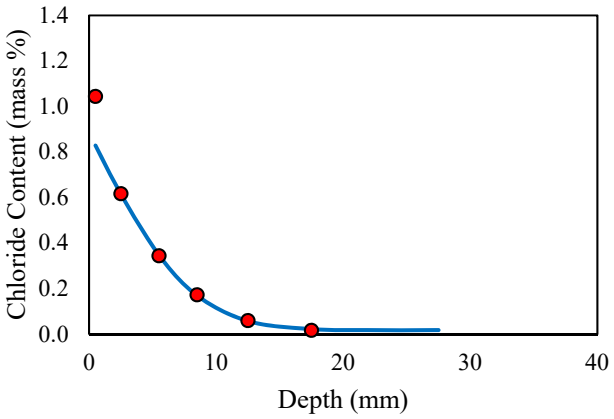

Mix No.	15
Mix ID	C-F20S6
Exposure time (months)	12
Diffusion (m^2/s)	0.62×10^{-12}
Cs (mass %)	0.883
C_i (mass %)	0.17
R^2	1.000

Figure B-15: Chloride bulk diffusion results for Mix 15 at one year exposure

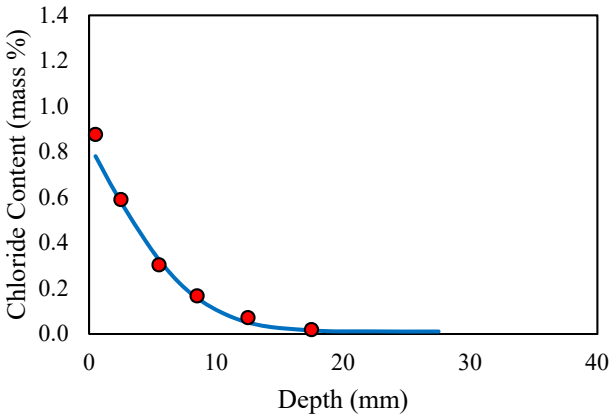

Mix No.	16
Mix ID	C-F20S8
Exposure time (months)	12
Diffusion (m^2/s)	0.63×10^{-12}
Cs (mass %)	0.833
C_i (mass %)	0.011
R^2	0.995

Figure B-16: Chloride bulk diffusion results for Mix 16 at one year exposure

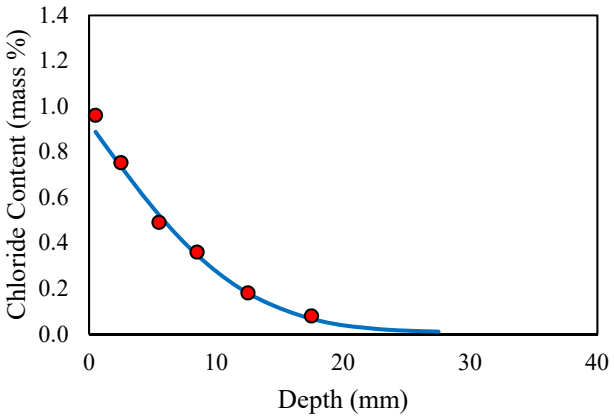

Mix No.	17
Mix ID	C-F20S8h
Exposure time (months)	12
Diffusion (m^2/s)	1.42×10^{-12}
Cs (mass %)	0.927
C_i (mass %)	0.007
R^2	0.994

Figure B-17: Chloride bulk diffusion results for Mix 17 at one year exposure

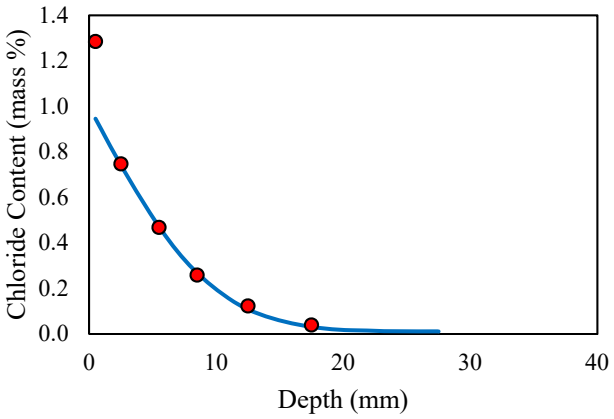

Mix No.	18
Mix ID	C-F20M6
Exposure time (months)	12
Diffusion (m^2/s)	0.91×10^{-12}
Cs (mass %)	0.998
C_i (mass %)	0.011
R^2	0.999

Figure B-18: Chloride bulk diffusion results for Mix 18 at one year exposure

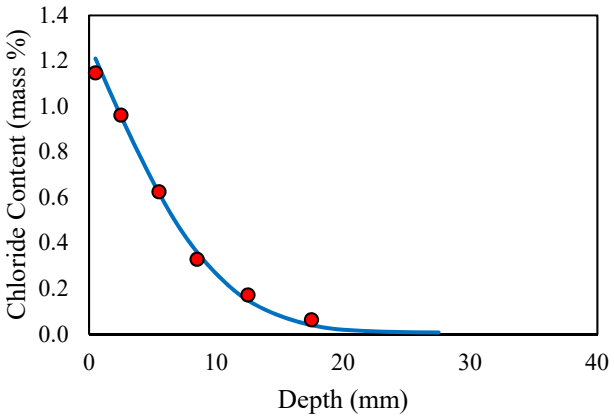

Mix No.	19
Mix ID	C-F20M8
Exposure time (months)	12
Diffusion (m^2/s)	0.98×10^{-12}
Cs (mass %)	1.275
C_i (mass %)	0.007
R^2	0.997

Figure B-19: Chloride bulk diffusion results for Mix 19 at one year exposure

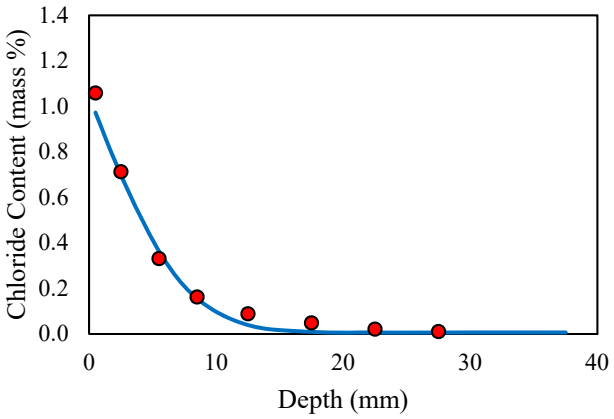

Mix No.	20
Mix ID	C-F20M10
Exposure time (months)	12
Diffusion (m^2/s)	0.54×10^{-12}
Cs (mass %)	1.044
C_i (mass %)	0.006
R^2	0.991

Figure B-20: Chloride bulk diffusion results for Mix 20 at one year exposure

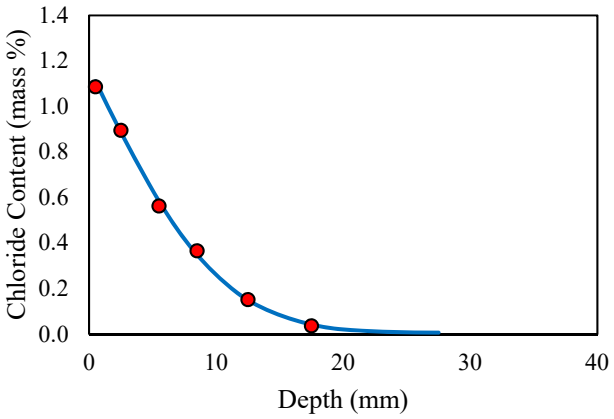

Mix No.	21
Mix ID	C-F20M10h
Exposure time (months)	12
Diffusion (m^2/s)	1.04×10^{-12}
Cs (mass %)	1.168
C_i (mass %)	0.005
R^2	0.998

Figure B-21: Chloride bulk diffusion results for Mix 21 at one year exposure

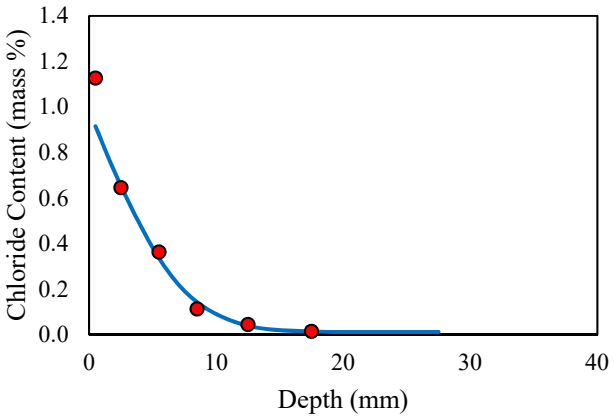

Mix No.	22
Mix ID	C-G55M8
Exposure time (months)	12
Diffusion (m^2/s)	0.51×10^{-12}
Cs (mass %)	0.983
C_i (mass %)	0.012
R^2	0.994

Figure B-22: Chloride bulk diffusion results for Mix 22 at one year exposure

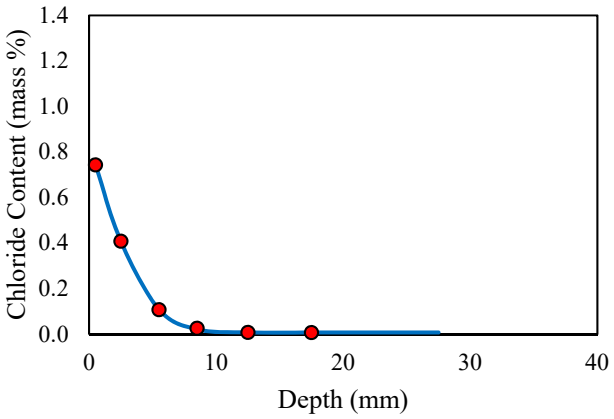

Mix No.	23
Mix ID	C-G55M10
Exposure time (months)	12
Diffusion (m^2/s)	0.20×10^{-12}
Cs (mass %)	0.837
C_i (mass %)	0.007
R^2	1.000

Figure B-23: Chloride bulk diffusion results for Mix 23 at one year exposure

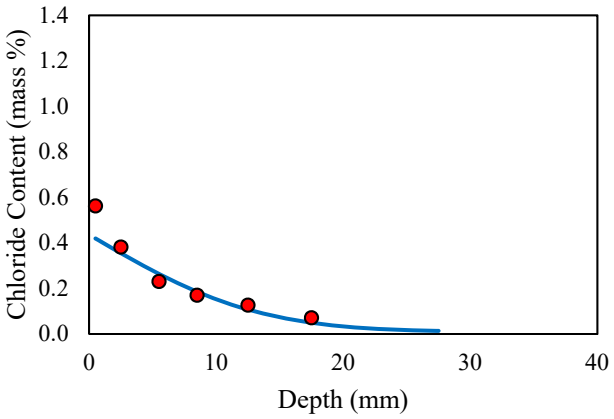

Mix No.	24
Mix ID	CV-100
Exposure time (months)	12
Diffusion (m^2/s)	1.70×10^{-12}
Cs (mass %)	0.436
C_i (mass %)	0.010
R^2	0.952

Figure B-24: Chloride bulk diffusion results for Mix 24 at one year exposure

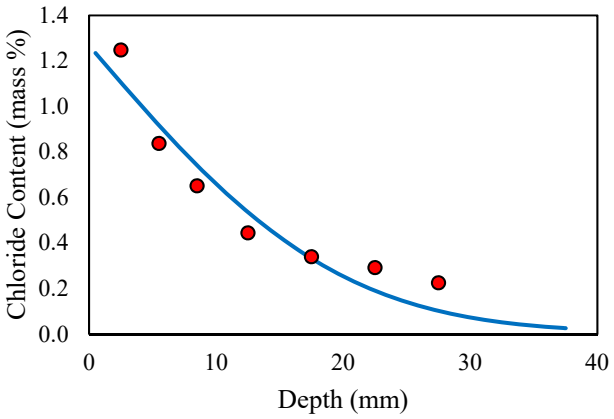

Mix No.	25
Mix ID	CV-100h
Exposure time (months)	12
Diffusion (m^2/s)	3.80×10^{-12}
Cs (mass %)	1.267
C_i (mass %)	0.006
R^2	0.922

Figure B-25: Chloride bulk diffusion results for Mix 25 at one year exposure

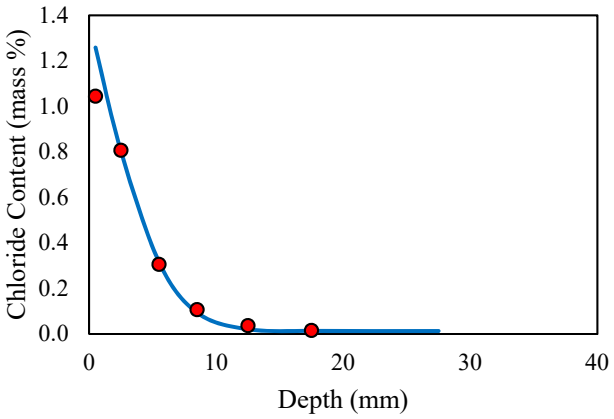

Mix No.	26
Mix ID	CV-F10G60
Exposure time (months)	12
Diffusion (m^2/s)	0.32×10^{-12}
Cs (mass %)	1.379
C_i (mass %)	0.013
R^2	0.999

Figure B-26: Chloride bulk diffusion results for Mix 26 at one year exposure

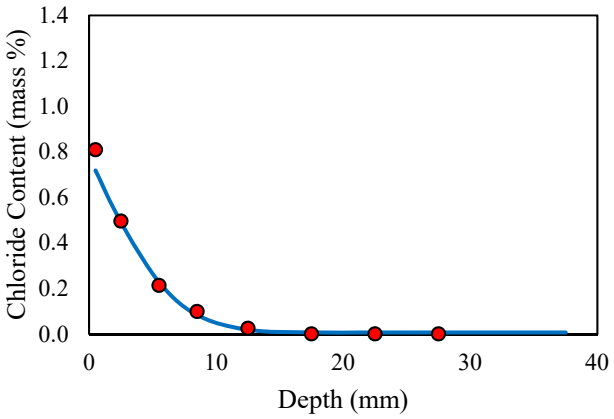

Mix No.	27
Mix ID	CV-F20S8
Exposure time (months)	12
Diffusion (m^2/s)	0.42×10^{-12}
Cs (mass %)	0.778
C_i (mass %)	0.007
R^2	0.997

Figure B-27: Chloride bulk diffusion results for Mix 27 at one year exposure

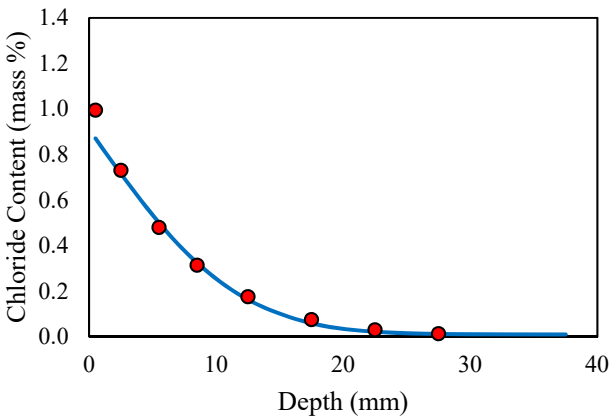

Mix No.	28
Mix ID	CV-M10
Exposure time (months)	12
Diffusion (m^2/s)	1.31×10^{-12}
Cs (mass %)	0.910
C_i (mass %)	0.009
R^2	0.997

Figure B-28: Chloride bulk diffusion results for Mix 28 at one year exposure

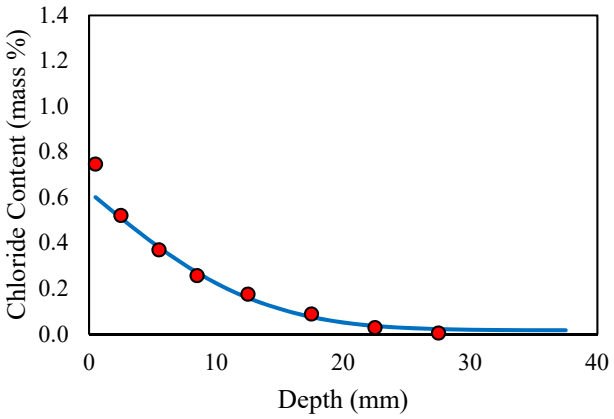

Mix No.	29
Mix ID	CL-100
Exposure time (months)	12
Diffusion (m^2/s)	1.75×10^{-12}
Cs (mass %)	0.624
C_i (mass %)	0.016
R^2	0.994

Figure B-29: Chloride bulk diffusion results for Mix 29 at one year exposure

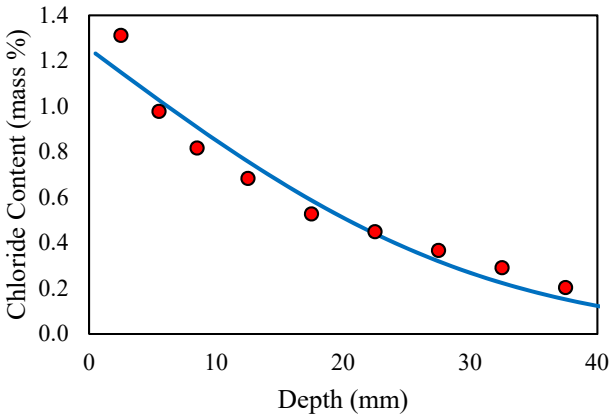

Mix No.	30
Mix ID	CL-100h
Exposure time (months)	12
Diffusion (m^2/s)	9.19×10^{-12}
Cs (mass %)	1.253
C_i (mass %)	0.002
R^2	0.948

Figure B-30: Chloride bulk diffusion results for Mix 30 at one year exposure

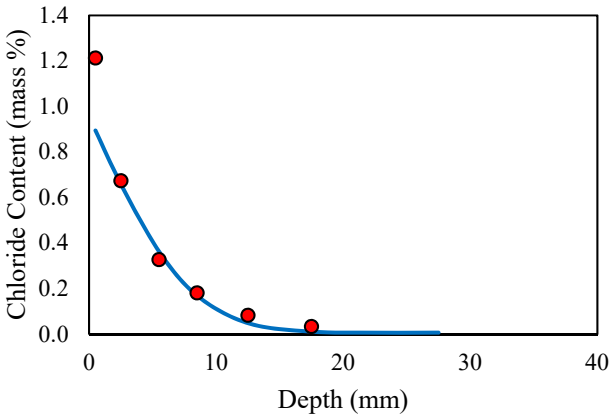

Mix No.	31
Mix ID	CL-F10G60
Exposure time (months)	12
Diffusion (m^2/s)	0.61×10^{-12}
Cs (mass %)	0.955
C_i (mass %)	0.006
R^2	0.991

Figure B-31: Chloride bulk diffusion results for Mix 31 at one year exposure

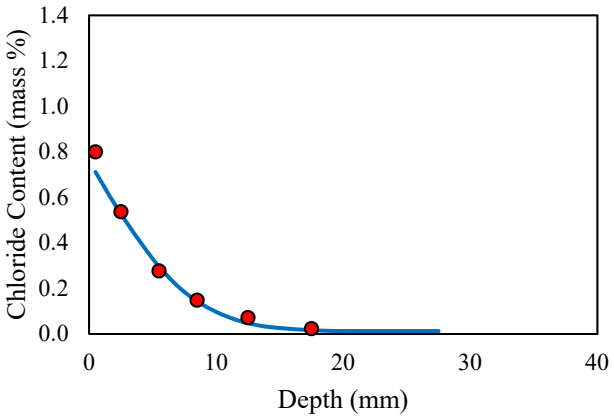

Mix No.	32
Mix ID	CL-F20S8
Exposure time (months)	12
Diffusion (m^2/s)	0.00×10^{-12}
Cs (mass %)	0.759
C_i (mass %)	0.013
R^2	0.995

Figure B-32: Chloride bulk diffusion results for Mix 32 at one year exposure

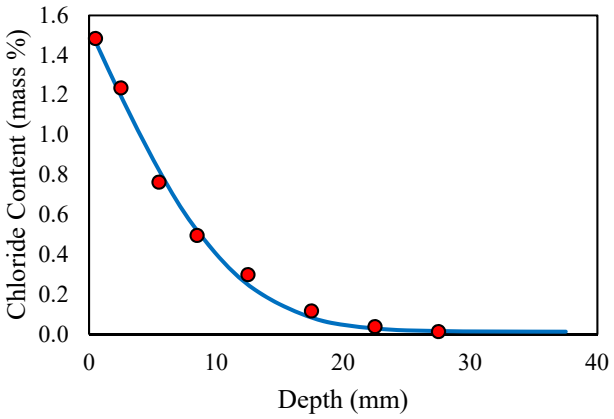

Mix No.	33
Mix ID	CL-M10
Exposure time (months)	12
Diffusion (m^2/s)	1.22×10^{-12}
Cs (mass %)	1.538
C_i (mass %)	0.012
R^2	0.993

Figure B-33: Chloride bulk diffusion results for Mix 33 at one year exposure

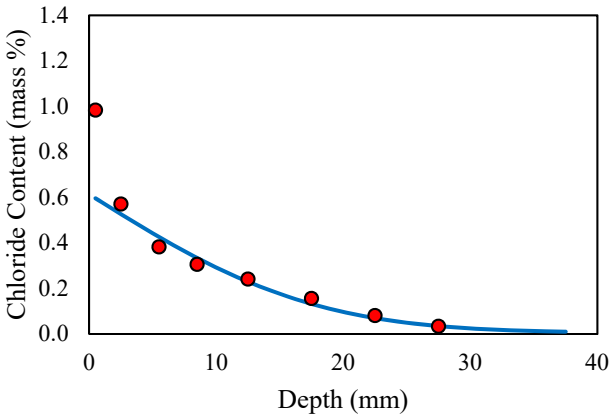

Mix No.	34
Mix ID	CHA-100
Exposure time (months)	12
Diffusion (m^2/s)	3.06×10^{-12}
Cs (mass %)	0.613
C_i (mass %)	0.006
R^2	0.974

Figure B-34: Chloride bulk diffusion results for Mix 34 at one year exposure

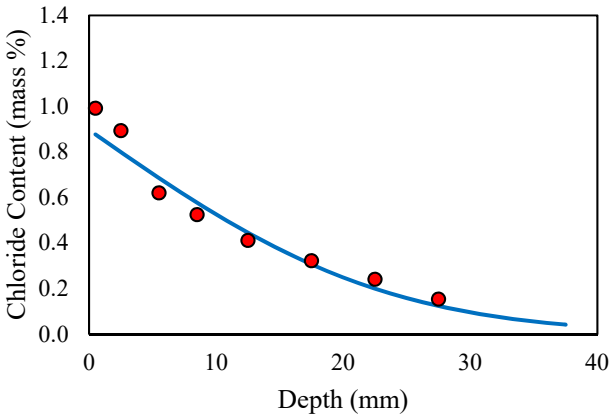

Mix No.	35
Mix ID	CHA-100h
Exposure time (months)	12
Diffusion (m^2/s)	5.28×10^{-12}
Cs (mass %)	0.896
C_i (mass %)	0.006
R^2	0.949

Figure B-35: Chloride bulk diffusion results for Mix 35 at one year exposure

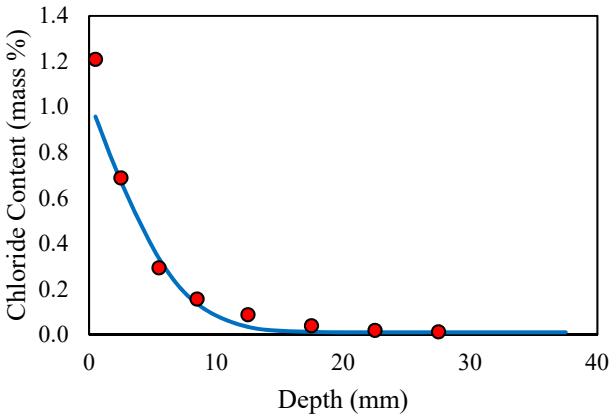

Mix No.	36
Mix ID	CHA-F10G60
Exposure time (months)	12
Diffusion (m^2/s)	0.48×10^{-12}
Cs (mass %)	1.031
C_i (mass %)	0.010
R^2	0.987

Figure B-36: Chloride bulk diffusion results for Mix 36 at one year exposure

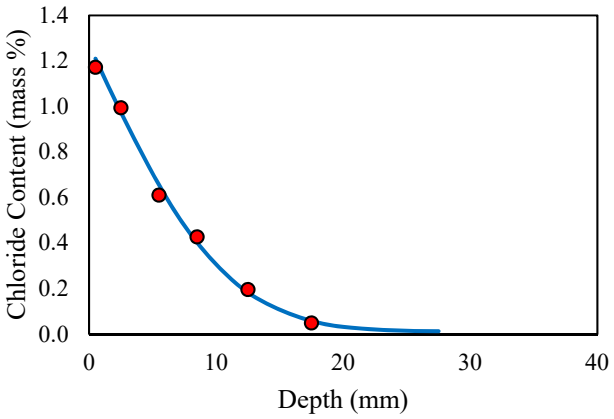

Mix No.	37
Mix ID	CHA-F20S8
Exposure time (months)	12
Diffusion (m^2/s)	1.12×10^{-12}
Cs (mass %)	1.269
C_i (mass %)	0.011
R^2	0.994

Figure B-37: Chloride bulk diffusion results for Mix 37 at one year exposure

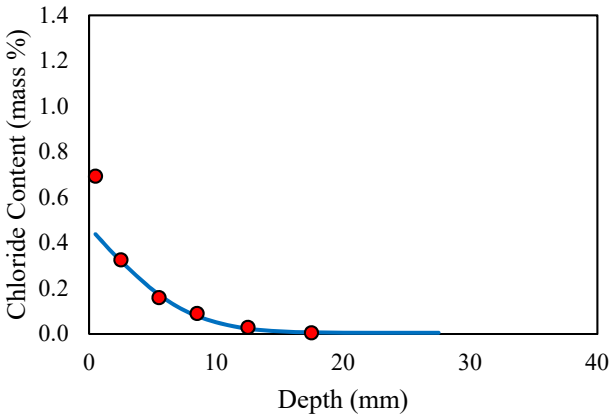

Mix No.	38
Mix ID	CHA-M10
Exposure time (months)	12
Diffusion (m^2/s)	0.58×10^{-12}
Cs (mass %)	0.469
C_i (mass %)	0.005
R^2	0.994

Figure B-38: Chloride bulk diffusion results for Mix 38 at one year exposure

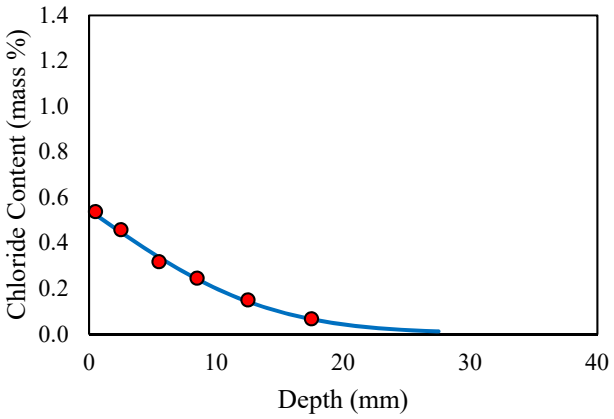

Mix No.	39
Mix ID	C-100SS
Exposure time (months)	12
Diffusion (m^2/s)	0.58×10^{-12}
Cs (mass %)	0.544
C_i (mass %)	0.005
R^2	0.994

Figure B-39: Chloride bulk diffusion results for Mix 39 at one year exposure

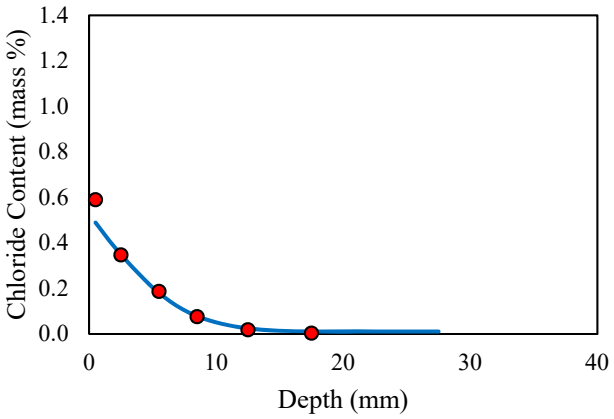

Mix No.	40
Mix ID	C-F20S8SS
Exposure time (months)	12
Diffusion (m^2/s)	0.50×10^{-12}
Cs (mass %)	0.525
C_i (mass %)	0.011
R^2	0.999

Figure B-40: Chloride bulk diffusion results for Mix 40 at one year exposure

APPENDIX C: EFFECTIVE CHLORIDE DIFFUSION: 6 MONTHS EXPOSURE

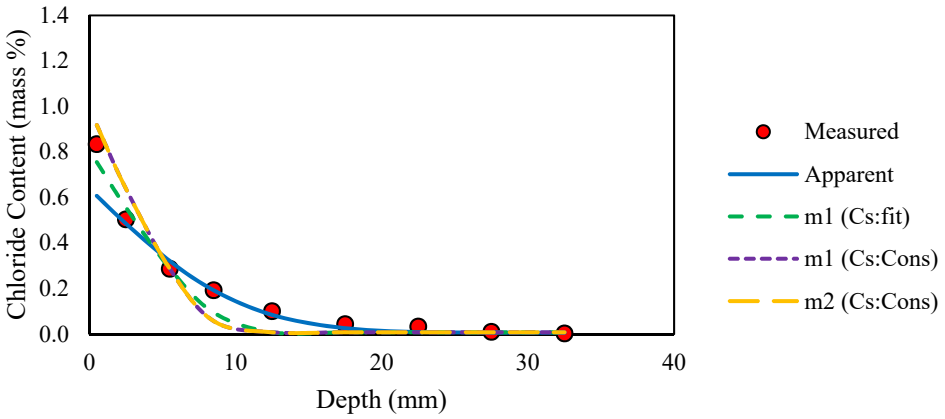

Figure C-1: Effective Chloride bulk diffusion results for Mix 1 at six month exposure

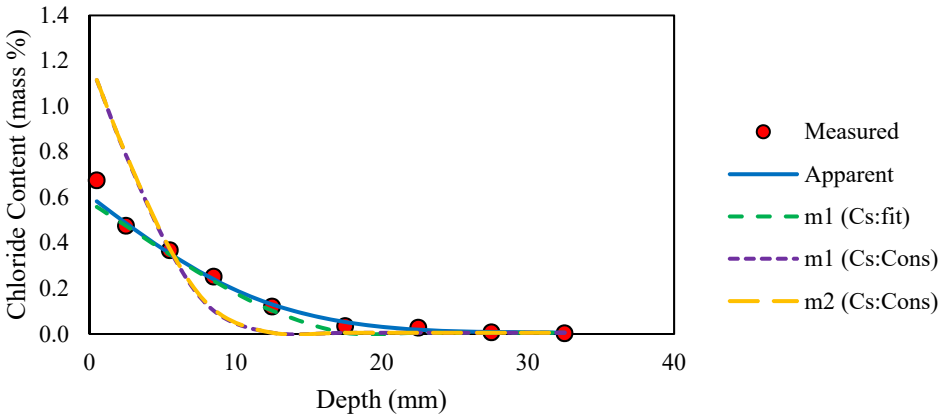

Figure C-2: Effective Chloride bulk diffusion results for Mix 2 at six month exposure

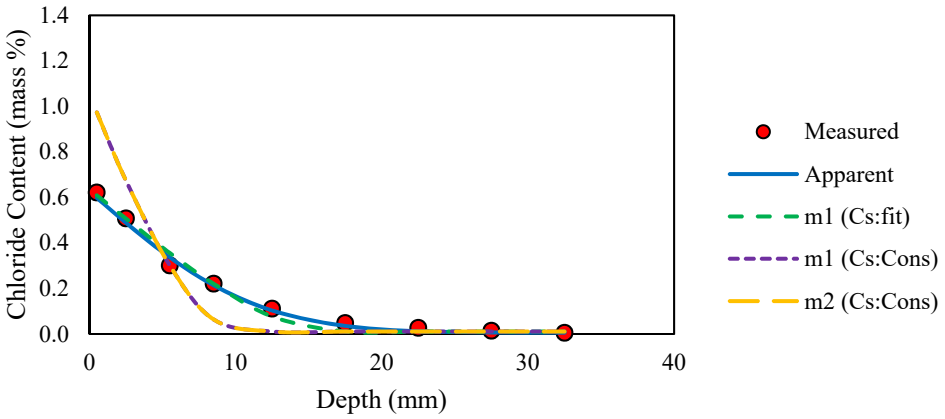

Figure C-3: Effective Chloride bulk diffusion results for Mix 3 at six month exposure

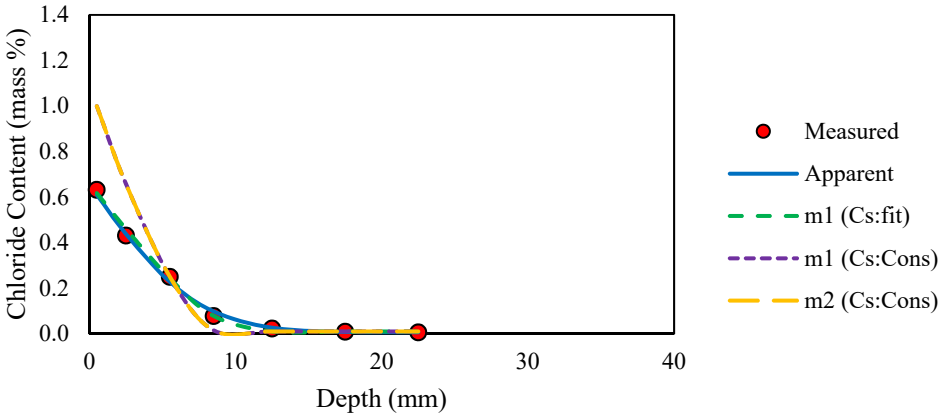

Figure C-4: Effective Chloride bulk diffusion results for Mix 4 at six month exposure

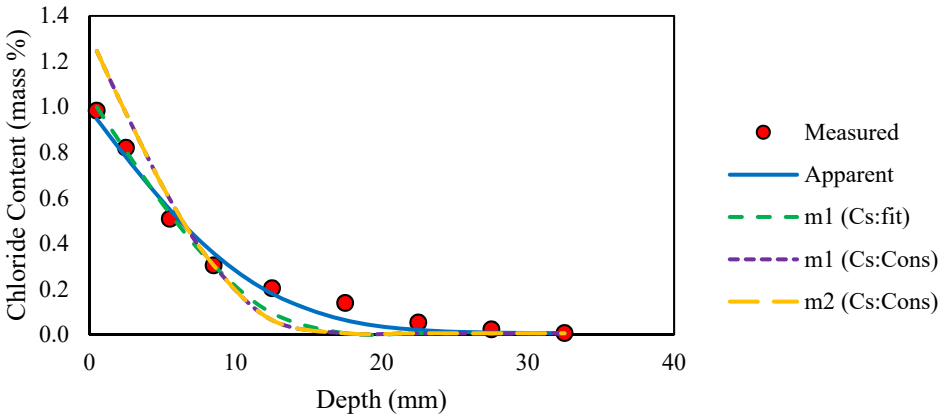

Figure C-5: Effective Chloride bulk diffusion results for Mix 5 at six month exposure

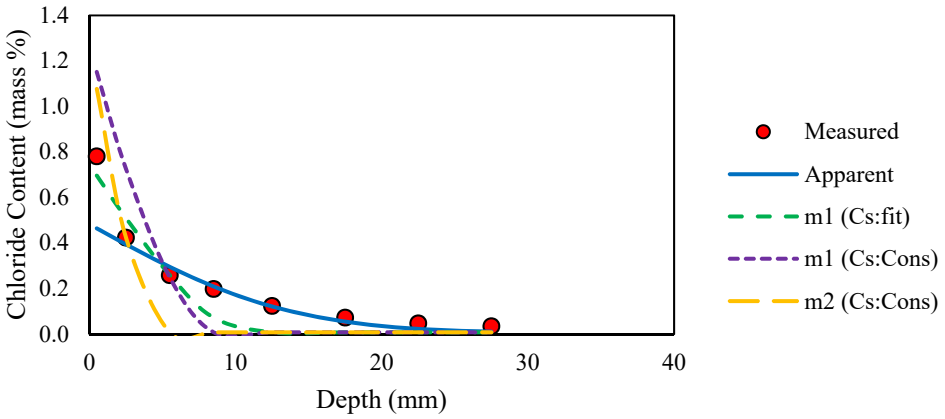

Figure C-6: Effective Chloride bulk diffusion results for Mix 6 at six month exposure

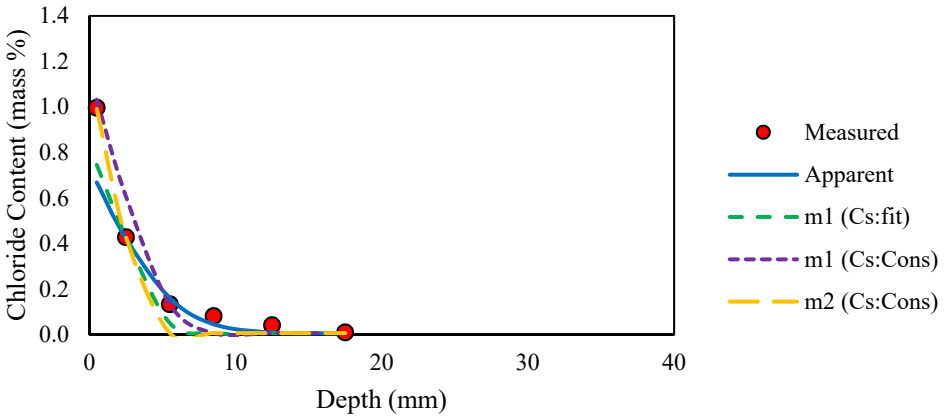

Figure C-7: Effective Chloride bulk diffusion results for Mix 7 at six month exposure

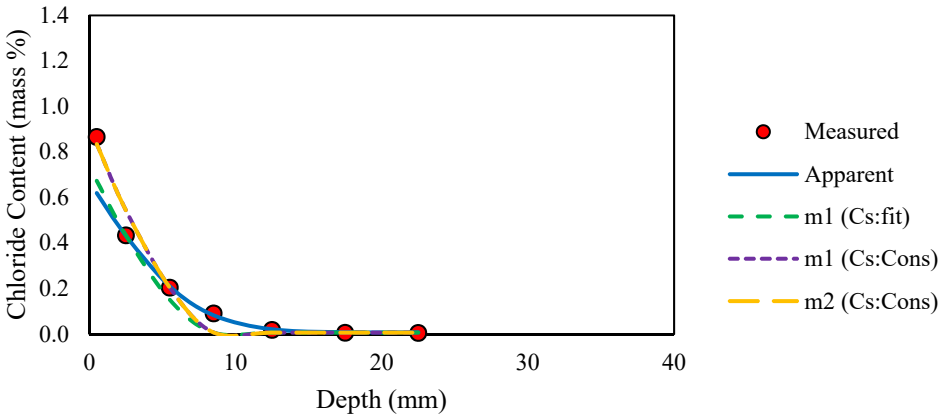

Figure C-8: Effective Chloride bulk diffusion results for Mix 8 at six month exposure

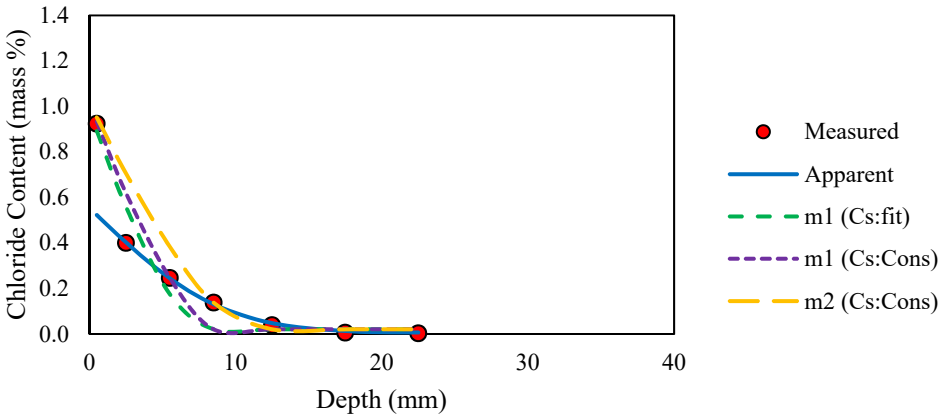

Figure C-9: Effective Chloride bulk diffusion results for Mix 9 at six month exposure

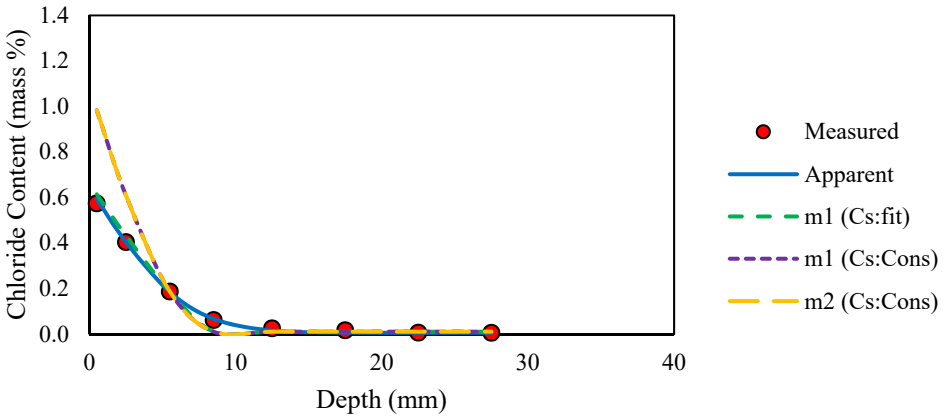

Figure C-10: Effective Chloride bulk diffusion results for Mix 10 at six month exposure

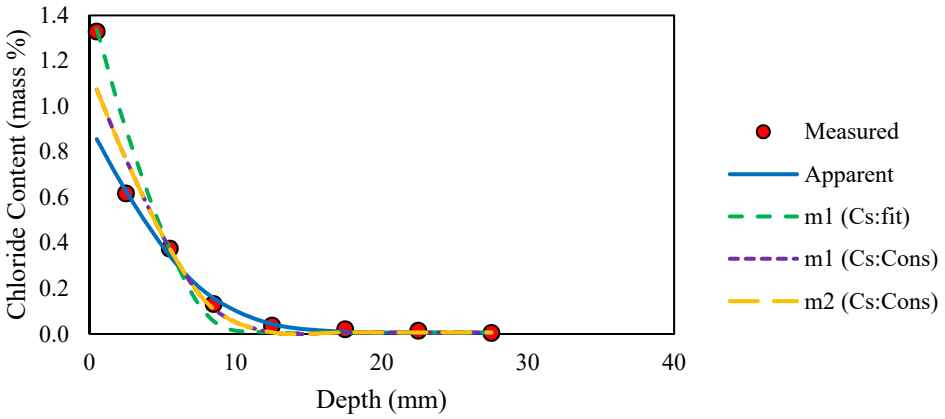

Figure C-11: Effective Chloride bulk diffusion results for Mix 11 at six month exposure

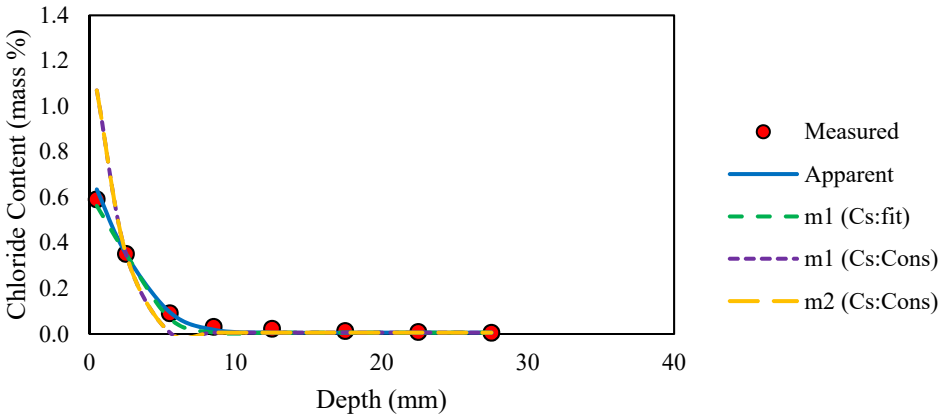

Figure C-12: Effective Chloride bulk diffusion results for Mix 12 at six month exposure

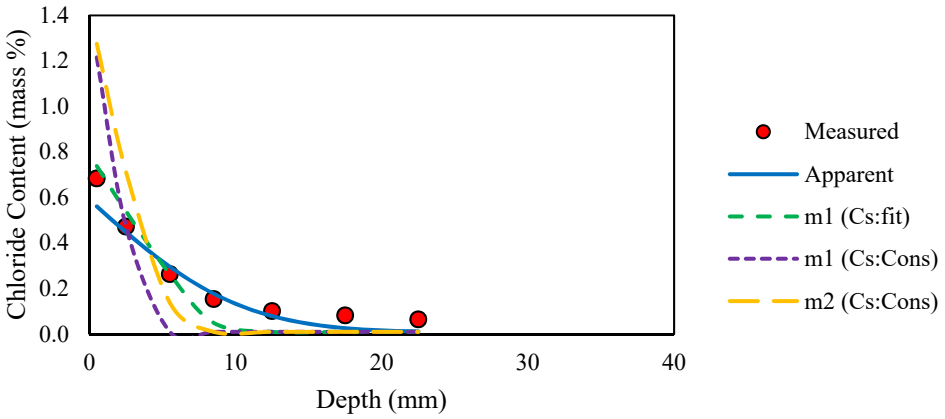

Figure C-13: Effective Chloride bulk diffusion results for Mix 13 at six month exposure

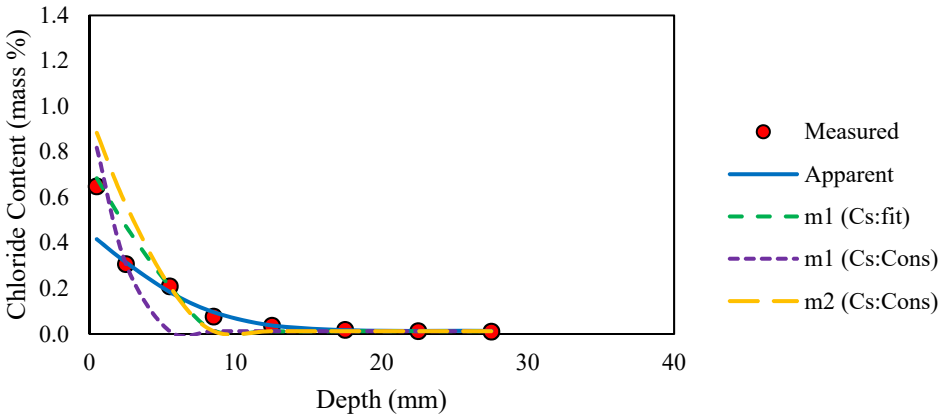

Figure C-14: Effective Chloride bulk diffusion results for Mix 14 at six month exposure

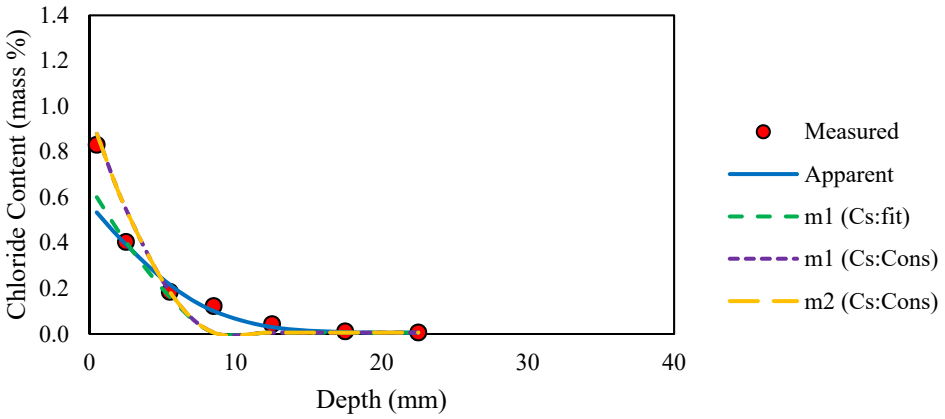

Figure C-15: Effective Chloride bulk diffusion results for Mix 15 at six month exposure

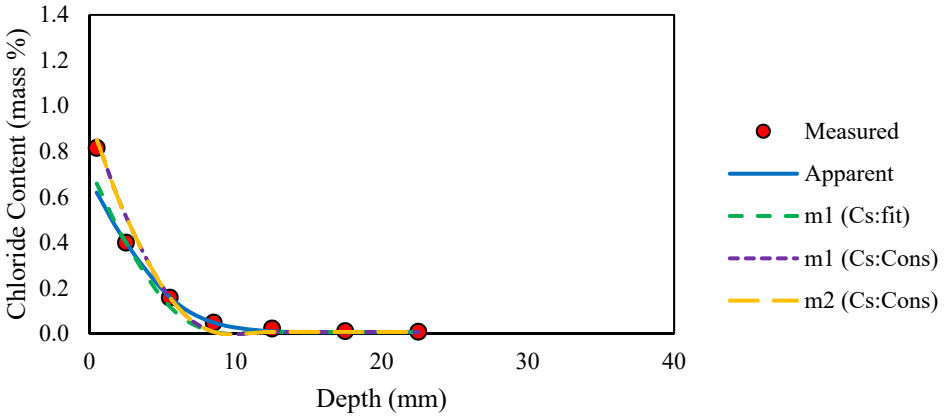

Figure C-16: Effective Chloride bulk diffusion results for Mix 1 at six month exposure

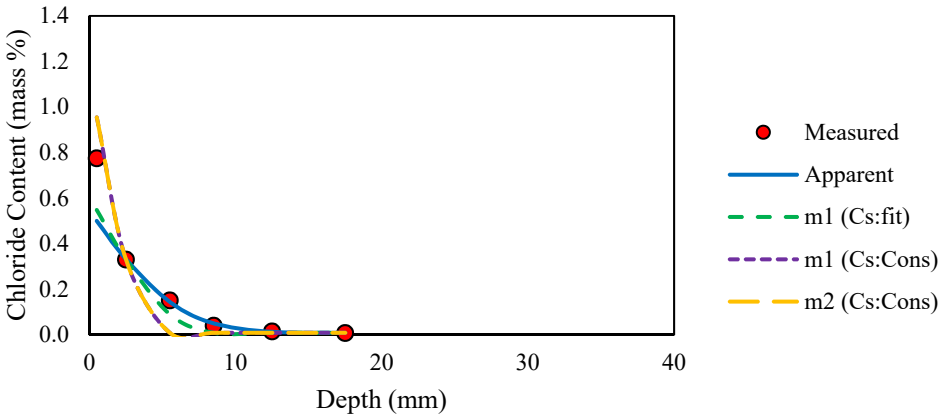

Figure C-17: Effective Chloride bulk diffusion results for Mix 17 at six month exposure

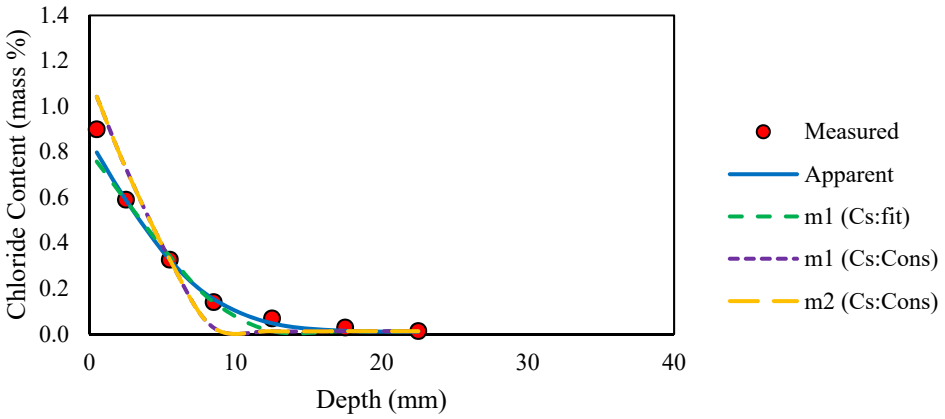

Figure C-18: Effective Chloride bulk diffusion results for Mix 18 at six month exposure

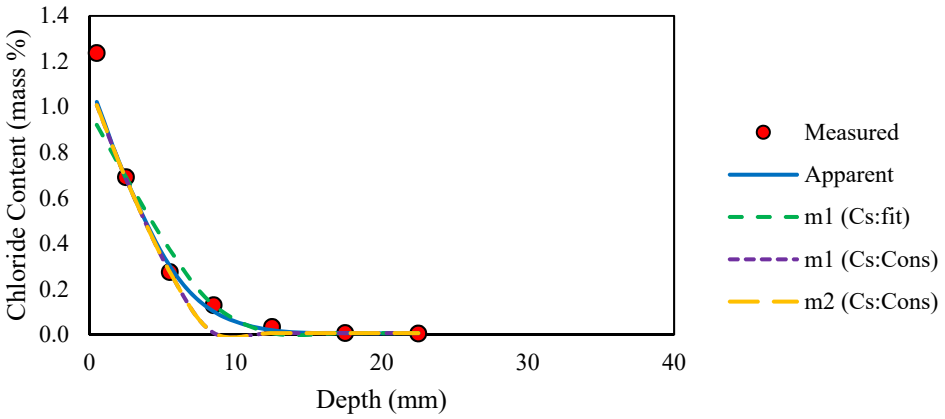

Figure C-19: Effective Chloride bulk diffusion results for Mix 19 at six month exposure

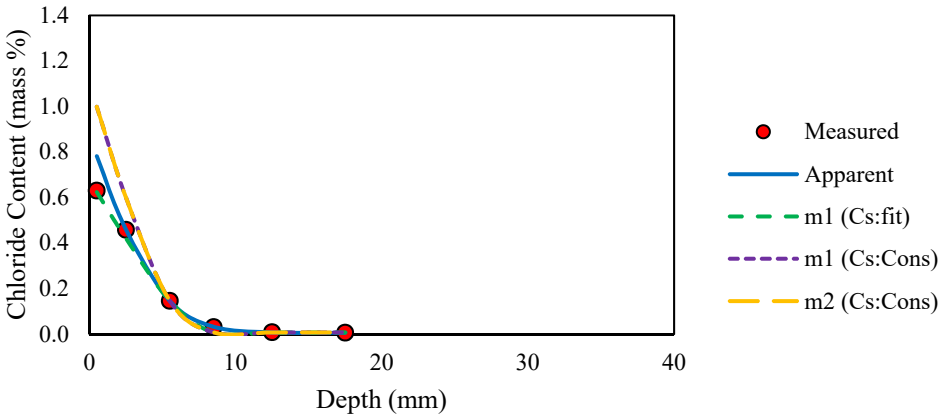

Figure C-20: Effective Chloride bulk diffusion results for Mix 20 at six month exposure

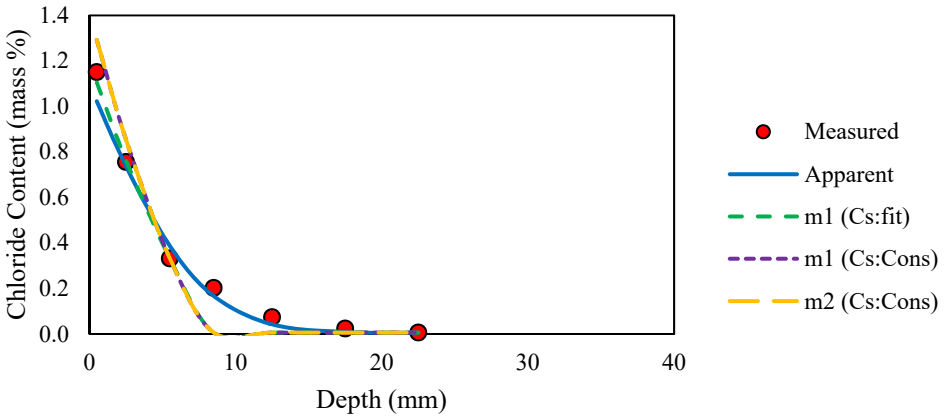

Figure C-21: Effective Chloride bulk diffusion results for Mix 21 at six month exposure

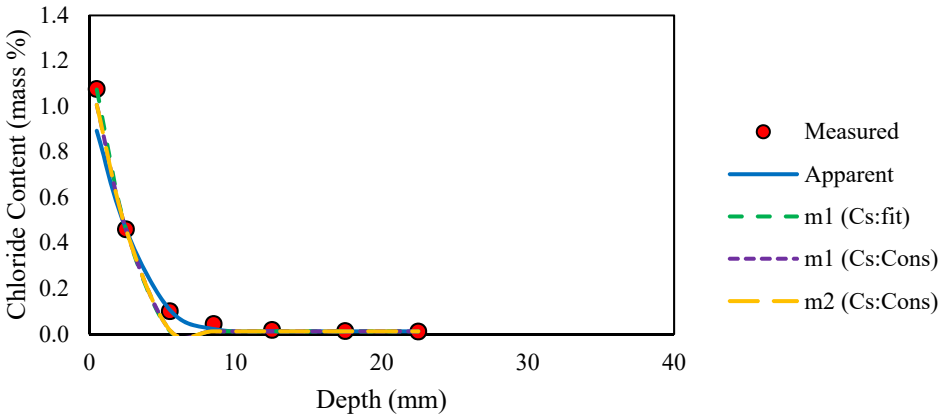

Figure C-22: Effective Chloride bulk diffusion results for Mix 1 at six month exposure

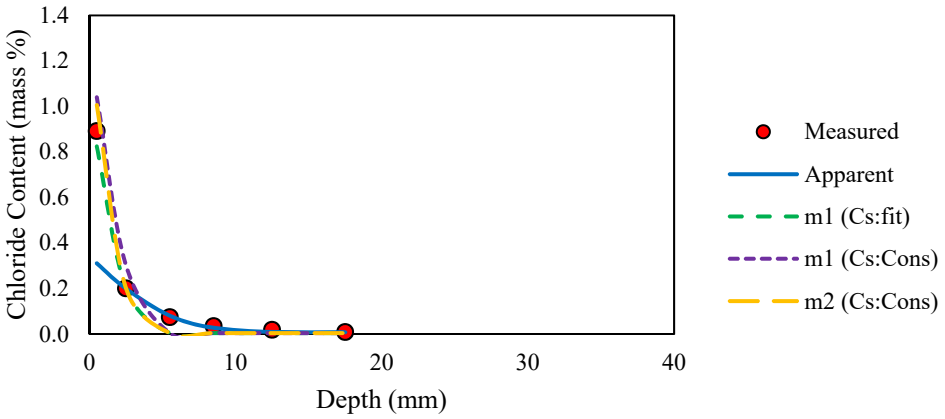

Figure C-23: Effective Chloride bulk diffusion results for Mix 23 at six month exposure

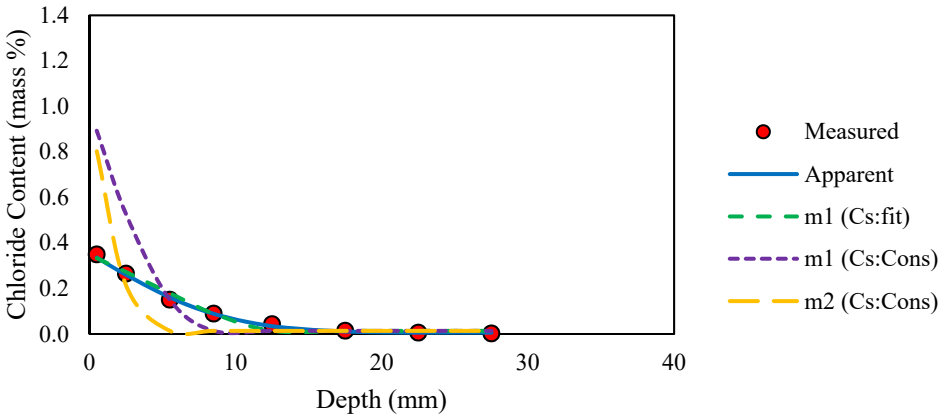

Figure C-24: Effective Chloride bulk diffusion results for Mix 24 at six month exposure

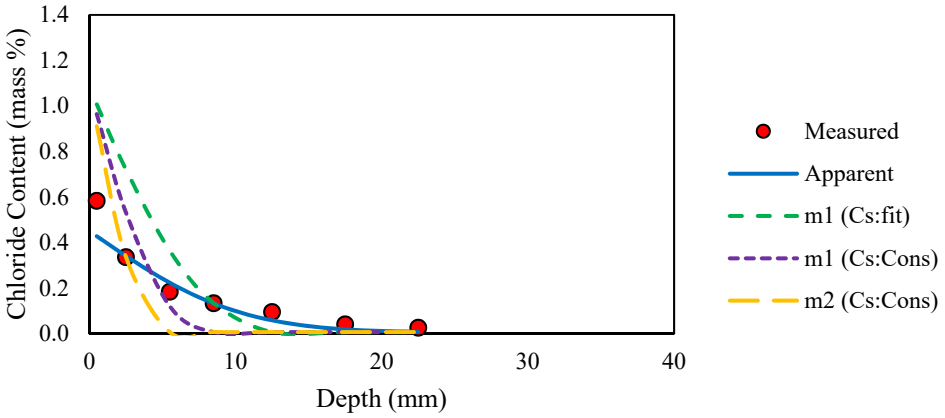

Figure C-25: Effective Chloride bulk diffusion results for Mix 25 at six month exposure

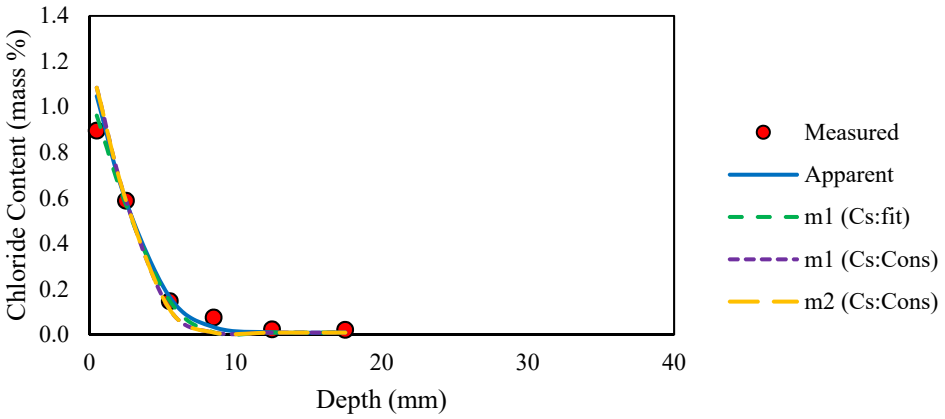

Figure C-26: Effective Chloride bulk diffusion results for Mix 26 at six month exposure

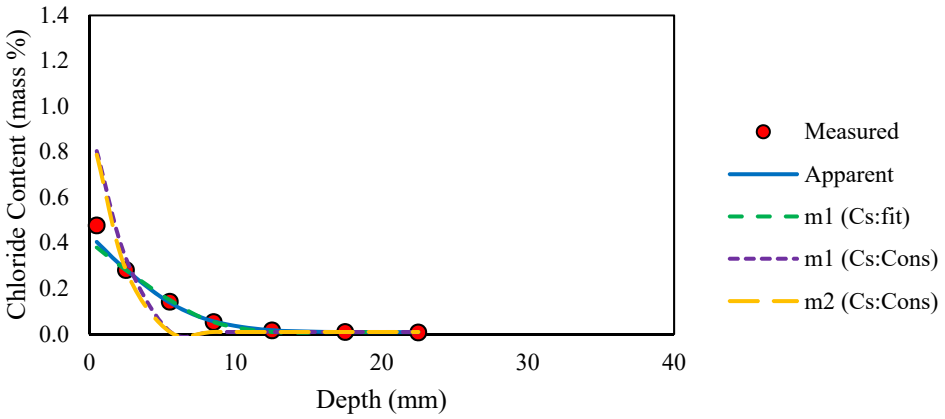

Figure C-27: Effective Chloride bulk diffusion results for Mix 27 at six month exposure

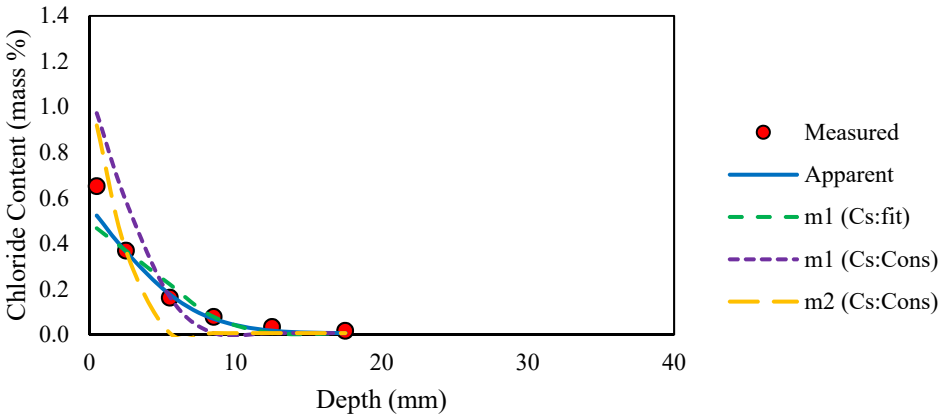

Figure C-28: Effective Chloride bulk diffusion results for Mix 28 at six month exposure

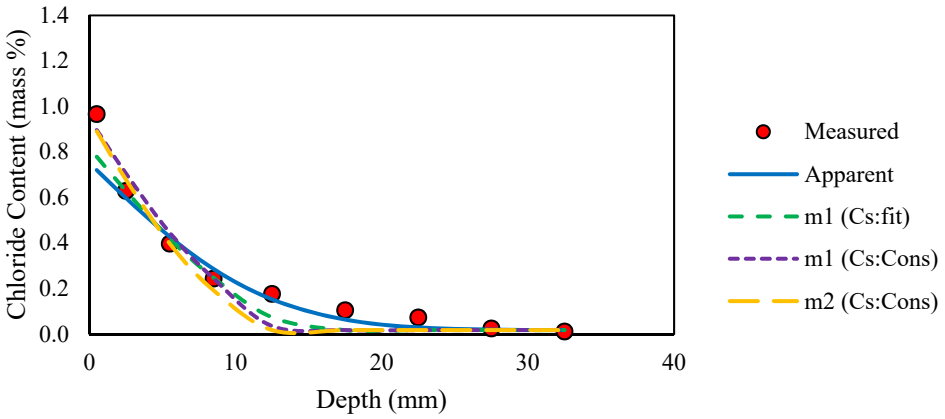

Figure C-29: Effective Chloride bulk diffusion results for Mix 29 at six month exposure

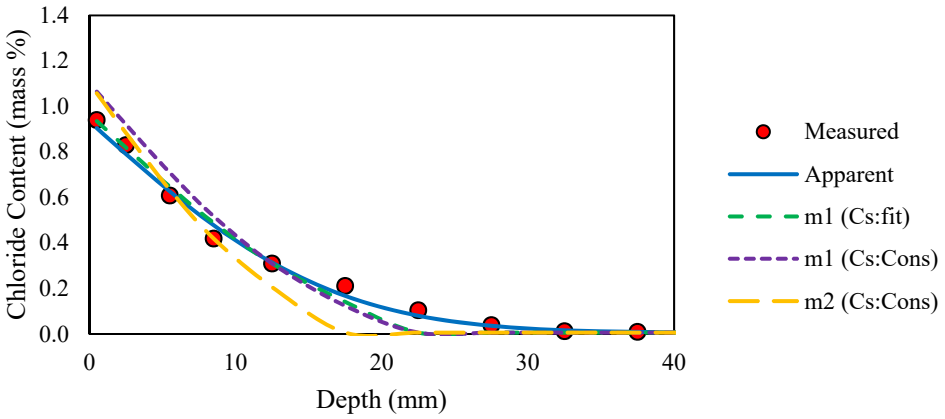

Figure C-30: Effective Chloride bulk diffusion results for Mix 30 at six month exposure

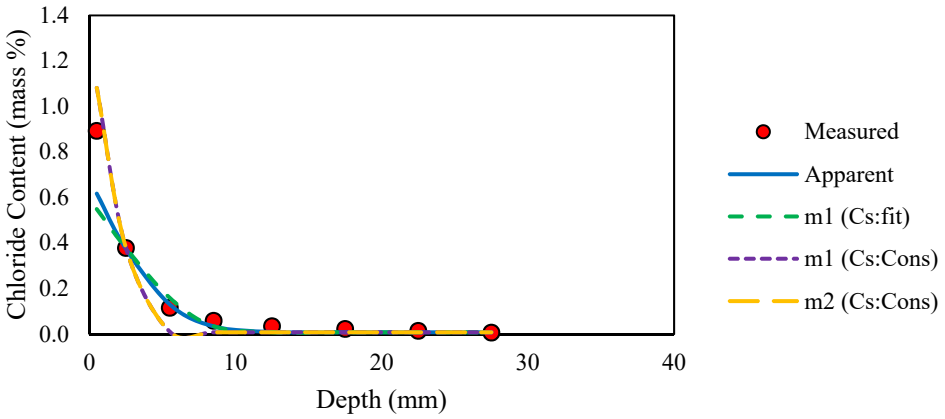

Figure C-31: Effective Chloride bulk diffusion results for Mix 31 at six month exposure

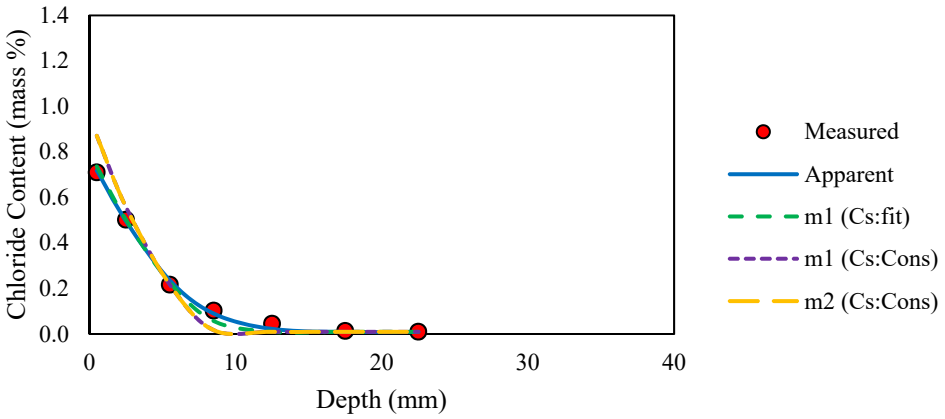

Figure C-32: Effective Chloride bulk diffusion results for Mix 32 at six month exposure

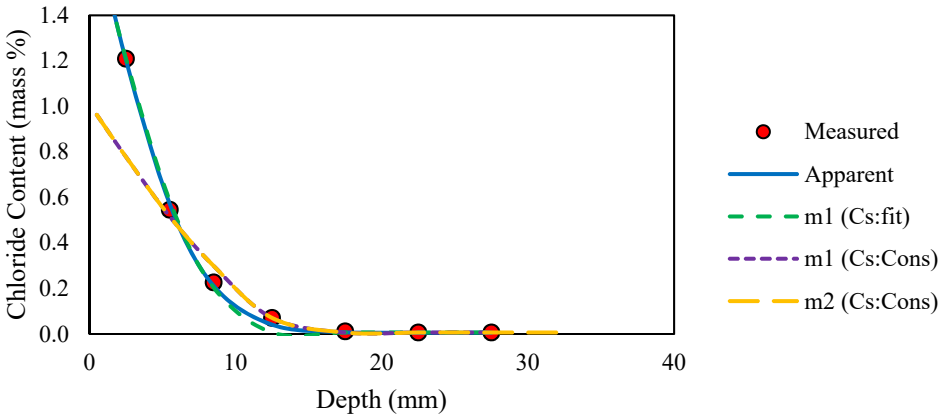

Figure C-33: Effective Chloride bulk diffusion results for Mix 33 at six month exposure

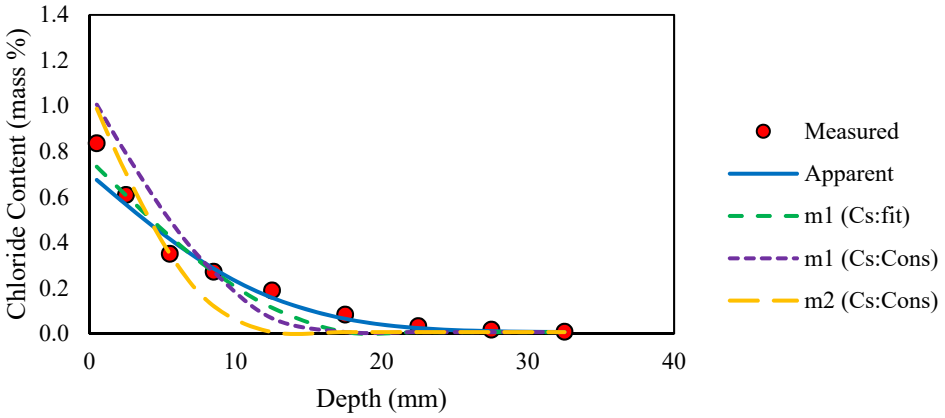

Figure C-34: Effective Chloride bulk diffusion results for Mix 34 at six month exposure

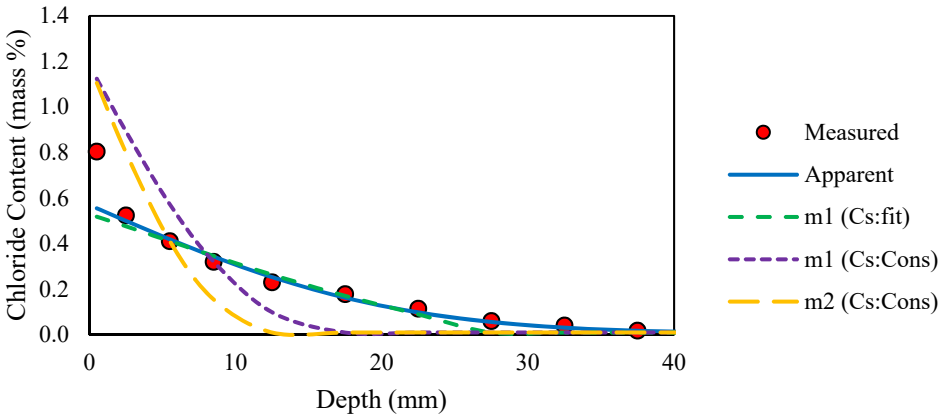

Figure C-35: Effective Chloride bulk diffusion results for Mix 35 at six month exposure

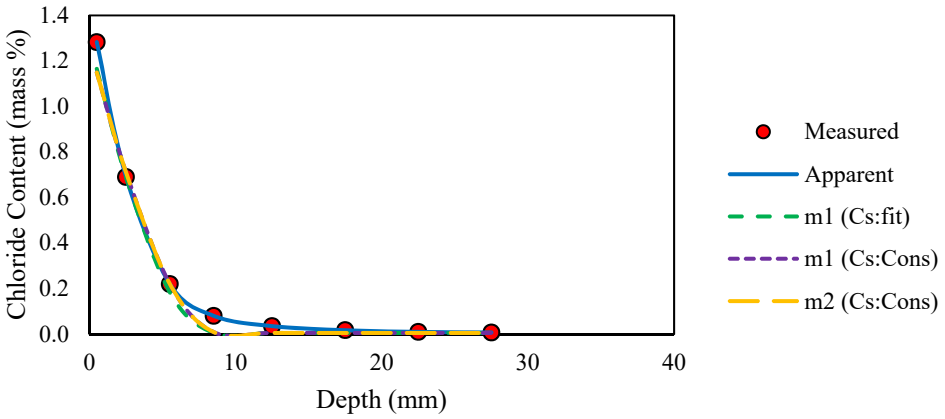

Figure C-36: Effective Chloride bulk diffusion results for Mix 36 at six month exposure

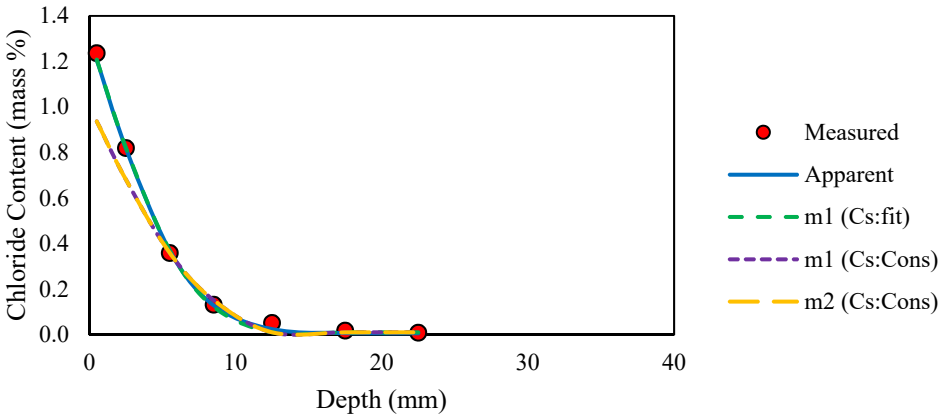

Figure C-37: Effective Chloride bulk diffusion results for Mix 37 at six month exposure

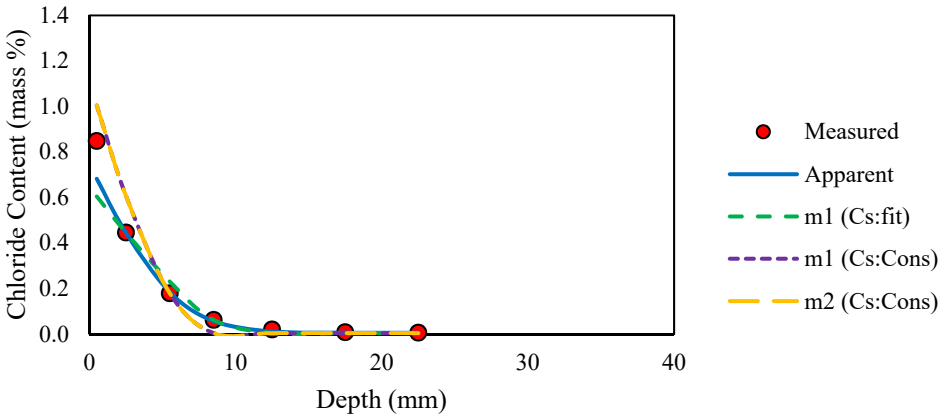

Figure C-38: Effective Chloride bulk diffusion results for Mix 38 at six month exposure

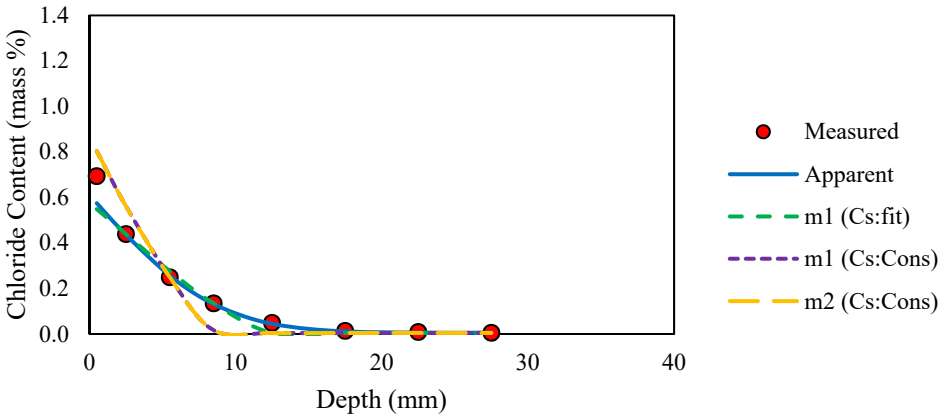

Figure C-39: Effective Chloride bulk diffusion results for Mix 39 at six month exposure

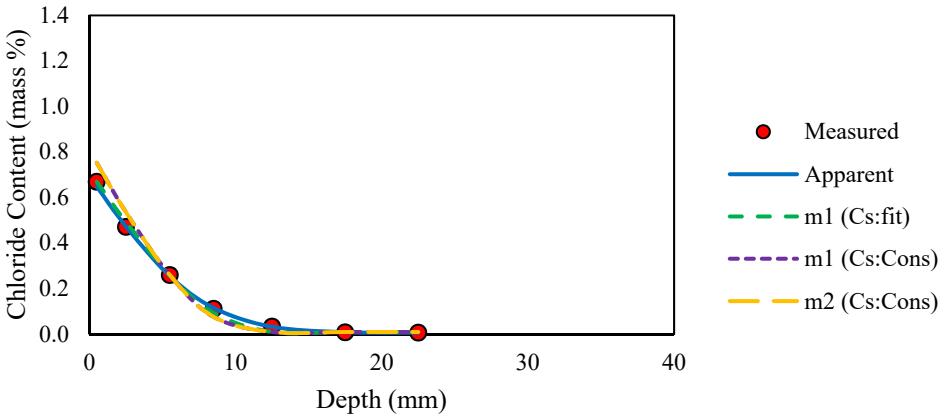

Figure C-40: Effective Chloride bulk diffusion results for Mix 40 at six month exposure

APPENDIX D: EFFECTIVE CHLORIDE DIFFUSION: 12 MONTHS EXPOSURE

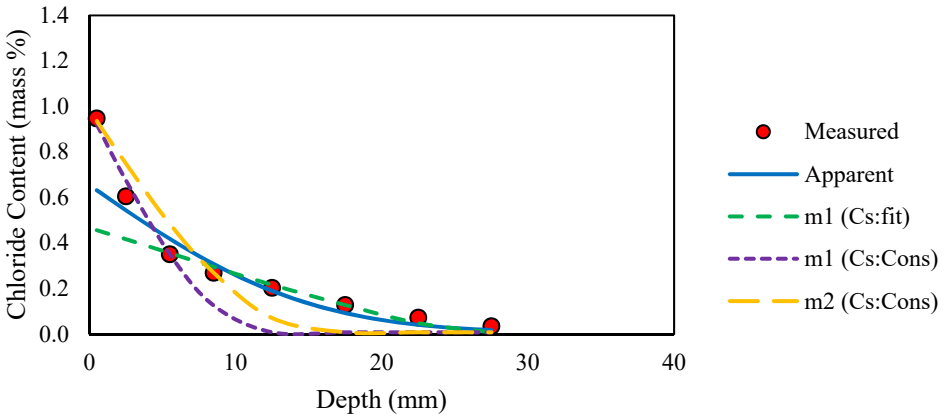

Figure D-1: Effective Chloride bulk diffusion results for Mix 1 at one-year exposure

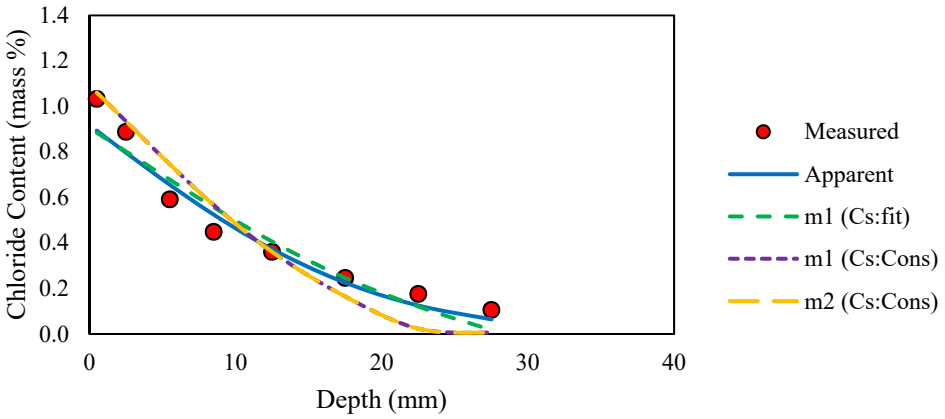

Figure D-2: Effective Chloride bulk diffusion results for Mix 2 at one-year exposure

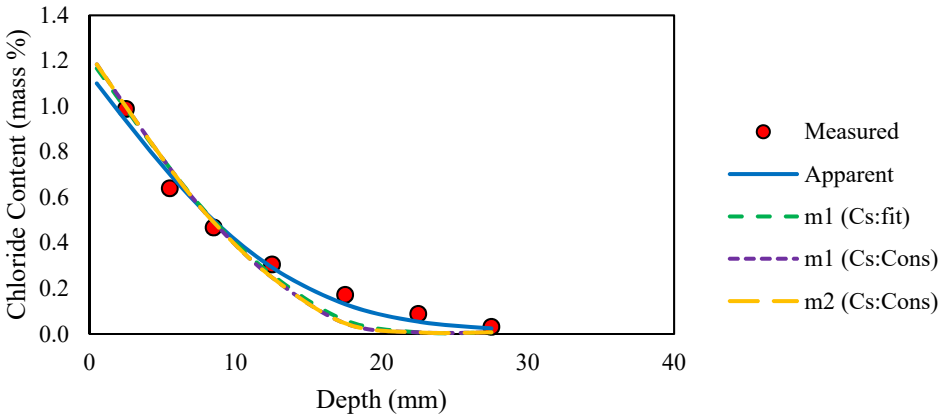

Figure D-3: Effective Chloride bulk diffusion results for Mix 3 at one-year exposure

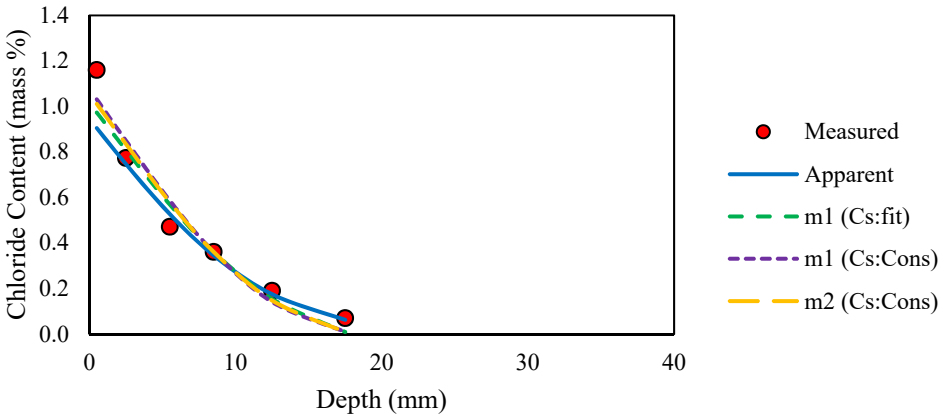

Figure D-4: Effective Chloride bulk diffusion results for Mix 4 at one-year exposure

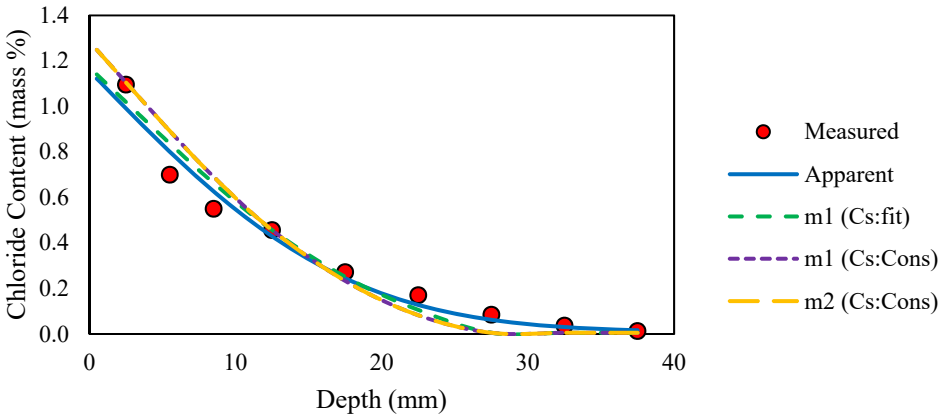

Figure D-5: Effective Chloride bulk diffusion results for Mix 5 at one-year exposure

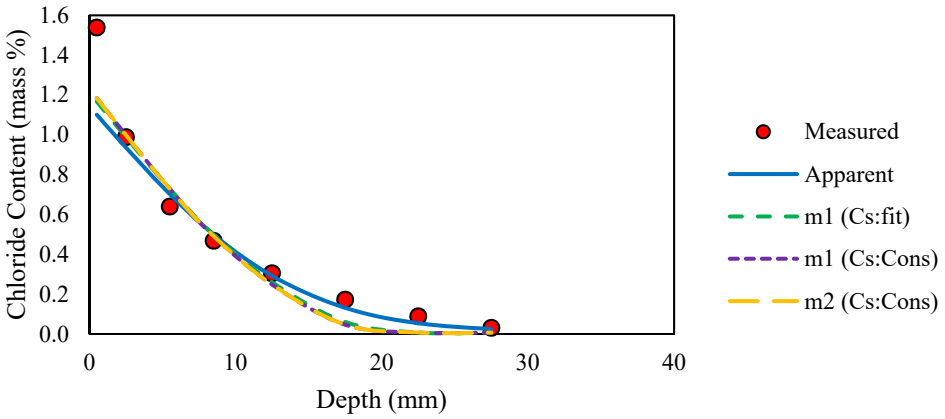

Figure D-6: Effective Chloride bulk diffusion results for Mix 6 at one-year exposure

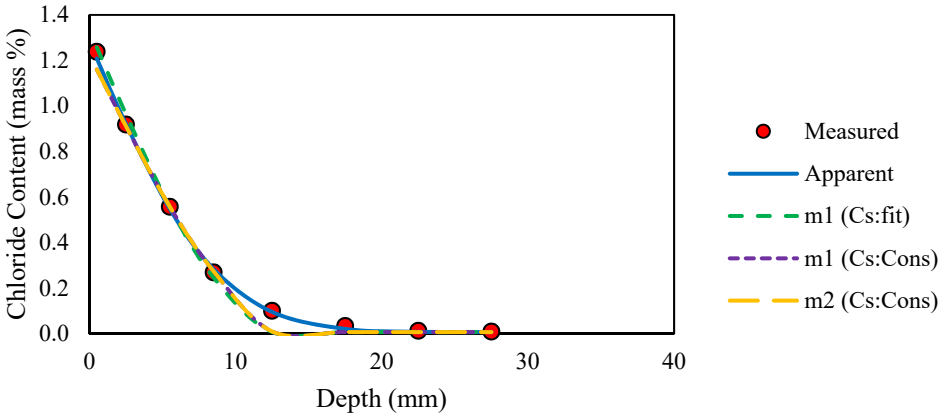

Figure D-7: Effective Chloride bulk diffusion results for Mix 7 at one-year exposure

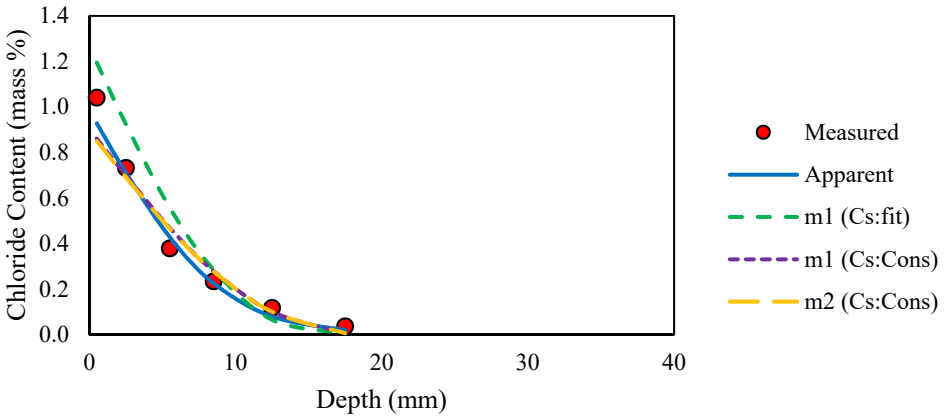

Figure D-8: Effective Chloride bulk diffusion results for Mix 8 at one-year exposure

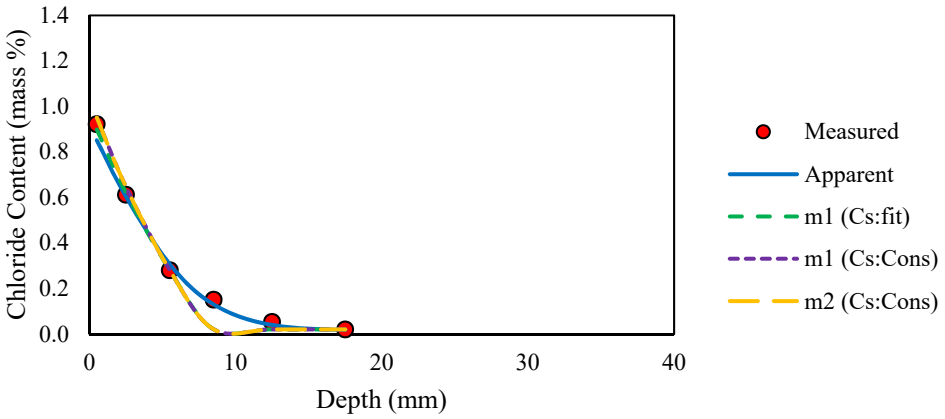

Figure D-9: Effective Chloride bulk diffusion results for Mix 9 at one-year exposure

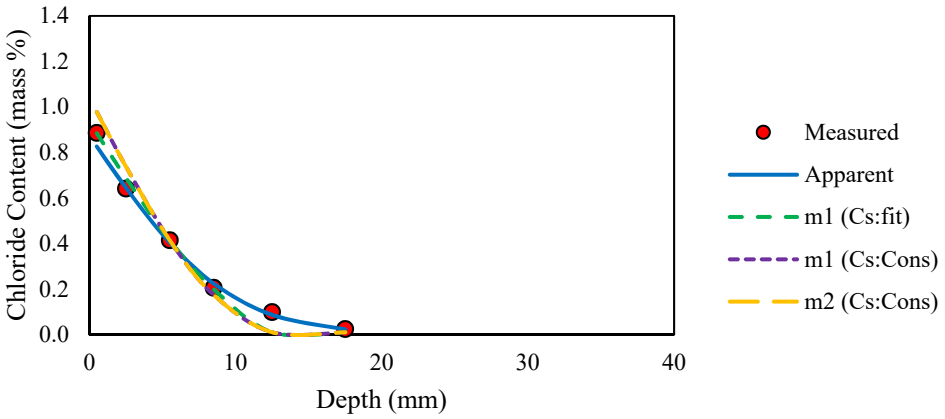

Figure D-10: Effective Chloride bulk diffusion results for Mix 10 at one-year exposure

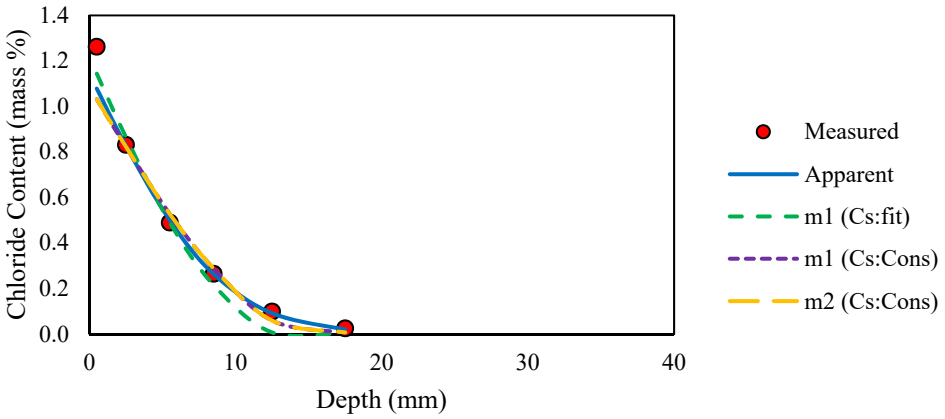

Figure D-11: Effective Chloride bulk diffusion results for Mix 11 at one-year exposure

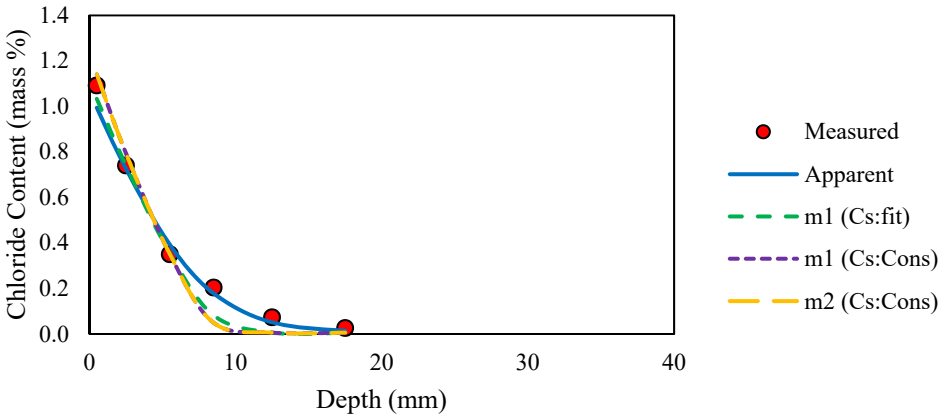

Figure D-12: Effective Chloride bulk diffusion results for Mix 12 at one-year exposure

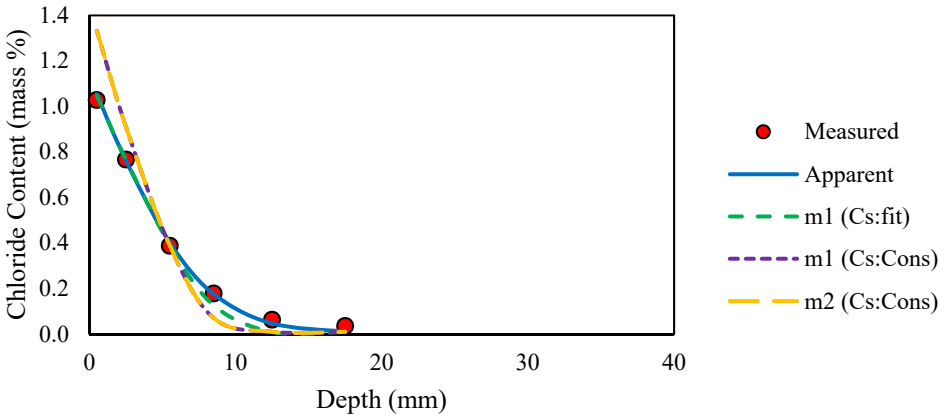

Figure D-13: Effective Chloride bulk diffusion results for Mix 13 at one-year exposure

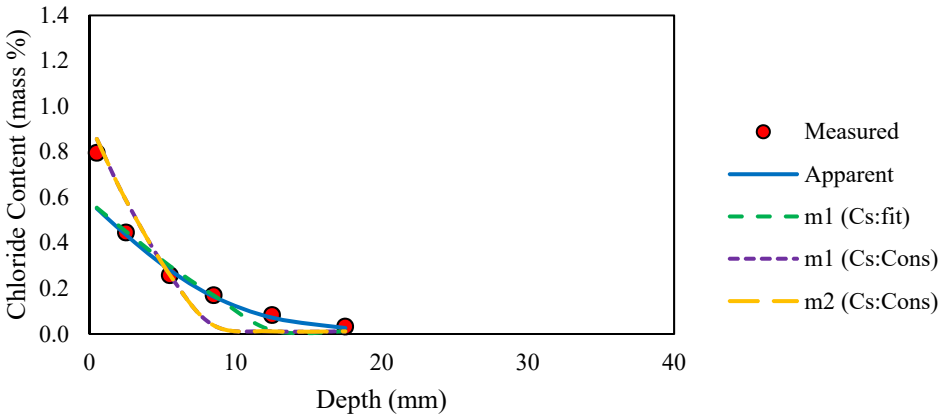

Figure D-14: Effective Chloride bulk diffusion results for Mix 14 at one-year exposure

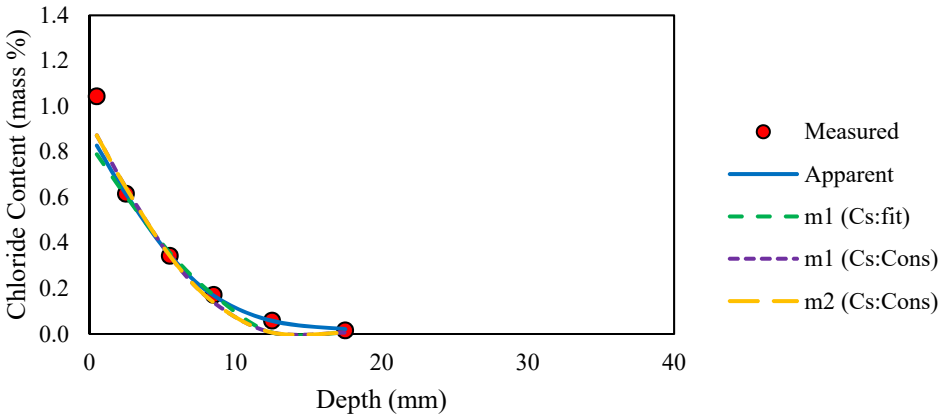

Figure D-15: Effective Chloride bulk diffusion results for Mix 15 at one-year exposure

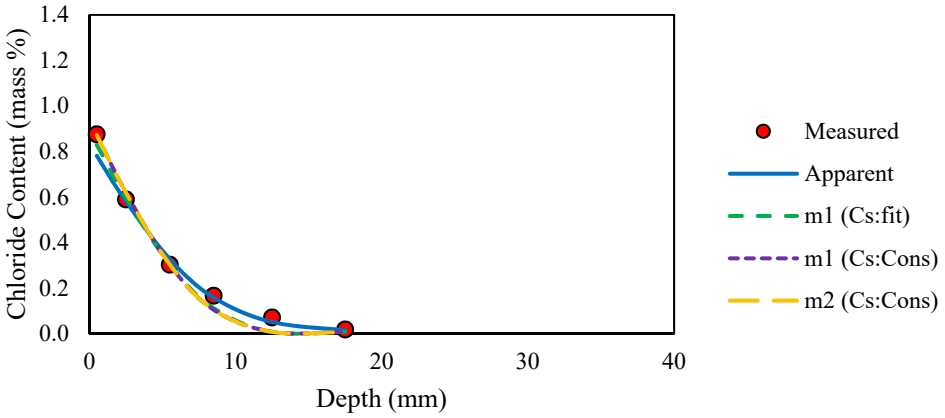

Figure D-16: Effective Chloride bulk diffusion results for Mix 16 at one-year exposure

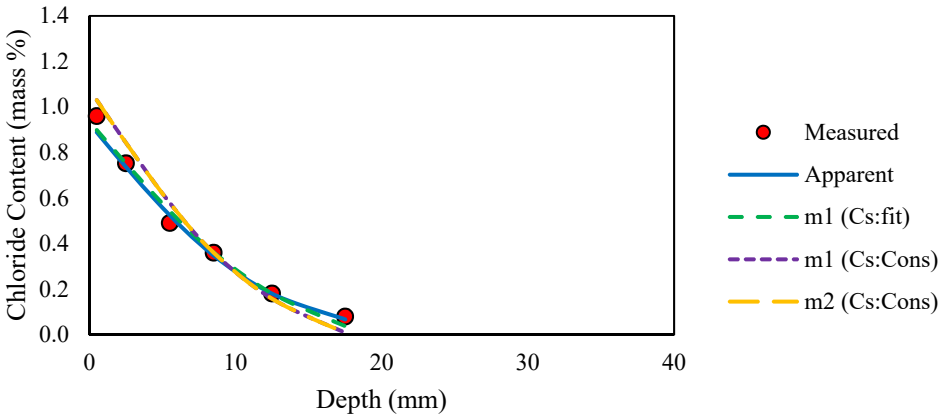

Figure D-17: Effective Chloride bulk diffusion results for Mix 17 at one-year exposure

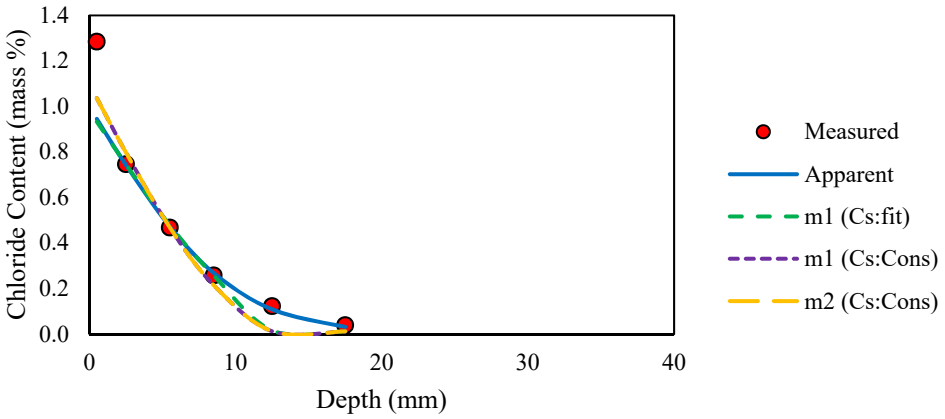

Figure D-18: Effective Chloride bulk diffusion results for Mix 18 at one-year exposure

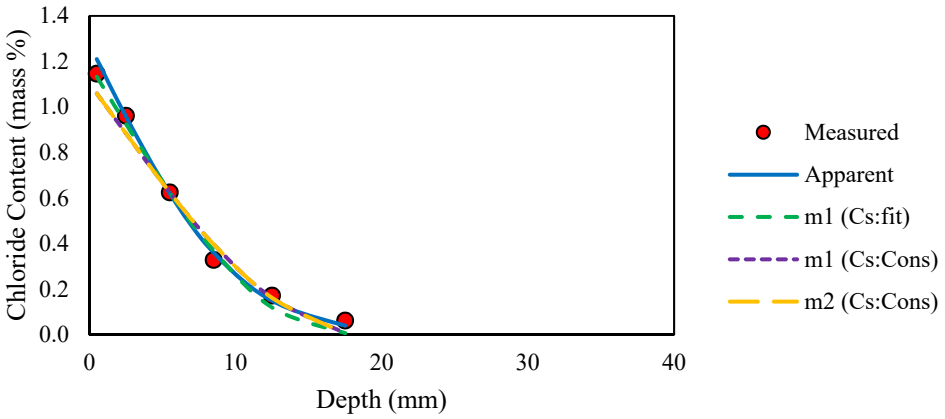

Figure D-19: Effective Chloride bulk diffusion results for Mix 19 at one-year exposure

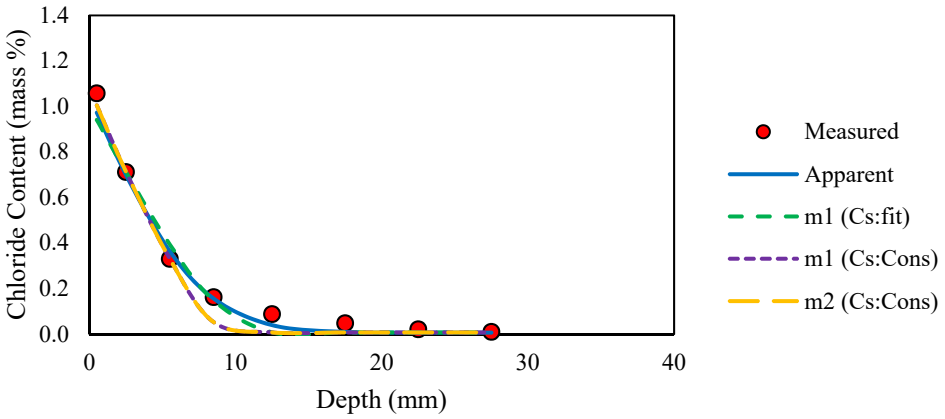

Figure D-20: Effective Chloride bulk diffusion results for Mix 20 at one-year exposure

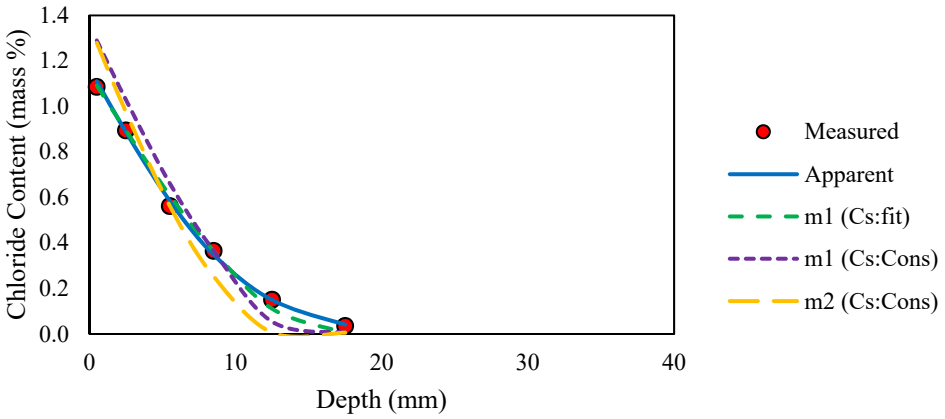

Figure D-21: Effective Chloride bulk diffusion results for Mix 21 at one-year exposure

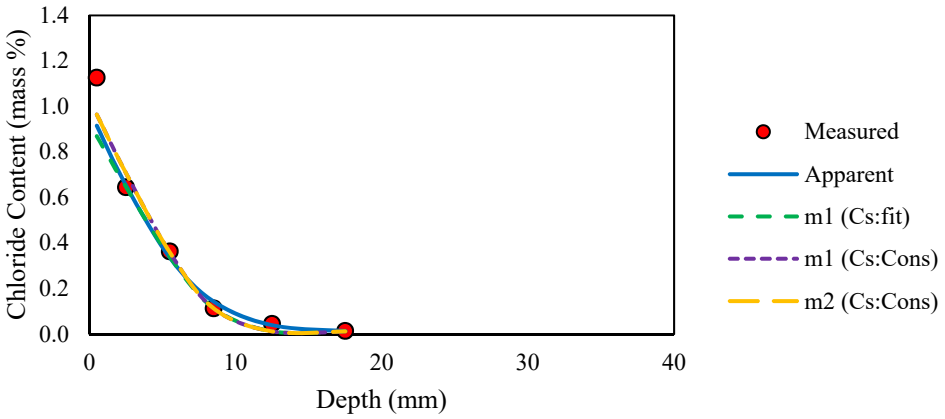

Figure D-22: Effective Chloride bulk diffusion results for Mix 22 at one-year exposure

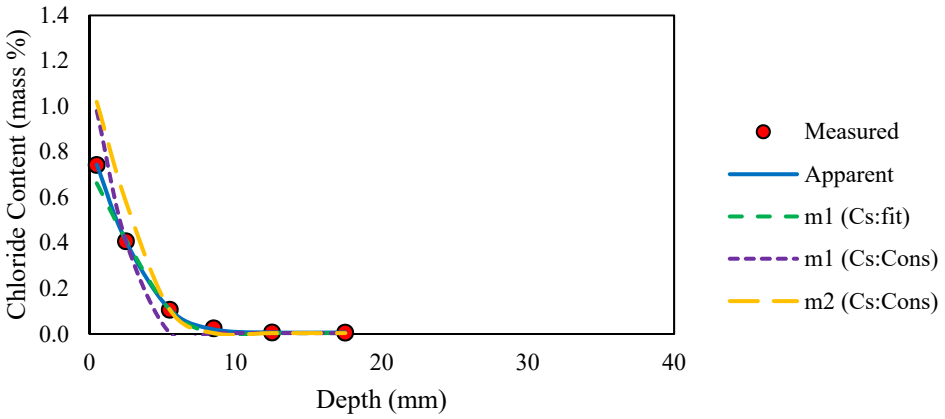

Figure D-23: Effective Chloride bulk diffusion results for Mix 23 at one-year exposure

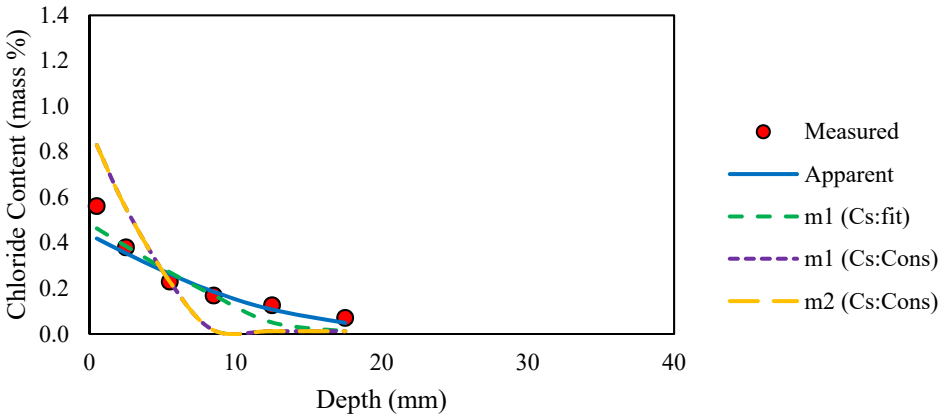

Figure D-24: Effective Chloride bulk diffusion results for Mix 24 at one-year exposure

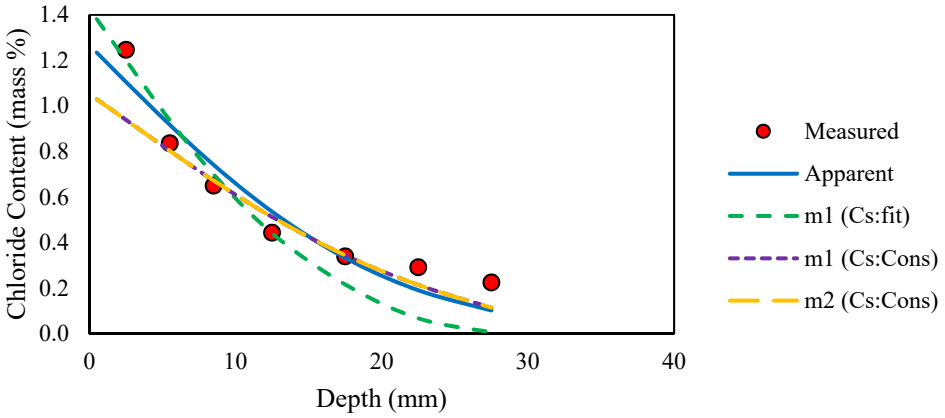

Figure D-25: Effective Chloride bulk diffusion results for Mix 25 at one-year exposure

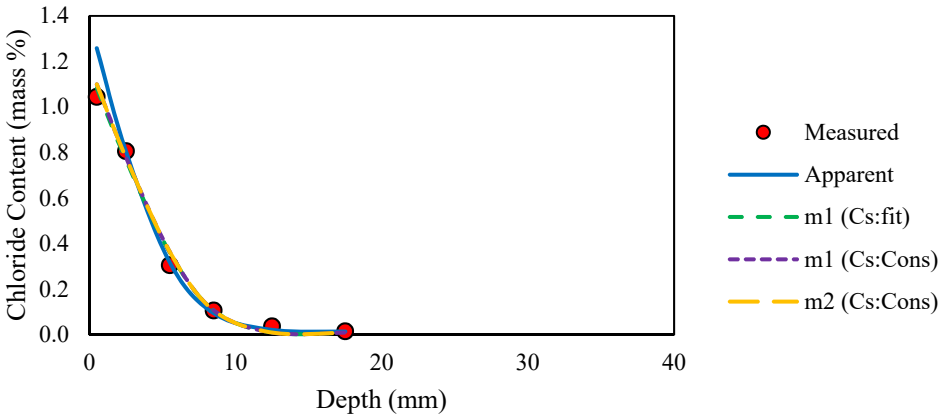

Figure D-26: Effective Chloride bulk diffusion results for Mix 26 at one-year exposure

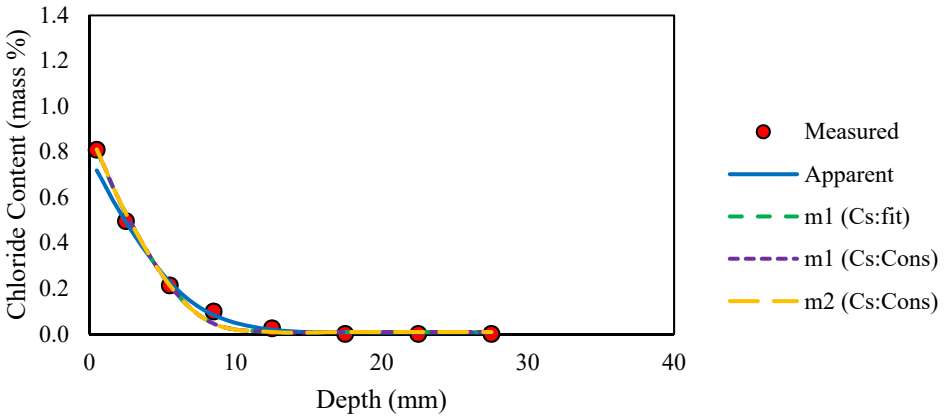

Figure D-27: Effective Chloride bulk diffusion results for Mix 27 at one-year exposure

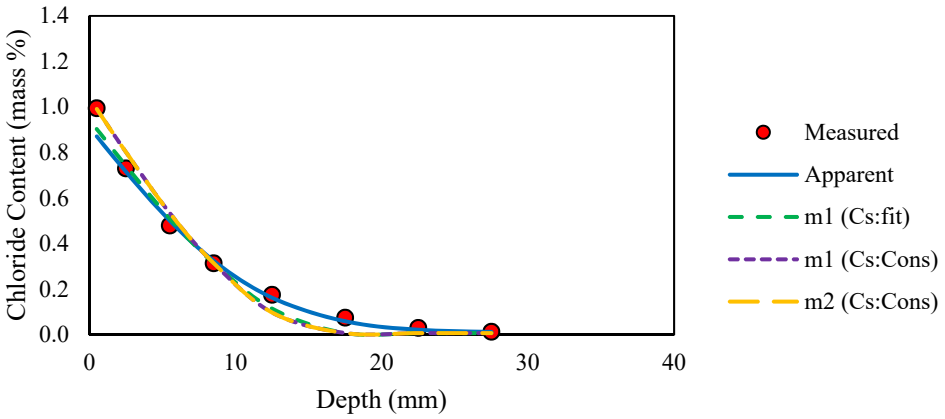

Figure D-28: Effective Chloride bulk diffusion results for Mix 28 at one-year exposure

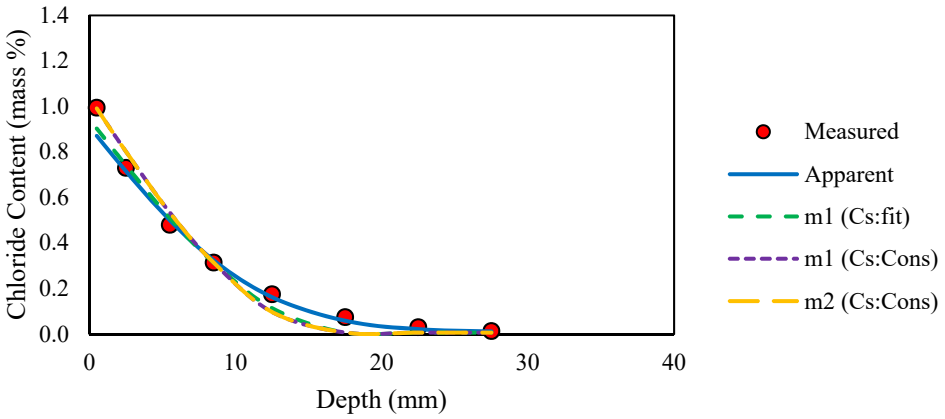

Figure D-29: Effective Chloride bulk diffusion results for Mix 29 at one-year exposure

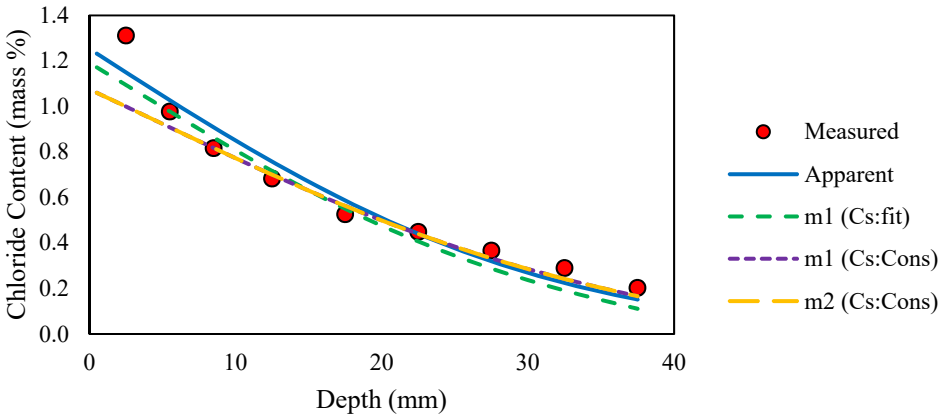

Figure D-30: Effective Chloride bulk diffusion results for Mix 30 at one-year exposure

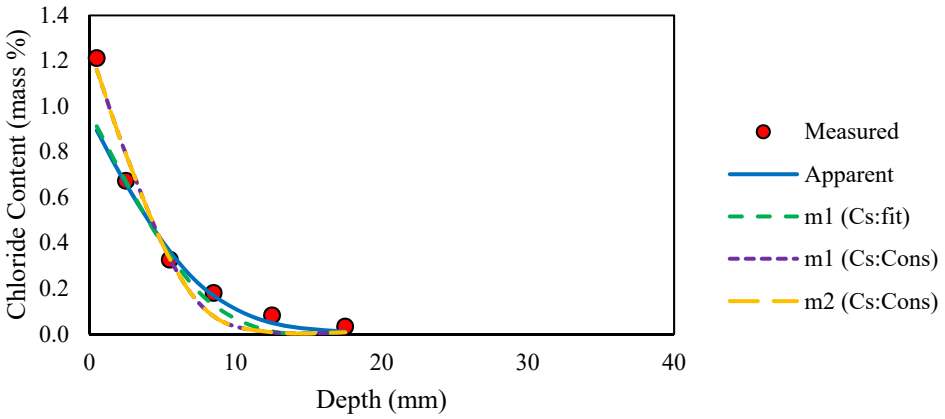

Figure D-31: Effective Chloride bulk diffusion results for Mix 31 at one-year exposure

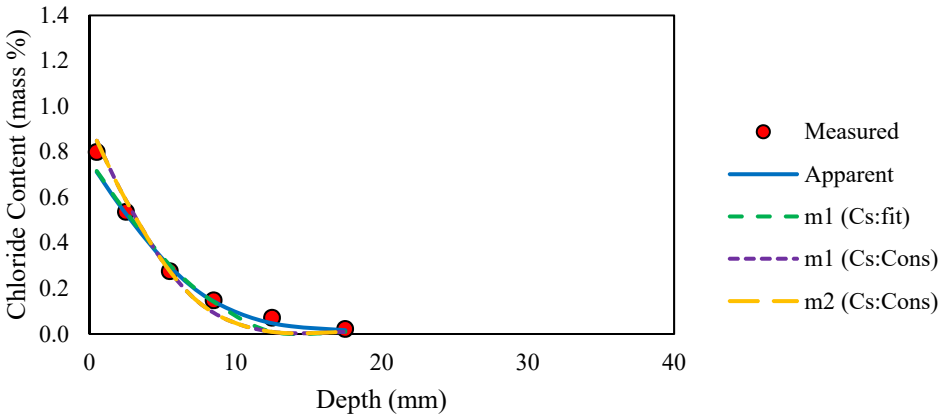

Figure D-32: Effective Chloride bulk diffusion results for Mix 32 at one-year exposure

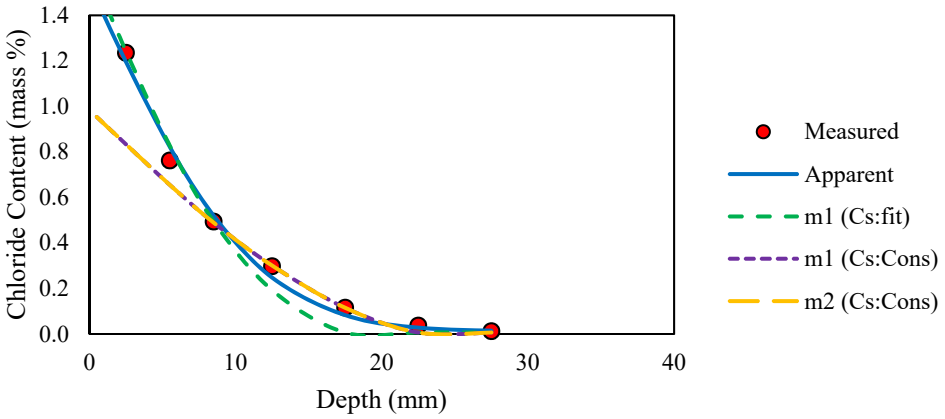

Figure D-33: Effective Chloride bulk diffusion results for Mix 33 at one-year exposure

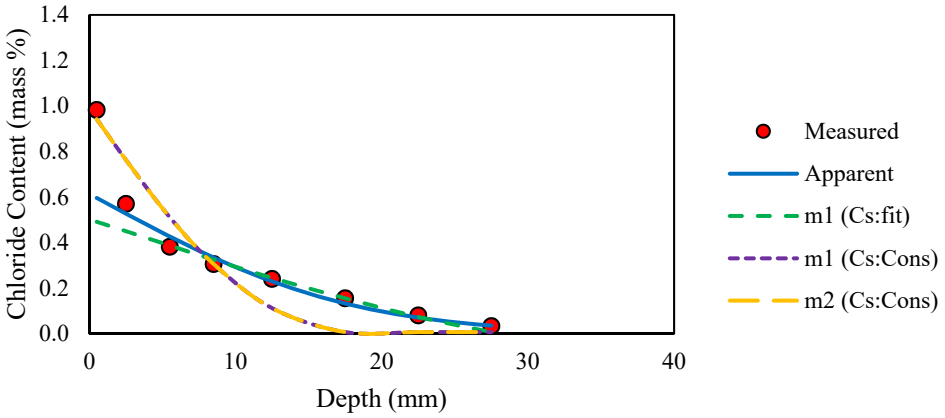

Figure D-34: Effective Chloride bulk diffusion results for Mix 34 at one-year exposure

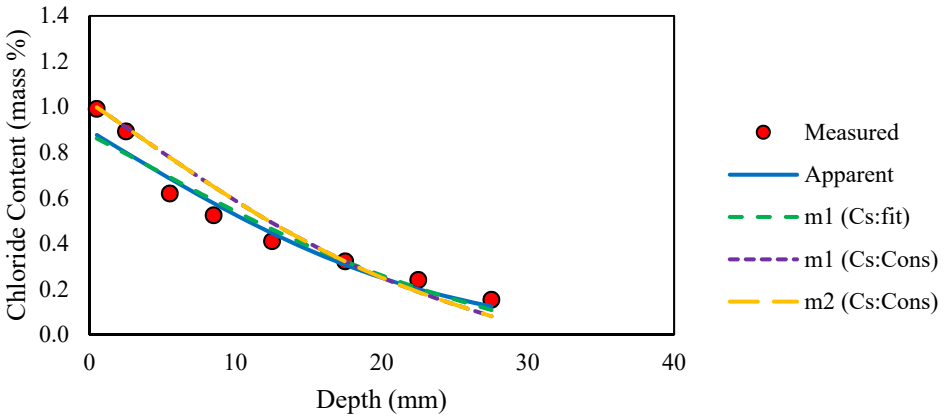

Figure D-35: Effective Chloride bulk diffusion results for Mix 35 at one-year exposure

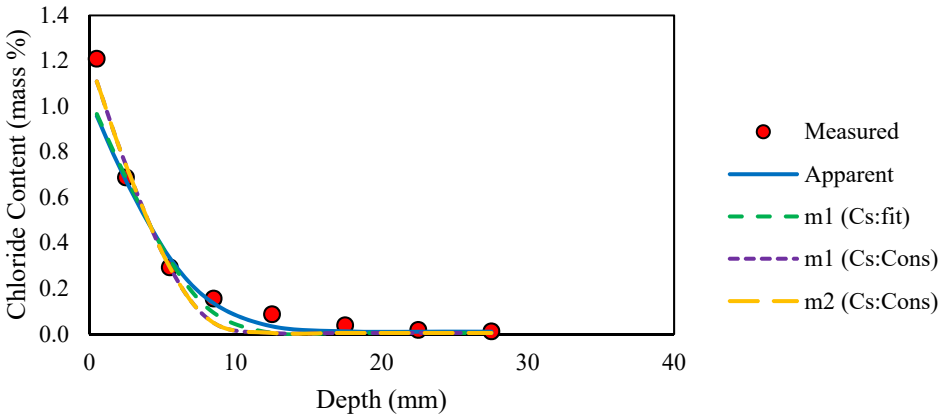

Figure D-36: Effective Chloride bulk diffusion results for Mix 36 at one-year exposure

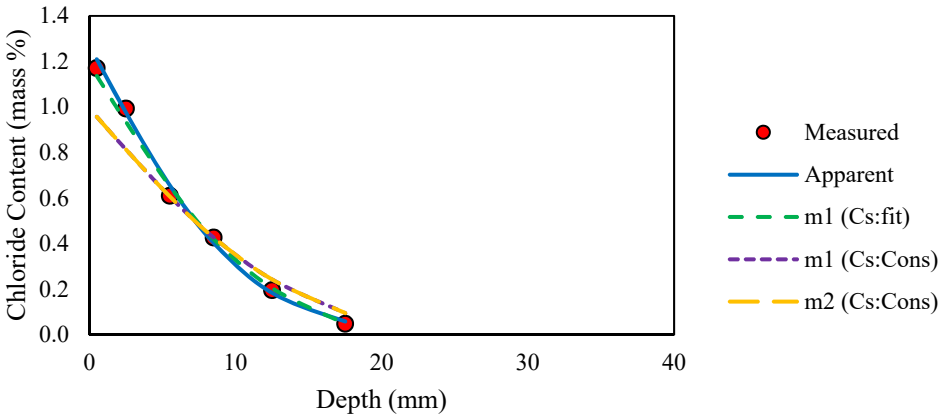

Figure D-37: Effective Chloride bulk diffusion results for Mix 37 at one-year exposure

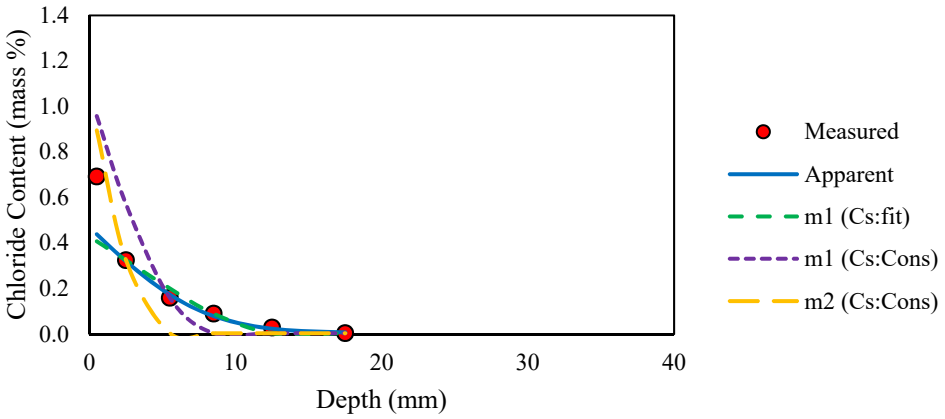

Figure D-38: Effective Chloride bulk diffusion results for Mix 38 at one-year exposure

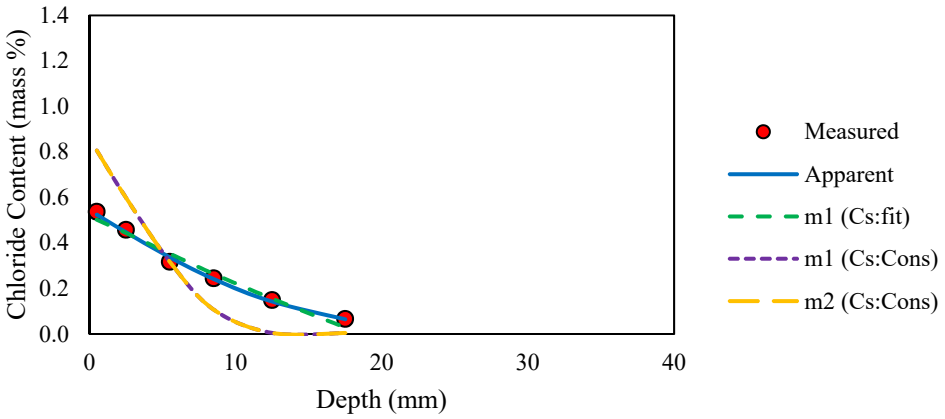

Figure D-39: Effective Chloride bulk diffusion results for Mix 39 at one-year exposure

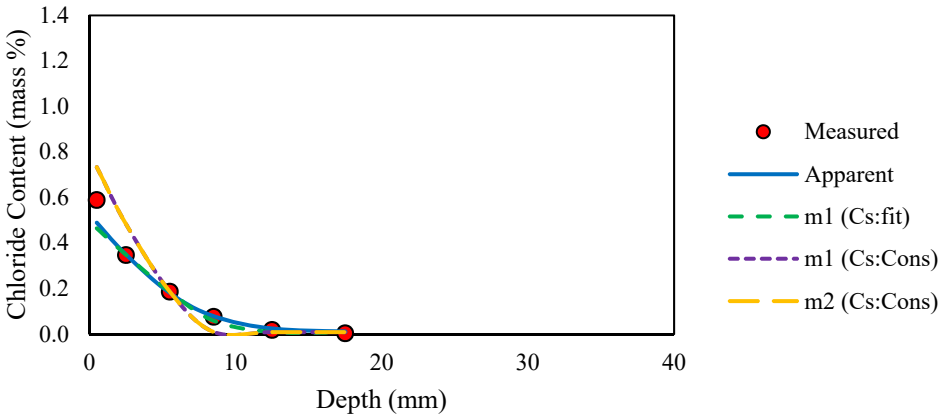

Figure D-40: Effective Chloride bulk diffusion results for Mix 40 at one-year exposure

APPENDIX E: EFFECTIVE CHLORIDE DIFFUSION PREDICTION FROM FORMATION FACTOR: 6 MONTHS EXPOSURE

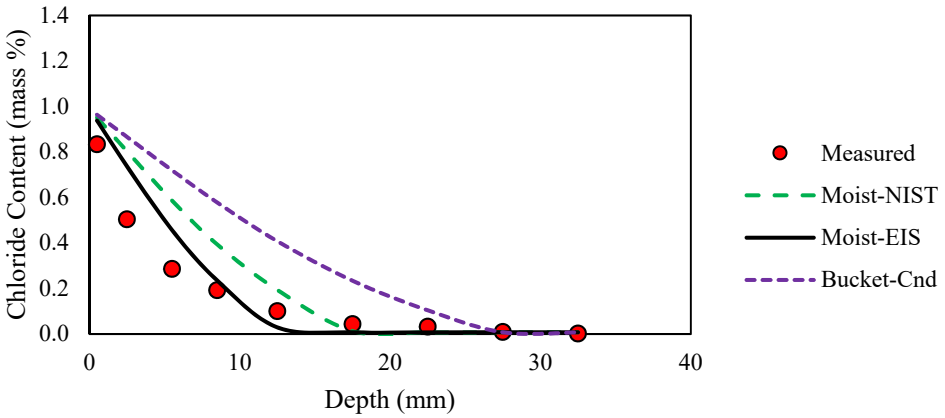

Figure E-1: Effective Chloride bulk diffusion using formation factor for Mix 1 at six month exposure

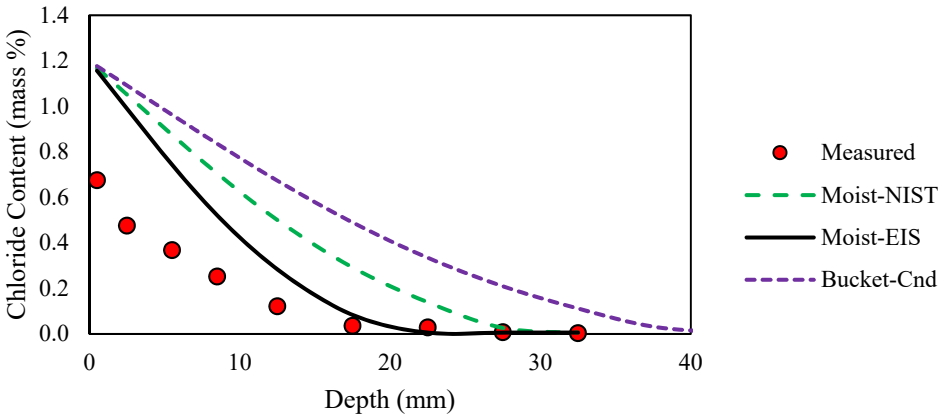

Figure E-2: Effective Chloride bulk diffusion using formation factor for Mix 2 at six month exposure

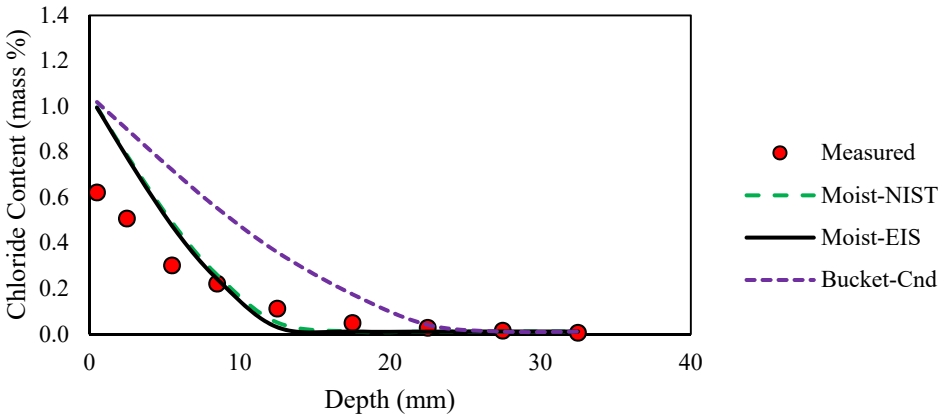

Figure E-3: Effective Chloride bulk diffusion using formation factor for Mix 3 at six month exposure

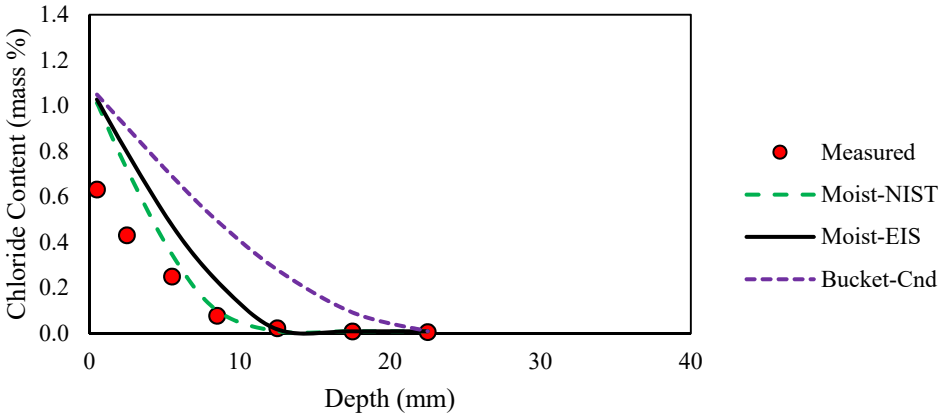

Figure E-4: Effective Chloride bulk diffusion using formation factor for Mix 4 at six month exposure

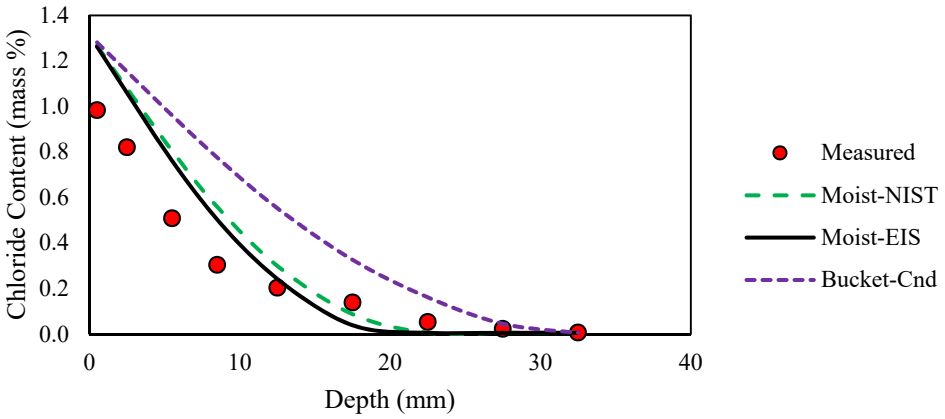

Figure E-5: Effective Chloride bulk diffusion using formation factor for Mix 5 at six month exposure

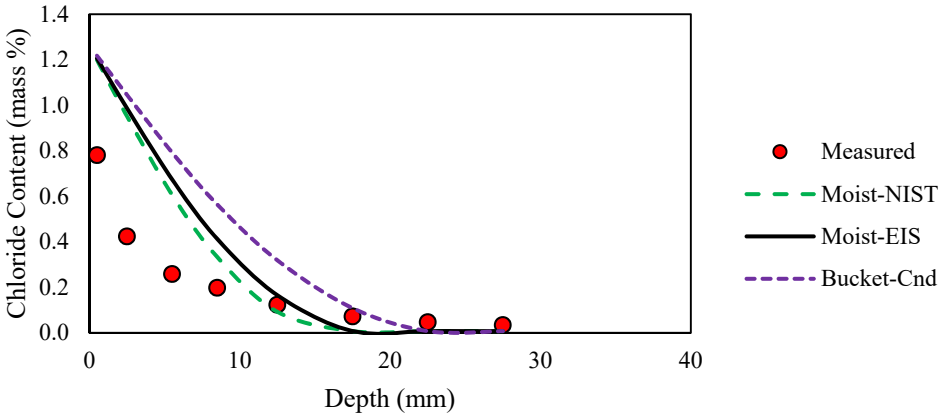

Figure E-6: Effective Chloride bulk diffusion using formation factor for Mix 6 at six month exposure

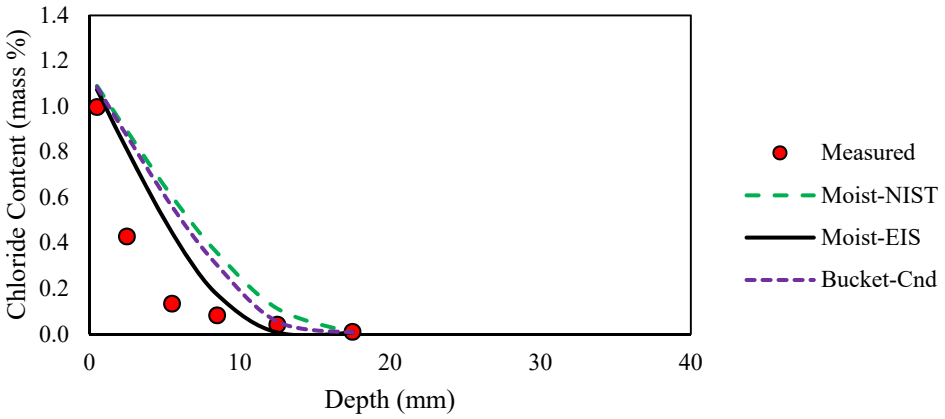

Figure E-7: Effective Chloride bulk diffusion using formation factor for Mix 7 at six month exposure

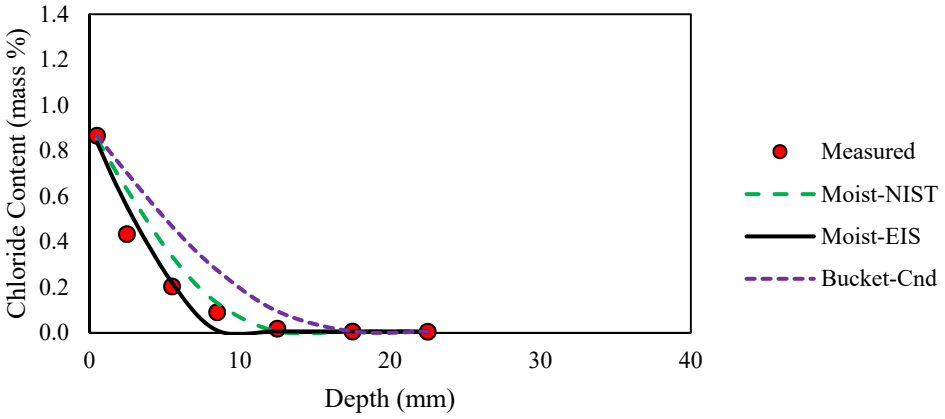

Figure E-8: Effective Chloride bulk diffusion using formation factor for Mix 8 at six month exposure

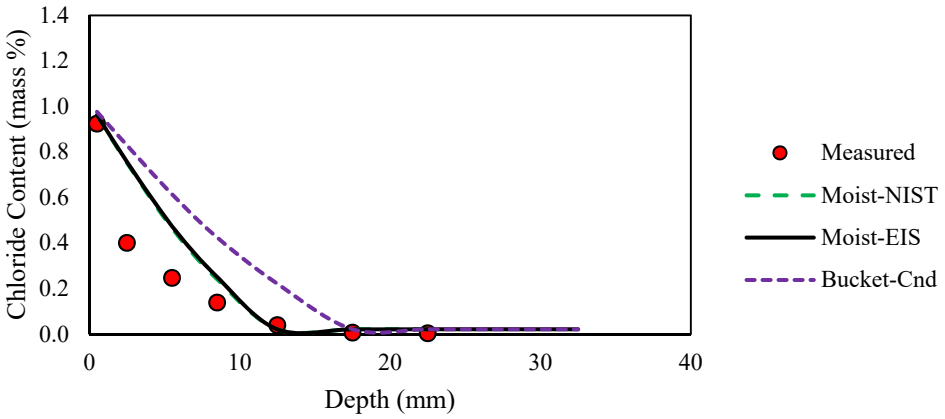

Figure E-9: Effective Chloride bulk diffusion using formation factor for Mix 9 at six month exposure

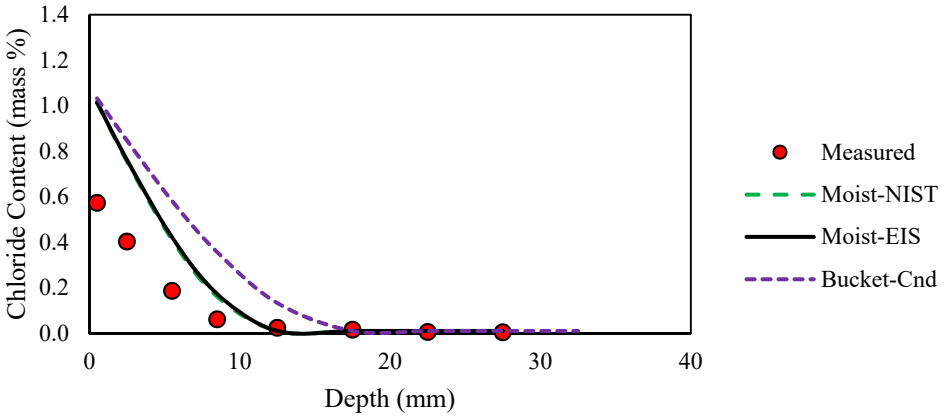

Figure E-10: Effective Chloride bulk diffusion using formation factor for Mix 10 at six month exposure

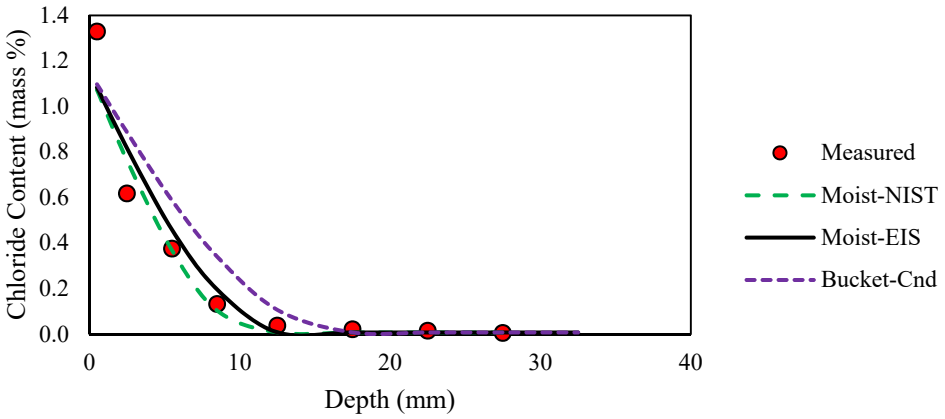

Figure E-11: Effective Chloride bulk diffusion using formation factor for Mix 11 at six month exposure

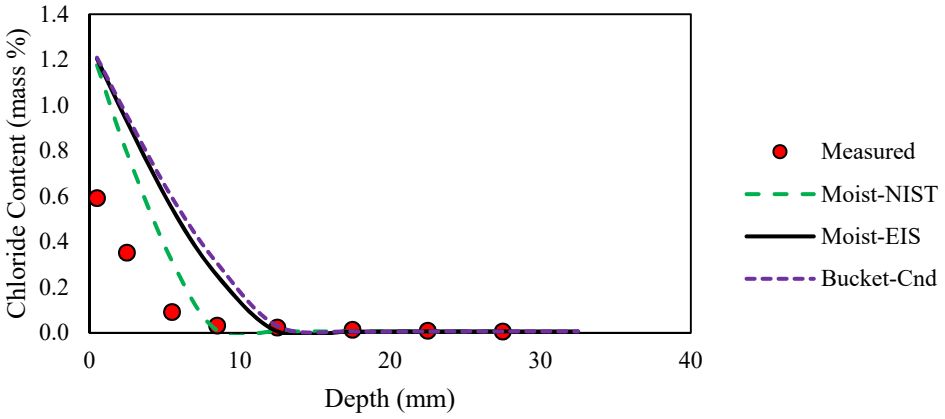

Figure E-12: Effective Chloride bulk diffusion using formation factor for Mix 12 at six month exposure

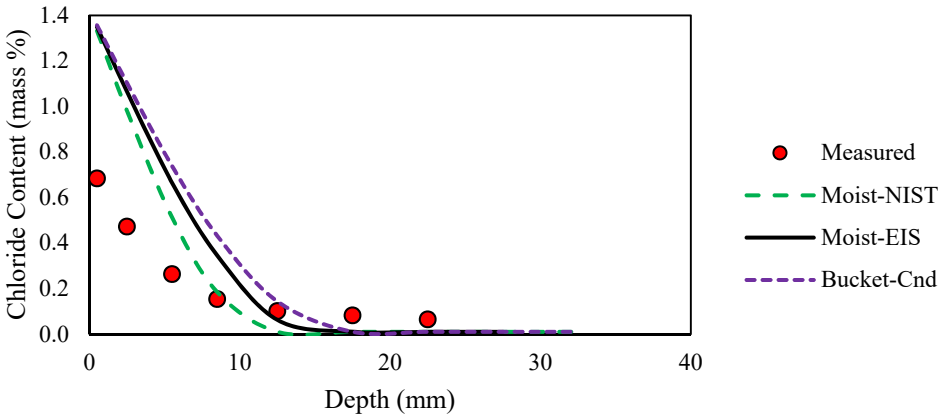

Figure E-13: Effective Chloride bulk diffusion using formation factor for Mix 13 at six month exposure

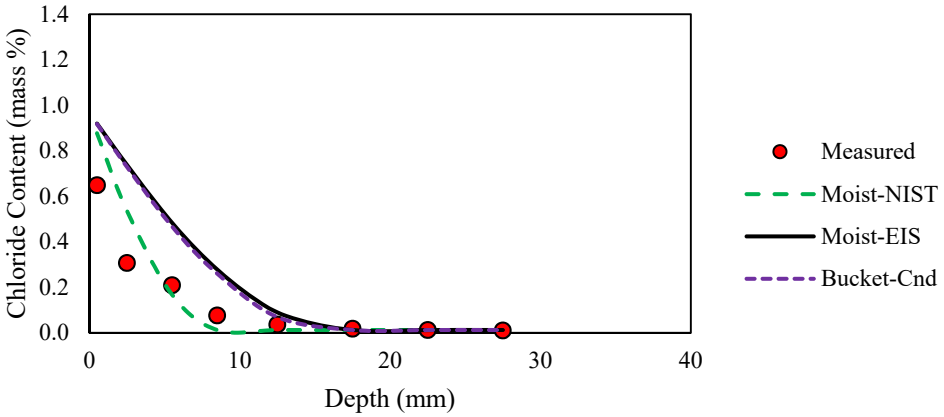

Figure E-14: Effective Chloride bulk diffusion using formation factor for Mix 14 at six month exposure

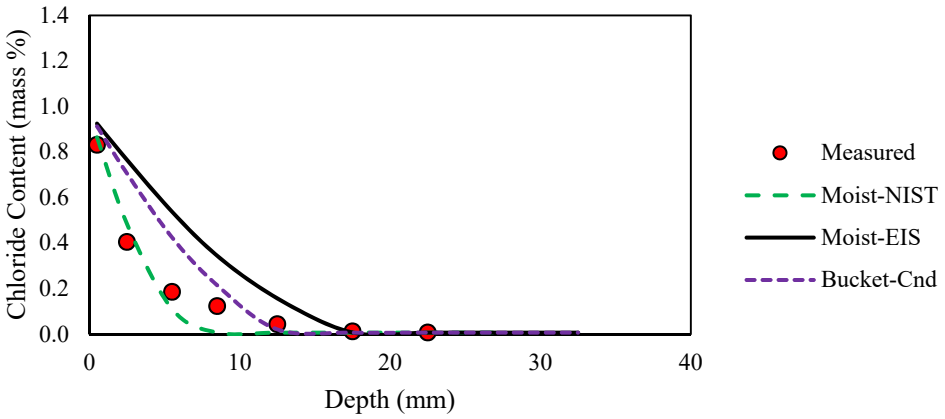

Figure E-15: Effective Chloride bulk diffusion using formation factor for Mix 15 at six month exposure

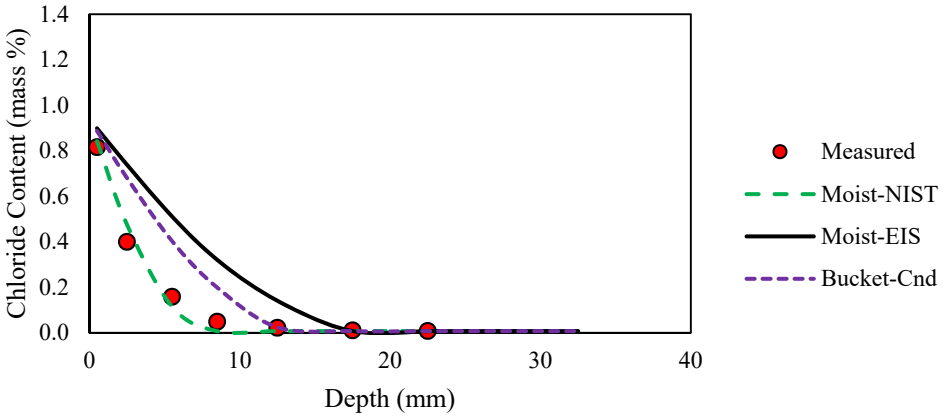

Figure E-16: Effective Chloride bulk diffusion using formation factor for Mix 16 at six month exposure

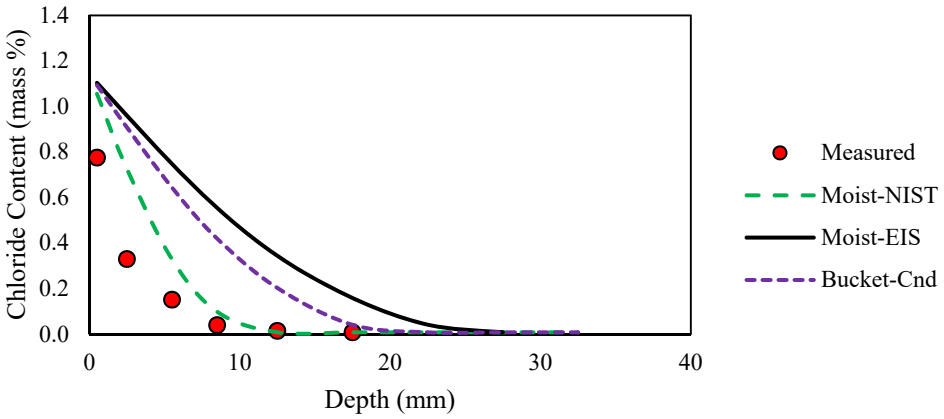

Figure E-17: Effective Chloride bulk diffusion using formation factor for Mix 17 at six month exposure

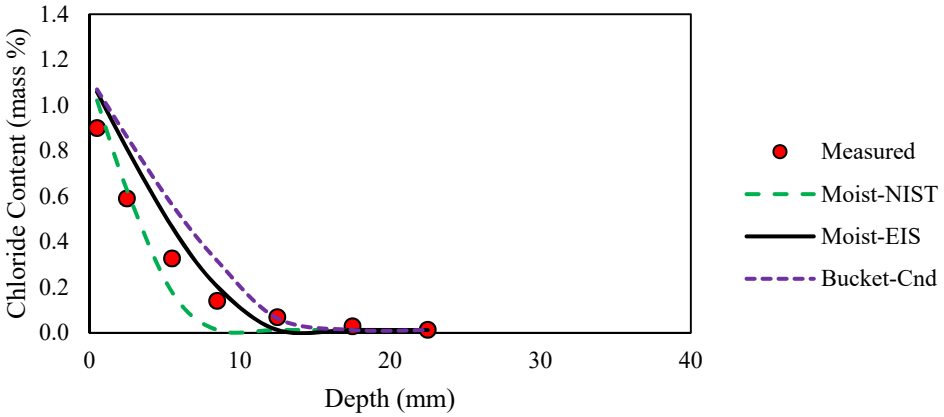

Figure E-18: Effective Chloride bulk diffusion using formation factor for Mix 18 at six month exposure

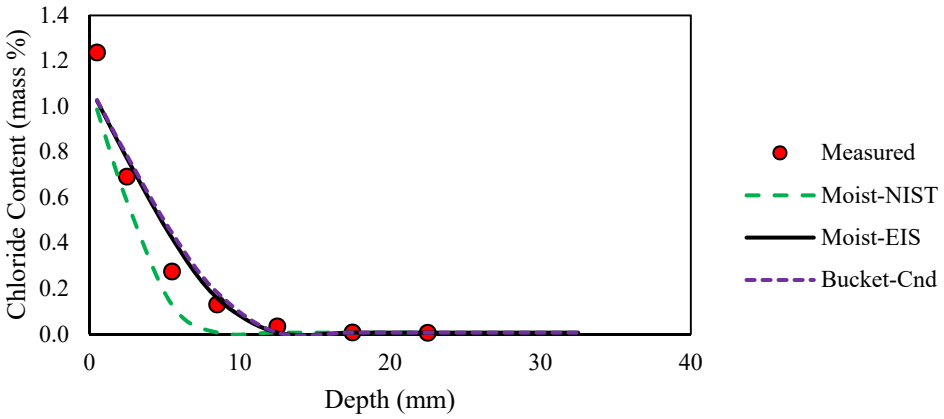

Figure E-19: Effective Chloride bulk diffusion using formation factor for Mix 19 at six month exposure

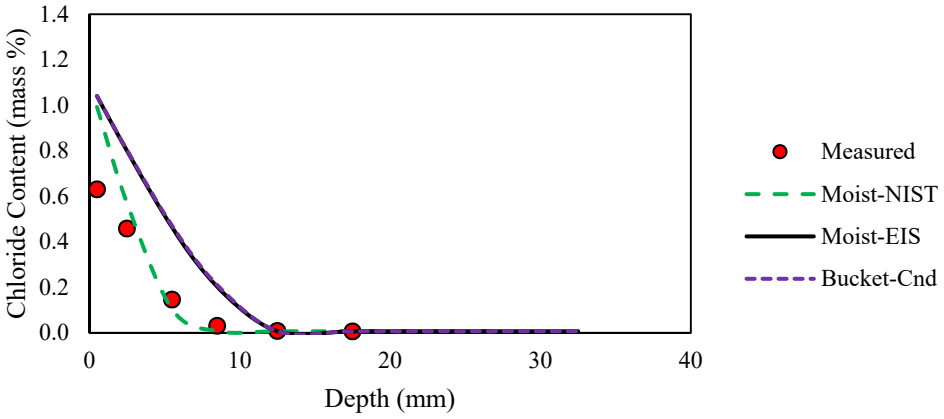

Figure E-20: Effective Chloride bulk diffusion using formation factor for Mix 20 at six month exposure

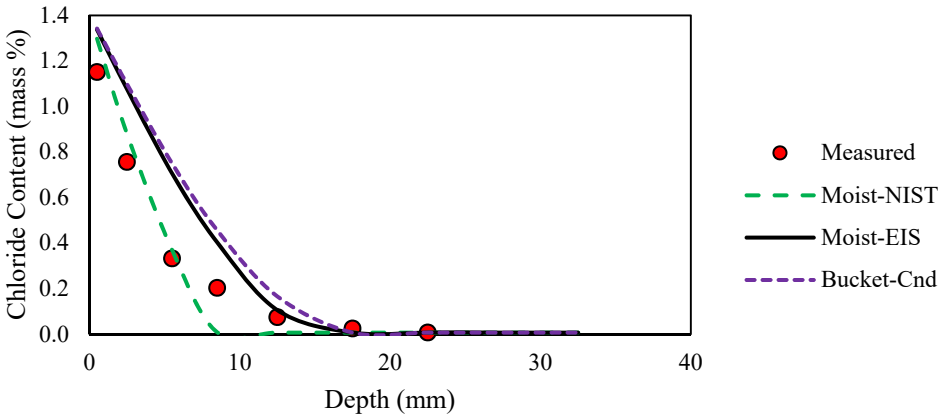

Figure E-21: Effective Chloride bulk diffusion using formation factor for Mix 21 at six month exposure

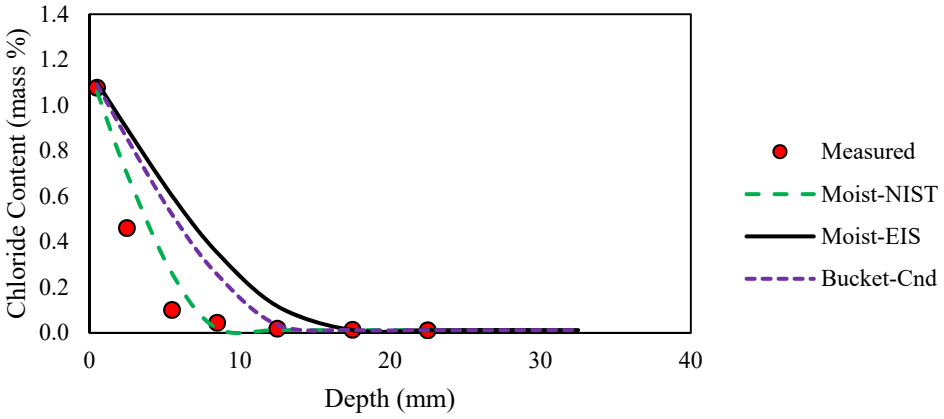

Figure E-22: Effective Chloride bulk diffusion using formation factor for Mix 22 at six month exposure

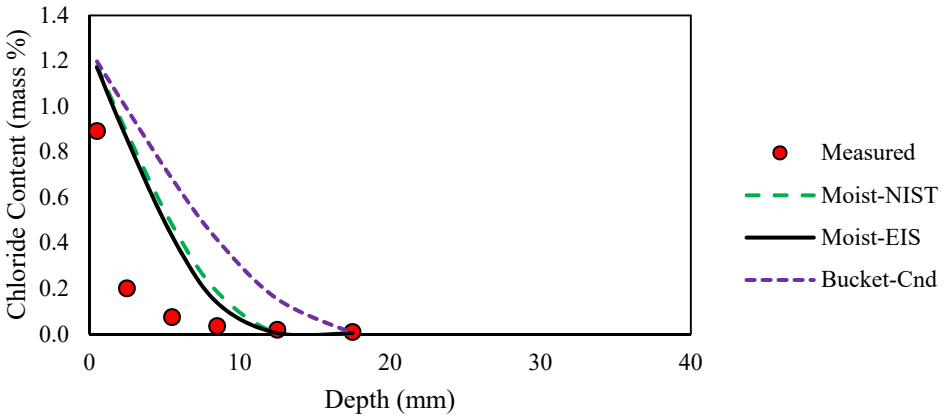

Figure E-23: Effective Chloride bulk diffusion using formation factor for Mix 23 at six month exposure

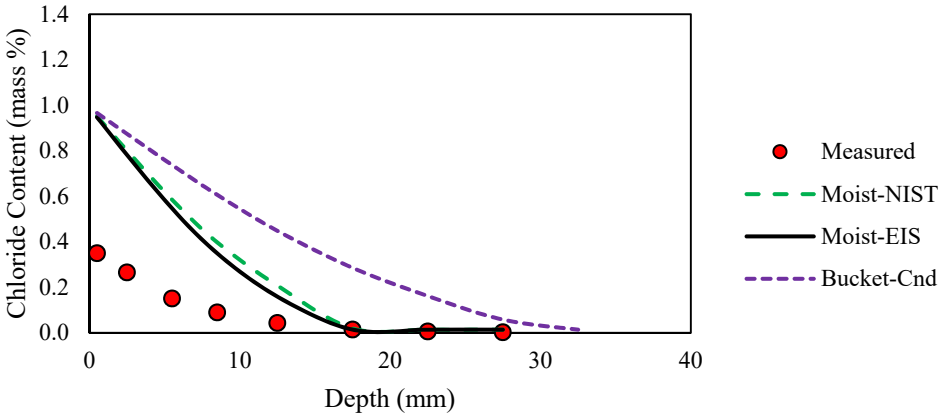

Figure E-24: Effective Chloride bulk diffusion using formation factor for Mix 24 at six month exposure

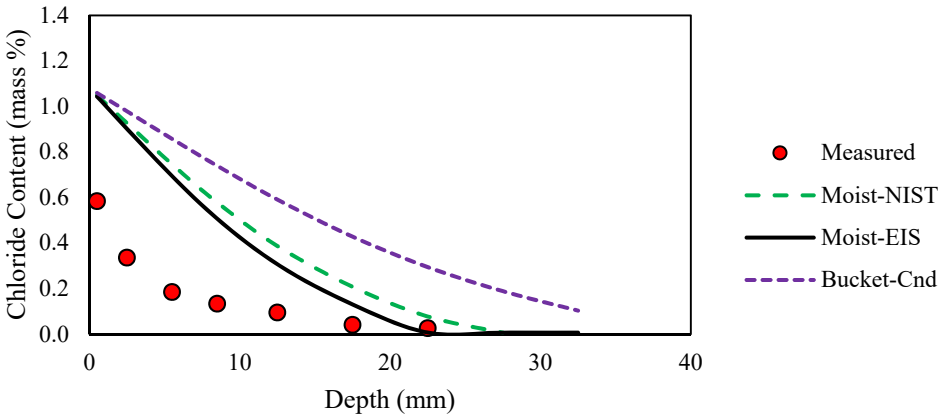

Figure E-25: Effective Chloride bulk diffusion using formation factor for Mix 25 at six month exposure

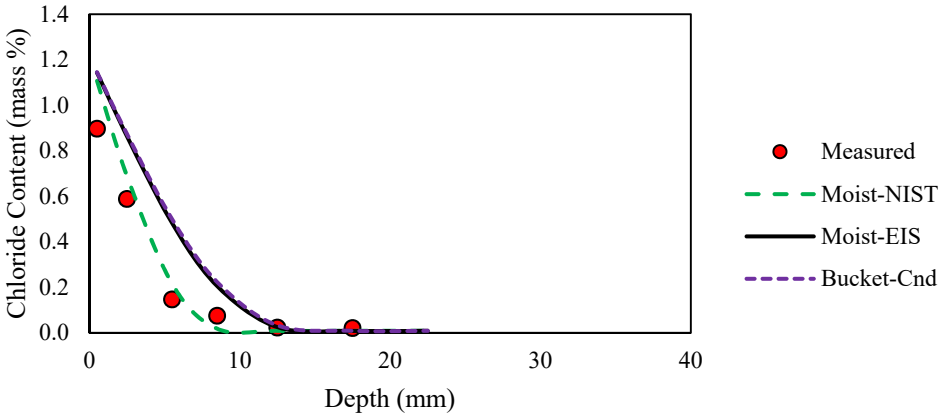

Figure E-26: Effective Chloride bulk diffusion using formation factor for Mix 26 at six month exposure

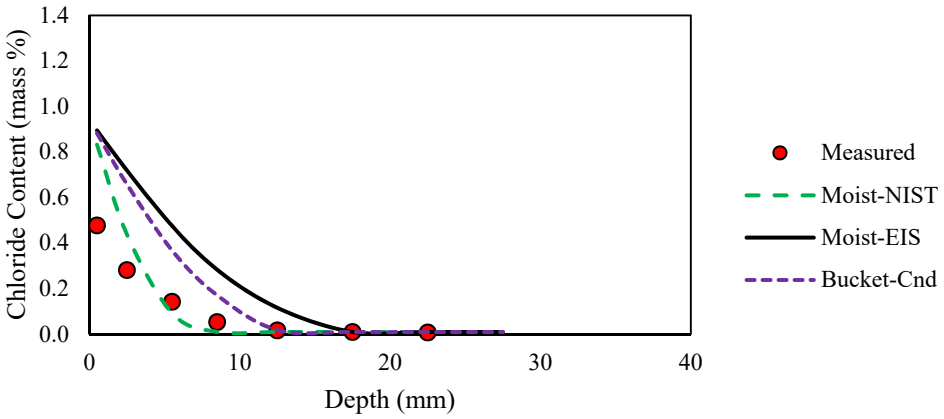

Figure E-27: Effective Chloride bulk diffusion using formation factor for Mix 27 at six month exposure

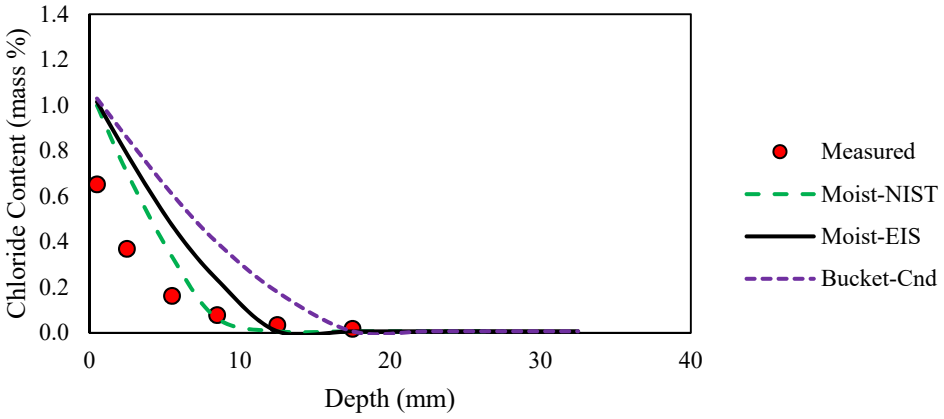

Figure E-28: Effective Chloride bulk diffusion using formation factor for Mix 28 at six month exposure

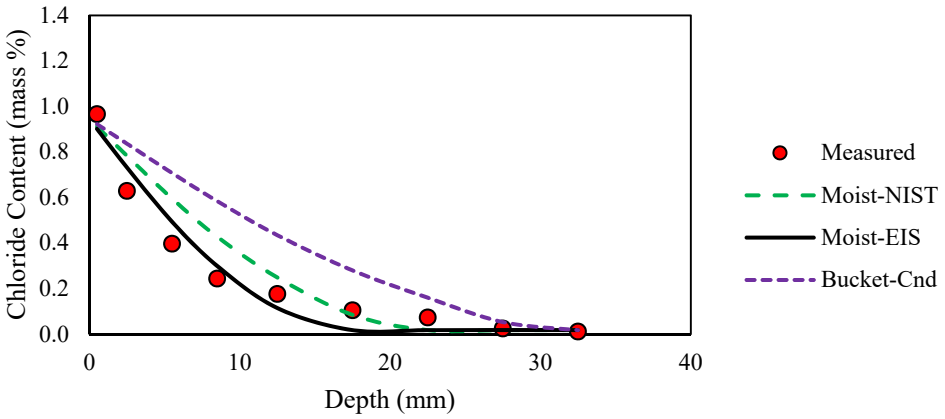

Figure E-29: Effective Chloride bulk diffusion using formation factor for Mix 29 at six month exposure

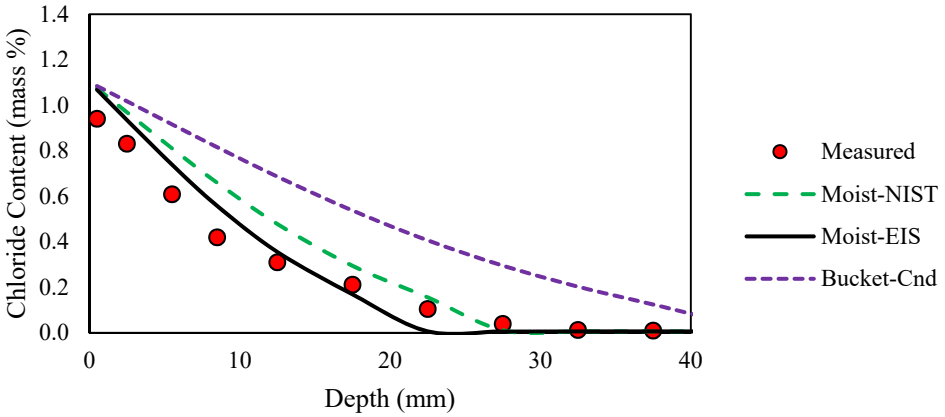

Figure E-30: Effective Chloride bulk diffusion using formation factor for Mix 30 at six month exposure

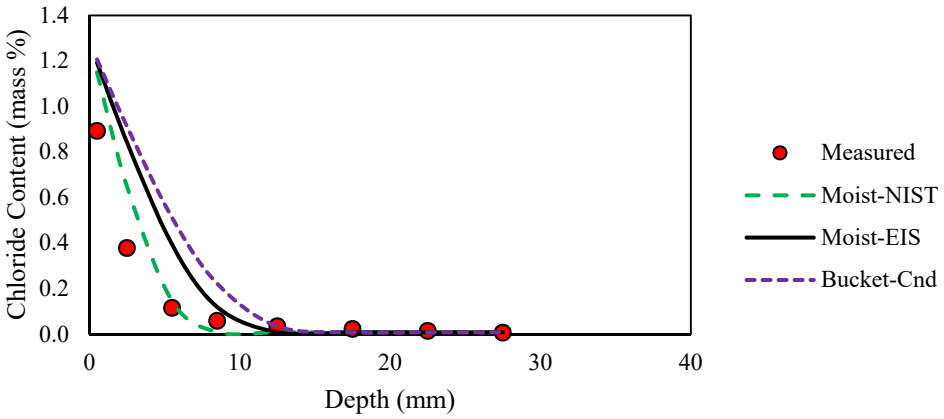

Figure E-31: Effective Chloride bulk diffusion using formation factor for Mix 31 at six month exposure

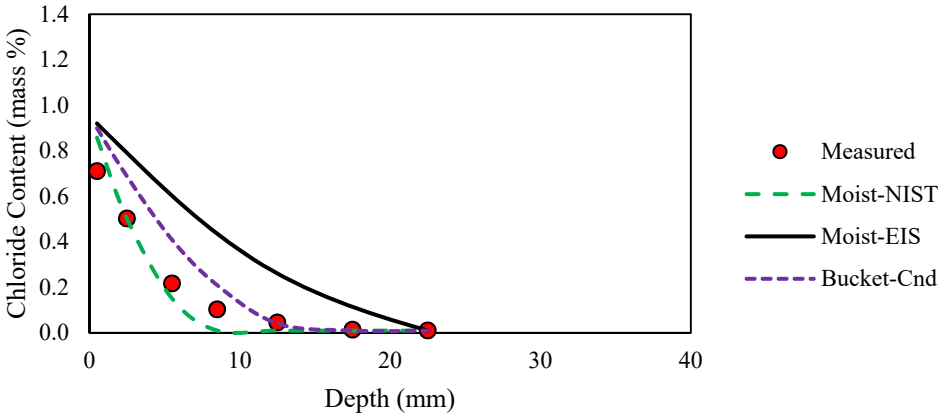

Figure E-32: Effective Chloride bulk diffusion using formation factor for Mix 32 at six month exposure

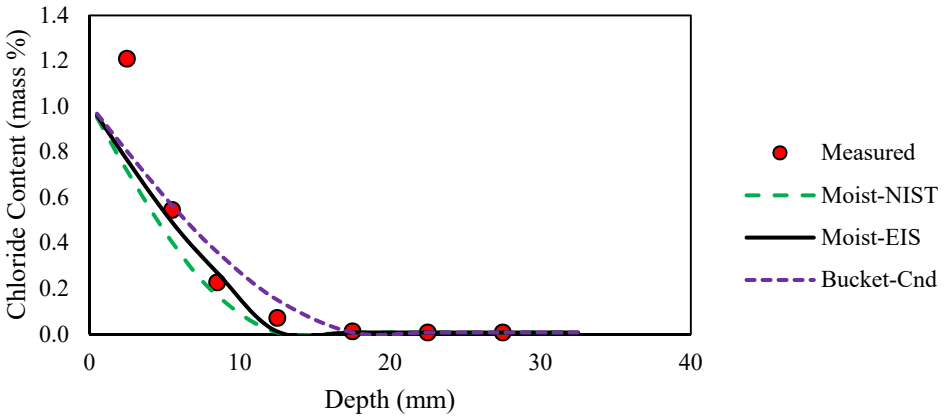

Figure E-33: Effective Chloride bulk diffusion using formation factor for Mix 33 at six month exposure

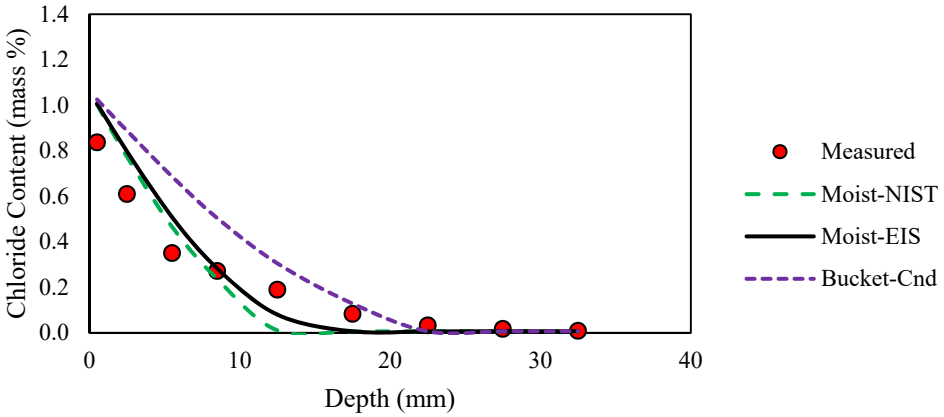

Figure E-34: Effective Chloride bulk diffusion using formation factor for Mix 34 at six month exposure

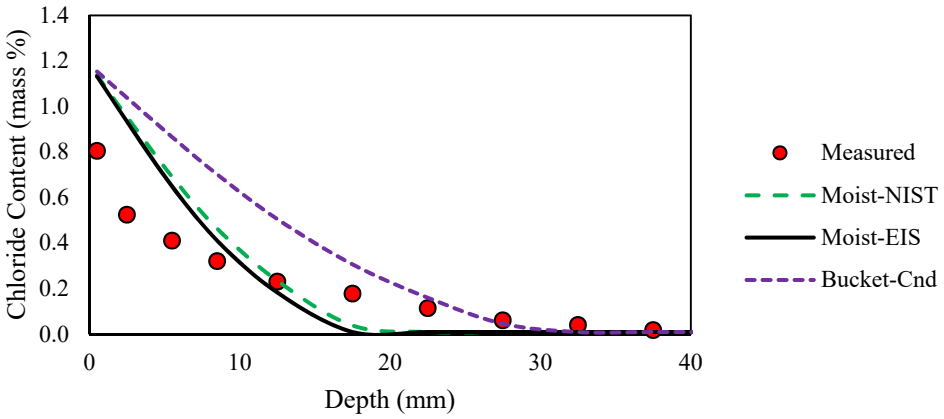

Figure E-35: Effective Chloride bulk diffusion using formation factor for Mix 35 at six month exposure

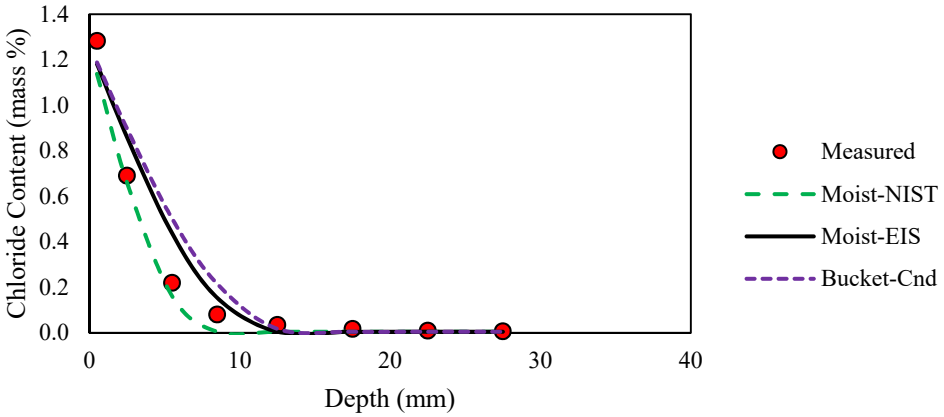

Figure E-36: Effective Chloride bulk diffusion using formation factor for Mix 36 at six month exposure

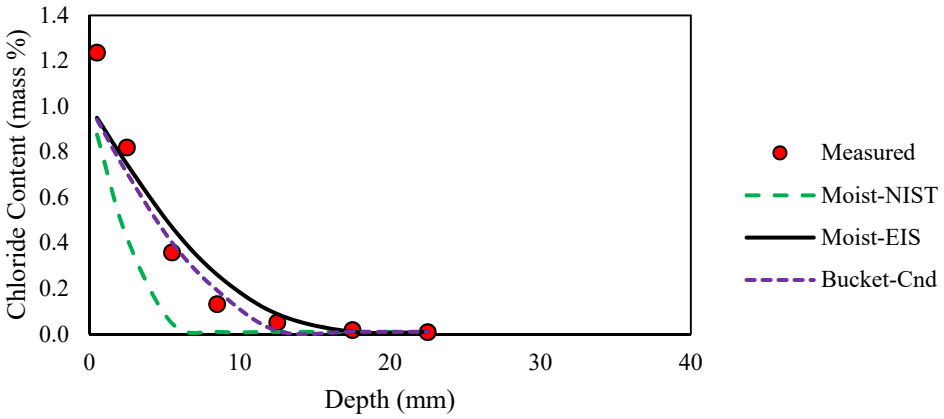

Figure E-37: Effective Chloride bulk diffusion using formation factor for Mix 37 at six month exposure

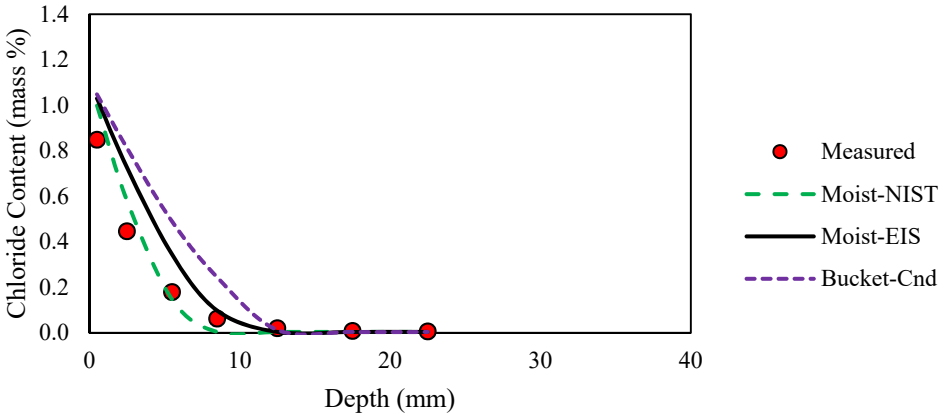

Figure E-38: Effective Chloride bulk diffusion using formation factor for Mix 38 at six month exposure

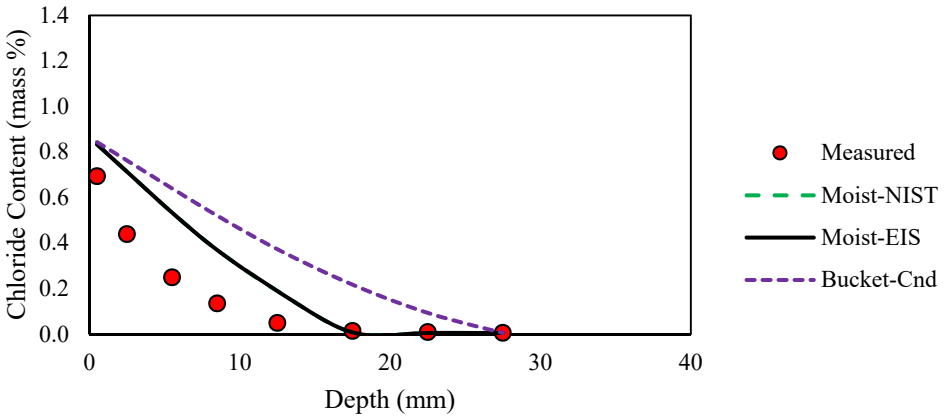

Figure E-39: Effective Chloride bulk diffusion using formation factor for Mix 39 at six month exposure

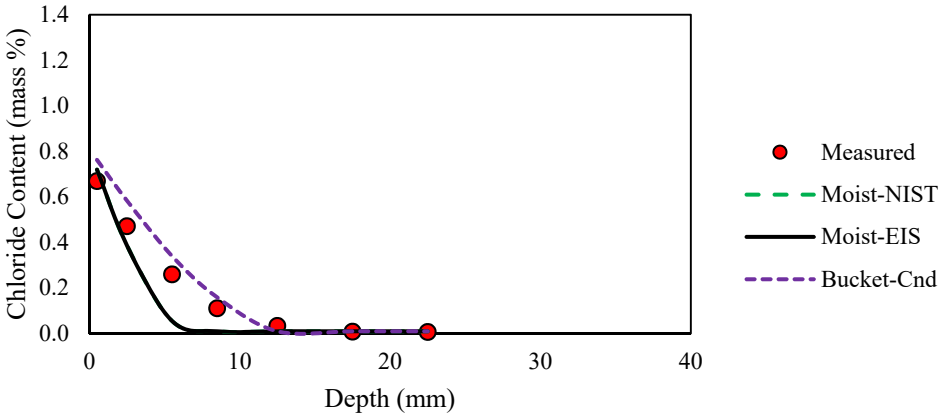

Figure E-40: Effective Chloride bulk diffusion using formation factor for Mix 40 at six month exposure

APPENDIX F: EFFECTIVE CHLORIDE DIFFUSION PREDICTION FROM FORMATION FACTOR: 12 MONTHS EXPOSURE

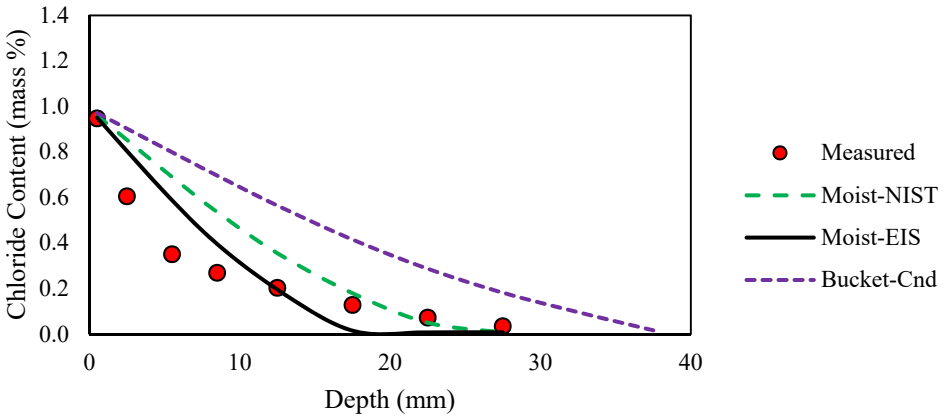

Figure F-1: Effective Chloride bulk diffusion using formation factor for Mix 1 at one year exposure

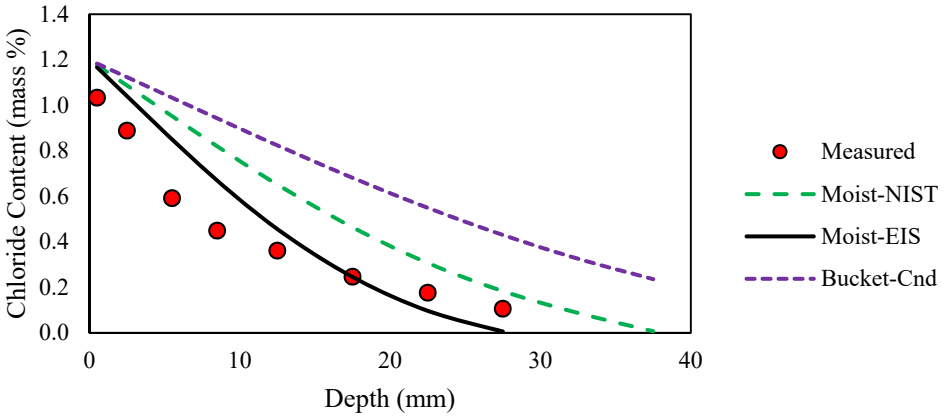

Figure F-2: Effective Chloride bulk diffusion using formation factor for Mix 2 at one year exposure

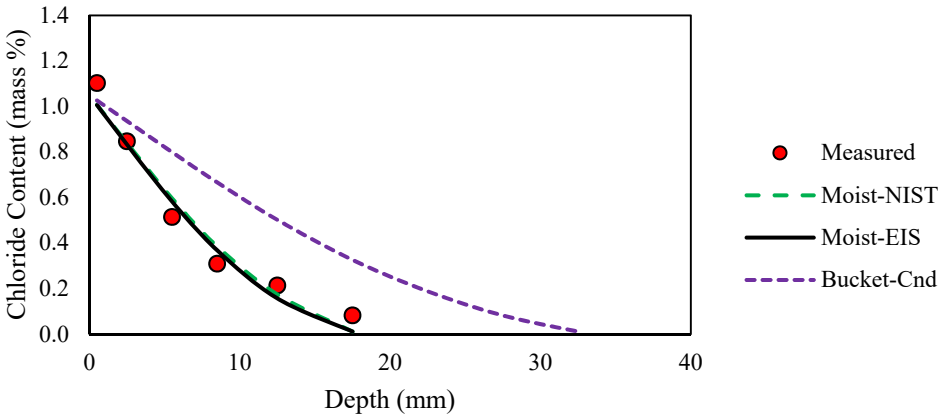

Figure F-3: Effective Chloride bulk diffusion using formation factor for Mix 3 at one year exposure

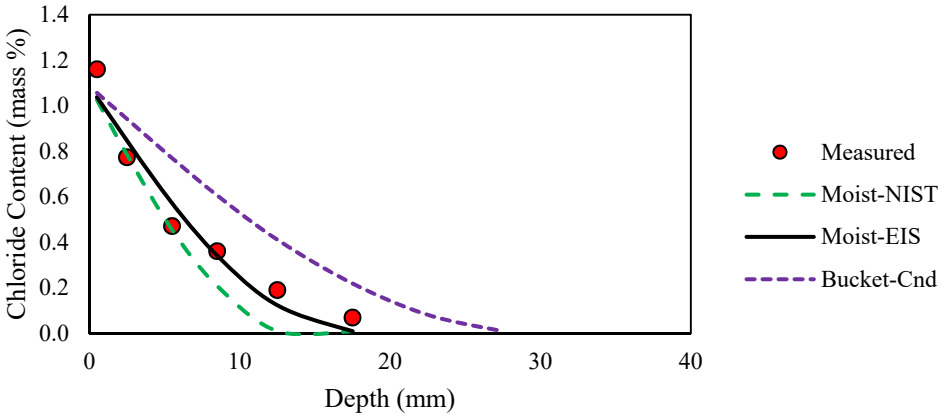

Figure F-4: Effective Chloride bulk diffusion using formation factor for Mix 4 at one year exposure

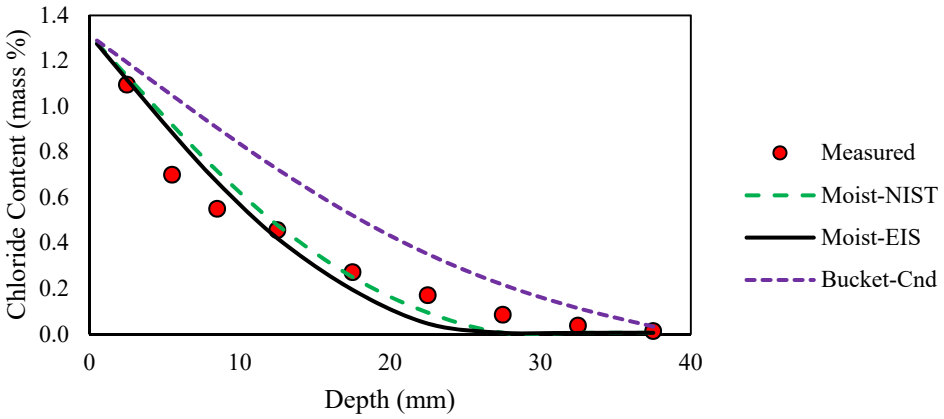

Figure F-5: Effective Chloride bulk diffusion using formation factor for Mix 5 at one year exposure

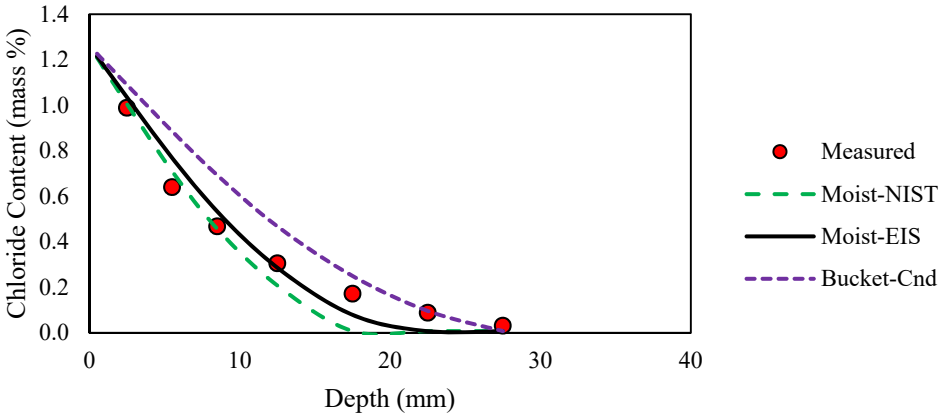

Figure F-6: Effective Chloride bulk diffusion using formation factor for Mix 6 at one year exposure

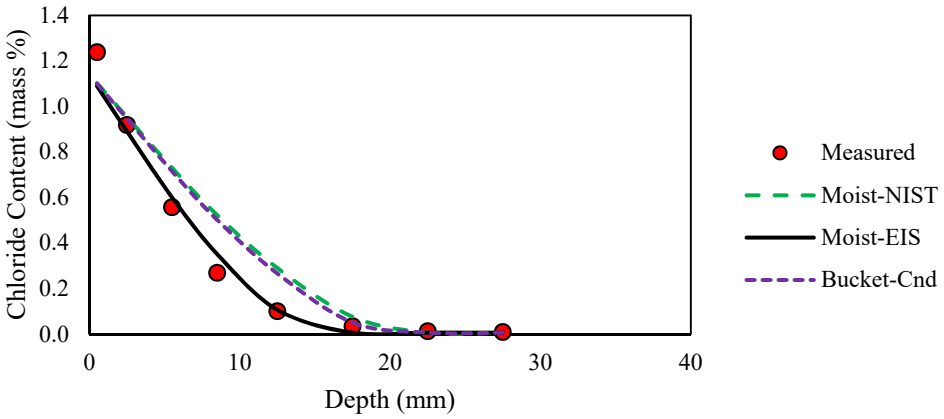

Figure F-7: Effective Chloride bulk diffusion using formation factor for Mix 7 at one year exposure

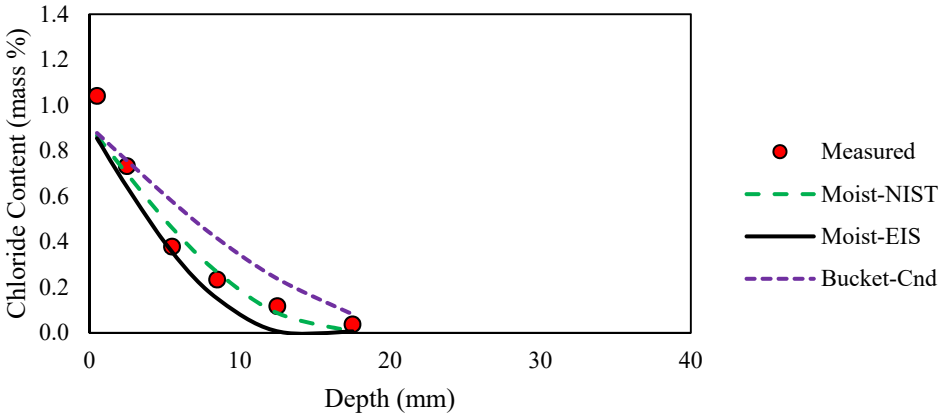

Figure F-8: Effective Chloride bulk diffusion using formation factor for Mix 8 at one year exposure

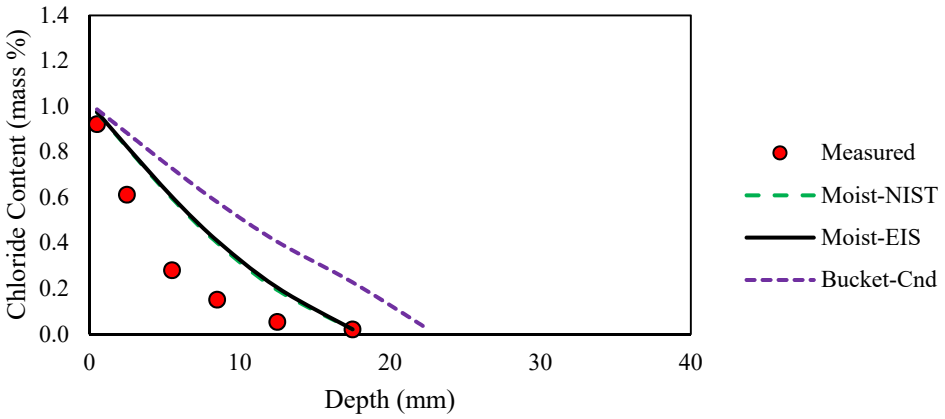

Figure F-9: Effective Chloride bulk diffusion using formation factor for Mix 9 at one year exposure

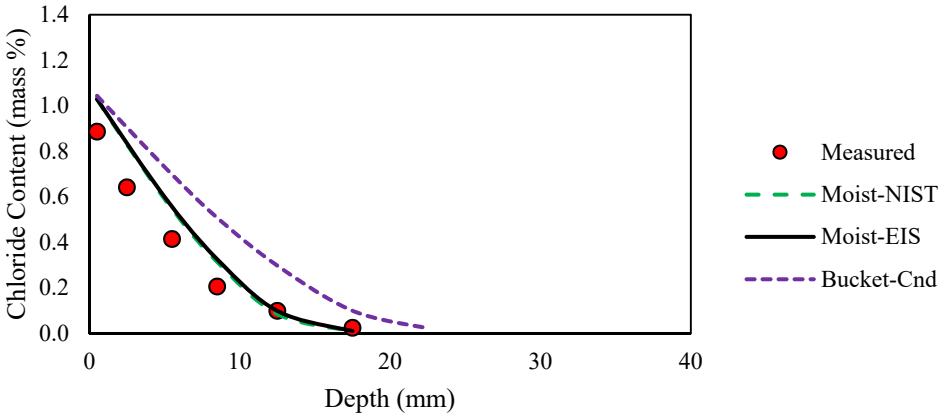

Figure F-10: Effective Chloride bulk diffusion using formation factor for Mix 10 at one year exposure

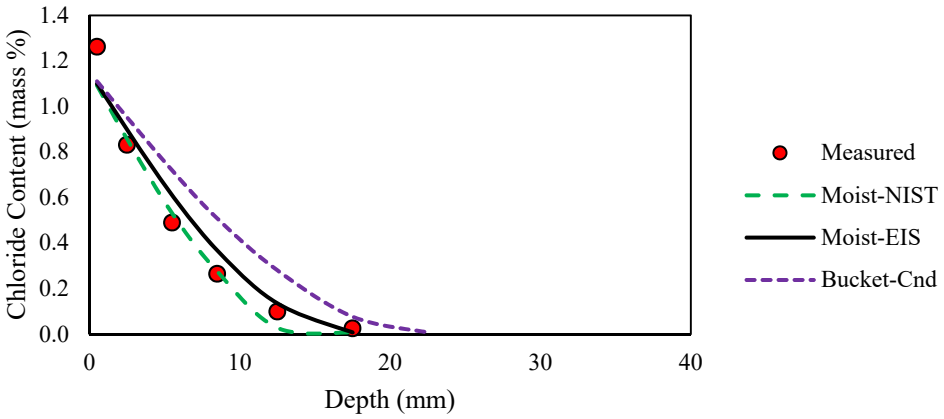

Figure F-11: Effective Chloride bulk diffusion using formation factor for Mix 11 at one year exposure

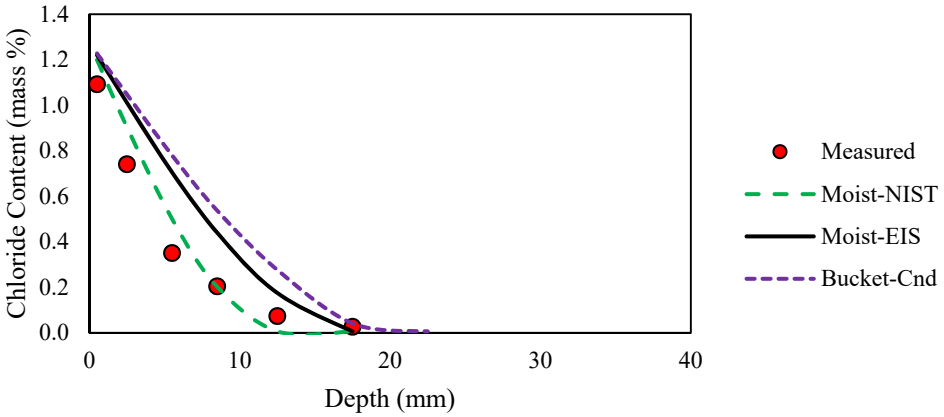

Figure F-12: Effective Chloride bulk diffusion using formation factor for Mix 12 at one year exposure

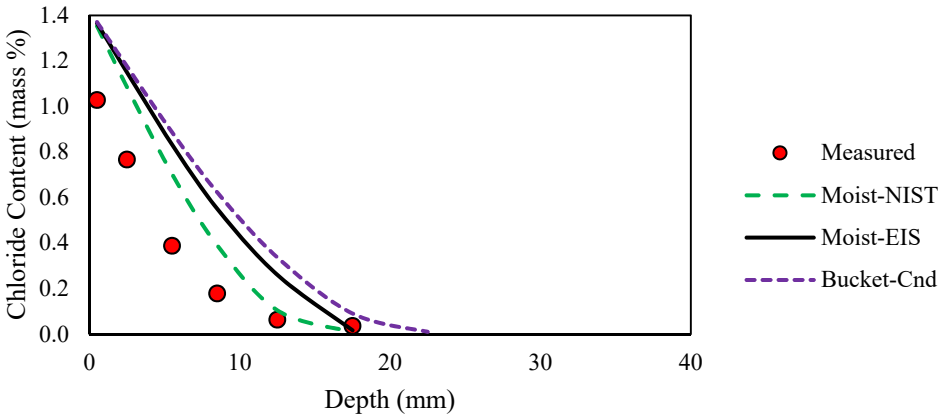

Figure F-13: Effective Chloride bulk diffusion using formation factor for Mix 13 at one year exposure

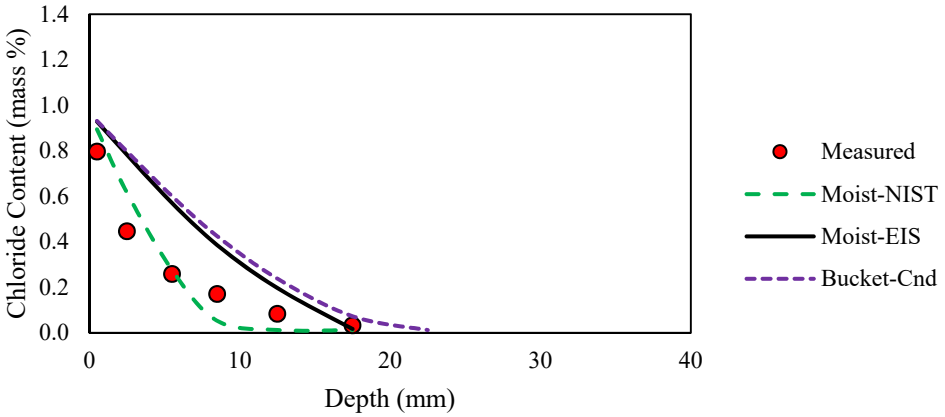

Figure F-14: Effective Chloride bulk diffusion using formation factor for Mix 14 at one year exposure

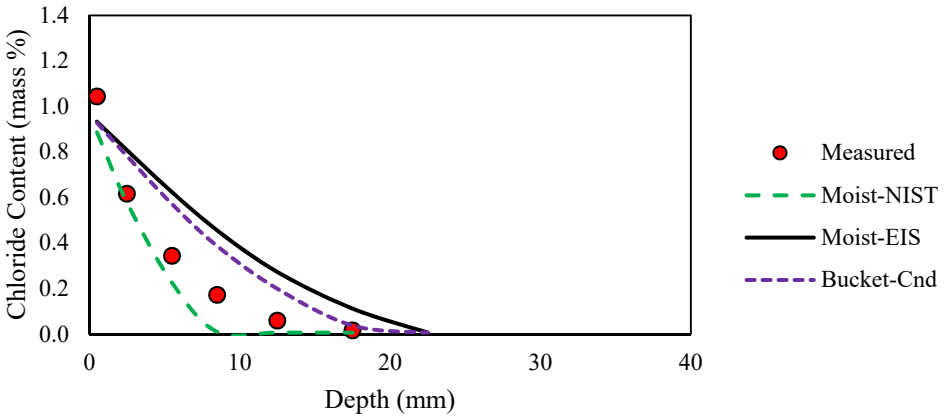

Figure F-15: Effective Chloride bulk diffusion using formation factor for Mix 15 at one year exposure

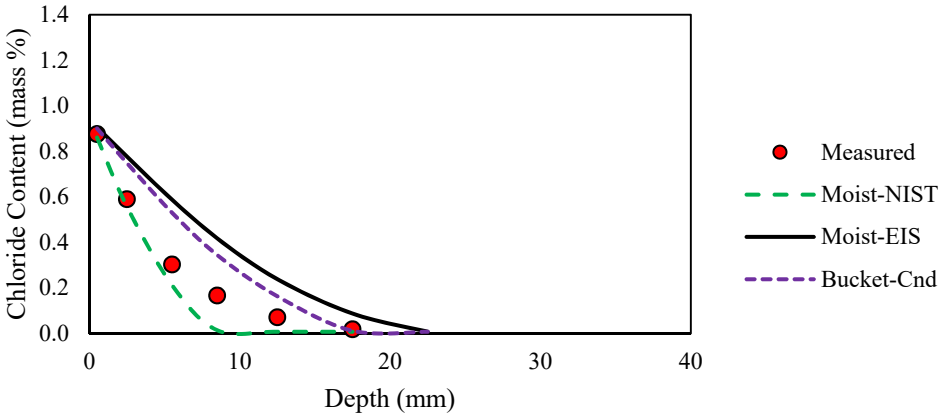

Figure F-16: Effective Chloride bulk diffusion using formation factor for Mix 16 at one year exposure

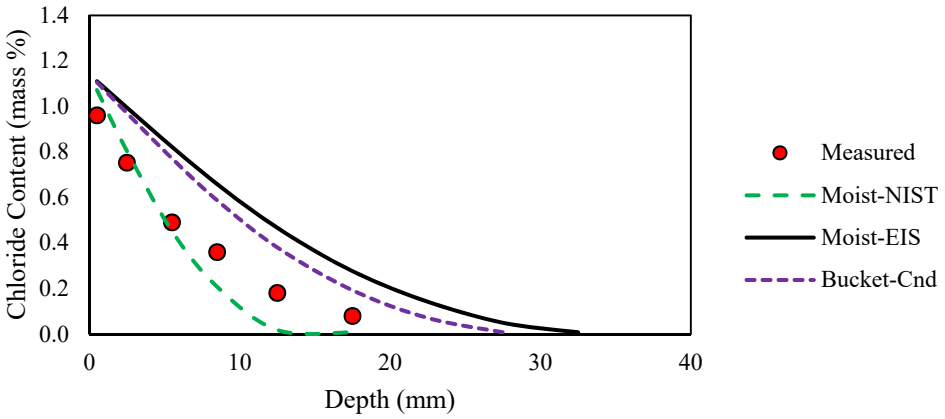

Figure F-17: Effective Chloride bulk diffusion using formation factor for Mix 17 at one year exposure

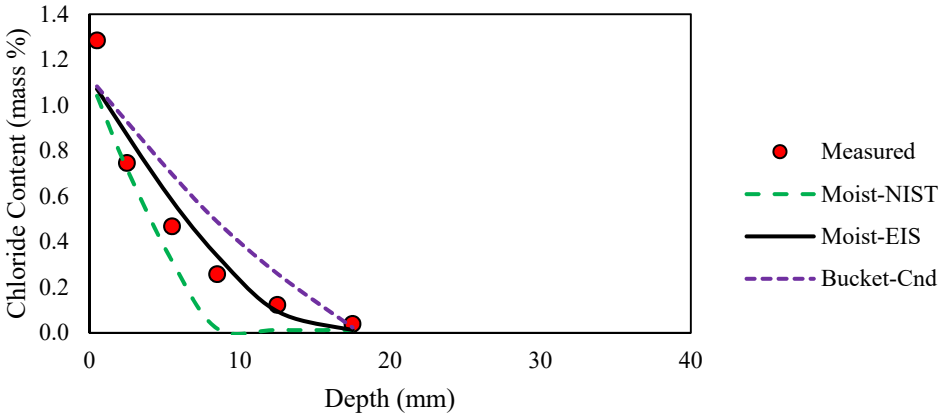

Figure F-18: Effective Chloride bulk diffusion using formation factor for Mix 18 at one year exposure

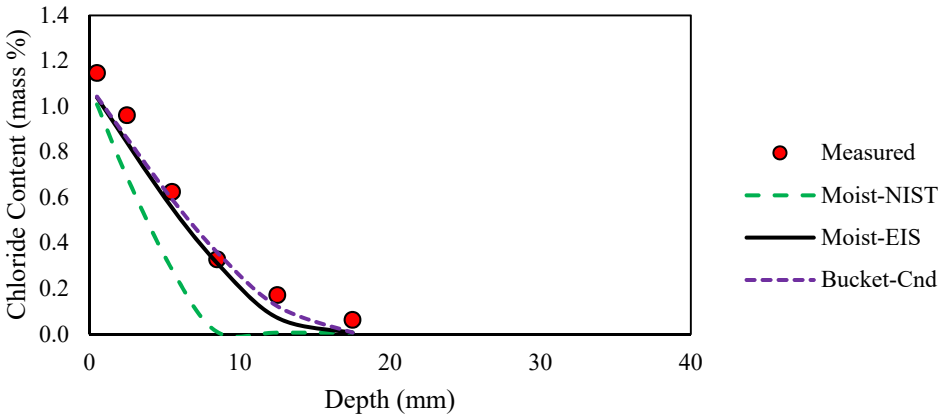

Figure F-19: Effective Chloride bulk diffusion using formation factor for Mix 19 at one year exposure

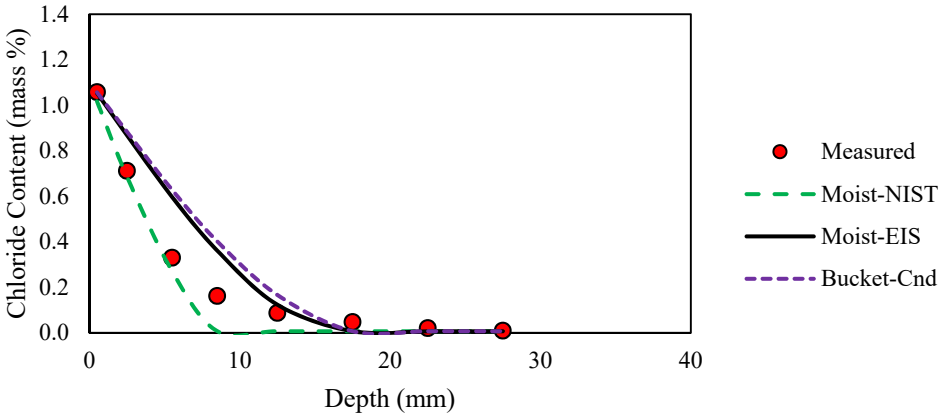

Figure F-20: Effective Chloride bulk diffusion using formation factor for Mix 20 at one year exposure

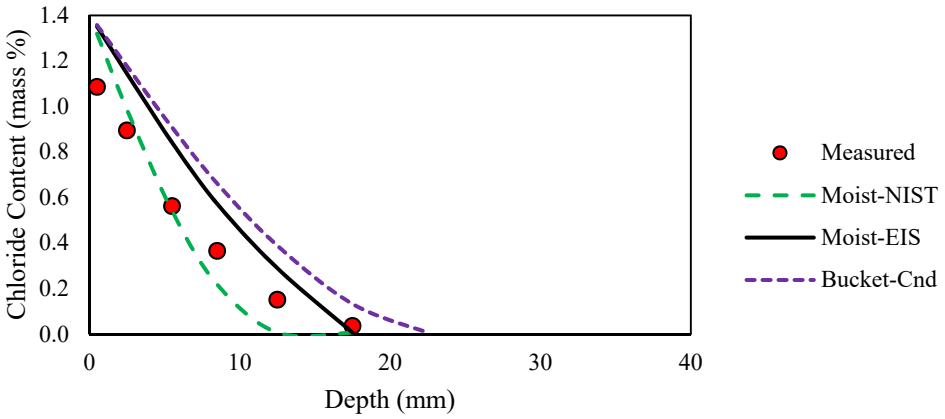

Figure F-21: Effective Chloride bulk diffusion using formation factor for Mix 21 at one year exposure

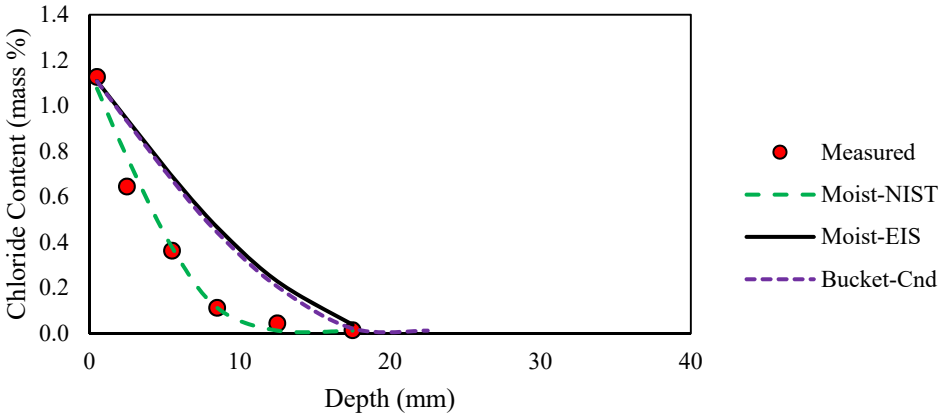

Figure F-22: Effective Chloride bulk diffusion using formation factor for Mix 22 at one year exposure

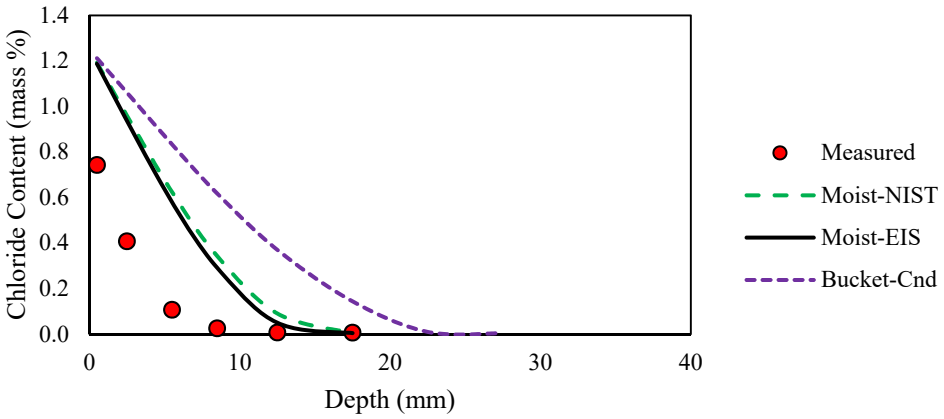

Figure F-23: Effective Chloride bulk diffusion using formation factor for Mix 23 at one year exposure

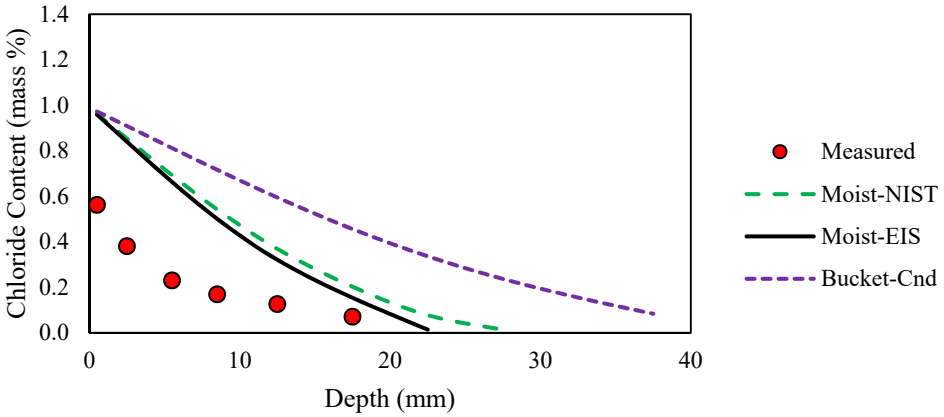

Figure F-24: Effective Chloride bulk diffusion using formation factor for Mix 24 at one year exposure

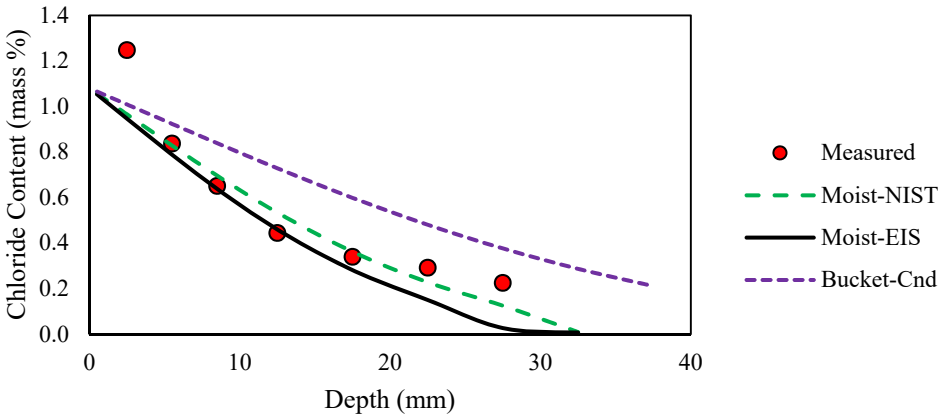

Figure F-25: Effective Chloride bulk diffusion using formation factor for Mix 25 at one year exposure

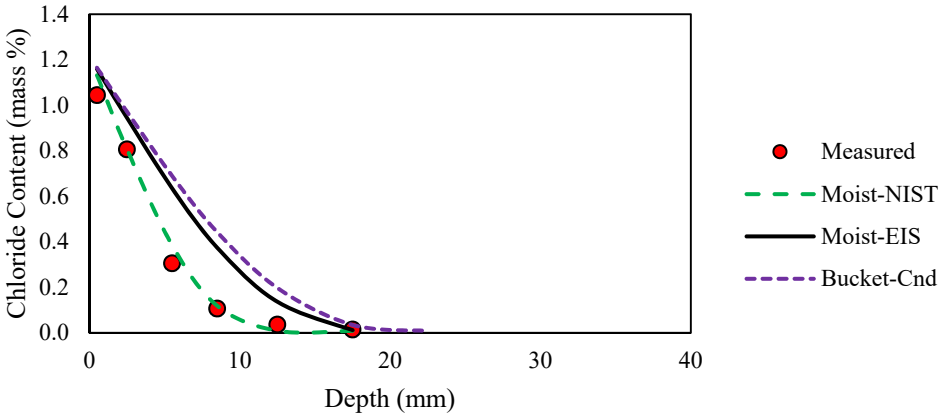

Figure F-26: Effective Chloride bulk diffusion using formation factor for Mix 26 at one year exposure

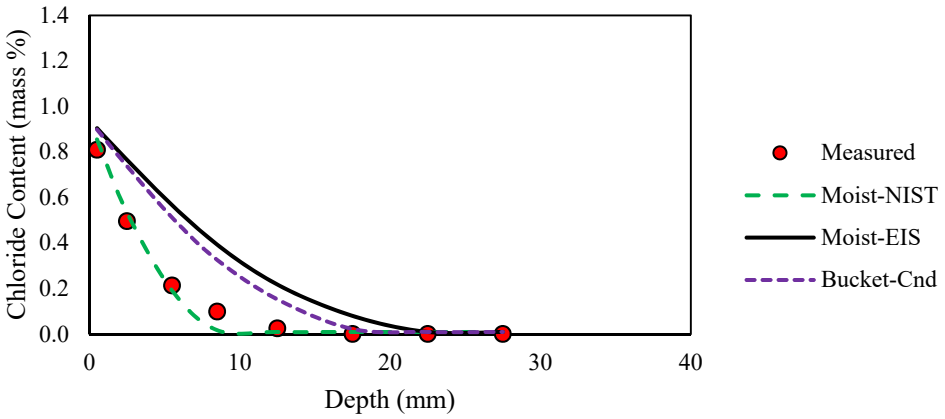

Figure F-27: Effective Chloride bulk diffusion using formation factor for Mix 27 at one year exposure

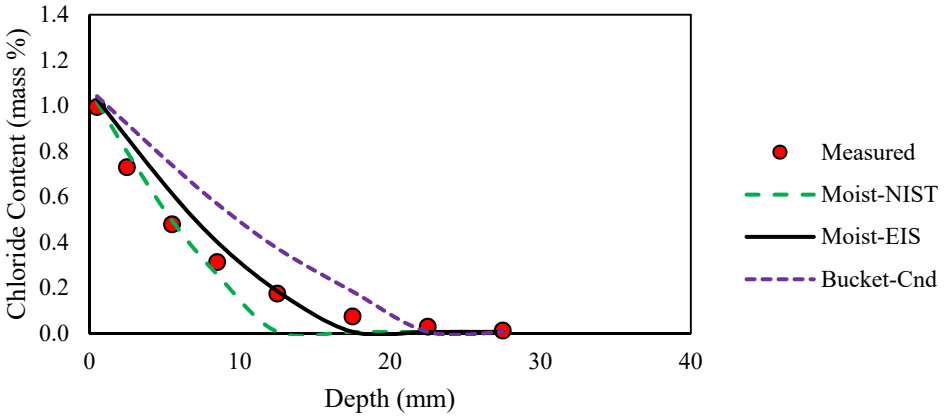

Figure F-28: Effective Chloride bulk diffusion using formation factor for Mix 28 at one year exposure

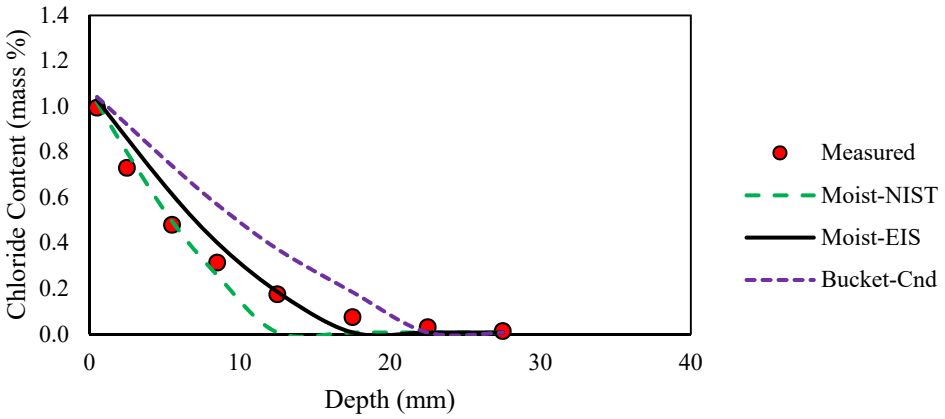

Figure F-29: Effective Chloride bulk diffusion using formation factor for Mix 29 at one year exposure

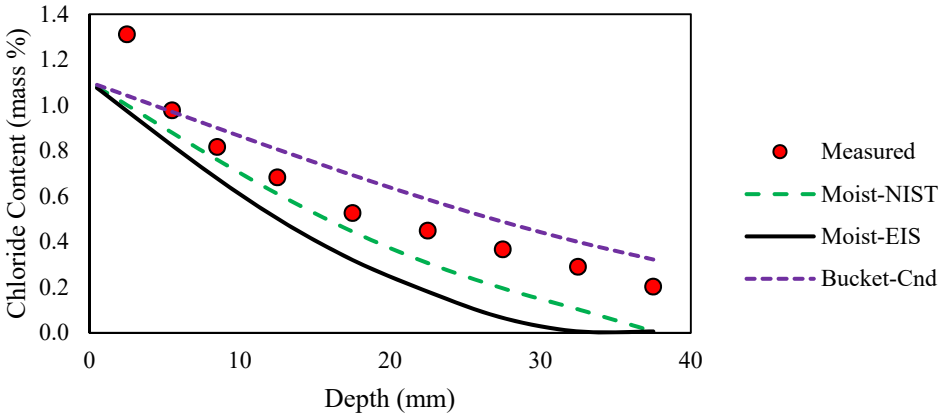

Figure F-30: Effective Chloride bulk diffusion using formation factor for Mix 30 at one year exposure

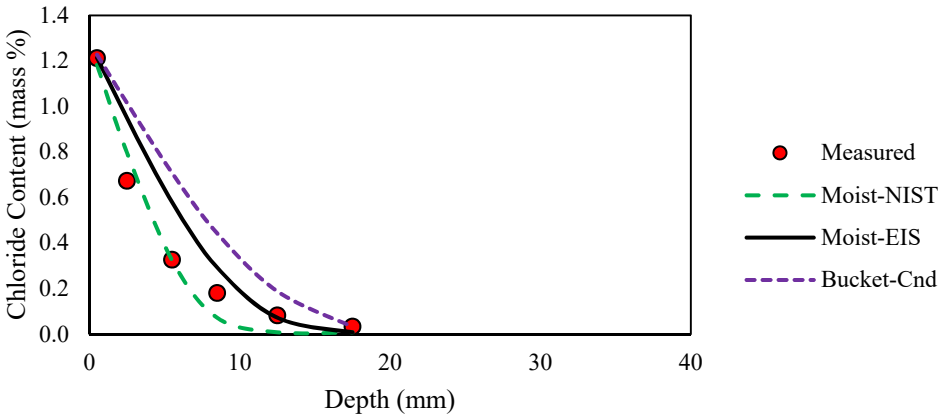

Figure F-31: Effective Chloride bulk diffusion using formation factor for Mix 31 at one year exposure

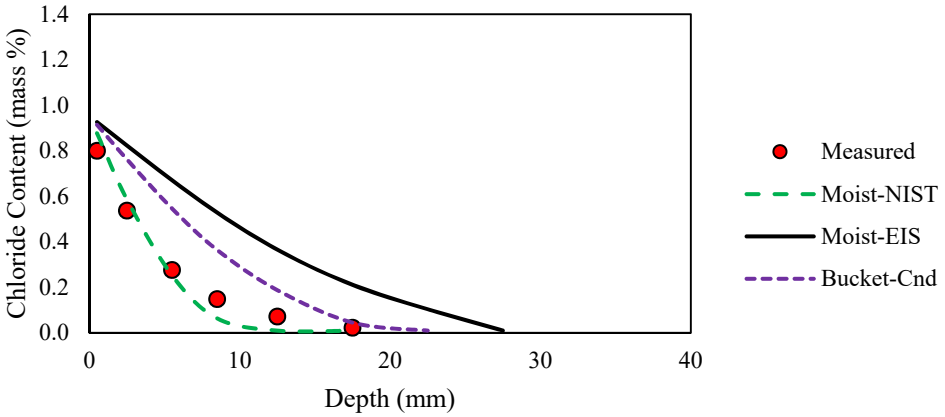

Figure F-32: Effective Chloride bulk diffusion using formation factor for Mix 32 at one year exposure

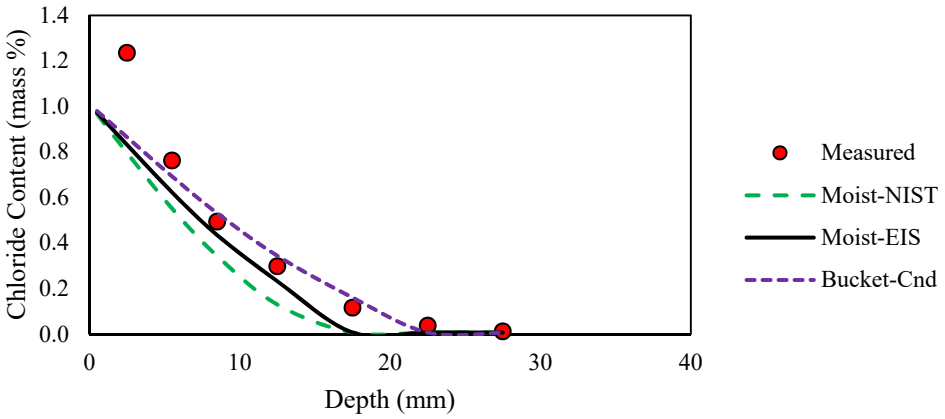

Figure F-33: Effective Chloride bulk diffusion using formation factor for Mix 33 at one year exposure

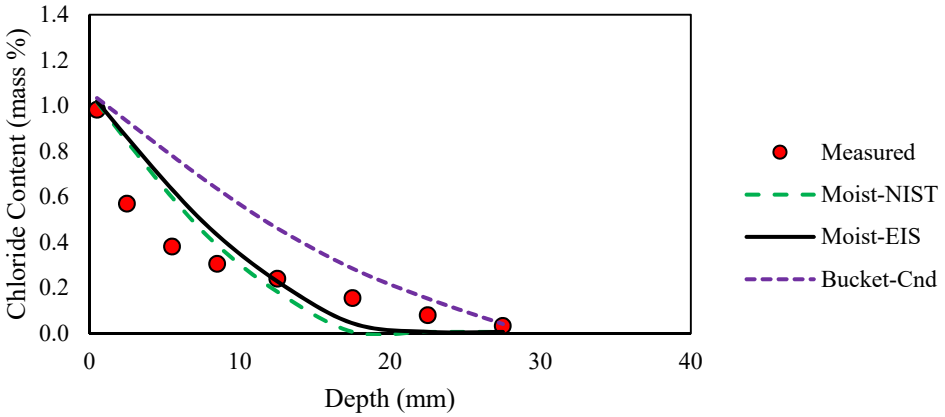

Figure F-34: Effective Chloride bulk diffusion using formation factor for Mix 34 at one year exposure

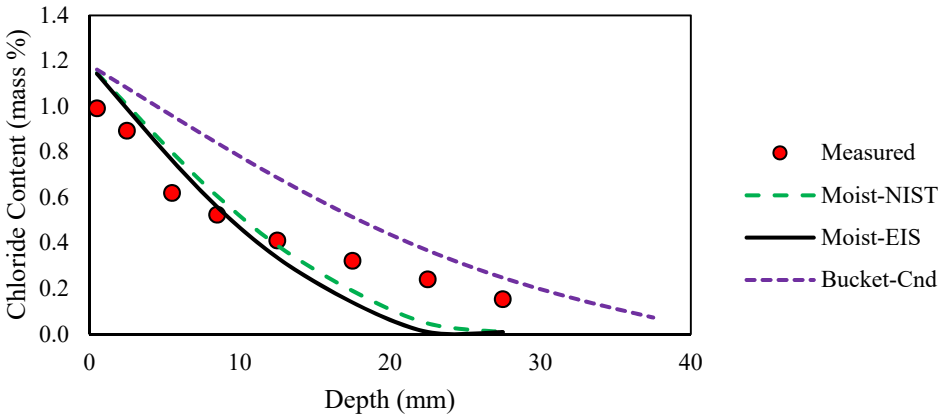

Figure F-35: Effective Chloride bulk diffusion using formation factor for Mix 35 at one year exposure

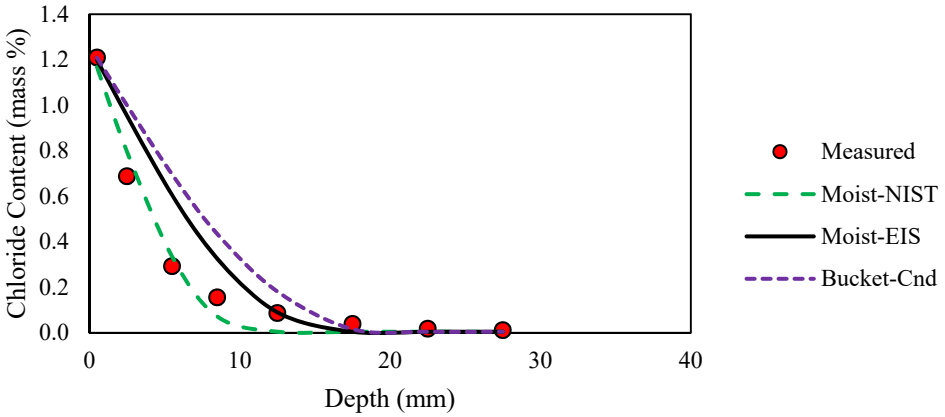

Figure F-36: Effective Chloride bulk diffusion using formation factor for Mix 36 at one year exposure

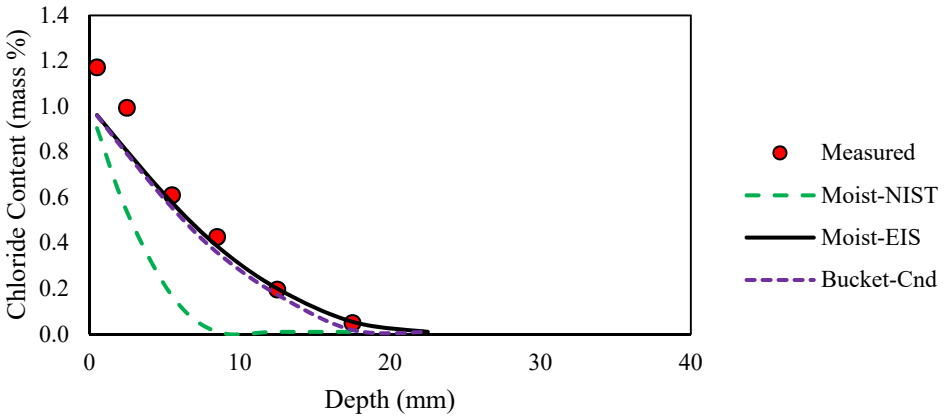

Figure F-37: Effective Chloride bulk diffusion using formation factor for Mix 37 at one year exposure

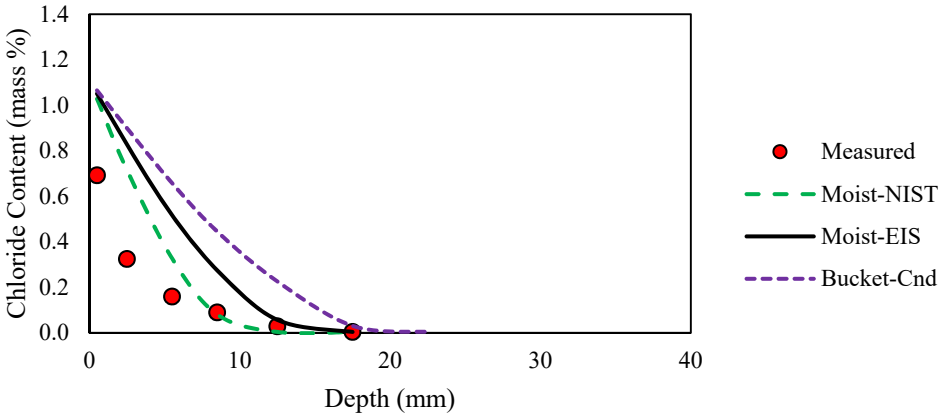

Figure F-38: Effective Chloride bulk diffusion using formation factor for Mix 38 at one year exposure

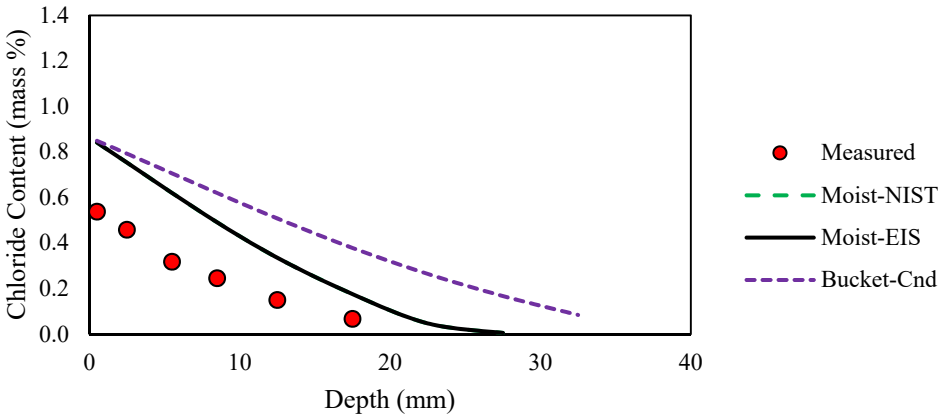

Figure F-39: Effective Chloride bulk diffusion using formation factor for Mix 39 at one year exposure

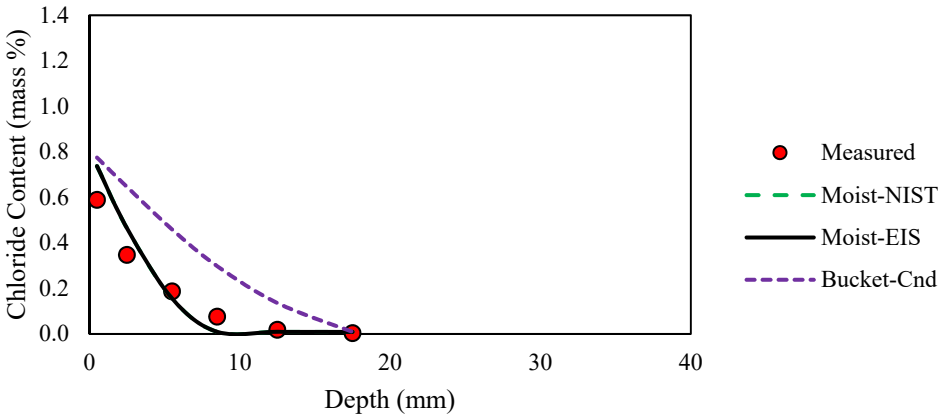

Figure F-40: Effective Chloride bulk diffusion using formation factor for Mix 40 at one year exposure

APPENDIX G: CHLORIDE PROFILE MEASUREMENTS FROM CORED SAMPLE SURFACE AND BULK DIFFUSION EXPERIMENTS

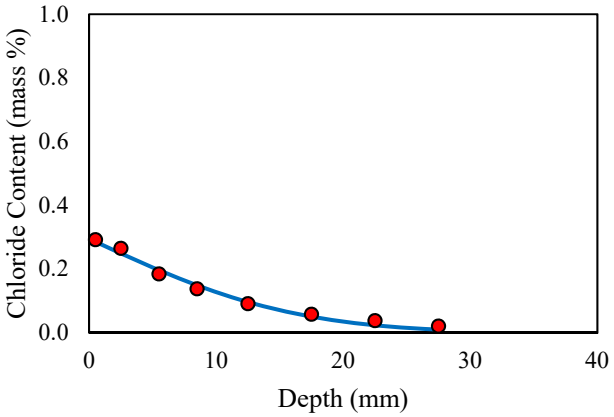

Mix No.	1-1
Mix ID	CEM
Exposure time (years)	13
Diffusion (m^2/s)	0.20×10^{-12}
Cs (mass %)	0.295
C_i (mass %)	0.001
R^2	0.988

Figure G-1: Chloride bulk diffusion results for Mix 1-1 of Key Royal Bridge at 13 years of exposure

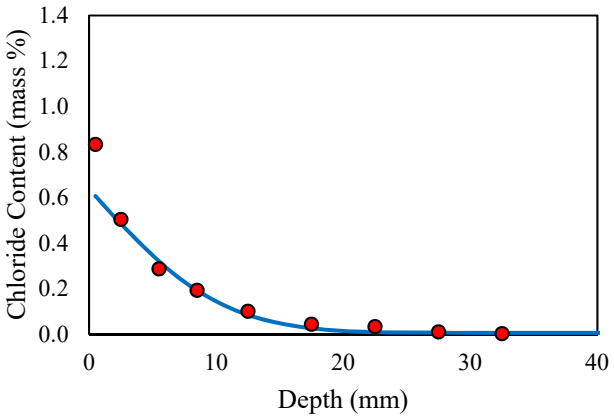

Mix No.	1-2
Mix ID	CEM
Exposure time (years)	13
Diffusion (m^2/s)	0.26×10^{-12}
Cs (mass %)	0.351
C_i (mass %)	0.001
R^2	0.956

Figure G-2: Chloride bulk diffusion results for Mix 1-2 of Key Royal Bridge at 13 years of exposure

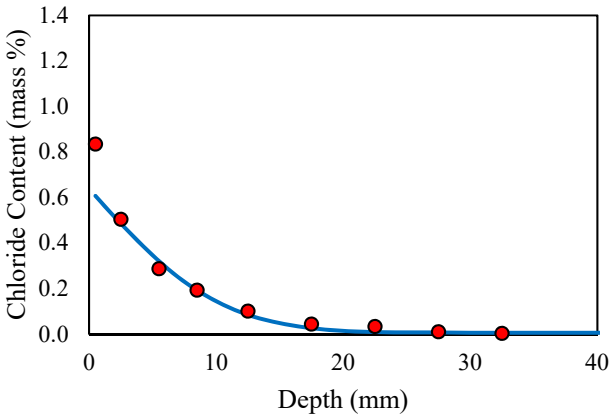

Mix No.	1-3
Mix ID	CEM
Exposure time (years)	13
Diffusion (m^2/s)	1.11×10^{-12}
Cs (mass %)	0.482
C_i (mass %)	0.001
R^2	0.956

Figure G-3: Chloride bulk diffusion results for Mix 1-3 of Key Royal Bridge at 13 years of exposure

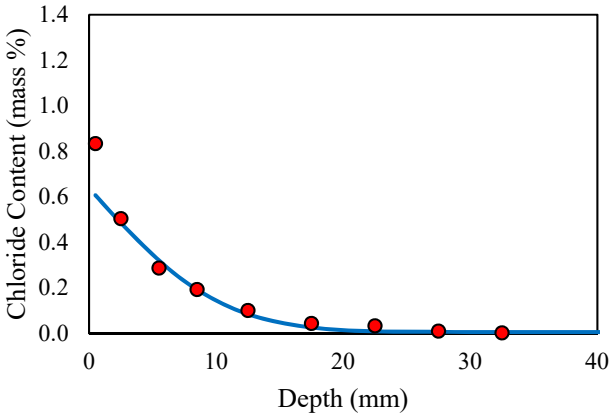

Mix No.	1
Mix ID	CEM
Exposure time (months)	6
Diffusion (m^2/s)	3.21×10^{-12}
Cs (mass %)	0.738
C_i (mass %)	0.001
R^2	0.986

Figure G-4: Chloride bulk diffusion results for Mix 1 of Key Royal Bridge after 6 months of exposure

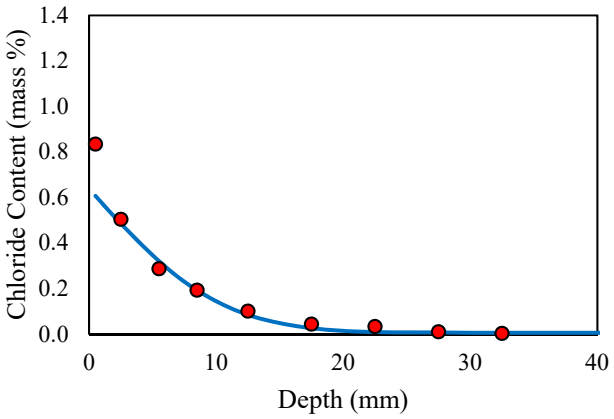

Mix No.	2-1
Mix ID	UFA
Exposure time (years)	13
Diffusion (m^2/s)	0.06×10^{-12}
Cs (mass %)	0.273
C_i (mass %)	0.001
R^2	0.996

Figure G-5: Chloride bulk diffusion results for Mix 2-1 of Key Royal Bridge at 13 years of exposure

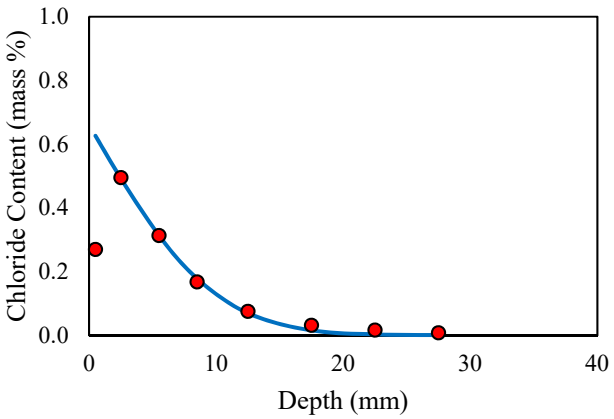

Mix No.	2-2
Mix ID	UFA
Exposure time (years)	13
Diffusion (m^2/s)	0.07×10^{-12}
Cs (mass %)	0.660
C_i (mass %)	0.001
R^2	0.998

Figure G-6: Chloride bulk diffusion results for Mix 2-2 of Key Royal Bridge at 13 years of exposure

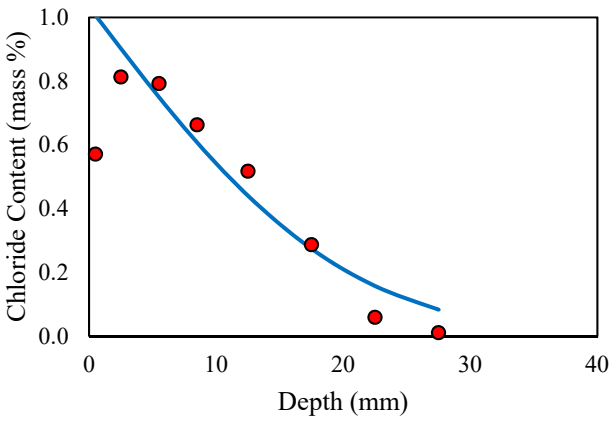

Mix No.	2-3
Mix ID	UFA
Exposure time (years)	13
Diffusion (m^2/s)	0.30×10^{-12}
Cs (mass %)	1.033
C_i (mass %)	0.001
R^2	0.954

Figure G-7: Chloride bulk diffusion results for Mix 2-3 of Key Royal Bridge at 13 years of exposure

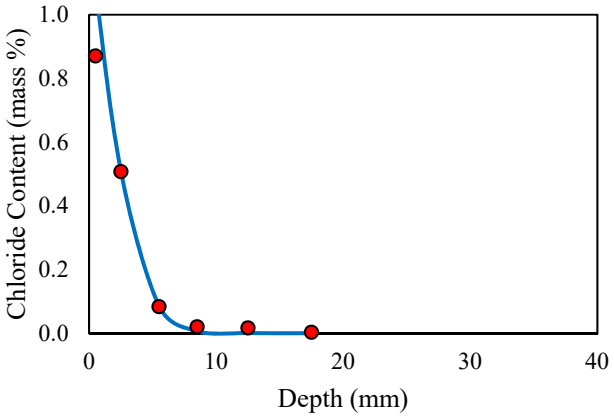

Mix No.	2
Mix ID	UFA
Exposure time (months)	6
Diffusion (m^2/s)	0.29×10^{-12}
Cs (mass %)	1.242
C_i (mass %)	0.001
R^2	0.999

Figure G-8: Chloride bulk diffusion results for Mix 2 of Key Royal Bridge after 6 months of exposure

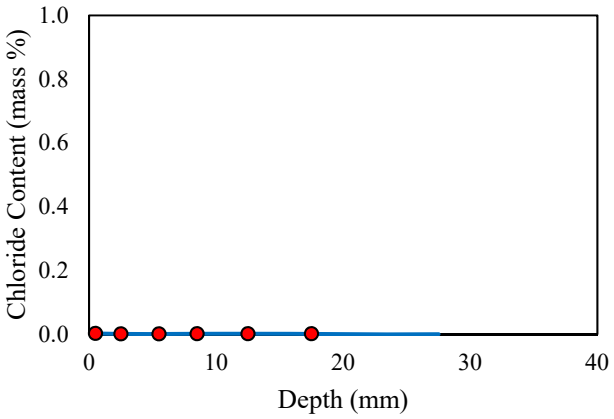

Mix No.	3-1
Mix ID	FA
Exposure time (years)	13
Diffusion (m^2/s)	0.00×10^{-12}
Cs (mass %)	0.000
C_i (mass %)	0.001
R^2	-

Figure G-9: Chloride profile results for Mix 3-1 of Key Royal Bridge at 12 years of field exposure

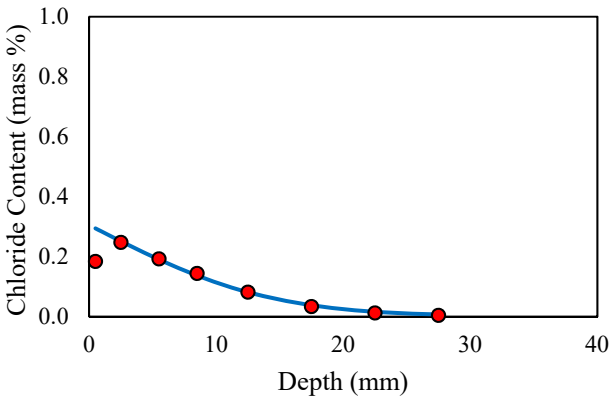

Mix No.	3-2
Mix ID	FA
Exposure time (years)	13
Diffusion (m^2/s)	0.15×10^{-12}
Cs (mass %)	0.305
C_i (mass %)	0.001
R^2	0.998

Figure G-10: Chloride profile results for Mix 3-2 of Key Royal Bridge at 12 years of field exposure

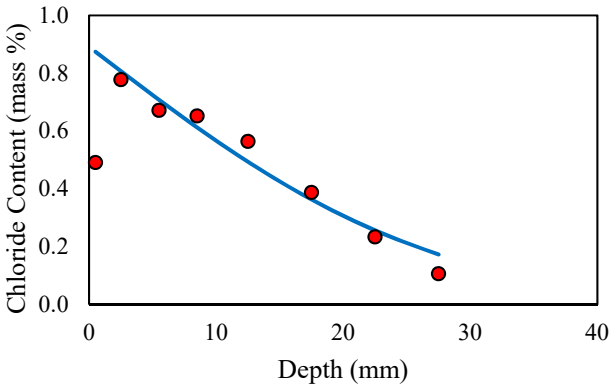

Mix No.	3-3
Mix ID	FA
Exposure time (years)	13
Diffusion (m^2/s)	0.54×10^{-12}
Cs (mass %)	0.891
C_i (mass %)	0.001
R^2	0.963

Figure G-11: Chloride profile results for Mix 3-3 of Key Royal Bridge at 12 years of field exposure

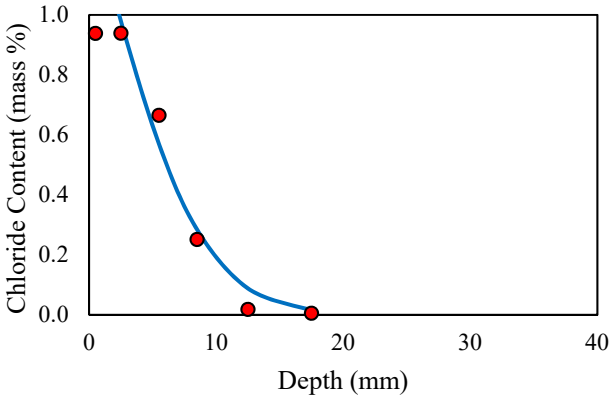

Mix No.	3
Mix ID	FA
Exposure time (months)	6
Diffusion (m^2/s)	1.42×10^{-12}
Cs (mass %)	1.380
C_i (mass %)	0.001
R^2	0.977

Figure G-12: Chloride bulk diffusion results for Mix 3 of Key Royal Bridge after 6 months of exposure

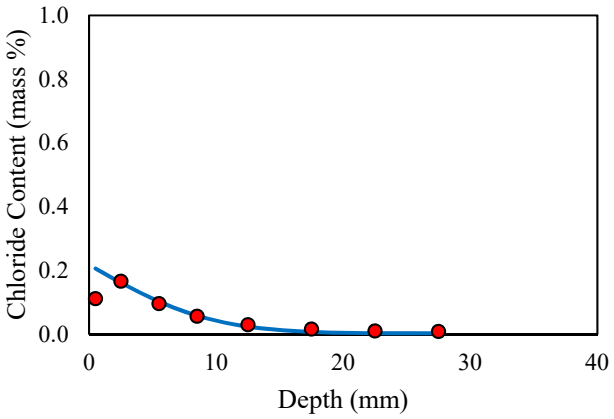

Mix No.	4-1
Mix ID	SF
Exposure time (years)	13
Diffusion (m^2/s)	0.07×10^{-12}
Cs (mass %)	0.217
C_i (mass %)	0.002
R^2	0.993

Figure G-13: Chloride profile results for Mix 4-1 of Key Royal Bridge at 12 years of field exposure

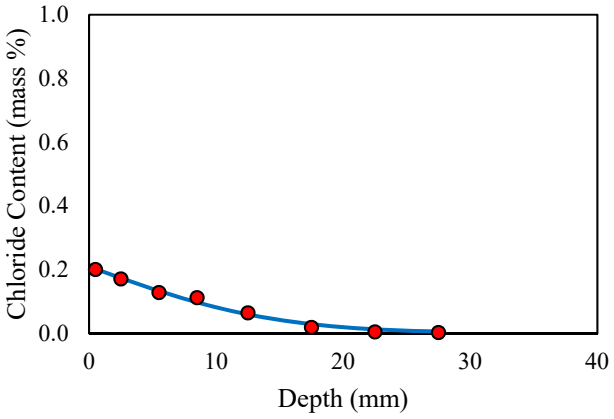

Mix No.	4-2
Mix ID	SF
Exposure time (years)	13
Diffusion (m^2/s)	0.16×10^{-12}
Cs (mass %)	0.209
C_i (mass %)	0.002
R^2	0.985

Figure G-14: Chloride profile results for Mix 4-2 of Key Royal Bridge at 12 years of field exposure

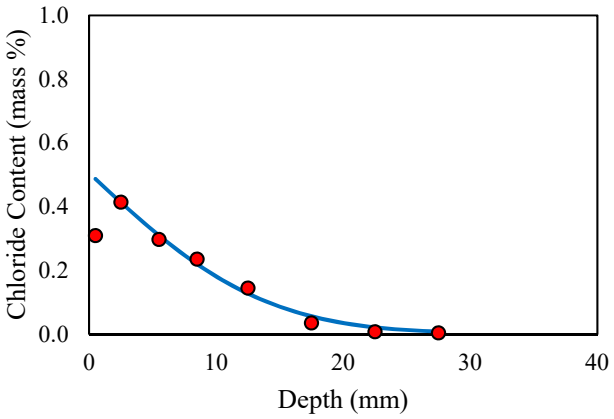

Mix No.	4-3
Mix ID	SF
Exposure time (years)	13
Diffusion (m^2/s)	0.14×10^{-12}
Cs (mass %)	0.505
C_i (mass %)	0.002
R^2	0.992

Figure G-15: Chloride profile results for Mix 4-3 of Key Royal Bridge at 12 years of field exposure

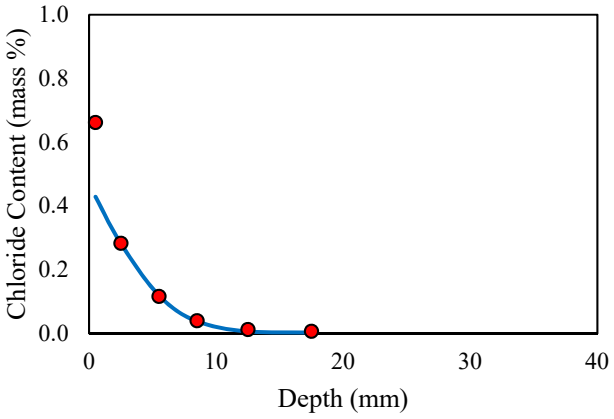

Mix No.	4
Mix ID	SF
Exposure time (months)	6
Diffusion (m^2/s)	0.72×10^{-12}
Cs (mass %)	0.467
C_i (mass %)	0.002
R^2	0.999

Figure G-16: Chloride bulk diffusion results for Mix 4 of Key Royal Bridge after 6 months of exposure

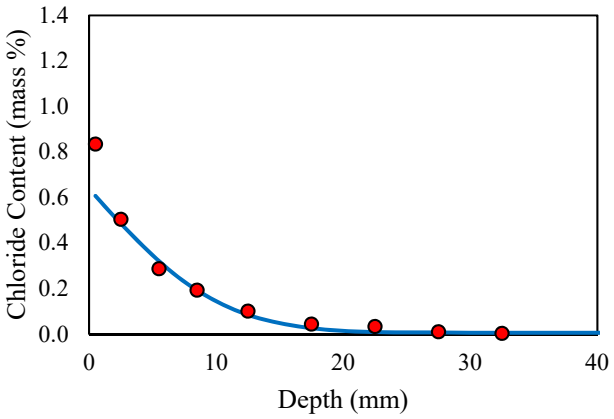

Mix No.	5-1
Mix ID	MET
Exposure time (years)	13
Diffusion (m^2/s)	0.09×10^{-12}
Cs (mass %)	0.403
C_i (mass %)	0.006
R^2	0.981

Figure G-17: Chloride profile results for Mix 5-1 of Key Royal Bridge at 12 years of field exposure

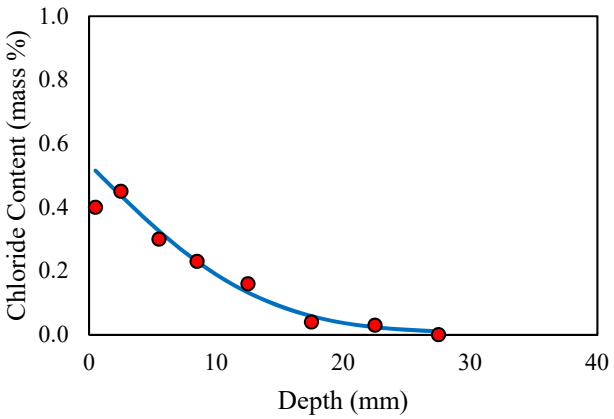

Mix No.	5-2
Mix ID	MET
Exposure time (years)	13
Diffusion (m^2/s)	0.14×10^{-12}
Cs (mass %)	0.535
C_i (mass %)	0.006
R^2	0.987

Figure G-18: Chloride profile results for Mix 5-2 of Key Royal Bridge at 12 years of field exposure

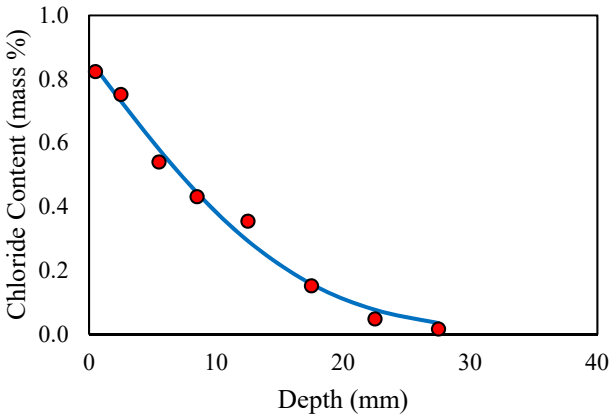

Mix No.	5-3
Mix ID	MET
Exposure time (years)	13
Diffusion (m^2/s)	0.20×10^{-12}
Cs (mass %)	0.862
C_i (mass %)	0.006
R^2	0.984

Figure G-19: Chloride profile results for Mix 5-3 of Key Royal Bridge at 12 years of field exposure

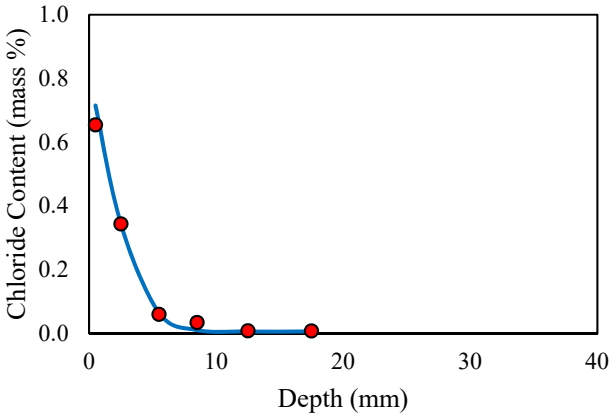

Mix No.	5
Mix ID	MET
Exposure time (months)	6
Diffusion (m^2/s)	0.30×10^{-12}
Cs (mass %)	0.821
C_i (mass %)	0.006
R^2	0.995

Figure G-20: Chloride bulk diffusion results for Mix 5 of Key Royal Bridge after 6 months of exposure

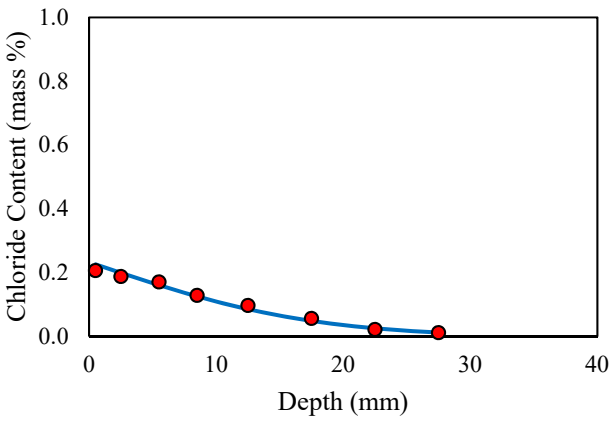

Mix No.	6-1
Mix ID	BFS
Exposure time (years)	13
Diffusion (m^2/s)	0.23×10^{-12}
Cs (mass %)	0.232
C_i (mass %)	0.001
R^2	0.987

Figure G-21: Chloride profile results for Mix 6-1 of Key Royal Bridge at 12 years of field exposure

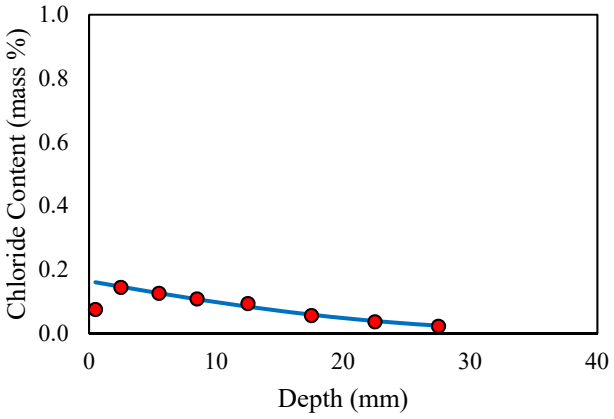

Mix No.	6-2
Mix ID	BFS
Exposure time (years)	13
Diffusion (m^2/s)	0.44×10^{-12}
Cs (mass %)	0.164
C_i (mass %)	0.001
R^2	0.990

Figure G-22: Chloride profile results for Mix 6-2 of Key Royal Bridge at 12 years of field exposure

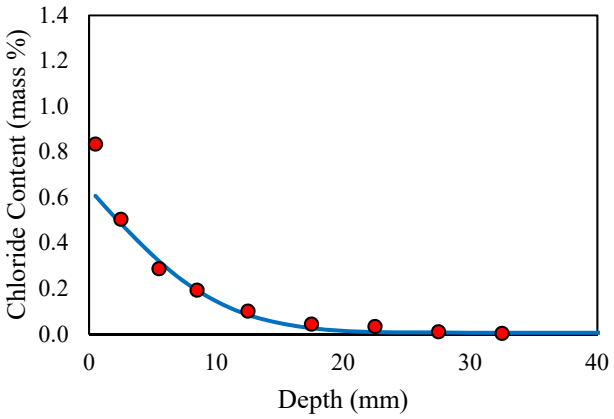

Mix No.	6-3
Mix ID	BFS
Exposure time (years)	13
Diffusion (m^2/s)	0.027×10^{-12}
Cs (mass %)	0.413
C_i (mass %)	0.001
R^2	0.985

Figure G-23: Chloride profile results for Mix 6-3 of Key Royal Bridge at 12 years of field exposure

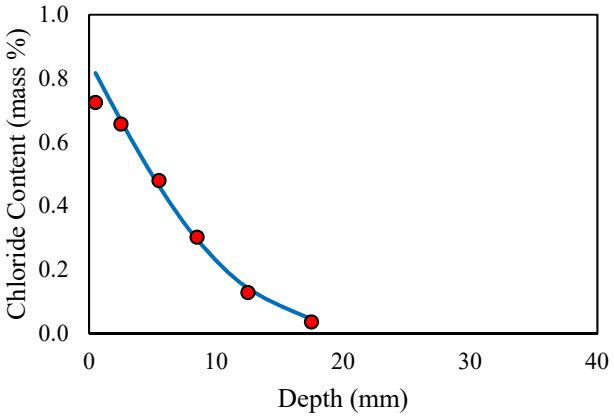

Mix No.	6
Mix ID	BFS
Exposure time (months)	6
Diffusion (m^2/s)	2.56×10^{-12}
Cs (mass %)	0.855
C_i (mass %)	0.001
R^2	0.997

Figure G-24: Chloride bulk diffusion results for Mix 6 of Key Royal Bridge after 6 months of exposure